TÉCNICO LISBOA

UNIVERSIDADE DE LISBOA

INSTITUTO SUPERIOR TÉCNICO

Development of a Biocompatible, Electroconductive, Elastomeric Construct for Use as a Somatosensory System Microenvironment

Siddhi Bianca Camila Lama

Supervisor: Doctor Frederico Castelo Alves Ferreira

Co-Supervisors: Doctor Ann Marie Rajnicek

Doctor Jorge Manuel Mateus Martins

Thesis approved in public session to obtain the PhD Degree in Bioengineering

Jury final classification: Pass with Distinction

2019

UNIVERSIDADE DE LISBOA
INSTITUTO SUPERIOR TÉCNICO

Development of a Biocompatible, Electroconductive, Elastomeric Construct for Use as a Somatosensory System Microenvironment

Siddhi Bianca Camila Lama

Supervisor: Doctor Frederico Castelo Alves Ferreira
Co-Supervisors: Doctor Ann Marie Rajnicek
Doctor Jorge Manuel Mateus Martins

Thesis approved in public session to obtain the PhD Degree in Bioengineering

Jury final classification: Pass with Distinction

Jury

Chairperson: Doctor Joaquim Manuel Sampaio Cabral, Instituto Superior Técnico, Universidade de Lisboa

Members of the Committee:
Doctor Carlos Enrique Aleman Llanso, Escola Tècnica Superior d'Enginyeria Industrial de Barcelona, Universitat Politècnica de Catalunya, Espanha
Doctor Joaquim Manuel Sampaio Cabral, Instituto Superior Técnico, Universidade de Lisboa
Doctor Jorge Manuel Ferreira Morgado, Instituto Superior Técnico, Universidade de Lisboa
Doctor Eirini Velliou, Faculty of Engineering and Physical Sciences, University of Surrey, UK
Doctor Frederico Castelo Alves Ferreira, Instituto Superior Técnico, Universidade de Lisboa

Funding Institutions
This research was funded by "Fundação para a Ciência e Tecnologia" (MIT-Portugal Scholarship) through the PhD grant with reference (SFRH/BD/52338/2013)

2019

RESUMO

Ao longo da existência humana, a perda de membros foi considerada um prejuízo irreversível e perda permanente de função. Até recentemente, a restauração do feedback sensorial para usuários de próteses e indivíduos com neuropatias variadas era inimaginável. No entanto, desenvolvimentos multidisciplinares tornaram a recuperação dessa função cada vez mais factível. A falta de pele inervada, que permite que uma miríade de estímulos táteis seja detetada e interpretada, tem sido um dos principais obstáculos na restauração do feedback sensorial completo. Isso foi combatido através do design de substitutos artificiais da pele, permitindo aos usuários um feedback sensorial parcial, mas não padrão. Esta tese enfoca a criação de um sistema somatossensorial de bioengenharia, tanto em termos de substrato micro ambiental como em ambiente celular. Nós criamos um modelo de sistema somatossensorial projetando uma construção tridimensional, biocompatível, elastomérica, eletrocondutora, permeável, sensível à pressão, capaz de atuar como uma interface para as células do sistema somatossensorial. A validação dos componentes individuais e do constructo completo foi realizada. Começamos avaliando métodos mecânicos, avaliando as propriedades de deformação elástica, alongamento na ruptura e fadiga. Em seguida, analisamos a condutividade eléctrica, tanto em estase como durante vários pontos de fadiga eletromecânica, bem como em ambientes secos e líquidos. Além disso, avaliamos a piezoeletricidade do constructo, validando o uso da capacidade do nosso constructo para funcionar como um elétrodo macio. A análise do nosso sistema somatossensorial foi validada com vários tipos de células encontradas no sistema somatossensorial, tais como: fibroblastos, queratinócitos, células de Schwann, células ganglionares da raiz dorsal e células progenitoras neuropáticas. Citotoxicidade, adesão, expansão e diferenciação foram todas avaliadas. Além disso, células neurais e co-culturas contendo células neurais foram avaliadas em campos elétricos para entender os efeitos da eletricidade no nosso modelo de sistema somatossensorial. Experimentos de campo elétrico usando tais estruturas (scaffolds) podem eventualmente tornar-se um método padrão para realizar modelagem in vitro de terapias do sistema somatossensorial baseadas em eletricidade. Sistemas somatossensoriais de bioengenharia podem ser potencialmente integrados em interfaces homem-máquina bidirecionais, levando a uma função sensorial melhorada para usuários de próteses e possibilitando a criação de modelos de doenças do sistema somatossensorial que possam ajudar a entender as neuropatias sensoriais e analgesia congênita.

Palavras-chave: Polímeros biocompatíveis, elastômeros, propriedades mecânicas, eletrocondutores, piezoeletricidade

ABSTRACT

Throughout human existence, limb loss has been considered an irreversible detriment and permanent loss of function. Until recently, restoration of sensory feedback for prosthesis users and subjects with varied neuropathies was unimaginable. However, multidisciplinary developments have made recovery of this function increasingly attainable. Lack of innervated skin, which allows for a myriad of tactile stimuli to be detected and interpreted, has been one of the key hindrances in the restoration of complete sensory feedback. This has been combated through design of artificial skin substitutes, enabling users with partial—but not standard—sensory feedback. This thesis focuses on the creation of a bioengineered somatosensory system, both in terms of the micro-environmental substrate and cellular environment. We went about creating a physical somatosensory system model by designing a biocompatible, elastomeric, electroconductive, perdurable, pressure-sensitive, three-dimensional construct capable of acting as an interface for somatosensory system cells. Validation of both individual components and the complete construct was performed. We began by assessing mechanical methods, assessing the tensile deformation, elongation at break, and fatigue properties. We subsequently analysed electroconductivity, both in stasis and during various points of electro-mechanical fatigue, as well as in dry and liquid environments. Furthermore, we assessed the piezoelectricity of the construct, validating the use of our construct's ability to function as a soft electrode. Analysis of our somatosensory system construct was validated with various cell types found in the somatosensory system, namely: fibroblasts, keratinocytes, Schwann cells, and dorsal root ganglion cells. Material cytotoxicity and cellular adhesion, expansion, and differentiation on materials were all assessed. Additionally, neural cells and co-cultures containing neural cells were assessed under electrical fields to understand the effects of electricity on our somatosensory system model. Electrical field experiments using such scaffolds can eventually become a standard method of performing *in vitro* modelling of electricity-based somatosensory system therapies. Bioengineered somatosensory systems can potentially be integrated into novel, bi-directional human-machine interfaces, leading to enhanced sensory function for users of prostheses and enable the creation of somatosensory system disease models to better understand sensory neuropathies and congenital analgesia.

Keywords: Biocompatible polymers, elastomers, mechanical properties, electroconductive, piezoelectricity

RESUMO ALARGADO

Como seres humanos, damos por certo nossa capacidade de sentir prazer, dor, temperatura, textura e uma miríade de outras sensações através da estereognosia. De fato, a sensibilidade tátil tem sido tida como certa ao longo do tempo em que as modalidades sensoriais humanas têm sido pesquisadas há menos de dois séculos. O sistema somatossensorial humano desempenha um papel fundamental nas funções exterorrecional, interoceptiva e proprioceptiva, cujos papéis estão relacionados à percepção dos estímulos, reação aos estímulos e controle da posição e do equilíbrio corporal, respectivamente. Todos os três são críticos para a função completa do corpo humano, sensibilidade e feedback sensorial.

Embora a totalidade do sistema somatossensorial seja incrivelmente complexa, esta tese optou por enfocar seus componentes exterorreceptivos e proprioceptivos por causa da relação entre essas partes do sistema somatossensorial e os estímulos externos. Escolhemos especificamente estudar a relação da pele com as funções exterorreceptivas e proprioceptivas. A função exterorreceptiva refere-se a uma variedade de sensações superficiais, como dor, prazer e temperatura. O sistema somatossensorial detecta sensações exterorreceptivas via neurônios sensoriais nos gânglios da raiz dorsal e nos gânglios sensitivos cranianos. Dentro do sistema nervoso, os gânglios da raiz dorsal pseudo-unipolar estendem-se simultaneamente aos seus alvos periféricos e à medula espinal, ou núcleos da coluna dorsal do tronco cerebral. Enquanto isso, a pele é inervada por mecanoreceptores de baixo e alto limiar capazes ou respondendo a uma variedade de estímulos inócuos e prejudiciais. Existem vários mecanorreceptores especializados na pele relacionados com a função exteroceptiva, em particular, terminações nervosas livres no plexo do cabelo radicular, nos bulbos finais de Krauses, nos corpúsculos de Meissner e nos discos de Merkels. A função proprioceptiva contribui para a consciência corporal, o movimento e o controle. Semelhante à cinestesia e ao sistema vestibular, a propriocepção fornece um feedback sensorial que permite a precisão da posição e movimento do membro, a tensão e o equilíbrio. Os proprioceptores são normalmente encontrados em órgãos tendinosos de Golgi, fusos musculares e dentro e ao redor das cápsulas articulares. Eles são capazes de influenciar os nervos motores, fazendo sinapses com os neurônios motores inferiores e com o sistema nervoso central, a fim de interpretar sinais e até mesmo induzir movimentos reflexos. Os dois principais tipos de proprioceptores são corpúsculos de Pacini e terminações de Ruffini.

A função e a disfunção somatossensorial continuam sendo assuntos extremamente complexos que afetam uma série de condições, desde a perda do membro até as neuropatias autonômicas e periféricas. A perda de membros, em particular, é tipicamente considerada um prejuízo irreversível, pois resulta em perda permanente de função, irregularidades sensoriais, como a síndrome do membro fantasma, e é frequentemente associada ao estigma psicossocial que resulta em problemas de saúde mental. As próteses tentaram substituir os membros e dígitos perdidos por milhares de anos. No entanto, muitos deles funcionam principalmente como dispositivos cosméticos passivos, não dando aos usuários nenhum feedback sensorial e agindo como pouco mais que ganchos. Nos últimos anos, próteses osteointegradas e mioelétricas tornaram-se popularizadas, e os ensaios clínicos em andamento envolveram até mesmo a incorporação de eletrodos implantáveis. Essas novas próteses integradas incluem componentes que permitem a estimulação neural e musculoesquelética. Isto levou a avanços revolucionários, melhorando a amplitude de movimento e controle. Apesar disso, esses dispositivos biomédicos ainda não podem fornecer aos usuários um feedback sensorial e, conseqüentemente, permanecem a anos de mimetizar com sucesso a função motora e somatossensorial completa. A falta de pele inervada, que permite que uma miríade de estímulos táteis seja detectada e interpretada, é um obstáculo fundamental para dar aos amputados um feedback sensorial completo. Isso foi combatido através do uso de eletrodos implantáveis e do design de substitutos artificiais da pele, permitindo aos usuários um feedback sensorial parcial, mas não padrão. A única maneira de restaurar atualmente a função do sistema somatossensorial é através do transplante. Embora os recentes avanços nas cirurgias de tecidos compostos tenham permitido o transplante completo dos membros, os imunossupressores ao longo da vida e as avaliações psicológicas são obrigatórios, tornando essa técnica inadequada para todos os amputados.

Neuropatias autonômicas e periféricas são outras questões do sistema somatossensorial que requerem uma compreensão adicional do sistema somatossensorial em nível celular antes que possam ser totalmente resolvidas. Este crescente campo de conhecimento foi determinado por ter um componente genético graças a casos hereditários, onde famílias inteiras com percepção alterada de dor foram identificadas. No entanto, várias neuropatias resultam mais tarde na vida devido a doença e / ou lesão. Essas neuropatias podem ser debilitantes e, em muitos casos, os medicamentos padrão usados para controlar a dor são inúteis. A estimulação elétrica do nervo, disponível nos formatos externo e interno, tem sido usada para combater a disfunção do sistema

somatossensorial, reduzindo os sintomas como hiperalgesia e inflamação e alteração dos níveis de neurotransmissores envolvidos na patologia. No entanto, essas técnicas terapêuticas foram desenvolvidas apenas na década de 1960. Em muitos países, eles estão disponíveis apenas como tratamentos experimentais ou privados. Estudos adicionais sobre a influência de campos elétricos no sistema somatossensorial são essenciais para entender as mudanças em nível celular e molecular, a fim de avançar na pesquisa neste campo. Esta tese enfoca a criação de um sistema somatossensorial de bioengenharia, tanto em termos de substrato micro-ambiental e ambiente celular. A bioengenharia bem-sucedida do sistema somatossensorial pode ser integrada a interfaces homem-máquina novas e bidirecionais, levando a uma função sensorial aprimorada para usuários de próteses. Até recentemente, a restauração do feedback sensorial para usuários de próteses e indivíduos com neuropatias variadas era inimaginável. No entanto, os avanços nos campos científicos multidisciplinares tornaram possível uma recuperação potencial da função. Nós criamos o nosso próprio ambiente de sistema somatossensorial projetando uma construção tridimensional, biocompatível, elastomérica, eletrocondutora, perdurável, sensível à pressão. Esta construção é capaz de atuar como uma interface para o sistema somatossensorial de bioengenharia e modelos de pele. A análise da sensibilidade dos mecanorreceptores da pele em um microambiente apropriado aumentaria a compreensão de aspectos da função somatossensorial que são difíceis de serem replicados na substituição artificial de membros ou que se recuperam totalmente por meio de transplante. Além disso, isso permitiria a criação de modelos melhorados de patologia do sistema somatossensorial para melhor compreender as neuropatias sensoriais e a analgesia congênita. Isto permitiria adicionalmente compreender melhor as terapias de campo elétrico a nível celular e molecular. Para criar uma construção, validamos os componentes individuais e o modelo completo. Começamos avaliando as propriedades mecânicas (nomeadamente a deformação à tração, o alongamento na ruptura e as propriedades de fadiga) de nossas misturas elastoméricas selecionadas e materiais fibrosos e flexíveis para identificar quais materiais tinham módulos de deformação semelhantes àqueles da pele. Como a pele é um material anisotrópico único, com capacidade de regeneração in vivo, usamos pele suína fresca para realizar nossa análise comparativa. Descobrimos que o nosso material selecionado não só tinha um módulo de Young semelhante ao da pele, mas era capaz de resistir a grandes quantidades de fadiga mecânica, apenas se deformando depois de passar por substancial alongamento. Além disso, fomos capazes de eliminar materiais da seleção processada com base em fatores como a fadiga baseada na desidratação. Em seguida, analisamos a eletrocondutividade em ambientes secos e líquidos para validar o comportamento de cada componente individualmente, bem como o

construto completo. Também avaliamos o elastômero eletrocondutivo e o elastômero eletrocondutor piezoelétrico em estase e em vários pontos de tensão para avaliar a fadiga eletromecânica e piezoelétrica. Finalmente, fomos capazes de criar elastômeros eletrocondutores com valores de resistência variável e controlada, otimizando a camada piezelétrica. Isso nos permitiu avaliar a piezoeletricidade da construção, validando sua capacidade de funcionar como um eletrodo macio. A análise celular do nosso sistema somatossensorial foi realizada com vários tipos celulares encontrados no sistema somatossensorial, a saber: fibroblastos, queratinócitos, células de Schwann, células ganglionares da raiz dorsal e células progenitoras neuronais (ReN). A citotoxicidade foi avaliada segundo os padrões ISO usando fibroblastos L929. A adesão, expansão e diferenciação de longo prazo foram avaliadas usando queratinócitos, células de Schwann, células ganglionares da raiz dorsal e células ReN. Além disso, as células neurais e co-culturas contendo células neurais foram avaliadas em campos elétricos para entender os efeitos da eletricidade nas células que residem dentro do nosso microambiente projetado. Nossos achados sugerem que nosso material é um substrato preferido para análise celular de longo prazo, cicatrização de feridas, proliferação e modelagem de diferenciação. Outros estudos podem ser realizados para avaliar os efeitos do estresse físico e da atividade eletromecânica e piezelétrica ao utilizar este material em cultura de células. Esta tese fornece as validações fundamentais necessárias para usar o nosso construto para criar produtos que podem ser implantados ou usados a longo prazo. Experimentos de campo elétrico usando nossa construção 3-D podem, eventualmente, ser usados como um microambiente padrão ao realizar a modelagem in vitro de sistemas somatossensoriais, bem como avaliações da terapêutica do sistema somatossensorial baseado em eletricidade.

Palavras-chave: Polímeros biocompatíveis, elastômeros, propriedades mecânicas, eletrocondutores, piezoeletricidade

ACKNOWLEDGEMENTS

I would like to begin by thanking the MIT Portugal PhD programme selection committee for giving me the opportunity to be a part of this program. Thank you to Fundação para a Ciência e Tecnologia (FCT) for the financial support that allowed me to pursue my PhD studies through the SFRH/BD/52338/2013 PhD grant.

Thank you to everyone at Instituto Superior Técnico (IST) at the University of Lisboa. Thank you to Professor Joaquim Sampaio Cabral for accepting me into IST's IBB Group, where I was able to develop my project. Particular thanks to my principal supervisor, Doctor Frederico Ferreira, for allowing me to be creative and innovative throughout the duration of my doctoral studies and for sharing his experience and knowledge with me. Thank you for giving me an incredible amount of freedom that inspired me throughout the course of my PhD. Thank you as well to my co-supervisor, Dr. Jorge Martins, for the support and insight he provided throughout the development of this project. Thank you to Dr. Jorge Morgado for all his help with my electroconductivity tests; one of the most challenging parts of this project.

Thank you to my colleagues at the IBB, particularly Carlos Rodrigues, Ana Fernandes-Platzgummer, Marcia Mata, Teresa Esteves, and Ricardo Manuel Ferreira dos Santos Pereira, who helped me enormously throughout the duration of my doctoral studies. Thank you to Ermelinda Macoas and Isabel Nogueira, who were an invaluable help with imaging analyses. Thank you to my peers at IST who directly or indirectly influenced my work, particularly Miriam Sousa, Carla Moura, Flavio Ferreira, Fabio Garrudo, Tania Baltazar, Laura Sordini, Silvia Gonella, and Rolando Matos. Notable thanks to Alexandre Ribeiro, who was available at all hours of the day for assistance with electroconductivity work: I could not have done this without you.

Thank you to the University of Aberdeen, particularly Dr. Colin McCaig and Dr. Ann Rajnicek for being so open to new, collaborative work and allowing me to join their team. Thank you to my peers there, particularly Alba Guijarro-Belmar and Anna Varone for helping me learn new techniques. A special thanks to Lion Budrass for making my time at the University of Aberdeen great fun, continuing to work with me even after my departure, and being a constant inspiration.

Thank you to Universidad Autonoma de Barcelona (UAB), particularly Nieves Casan-Pastor for accepting me into her group and facilitating a variety of experiments I could not have learned elsewhere, and Llibertat Abad for teaching me new techniques that were fundamental to this work.

Thank you to the Universidad Polytechnica de Catalunya (UPC), particularly Dr. Eloi Pineda, who was incredibly welcoming and has been extremely helpful throughout the duration of my studies; his friendliness led me to other professors at the UPC who ended up making invaluable contributions to my work. Thank you to Dr. Carlos Aleman, Dr. Francisco Estrany Coda, and Dr. Francisco Casellas, who were incredibly kind, generous with their time, and helpful throughout the course of my doctoral studies: Your support was invaluable.

Thank you to my magnificent friends throughout Europe who have become my family since I moved to this continent. To Chavez Hyndman, Edward Hartwell Goose, Emma Elizabeth Bird, Linden Watts, Melissa R. Wright, Miranda Solomon, Robert Stafford-Williams, Rúna Chapple-Smith, and Sara Mickle for being the most positive, encouraging friends, especially throughout the writing process. Special thanks to Song Yee, Dane Glasby, Enmanuel Simoes, Farid Singh, Rosie Harrison Flower, and Yury Bolotov — I could not have completed my thesis-related work without your help. Thank you for your endless encouragement, inspiration, and support.

TABLE OF CONTENTS

RESUMO ..... **iii**
ABSTRACT ..... **iv**
RESUMO ALARGADO ..... **v**
ACKNOWLEDGEMENTS ..... **ix**
TABLE OF CONTENTS ..... **xii**
LIST OF TABLES ..... **xviii**
LIST OF FIGURES ..... **xx**
LIST OF EQUATIONS ..... **xxiii**
ABBREVIATIONS ..... **xxiv**

1. INTRODUCTION AND STATE OF THE ART **1**
1.1 **Introduction** 2
1.2 **Motivation, Objectives, Research Questions and Strategy** 2
1.3 **State of the Art** 8
1.3.1 Motivation for the Creation of a Biocompatible, Electroconductive Elastomer 8
1.3.2 An Overview of the Somatosensory System 13
1.3.3 Electrical Stimulation for Wound Healing and Regeneration 15
1.3.4 Electrical Stimulation as a Neurostimulatory Technique 17
1.3.5 Soft Biocompatible and Electroconductive Materials Used in Neurostimulation 19
1.3.6 Summary of Electroconductive and/or Pressure-Sensitive Elastomer Constructs .23
1.4 **References** 29

2. MATERIALS AND METHODOLOGY **38**
2.1. **Outline** 39
2.2. **Polymers, Organic Materials, and Solvents** 39
2.2.1 Selected Polymers and Solvents Used for Their Dissolution. 39
2.2.2 Flexible Polymers and Preparation of Casting Solutions 42
Polyimide (PI) 42
Poly(methyl methacrylate) (PMMA) 42
Poly(vinylidenefluoride-co-trifluoroethylene) (P(VDF-TrFE)) 43
Polyacrylonitrile (PAN) 43
Polyvinylpyrrolidone (PVP) 43
Polysulfone (PSU) 43
2.2.3 Elastic Polymers and Preparation of Casting Solutions 44
Polyisoprene 44
Poly(butadiene) 43
Poly(styrene-isoprene-styrene): Kraton D1161 43
Poly(styrene-butadiene-styrene): Kraton D1152 43
Kaneka SIBSTAR™ 062T and 062M 45
2.2.4 Electroconductive materials 45
Electroconductive Flexible Polymers 45
Conjugated Electroconductive Polymers 45
Iridium Oxide 46
Carbon-Based Materials 46
2.2.5 Organic Materials 46

2.3. **Polymeric Material Deposition Methodologies (Chapter 3)** 47

2.3.1 Preparation and Cleaning of Substrates for Cast Samples 47
2.3.2 Defined-Area Drop Casting of Elastomers 47
2.3.3 Tape Casting (Casting Knife) of P(VDF-TrFE) 49
2.3.4 Spin Coating 50
Flexible Spin Coated Polymers (PI, PAN, PMMA, P(VDF-TrFE) 52
Electroconductive Spin Coated Polymers (PEDOT:PSS, P3HT, and PPY) 52

2.3.5 Electrospinning (PI, PANI, PMMA, PVDF-Tre, PAN, PSU, Kraton D1152, PVP, PVP/IrO2,) 53
Polyimide 55
Poly(methyl methacrylate) (PMMA) 55
Poly(vinylidenefluoride-co-trifluoroethylene) (P(VDF-TrFE)) 56
Polyacrylonitrile (PAN) 56
Polysulfone (PSU) 56
Polyvinylpyrrolidone (PVP) and IrOX-PVP 56
Kraton D1152 (Poly(styrene-butadiene-styrene) 57
2.3.6 Dip Coating (Elastomers on PEDOT:PSS, P3HT, and PPY) 57

2.4. Preparation and Electrical Characterization of Electrical Materials (Chapter 4) 58
2.4.1 Iridium Oxide Synthesis With and Without Oxalate 58
Iridium Oxide Electrodeposition 58
Iridium Oxide Electrospinning 61
2.4.2 Surface-Coated Electroconductive Materials on Elastomers 61
Thermally Evaporated Materials (Gold, Titanium, and Platinum) 61
SP(2) Carbon Materials Blended With Elastomers 63
Painted Materials (Polymeric Platinum, Silver, Carbon Nanotube Pastes) 64
2.5 Preparation of the Three-Layered Construct (Chapters 3, 4 and 5) **64**
2.6 **Electrical Characterization Methods (Chapter 4)** 65
2.6.1 Electrical Conductivity Analysis 65
2.6.2 Potentiostat Electrochemical Impedance Spectroscopy (EIS) 67
2.7. **Mechanical Assessments (Chapter 3)** 67
2.7.1 Tensile Deformation Assessment 67
2.7.2 Fatigue Analysis 68
2.7.3 Elongation at Break Analysis 68
2.7.4 Electromechanical Characterization 68
2.8. **Piezoelectric Characterization of P(VDF-TrFE) (Chapter 4)** 69
2.8.1 P(VDF-TrFE) Phase Assessment through Fourier Transformation Infared Spectroscopy 69
2.8.2 P(VDF-TrFE) Piezoelectric Functionality and Validation 69
2.9. **Cultured Cells, Media, Substrates and Analysis (Chapter 5)** 71
2.9.1 Cell Culture Supports 71
Cell Culture Supports: Creation of Complete Constructs 71
3D-Printed Holding Samples Wells 71
2.9.2 Cell Types, Media, and Basic Cell Culture Protocols 73
L929 Fibroblasts and Fibroblast Assays 73
Fibroblast Cell Counting 74
Fibroblast Cell Passaging 74
Fibroblast Cryopreservation 75

ReN Cells 75

ReN Cell Media 76
ReN Cell Culture Substrate Preparation 76
ReN Cell Thawing and Expansion 77
ReN Cell Passaging 77
ReN Cell Cryopreservation 78
Human Dorsal Root Ganglion (hDRG) Cells 78
Media for hDRG Cells 78
Culturing Cryopreserved hDRG Cells 78
Passaging of hDRG Cells 79
Subcloning of hDRG Cells 79
Cryopreservation of hDRG Cells 79
Human Keratinocyte Cells (hKeratinocyte or HEKa-APF) 80
hKeratinocyte Cell Media 80
hKeratinocyte Substrate Preparation 80
hKeratinocyte Cell Thawing and Expansion 80
hKeratinocyte Cell Passaging 80
hKeratinocyte Cell Cryopreservation 81
Human Schwann Cells 81
Human Schwann Cell Media 81
Culturing human Schwann Cells 81
Passaging Human Schwann Cells 81
Cryopreservation of Human Schwann Cells 82
Keratinocyte-Dorsal Root Ganglion Cell Culture 82
Human Keratinocyte-Dorsal Root Ganglion Co-Culture 82
Fibroblast, Keratinocyte, Dorsal Root Ganglion, Schwann Cell Co-Culture 83
2.9.3 ISO Standard Cytotoxicity Assays 84
Preparation of Materials for Cytoxicity Tests 84
Indirect Contact Assays 85
Direct Contact Assays 85
Alamar Blue Assay (24 well-plate) 85
2.9.4 Cell Fixation and Staining 86
Mammalian Cell Fixation and Permeabilization 86
Staining of Fixed Cells 86
Immunocytochemistry 86
Cell Dehydration 87
Live-Dead Cell Staining 87
Live Cell Staining (Cell-Specific Trackers) 88
Cell Tracker Fluorescent Probe 88
NeuroTrace Fluorescent Nissl Stain 88
Alkaline Phosphatase Live Stain 88
2.9.5 Cell Culture and Culture in Electrical Fields 89
Mammalian Adhesion Assays 89
Mammalian Electrical Field Scaffold Set-up 89
Mammalian Electrical Field Experimental Set-up 90
Mammalian Electrical Field Culture and Expansion 90
Mammalian Electrical Field Differentiation 91
2.10 **Microscopy and Other Assessments of the Construct (Chapter 5)** 91
2.10.1 Fluorescence Microscopy Imaging 91
2.10.2 Scanning Electron Microscopy (SEM) 91
2.10.3 Confocal Microscopy 92
2.10.4 Energy-dispersive X-ray spectroscopy (EDX) 92

2.10.5 Atomic Force Microscopy (AFM) 92
2.10.6 Contact Angle 93
2.11 **References** 94

3. MECHANICAL ASSESSMENT OF SELECTED POLYMERS AND THE COMPLETE CONSTRUCT **97**
3.1. **Outline** 98
3.2. **Introduction** 99
3.2.1 The Mechanical Properties of Skin vs. Skin Substrates 99
3.2.2 Flexible vs Elastic materials 102
3.2.3 Uses for Bioengineered Flexible Materials 104
3.2.4 Uses for Bioengineered Thermoplastic Elastomers 105
3.3. **Results** 108
3.3.1 Preliminary Assessment of Flexible Polymers for Skin Substrate Creation 108
3.3.2 Assessment and Processing of Elastic Polymers for Skin Substrate Creation 114
3.3.3 Tensile Deformation of Skin and Polymers 121
Young's Moduli for Elastomers, Flexible Polymers and Skin 122
Stress-Strain Curves of Elastomers, Flexible Polymers and Skin 126
Elongation at Break Properties of Selected Elastomers and Flexible Polymers 131
Analysis of Young's Moduli, Stress-Strain Curves and Elongation at Break Data 133
3.3.4 Comparative Analysis of Skin and Elastomers through Fatigue Assessment 136
3.4 **Conclusions** 139
3.5 **References** 140

4. ELECTROCONDUCTIVE, ELECTROMECHANICAL, AND PIEZOELECTRIC BEHAVIOUR OF THE CONSTRUCT **146**
4.1 **Outline** 147
4.2. **Introduction** 148
4.2.1 Electroconductive Materials Used in Biocompatible Devices 148
4.2.2 Design and Development of a Novel Electroconductive Elastomer 148
4.3 **Results** 158
4.3.1 Conceptual Analysis: Creation of Electroconductive Elastomers and Initial Assessments 158
4.3.2 Experimental Creation of Electroconductive Elastomers & Initial Assessments. 159
4.3.3 Analysis of Electroconductive Elastomers 159
4.4 **Creation of the Complete Construct** 165
4.5 **Analysis of Electroconductive Elastomer and Full Construct** 167
4.6 **Electromechanical Assays of the Construct** 180
4.7 **Validation of Construct through Electromechanical Assessment** 187
4.8 **Piezoelectricity of P(VDF-TrFE) and the Complete Construct** 194
4.9 **Conclusions** 202
4.10 **References** 204

5. CELL-MATERIAL CHARACTERIZATION AND INTERACTIONS **209**
5.1. **Outline** 210
5.2. **Skin and Somatosensory System Modelling** 210
5.2.1 Introduction to Skin and Somatosensory System Models 210
5.2.2 Proposed Approach to Skin-Related Co-Culture 212
5.3. **ISO-Standard Cytotoxicity Tests and Adhesion Assays with L929 Fibroblasts** .215

5.4 **Co-Culture Model Development** 215
5.4.1 Justification of the Co Culture Model 224
5.4.2 Cell Culture Media and Co-Culture 227
5.5 **Scratch Assay of Co-culture Model** 233
5.6 **Validation of the Construct Using Human Somatosensory System Cells** 236
5.7 **Conclusions** 236
5.8 **References** 236

6. **OVERVIEW OF THE COMPLETE CONSTRUCT, CONCLUSIONS, AND FUTURE DIRECTIONS** 249
6.1. **Overview of the Complete Construct and Future Directions** 210
6.1.1 : Mechanical Elaboration and Validation of the Construct 250
6.1.2 : Electroconductive & Piezoelectric Elaboration & Validation of the Construct 251
6.1.3 : Construct Biocompatibility 254
6.2. **Conclusions** 210
6.3. **References** 210

APPENDIX **258**
2.**A: Materials and Methodology** 259
Combinations of PEDOT, P3HT, PPY with Elastic and Flexible Polymers 260
3.**A: Materials and Mechanics** 260
4.**A: Electrochemical Analysis** 264
5.**A: Cell Culture and Preliminary Biocompatibility Tests** 270
5.A.1 Primary Cell Culture 270
Rat Dorsal Root Ganglion (rDRG Cells) 270
rDRG Cell Media 270
rDRG Cell Harvesting 271
rDRG Substrate Pre-Coating and Cell Culture 271
Rat Keratinocyte Cells 273
rKeratinocyte Cell Media 274
rKeratinocyte Cell Harvesting 274
rKeratinocyte Cell Culture 275
Rat Dorsal Keratinocyte-Dorsal Root Ganglion Co-Culture 275
Xenopus Cell Culture 276
Xenopus Cell Media 276
Xenopus Cell Harvesting and Culture 276
Xenopus Cell Fixation and Permeabilization 277
Xenopus Electrical Field Experiments 277
5.A.2 Preliminary Biocompatibility Assessments 278
6.**A: References** 282

LIST OF TABLES

Chapter 1:

Table 1.1: Biocompatible Electroconductive and Piezoelectric Elastomer Constructs 21
Table 1.2: A Summary of Electroconductive and/or Pressure-Sensitive Elastomer Constructs 25

Chapter 2:

Table 2.1: Conductive/Piezoelectric Polymers Assessed for Electrospinning 40
Table 2.2: Insulating Polymers Assessed for Electrospun Mesh Creation 41
Table 2.3: Conjugated Conductive Polymers 42
Table 2.4: Settings for Wells Created on Makerbot Makerware Type II 73
Table 2.5: Cell Cultivation Standards 74
Table 2.6: Cell Passaging Standards 75
Table 2.7: N2 Media 76
Table 2.8: B27 Neural Differentiation Media 76
Table 2.9: Somatosensory System Co-Cultures 83
Table 2.10: Summary of ISO 10993-5:2009(E) Guidelines for Cytotoxicity Assays 84
Table 2.11: Antibodies Used in Immunocytochemistry 87

Chapter 3:

Table 3.1: Diameters of Electrospun Flexible Polymers 112
Table 3.2: Ranking System for Preliminary Evaluation of Flexible Polymers 112
Table 3.3: Flexible Polymers Assessed for Electrospun Mesh Creation 113
Table 3.4: Reported Properties of Selected Alkene-Styrene Copolymers 115
Table 3.5: Elastomers Assessed for Electrospun Mesh Creation 120
Table 3.6: Strain Amplitude & Cycles to Failure of Elastomers 138

Chapter 4:

Table 4.1: A Summary of Soft Electroconductive and/or Pressure Sensitive Constructs 150
Table 4.2: Gwent Platinum Paints 160
Table 4.3: Additives and Treatments Required for Construct Components 166
Table 4.4: Conductivity of Electroconductive Elastomers and Full Construct 169
Table 4.5: Circuit Components Following Incubation in PBS 175
Table 4.6: Resistances (R) and Conductivity (σ) for the Elastomer, Electroconductive Elastomer, and Full Construct Following Incubation in PBS 176
Table 4.7: One Way Anova for Elongation at Break Samples 185
Table 4.8: Tukey Significance Test for Elongation at Break Samples 185
Table 4.9: Fatigue Analysis of Elastomers and Electroconductive Elastomers 186
Table 4.10: Piezoelectric Response of P(VDF-TrFE) Electrospun Fibers 200

Appendix:

Table 2.A: Other Polymers Assessed for Electrospun Mesh Creation 259
Table 3.A: Contact Angle of Hydrated and Dehydrated SBS 264
Table 4.A.1: Electroconductive Materials Analysed for Use in Interface construct 268
Table 4.A.2: Controls for Preliminary Assessment of Polymer-Electroconductive Material Blends 268
Table 4.A.3: Preliminary Assessement of Polymer-Electroconductive Material Blends 269
Table 5.A.1: Bottenstein and Sato's Fluid and Bottenstein and Sato's Supplemented Fluid 270

Table 5.A.2: Retinal Buffer (Rb) and Papain-Rb Dissociating Solutions.....272
Table 5.A.3: Trypsin Inhibitor Dnase (Tid) Solution 273
Table 5.A.4: Fibrogen-Collagen Coating Solution 273
Table 5.A.5: Calcium-Based Media Solutions.....274
Table 5.A.6: Xenopus Dissection and Culture Solutions.....277

LIST OF FIGURES

Chapter 1:

Figure 1.1: Materials Selection and Visual Outline of the Thesis 4
Figure 1.2: Before and After Images of a Hand Transplant Patient 9
Figure 1.3: Components Required for Direct Neural Stimulation in a Prosthesis User 10
Figure 1.4: Stretchable Prosthetic Skin Equipped with Silicon Nanoribbon Arrays 11
Figure 1.5: Skin-Spinal Cord Interconnections within the Somatosensory System 14

Chapter 2:

Figure 2.1: Schematic of the Spin Coating Process 50
Figure 2.2: Schematic of the Vertical and Horizontal Electrospinning Process 54
Figure 2.3: Potentiodynamic Deposition of IrOx Coatings 59
Figure 2.4: Representation of the IrOx Electrodeposition Process 60
Figure 2.5: Schematic of Thermal Evaporation deposition 62
Figure 2.6: Representation of the 4-Point Probe Method 66
Figure 2.7:Depiction of the Pressurized Pneumatic Circuit and System 70
Figure 2.8: Assembly of the Pressurized Pneumatic Circuit 70
Figure 2.9: Customized Wells 72
Figure 2.10: Experimental Setup for Electrical Field Experiments 90
Figure 2.11: Schematic of Contact Angle Methodology 93

Chapter 3:

Figure 3.1: Polyimide 108
Figure 3.2: Poly(methyl-methacrylate) 109
Figure 3.3: Polyacrilonitrile 109
Figure 3.4: Polysulfone 110
Figure 3.5: Polyvinyl Pyrrolidone 110
Figure 3.6: Electrospun Poly(vinylidenefluoride-co-trifluorethylene) (P(VDF-TrFE)) 111
Figure 3.7: Electrospun kaneka Poly(styrene-β-isobutylene- β-styrene) in Chloroform 116
Figure 3.8: 1%wt Iron (III) p-toluenesulfonate and 10%wt Kraton D1152ES (SBS) 118
Figure 3.9: 10%wt Iron (III) p-toluenesulfonate and 10%wt Kraton D1152ES (SBS) 118
Figure 3.10: 10%wt Kraton D1152ES (SBS) and 20%wt Iron (III) p-toluenesulfonate 119
Figure 3.11: 10%wt Kraton D1152ES (SBS) & 16.5%wt Iron (III) p-toluenesulfonate in THF and Chloroform 119
Figure 3.12: Young's Moduli of Skin, Flexible Materials, and Elastomers 124
Figure 3.13: Stress-Strain Curves of Skin, Flexible Materials, and Elastomers 127
Figure 3.14: Elongation at Break Percentages of Elastomeric Polymeric 132
Figure 3.15: Load-Elongation and Stress-Strain Curves for Peripheral Nerve in a Digit 136
Figure 3.16: Fatigue Analysis of Elastomers and *Ex Vivo* Skin 137

Chapter 4:

Figure 4.1: Evaluation of the Kaneka SIBS + Platinum + Iridium Oxide Construct 159
Figure 4.2: Thermally Evaporated Gold and Platinum and Gwent Silver and Platinum Pastes atop Kaneka SIBSTAR™ (SIBS) 160
Figure 4.3: SEM of Stretched Silver Paint Atop Kaneka SIBS 161
Figure 4.4: SEM of Platinum Paint Atop Kaneka SIBS 162
Figure 4.5: Electrodeposited IrOx and Platinum Paint on Kaneka SIBSTAR™ 162
Figure 4.6: EDX Analysis of SIBS, Platinum, and Iridium 163

Figure 4.7: Creation of PVP-IrOx Nanofibers 164
Figure 4.8: Schematic of the Assessed Conductive Constructs 169
Figure 4.9: Bode Plots of the Full Construct, Electroconductive Elastomer, and Elastomer Base Following Incubation in PBS 173
Figure 4.10: Nyquist Plots of the Full Construct, Electroconductive Elastomerr, and Elastomer Base Following Incubation in PBS 174
Figure 4.11: Fitted Circuits Following Incubation in PBS 175
Figure 4.12: Bode Plots of the Full Construct, Electroconductive Elastomer, and Elastomer Base Without Incubation in PBS 178
Figure 4.13: Nyquist Plots of the Full Construct, Electroconductive Elastomer, and Elastomer Base Without Incubation in PBS 179
Figure 4.14: Fitted Circuit for the Full Construct Without Incubation in PBS 180
Figure 4.15: Stress-Strain Curves for Elastomers With and Without Platinum Coatings 181
Figure 4.16: Stress-Strain Curves for All Elastomers With and Without Platinum Coatings 182
Figure 4.17: Elongation at Break Data of Electroconductive Elastomers 184
Figure 4.18: Fatigue Analysis of Kraton D1152 and Kraton D1152-Polyisoprene With and Without Heat Treatment and With and Without Platinum 186
Figure 4.19: Electromechanical Strain (15%) of Elastomers and Polymeric Platinum 190
Figure 4.20: Electromechanical Strain (30%) of Elastomers and Polymeric Platinum 191
Figure 4.21: Electromechanical Strain (45%) of Elastomers and Polymeric Platinum 192
Figure 4.22: Hysteresis Analysis Comparing Heat-Treated and Platinum-Coated Elastomers 193
Figure 4.23: FTIR of P(VDF-TrFE) Powder 196
Figure 4.24: FTIR of Unheated Electrospun Fibers 197
Figure 4.25: FTIR of Electrospun Fibers Heated for 30 Minutes 198
Figure 4.26: FTIR of Electrospun Fibers Heated for 60 Minutes 198
Figure 4.27: P(VDF-TrFE) Compilation of FTIR Analysis 199
Figure 4.28: Schematic of the Pressurized Pneumatic Circuit 199
Figure 4.29: Schematic of the Soft Piezoelectric Electrodes 201

Chapter 5:

Figure 5.1: Impact of a Cell Culture Substrate's Mechanical Properties on Morphology 213
Figure 5.2: MTT Indirect Contact Assay 217
Figure 5.3: Direct Contact Assay 218
Figure 5.4: Direct Contact Assay and Calcein Staining 220
Figure 5.5: SEM Adhesion and Proliferation Analysis 221
Figure 5.6: SEM Cross Sections of Adhesion and Proliferation Analysis 222
Figure 5.7: Adhesion and Proliferation Assay of Planar and Electrospun Materials Through Confocal Microscopy 223
Figure 5.8: Keratinocyte-DRG in Epilife 228
Figure 5.9: Mixed Media Culture of Keratinocytes and Dorsal Root Ganglion Cells 230
Figure 5.10: Schwann Cells on Glass (AP and Nissl Live Stain) 231
Figure 5.11: Dorsal Root Ganglion Cells on Glass (AP Live Stain) 231
Figure 5.12: Keratinocytes on Glass (CMAC Stain) 232
Figure 5.13: Wound Healing Analysis 234
Figure 5.14: Fibroblasts on Aligned and Random Full Construct 237
Figure 5.15: Keratinocytes on Random and Aligned Full Construct 238
Figure 5.16: Dorsal Root Ganglions on Complete Construct 238

Figure 5.17: Keratinocyte-Dorsal Root Ganglion Co-Culture on D1152 & Platinum-Coated D1152 239
Figure 5.18: Keratinocyte-Dorsal Root Ganglion Biological Scaffold Formation 240
Figure 5.19: Keratinocyte-Dorsal Root Ganglion Co-Culture on Aligned Complete Construct 240
Figure 5.20: Fibroblast-K-DRG-Schwann Co-Culture on Aligned Complete Construct 241
Figure 5.21: Fibroblast-K-DRG-Schwann Co-Culture on Random Complete Construct 241
Figure 5.22: Fixed Fibroblast-K-DRG-Schwann Co-Culture on Complete Construct 242
Figure 5.23: Electrically-Stimulated Fibroblast-K-DRG-Schwann Co-Culture on Aligned and Random Constructs 243

Chapter 6:

Figure 6.1: Novel Electroconductive and Piezoelectric Constructs Developed 253

Appendix:

Figure 3.A.1: Sputtering of Kraton D1152ES (SBS) 260
Figure 3.A.2: Additional Images of Electrospun D1152ES (SBS) 261
Figure 3.A.3: Elongation at Break Graph for Flexible and Elastic Polymers 262
Figure 3.A.4: Maximum Elastomer Deformation 262
Figure 3.A.5: Thermogravimetric Analysis of Drop Cast Kaneka SIBSTAR^{TM}062M 263
Figure 4.A.1: Cyclic Voltammetry of Gwent Polymeric Platinum C2050804P9 265
Figure 4.A.2: Cyclic Voltammetry of Gwent Polymeric Platinum C2020322P6 266
Figure 4.A.3: Example of IrOx Electrodeposition of Thermally Evaporated Platinum 266
Figure 4.A.4: Electroconductive-Elastomer Combinations Assessed 267
Figure 5.A.1: Dissection of the Rat Spinal Column after a Sagittal Cut Along the Midline 268
Figure 5.A.2: *Xenopus* Neurons on (10%) Kraton D1161PT (SIS) 279
Figure 5.A.3: *Xenopus* Neurons on (10%) Kraton D1152ES (SBS) 280
Figure 5.A.4: Rat Cortical Neurons on (10%) Kraton D1152 281
Figure 5.A.5: Rat Neuron on (10%) Kraton D1161 281

LIST OF EQUATIONS

Chapter 2:

Equation 2.1: Calculation of Thickness During the Drop Casting Process.....49
Equation 2.2: The Linear Relation Used to Find the Resistance of the Material.....65
Equation 2.3: Electrical Resistivity ρ as Related to Resistance.....66
Equation 2.4: Electrical Conductivity.....66
Equation 2.5: Number of viable Cells Present per Quadrant.....74
Equation 2.6: Roughness Value.....92

Chapter 4:

Equation 4.1: Membrane Conductivity.....176

ABBREVIATONS

3D	**Three dimensional**
AFM	**Atomic force microscopy**
B27	**Serum-free supplement for neural growth**
CNT	**Carbon nanotubes**
DMAc	**Dimethylacetamide**
DMEM	**Dulbecco's modified Eagle's medium**
DMF	**Dimethylformamide**
DRG	**Dorsal Root Ganglion**
EF	**Electrical Field**
FBS	**Fetal Bovine Serum**
GPa	**Gigapascal**
HeKa-APF	**Adult Human Epidermal Keratinocytes (Animal Product-Free)**
IBB	**Institute for Biotechnology and Bioscience**
IrOx	**Iridium Oxide**
IST	**Instituto Superior Técnico**
ITO	**Indium Tin Oxide**
MSC	**Mesenchymal stem/stromal cells**
MPa	**Megapascal**
MW	**Molecular weight**
P3HT	**Poly(3-hexylthi ophene-2,5-diyl)**
PAN	**Polyacrilonitrile**
PANi	**Polyaniline**
PBS	**Phosphate buffered saline**
PDMS	**Polydimethylsiloxane**
PEDOT	**Poly 3,4-ethylenedioxythiophene**
PFA	**Paraformaldehyde**
PI	**Polyimide**
PMMA	**Poly(methyl methacrylate)**
PPO	**Polyphenelene oxide**
PPy	**Polypyrrole**
PSF	**Polysulfone**
PSS	**Poly(styrene sulfonic acid)**
P(VDF-TrFE)	**Poly[(vinylidenefluoride)-co-trifluoro ethylene]**
PVP	**Polyvinylpyrrolidone**
ReN	**ReNcell VM Human Neural Progenitor Cell Line**
SBS	**Styrene Butadiene Styrene**
SEM	**Scanning electron microscopy**
SIBS	**Styrene–isobutylene–styrene**
SIS	**Styrene Isoprene Styrene**
THF	**Tetrahydrofuran**
UV	**Ultraviolet**
v/v	**Volume of solute per volume of solvent**
w/v	**Weight of solute per volume of solvent**
O_2	**Oxygen molecule**

CHAPTER 1.

INTRODUCTION AND STATE OF THE ART

1.1 Introduction

Human beings often take their capacity for stereognosis for granted. Sensory modalities have only been studied for the last two centuries, and the somatosensory system remains one of the least studied human organ systems.[1] Despite this, the somatosensory system is spread throughout multiple parts of the body and is comprised of both external and internal sensory receptors.[2] Receptor pathways in the skin, joints and muscle communicate with root ganglion cells, so that sensory information moves through the medial lemniscal pathway and into the spinal cord and brainstem.[3] This allows the regulation of sensations such as pain, pleasure, temperature, and texture. The somatosensory system also controls perception and reaction to stimuli, as well as body position and balance.[1]

The complexity of the somatosensory system has allowed for a variety of models, both computational and cellular, to be created. However, most somatosensory system models are only focused on one sensory component of the somatosensory system microenvironment. Creation of more complex, multidimensional microenvironments would allow for the study of cells and tissue *in vitro*, while allowing their culture within structures that more similarly mimic their natural environment's mechanical and electrical properties.

1.2 Motivation, Objectives, Research Questions and Strategy

The aim of this project was to design, manufacture and characterize a biocompatible, elastomeric, electroconductive, perdurable, pressure-sensitive material construct to support a multidimensional somatosensory system interface.

The motivation to develop somatosensory system constructs is their use, primarily, as an interface for *in vitro* research. Although there are a variety of medications and medical treatments for somatosensory system disorders, these conditions are poorly understood. The treatment of these conditions is often simply to manage symptoms. However, a variety of these diseases have a complex, unknown pathology that manifests neurally, but is expressed via the skin - a tissue with unique viscoelastic properties. Somatosensory system constructs would enable the variety of cell types that make up this bodily system to be simultaneously cultured

together. This, in turn, would enable strategic modelling of neuronal pathways and cell-cell interactions.

Somatosensory system constructs also may have potential secondary applications as components of implantable and wearable biomedical devices. Throughout the development of the construct, we took into consideration advancements in multidisciplinary fields including prosthetic and neural cuff design, biomaterials research, and electrical and magnetic-based stimulation therapeutics. We particularly focused on the impact of electrical fields used in invasive and non-invasive neurostimulation and neuroprosthetic research, which allowed us to optimize the multipurpose design of our work.

Unlike other material constructs designed for neurostimulation or as wearables, we wanted our creation to be multipurpose and functionally implantable in various capacities. The construct created in this study needed to be capable of acting as an interface for bioengineered skin and somatosensory system models. We chose to bioengineer a construct that would be able to act as a multidimensional microenvironment for skin, given the few existing models capable of replicating a somatosensory system environment.

To our knowledge, the construct created during this thesis is unique. Both second skin and artificial skin substrates have been studied extensively and possess many of the same attributes. However, the properties of other similar constructs are critical discussed on section 1.3.6.

The material construct that was created also has potential uses as a soft electrode in neurostimulatory devices, as a component of neuroprostheses, and as substrate for both the modelling and expansion of autologous skin grafts prior to transplantation. Five main factors related to this construct will be discussed as objectives:

1) The mechanics of creating a soft, stretchable, electroconductive construct.
2) The electroconductive approaches required to maintain both high elasticity and low electrical resistivity in such a device.
3) The natural sensorial capacity of such a device, namely its piezoelectric qualities.
4) The biocompatibility of the full construct with various cell types, including an assessment of different co-culture systems

5) Creation of different co-culture systems to help model different aspects of the somatosensory system.

Given the complexity and multidisciplinary nature of this work, Figure 1.1 outlines the research strategy taken in this thesis. Chapters 3, 4, and 5 are comprised of three main bodies of work, namely: Materials based work, electroconductive and piezoelectric analyses, and finally, validation of biocompatibility and cellular analysis.

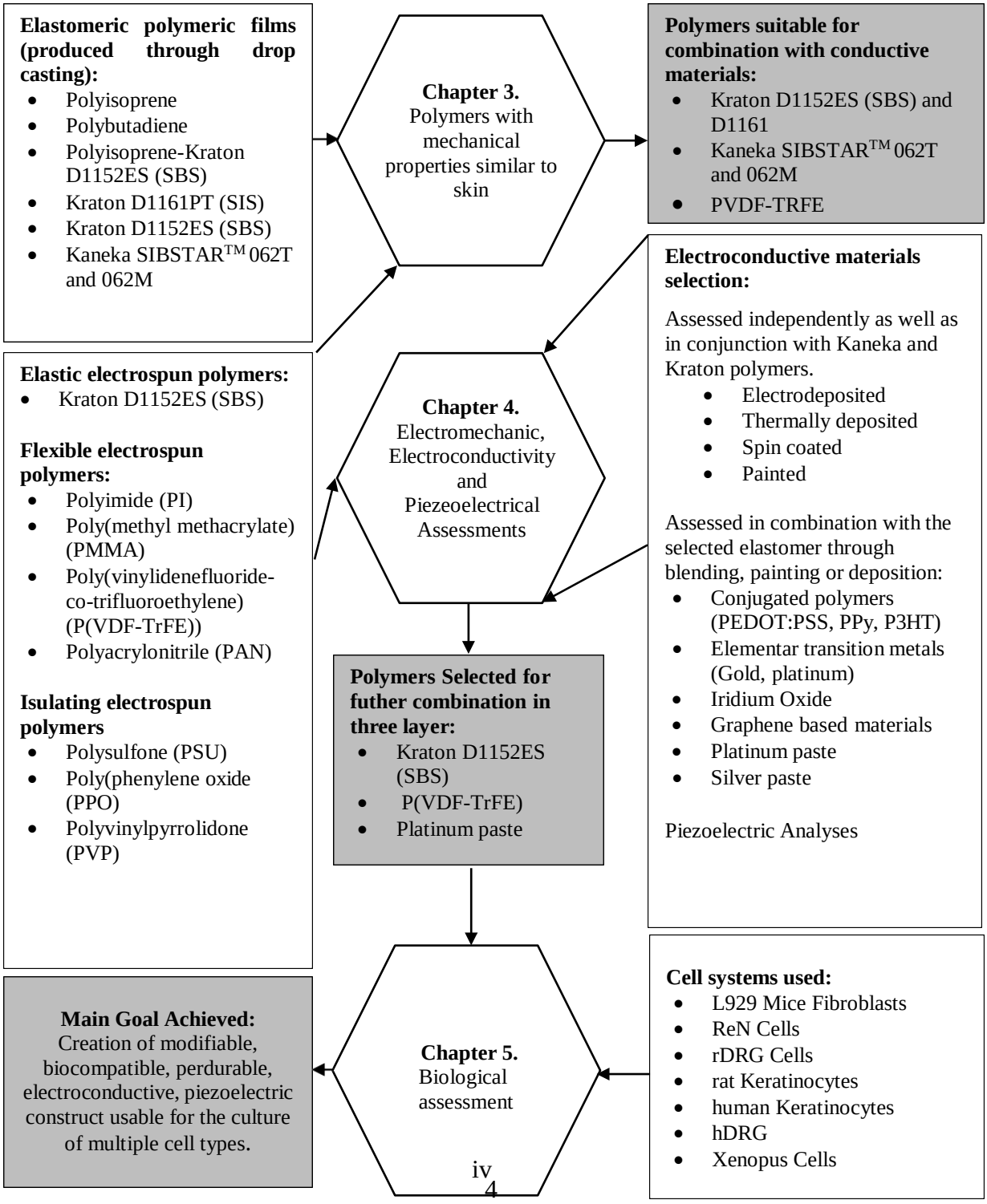

Figure 1.1: Materials Selection and Visual Outline of the Thesis

Commercially available materials were utilized in the research approach taken in order to mitigate further limits of supply. A three-layered approach was used to design this concept. This construct was comprised of elastomers, electroconductive materials, and piezoelectric polymers, in which:

i) Elastomers were selected from planar materials which had Young's moduli similar to skin, as well as electrospun materials that had structural properties more similar to those found in this organ. Not only was the initial stress-strain of importance, but capacity to withstand repeated fatigue and resist deformation.

ii) Electroconductive materials could be incorporated into the elastomer blend or utilized as a surface layer, providing the material did not greatly affect the mechanical properties and deformation of the elastomer. As with the primary layer, this material also had to retain its ability to be conductive under mechanical stress. Highly conductive materials capable of withstanding repeated strain were sought, given the incorporation of the potentially insulating third layer.

iii) A final piezoelectric material was utilized as a component that would provide stimulus to cells cultured on the construct. Planar piezoelectric sheets are less comparable to skin as they are prone to mechanical fatigue. Consequently, electrospun piezoelectric polymers were created. Such piezoelectrics would present a lower modulus and experience segmented fatigue during deformation.

The selection of such materials was the result of an intensive search across industrial and academic groups worldwide. Assembling these materials whilst maintaining the aforementioned properties required the development of several protocols and techniques. The final construct produced was designed to be soft and perdurable, rather than degradable or re-absorbed.

Materials characterization was performed in tandem to support and validate construct development. Specifically, mechanical, electroconductive and piezoelectric analyses were performed along with *in vitro* cellular analysis of the construct's individual components and the complete construct.

The studies comprised in this thesis were organized to answer the following research questions:

1. How does the functionality of elastomeric polymers compare to skin, specifically the tensile and fatigue properties? (Chapter 3)
   Rationale: This chapter focuses on the screening of soft materials that are appropriate for use as skin substitutes from a mechanical perspective. While mechanical properties of polymers are reported in the literature, few are compared to real-world systems. This study considers the full tensile strain curve and fatigue capacity of various materials before and after different processing techniques. Given that the mechanical properties of materials can be altered based on their conformations, different conformations of planar and porous materials are assessed. All results were directly compared with multiple regions of porcine skin.

2. Can elastomeric substrates possess electroconductive properties, despite the high electrical resistivity typically associated with soft materials? (Chapter 4)
   Rationale: Constructs involving electroconductive materials blended with elastomeric ones typically result in loss of electroconductivity or loss of elasticity. This chapter explored whether an elastomer with limited insulating properties exists, as well as different techniques that could facilitate the creation of an electroconductive elastomer with minimal loss of either property.

3. Does heat treatment impact the piezoelectric functionality of electrospun P(VDF-TrFE)? (Chapter 4)
   Rationale: Piezoelectrics integrated into any construct need to be combined in specific ways. While heat treatment of planar P(VDF-TrFE) is well-studied, similar data for electrospun or mechanically-produced fibers is limited. It is possible to over-heat P(VDF-TrFE), thereby reducing the piezoelectric functionality. This chapter focused on finding the optimal heat treatment for planar and electrospun P(VDF-TrFE) and identifying any processing limitations that could alter piezoelectric function.

4. Do the mechanical and insulating properties of elastomers impact piezoelectric functionality? (Chapter 4)

   Rationale: Piezoelectrics integrated into the construct must be created at certain thicknesses in order for a functional electrode to be formed. This chapter focused on identifying the processing requirements in order to seamlessly integrate all three layers of the construct: elastomer, electroconductive material, and piezoelectric. Furthermore, the effect of using a soft material as an electrode base was assessed in order to determine if this factor was self-limiting in the creation of the complete construct.

5. Can skin cells (namely fibroblasts and keratinocytes) as well as neuronal cells be grown on a piezoelectric, electroconductive, elastomeric construct? (Chapter 5)

   Rationale: A range of cells are found in skin, ranging from fibroblasts to keratinocytes to neuronal cells associated with sensory neuron pathways. Each cell type is known to have different preferences in terms of substrate type. This chapter focused on assessing the culture of four different cell types on each segment of the construct. Proliferation and long-term culture were both assessed. Furthermore, several co-culture models were created in order to identify growth patterns and proliferation that would occur when cells were allowed the opportunity to choose between porous, multi-layered substrates and textured, planar ones.

6. Is the creation of a biocompatible, elastomeric, electroconductive, perdurable, pressure-sensitive, three-dimensional construct feasible? (Chapter 6)

   Rationale: This chapter summarizes the results achieved to date and focuses on the discussion of future directions for this technology.

1.3 State of the Art

1.3.1 Motivation for the Creation of a Biocompatible, Electroconductive Elastomer

Human beings are able to perceive and understand complex environments through the combined functions of the central nervous system, musculature, and skin, regardless of the intricacy of the stimuli.[47] Skin functions as a barrier to pathogens while preventing excess water loss, and simultaneously receiving sensorial information from the environment.[48, 49] It allows for a myriad of tactile stimuli to be detected and interpreted. For example, the oiliness of a liquid is perceived as both resistance and smoothness, while awareness of snowfall versus hail requires pressure, temperature, and texture to be detected and processed. Skin acts as our first line of defence, and we are utterly dependent on its innervation to discern and interact with the world.

Lack of innervated skin can result following injury, illness, or even limb loss. Following most types of damage, skin is able to rapidly regenerate, restoring sensory function to the damaged area. However, severe damage can result in irreversible and devastating loss of function. Severe burns and limb loss lead to permanent sensory damage, as well as serious psychological and physiological effects. Historically, resolving severe damage to skin has involved some form of transplantation - the most reliable way of restoring somatosensory function. Skin grafting, which has been performed for over 3,000 years, enables neural migration from the grafted skin to nerve pathways within the injured region.[50, 51] Skin burns can be resolved through either autologous or allogenic transplantation, depending on the size of the affected area and the severity of the injury. In extreme cases, burns can be so severe that transplantation is not suitable, and amputations may be necessary. Amputations once implied permanent loss of function to the severed area. However, advances in composite tissue surgeries have enabled complete limb transplantation, allowing amputees the best chance of recovering both somatosensory and motor function.

Medical centres around the world offer composite tissue transplants for full limbs, but the eligibility criteria is quite stringent.[52] Following an amputation, candidates are selected based on varied anatomic and physiologic eligibility criteria, which includes an assessment of nerve conduction velocity and confirming a lack of immunosuppressive conditions.[52-55] Extensive

psychological and social assessments are also mandatory.[52-55] Regardless of fitness or desire for a limb, certain patients may always be deemed ineligible for transplantations due to a lack of the limb's representation in the brain. The longer the concept of the amputated limb remains within the brain, the less likely the amputee's brain is to accept a limb. If transplanted, such a patient would likely not be able to regain functionality of their new appendage.[47] Given the selectiveness of the process, composite tissue transplants are not suitable for all amputees. Approximately 113 hand transplants have been successfully performed since 1998—a tiny fraction of the total amputees worldwide.[52]

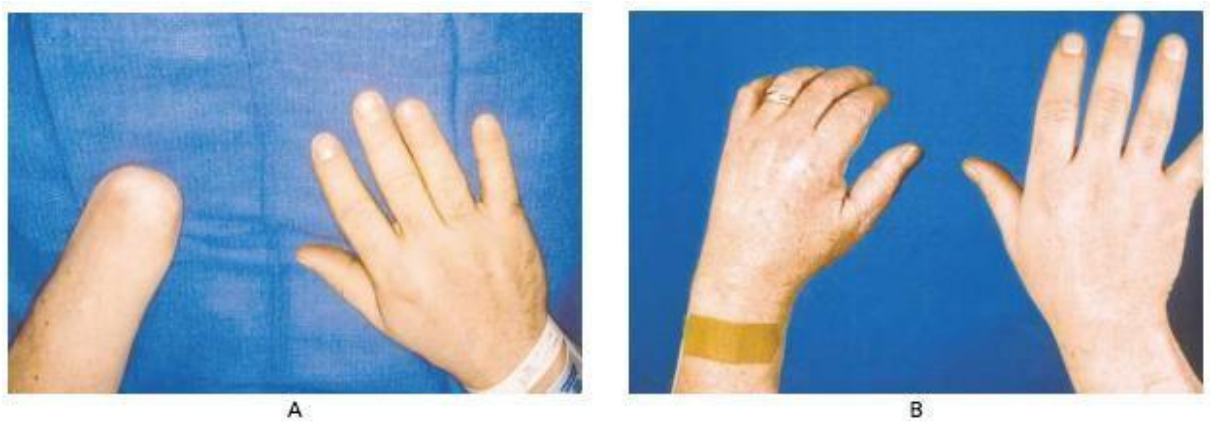

Figure 1.2: Before and After Images of a Hand Transplant Patient. Reproduced with permission from Jones et al., The New England Journal of Medicine 343.7 (2000): 468-473, Copyright Massachusetts Medical Society.[53]

Following transplantation, new nerve fibers must regenerate along the existing nerve pathways of the patient's stump and transplanted limb. This is a time-consuming process as nerve fibers grow at a maximum speed of 1mm/day.[55] Additionally, fibers are not guaranteed to migrate correctly along the original pathways. For instance, following a hand transplant, nerve fibers from one finger may regenerate into another, requiring the brain to completely reorganize its viewpoint of the somatosensory cortex.[55] This process consequently involves extensive physical therapy and psychological therapy, as patients struggle with limbs they feel no ownership of. Patients can expect to find themselves undergoing extensive physical therapy for six months or more.[56] Despite the rigorous pre-selection and post-assessment procedures, there is never any guarantee of regaining complete somatosensory function post-transplant.[57, 58] Return of motor and sensory function can take anything from months to years.[56] Optimizing this surgical technique going forward may require the addition of perdurable or long-life extra- or intra-neural electrodes to guide nerve pathways and accelerate rehabilitation.

An alternative to transplantation exists in the form of integrated prosthetics that utilize neural and musculoskeletal stimulation. With training, humans have been able to transfer hand sensitivity to foreign objects and perceive these objects as part of themselves.[47] Through osseointegration and similar surgical techniques, amputees can recognize prosthetics as an extension of themselves. This has increased more so with the development of myoelectric and neurally-controlled prosthetics, which often utilize implantable extra- and intra-muscular and/or extra- and intra-neural electrodes to create a human-machine interface to link body to prosthesis.[59-61] Such prostheses restore variable amounts of motion and movement control, depending on the prosthesis model and subject's nerve pathways.

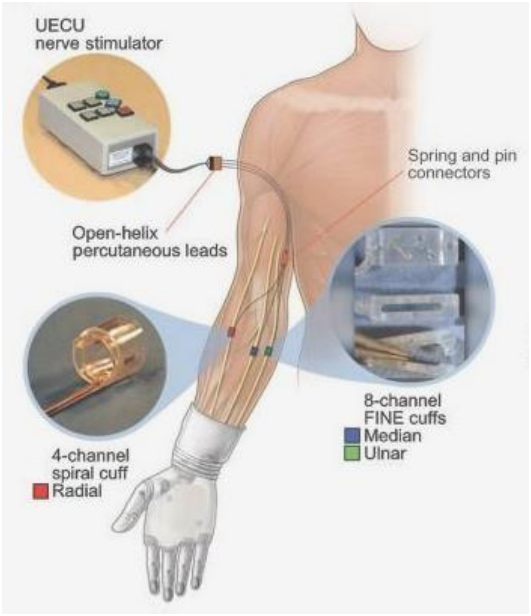

Figure 1.3: Components Required for Direct Neural Stimulation in a Prosthesis User.
Taken from Tan et al., Science Translational Medicine 6.257 (2014): 257ra138-257ra138.[63] Reprinted with permission from AAAS.

Neurally-controlled prosthetics are controlled by users through targeted innervation and subsequent thought-based control. However, these are particularly unique as they are capable of restoring partial somatosensory feedback through direct nerve stimulation. Neurostimulation techniques have allowed for pressure, pain, and various types of moving touch to be detectable thus far.[59-62] Despite restoring only limited somatosensory system function, the progress in this field has been ground breaking. However, although the neurostimulatory components required to restore sensory function have been successfully tested, they cannot yet be fully integrated into neuroprostheses. Due to the invasiveness of direct neural stimulation and lack of

miniaturization of the sensory feedback component, sensory feedback for neurally-controlled prosthesis users is still experimental and in limited clinical trials. However, sensor-embedded prostheses and various artificial skin substitutes have been developed as alternatives.

Artificial skin is often referred to by a variety of names, including electronic skin, e-skin, or second skin. Due to the overlap in other skin-based technologies, it should not be confused with the degradable biomaterials or biological sprays used on open body surfaces in order to prevent infection and promote wound healing (discussed further in section 1.3.5).[64-66] Artificial skin should not be confused with cosmesis, the process of making artificial limbs resemble organic limbs. Cosmesis tends to utilize vinyl or silicone based materials, focusing solely on replicating the natural appearance and texture of a limb. Although sensor-focused artificial skin and cosmesis may one day be integrated, none have thus far, though several prototypes are in development. The artificial skin discussed throughout this thesis refers to material-based products that are typically used to enhance robotics and prosthetics.[67]

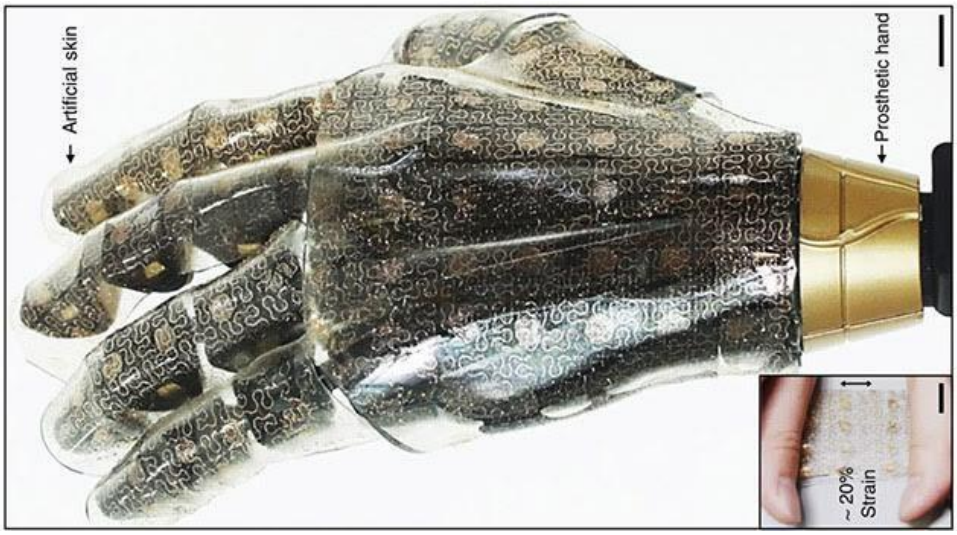

Figure 1.4: Stretchable Prosthetic Skin Equipped with Silicon Nanoribbon Arrays. Reprinted with permission from Springer Nature: Nature Communications. [Stretchable Silicon Nanoribbon Electronics for Skin Prosthesis, Jaemin Kim, Mincheol Lee, Hyung Joon Shim, Roozbeh Ghaffari, Hye Rim Cho et al.] Copyright 2014

The generalized goal of artificial skin substitutes is to create a construct that can mimic skin's sensory feedback and tactile function. Such products are typically flexible or elastic electronic constructs that equip users with increased sensory feedback. Currently, artificial skins are so advanced that they contain humidity, pressure, and temperature sensory arrays, in addition to electroresistive heaters and stretchable multi-electrode arrays for nerve stimulation.[68]

However, the creation of most artificial skins has been focused on only one or two sensory aspects. Certain artificial skin substitutes have a sense of pressure is equivalent to that of a human fingertip.[69] Others are capable of resistance over a 130 ºC temperature range, while others are capable of discriminating between both temperature and pressure.[70-73] Artificial skin substitutes may even have self-healing properties.[74]

Artificial skin substitutes must be integrated into prostheses or directly link to some aspect of the biological interface.[75] Despite the availability of highly stretchable electronic devices today, and several tactile and temperature sensors that perform better than human skin, most artificial skin substitutes struggle to combine these factors into a medically sound, long-term product.[76-78] Although integration and read-out of combined arrays can be both difficult and costly, the biggest issue by far is neural interfacing. The challenges to be addressed on materials/neural interface are primarily related to biocompatibility. There are also related concerns that electrodes, which are typically not made from soft materials, may fracture, enter the bloodstream, and cause internal damage.[68] However, advances in materials design, as shown in Table 1.2, will undoubtedly allow artificial skin products substitutes to soon become natural, integrated extensions of the human body.

Given the complexity of the somatosensory system and the variety of potential methods for the restoration of somatosensory function, neurostimulation through biocompatible, stretchable electronics is necessary to further research in composite tissue transplantation, neuroprosthetic design, and artificial skin substrates. Each field requires such materials to be modified in slightly different ways, but all have the same end goal.

To date, different studies have focused on different aspects of somatosensory system restoration such as: 1) understanding the somatosensory system, 2) the clinical relevance of neurostimulation in its ability to correct sensory dysfunction, and 3) materials research that can assist in the functional restoration of the somatosensory system.[27,30,48,63] The research presented in this thesis primarily focused on the latter: A materials-based approach. Rather than replicate individual aspects of the somatosensory system individually, a system was developed that could support the function of a healthy somatosensory system. We propose the creation of a system that can be used to repair, restore and enhance somatosensory system function, rather than create a novel somatosensory system from the ground up.

1.3.2 An Overview of the Somatosensory System

As human beings, we take for granted our ability to feel pleasure, pain, temperature, texture, and a myriad of other sensations through stereognosis. Indeed, tactile sensibility has been so taken for granted throughout the human experience that analysis of human sensory modalities has been researched for less than two centuries.[1] Novel aspects of the somatosensory system are still constantly being discovered. For instance, five novel chemoreceptors– specifically, olfactory receptors, typically found in nasal epithelium– were recently identified within keratinocytes, the skin's primary cell type.[48] The human somatosensory system is notably complex as it plays a role in exteroreceptive, interoceptive, and proprioceptive functions– whose roles are related to perception of stimuli, reaction to stimuli, and control of body position and balance, respectively.[1] All three aspects are critical to the complete function, sensibility, and sensory feedback of the body's limbs and digits.

Exteroreceptive function refers to a variety of superficial sensations such as pain, pleasure, and temperature. Skin is innervated by both low and high threshold mechanoreceptors capable of responding to a variety of innocuous and harmful stimuli.[1] Several types of specialized mechanoreceptors exist in the skin: In particular, free nerve endings on the root hair plexus, Krause's end bulbs, Meissner's corpuscles, and Merkel's discs. As we experience superficial sensations, these signals are perceived by our skin's receptors and travel through our myelinated nerves. Exteroreceptive sensations travel via sensory neurons into dorsal root ganglia and cranial sensory ganglia.[1] These dorsal root ganglia extend through the nervous system to their peripheral targets and the spinal cord, or dorsal column nuclei of the brainstem.[1]

Interoceptive function refers to the feeling of self: visceral feelings within the human body, such as those caused by vasomotor activity or thermoregulation, that have an inherent association with emotion and self-awareness.[79] The lamina I spinothalamocortical pathway, the most superficial layer of the spinal dorsal horn, conveys these types of sensations to the central nervous system via A- and C-fibers throughout the body.[79] This aspect of the somatosensory system is a complex function with various motor, sensory, and neuropsychological aspects.

Proprioceptive function contributes to bodily awareness, movement, and control.[80] Similar to kinaesthesia and the vestibular system, proprioception gives sensory feedback that enables accurate limb position and movement, tension, and balance.[80] Proprioceptors, typically Pacinian corpuscles and Ruffini endings, are typically found in Golgi tendon organs, muscle spindles, and in and around joint capsules.[81] They are able to influence motor nerves, synapsing with lower motor neurons and the central nervous system in order to interpret signals and even induce reflex movements.[82]

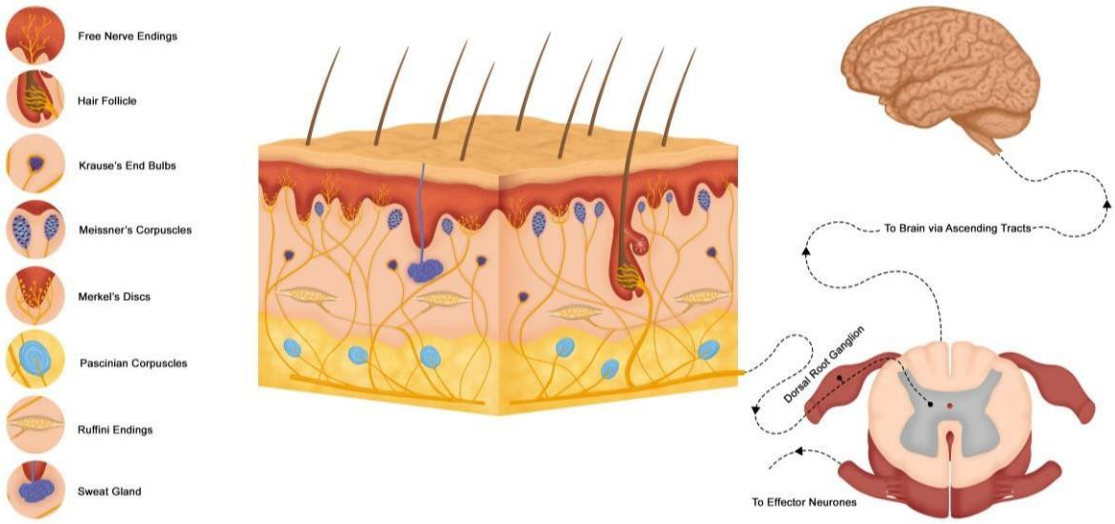

Figure 1.5: Skin-Spinal Cord Interconnections within the Somatosensory System. Diagram depicting the sensory neurons in the skin, alongside the pathway through the somatosensory system via the dorsal root ganglion and spinal cord to the brain.

Functional components of the somatosensory system can be lost with age, disease, nutrient deficiencies, or injury. In some cases, genetic mutations can alter somatosensory system function from birth, leading to conditions such as congenital analgesia.[74] Somatosensory system issues commonly arise from injuries to skin, nerves, or the brain. This is obvious with amputees or burn victims, where skin and nerve damage is evident. However, conditions such as multiple sclerosis, shingles, diabetes, and stroke can result in similar issues. Within the exteroceptive somatosensory system, this can present as neuropathic pain which can be perceived as burning, tingling, numbness, or aching. Such issues may resolve themselves with time, or evolve into debilitating conditions, including chronic neuropathic pain or fibromyalgia. Once malfunctioning or lost, somatosensory function can be challenging to regain. There are no known cures for genetic diseases, like congenital analgesia, that result in somatosensory system issues. Sensory malfunctions related to illness or injury are typically associated with

permanently damaged nerve pathways. Mononeuropathy and polyneuropathy can present as pain, hypersensitivity, and numbness, as well as various proprioceptive issues including weakness and mobility issues. Neuropathies can be treated through the administration of various medications, including corticosteroids, immunosuppressants, antidepressants, and opioids. However, neuropathies are often treatment-resistant. They may be so severe that elective amputations are sometimes requested.[83]

Interestingly enough, neurostimulatory technologies have become a promising therapy for treatment-resistant somatosensory disorders, including those which originate from neurodegenerative and autoimmune conditions.[84-86] Electrical stimulation has also been used to accelerate wound healing of the skin, and increase both cutaneous perfusion and venous flow.[87] Such therapeutic approaches involve stimulation of the brain or the damaged area of the body, and exist in both implantable and non-invasive formats.

1.3.3 Electrical Stimulation for Wound Healing and Regeneration

Electrical stimulation has been used therapeutically since 15 AD, when 'electric eel'-type fish were used to treat headaches, migraines, and gout.[88] Over the past 2,000 years, electrical stimulation has moved far past harnessing electricity from marine creatures. The development of defibrillators, pacemakers, and various other electricity-dependent medical devices have led to a greater understanding of human nervous system. Virtually all mammalian tissues are excitable due to the way that neuronal and muscle cells communicate. As such, electricity can be used to regulate various issues, including cardiac dysrhythmias, respiratory dysfunction, and nerve hypersensitivity.[88] In recent years, advances in electrical stimulation have been found to have noteworthy clinical implications in wound healing, the creation of neural interface systems, and neurostimulation therapies.

Electrical stimulation in the context of wound healing and tissue regeneration has been explored for many years. Studies of limb regeneration, which occurs naturally in organisms such as zebrafish, axolotls, salamanders, and cervines, have identified genetic and immunologic components involved in re-growing complete composite tissue.[89-91] Further exploration of limb regeneration under electric fields has led to a more in-depth understanding of cellular migration, proximal and distal wound healing, and the limitations of regenerative

ability in mammals.[92, 93] While non-mammalian models have provided us with excellent models that can be used to study these biological mechanisms, replicating such regenerative processes in mammalian limbs has been limited. However, the principles discovered through such studies have shown that electrical stimulation can be used to accelerate healing.

Epithelial and endothelial cells, fibroblasts, lymphocytes, macrophages, and neuronal cells are all receptive to electrical stimulation.[94] Electric fields have been show to activate ion transport and endogenous electric fields in damaged cells, help direct cell migration, and affect stem cell-based regenerative responses.[94] The induction of intracellular signalling has also been identified in keratinocytes and corneal epithelial cells following electrical stimulation.[95,96]

Electrical stimulation has shown particular promise in the treatment of chronic and non-healing wounds.[97-99] In humans, electrical stimulation has been shown to increase angiogenesis, improve tissue oxygenation, and improve the healing of venous insufficiency wounds, wounds resulting from non-ischemic diabetic neuropathy, and lower extremity ischemic wounds.[99] This type of electrical stimulation is typically performed with biocompatible substrates through a non-invasive format. Various electrical stimulation devices for wound healing exist. These include the branded products Procellera (a silver-zinc matrix on polyester) and Posifect (a battery-embedded hydrogel), as well as many unbranded electrical stimulation devices that have been used in clinical trials.[99-103] In addition to promoting wound healing, electrical stimulation can help prevent infection and reduce both pain and inflammation.[99-100]

Despite these successes, the current applied to produce each individual result is highly variable. This limits the use of each device. A neurostimulatory device will be capable of producing a large, variable-strength electric field, while products specifically designed for direct skin contact and wound healing will be far more limited. This ultimately means that there is no ‘one size fits all’ material that can be used when developing stimulatory bioelectrical devices. Given the rise of personalized medicine, novel devices should be customizable, or at a minimum less restrictive in the parameters that affect their conductivity. For research in this field to progress, device design and the duration of stimulation are also parameters that need to be optimized.[94]

1.3.4 Electrical Stimulation as a Neurostimulatory Technique

Neurostimulation is a bioelectric medicine that is available in both non-invasive and implanted formats. In the last few decades, various neurostimulation techniques have become popular, including (but not limited to): deep brain stimulation (DBS), vagus nerve stimulation (VNS), transcranial magnetic stimulation (TMS), motor cortex stimulation (MCS), and spinal cord stimulation (SCS).[104-107] Most neurostimulatory techniques are multipurpose; for instance, vagus nerve stimulation alone can be used to treat Alzheimer's disease, chronic heart failure, cluster headaches and migraines, treatment-resistant depression, epilepsy, inflammatory bowel disease, and rheumatoid arthritis.[107-114] VNS has also been shown to suppress pain.[115] Like VNS, spinal cord stimulation has also been used to treat chronic pain of various types.[116] However, it has become particularly renowned for helping paraplegics with regaining control of mobility.[117]

The clinical implications of neurostimulation are huge, given the wide range of medical treatments it is able to provide. Implantable neurostimulatory techniques are highly regulated, while non-invasive devices are readily available throughout the European Union and USA as portable, non-FDA approved devices. The difference between these techniques and treatment methods is based on three main factors: 1) The placement of the electrodes, 2) the frequency of the neurostimulation, and 3) the regularity of the stimulation. Although neurostimulation techniques can be literally "non-invasive", even external electrical stimulation can affect the cortical excitability of the brain in adverse and beneficial ways.[106]

For instance, spinal cord stimulation involves spinal surgery in order to implant an electrode array onto the epidural surface of the spinal cord. Weeks of recovery time must be factored in before commencing therapy. Spinal cord stimulation can vary, with commonly used frequencies at 15, 20, and 40 Hz for 0.21 milliseconds with a voltage range of 0-to-6 V. Positive results could be seen just weeks after stimulation.[117]

In contrast, implantable pulse generators used in vagus nerve stimulation for Alzheimer's disease, use a frequency 20 Hz and current 0.25 mA. Stimulation lasts for 30 second periods, with 5 minute breaks. Results can be seen within a three month period, but stimulation continues for a year or more. [107]

Finally, non-invasive neurostimulatory devices that use techniques like TMS – applied above the scalp – involves frequencies that range from 1 Hz to 20 Hz. Lower frequencies typically inhibit cortical excitability and higher frequencies increase it. However, neurostimulation using such techniques can be applied in a variety of ways. These different stimulatory protocols can in turn produce different amounts of aftereffects that can last for less than one hour or as long as eight. Non-invasive stimulation may occur one-to-five times a week for a few days, months, or longer.[107]

Non-invasive and invasive neurostimulatory techniques do not differ substantially in concept, but utilize completely different materials. Non-invasive neurostimulatory techniques typically utilize electrodes and a source to apply controlled current to a person's head or the site of nerve damage. Electrodes can be made out of a variety of metals, and direct contact is made through use of adhesive jellies or gels.[118] Alternatively, an electric current travelling through a coiled wire creates a magnetic field that can be placed upon the person to produce an alternative type of stimulation.[106] Unlike the electrical stimulation used in wound healing, TMS and other forms of neurostimulation typically require direct contact.

Invasive neurostimulatory techniques are similar in principle to non-invasive neurostimulation, but utilize implantable, miniaturized devices for electrostimulation instead of external ones. Invasive devices are FDA-approved, surgically implanted, and typically range between the size of a battery and that of a pill. Modern neurostimulatory devices typically consist of a soft polymeric component and an electroconductive component. Commonly implanted electroconductive materials include titanium nitride (TiN), iridium oxide (IrOx), and platinum (Pt), which are capable of capacitive, three-dimensional faradaic, and pseudocapacitive charge-injection mechanisms, respectively.[119] Such materials are selected as they are capable of producing reversible mechanisms of charge, are easily controlled, and do not result in the production of any unsafe, reactive species.[119] Implantable devices are typically for people with incurable neurological or inflammatory diseases that require regular electrical stimulation to remain asymptomatic. Neurostimulation can also be performed through nerve cuff electrodes, which may be implanted for the treatment of spinal cord injury, stroke, and sensory deficits.[119] Nerve cuff electrodes have also been implanted into amputees using neutrally-controlled prostheses in order to create a human-machine interface.[119-121] Such implants include non-

penetrating peripheral nerve cuff electrodes, spiral cuff electrodes, transversal intrafascicular multichannel electrodes, longitudinal intrafascicular electrodes, monopolar epimysial electrodes, and flat interface nerve electrodes.[119-121]

Currently, non-invasive neurostimulation is a fairly costly medical technique that is not yet available worldwide. It has remained somewhat experimental and unregulated. In contrast, implantable neurostimulation devices are becoming increasingly common, particularly through clinical trials. However, many (but not all) involve the use of materials that prevent future treatment via electromagnetic technologies and therapeutics (e.g., magnetic resonance imaging, ultrasounds, and diathermy). Neurostimulation devices are quite typically unable to work synergistically with other implanted electrostimulatory devices, such as pacemakers. They must also be replaced with some amount of regularity, depending on the model and purpose of the device.

1.3.5 Soft Biocompatible and Electroconductive Materials Used in Neurostimulation

There are a variety of materials that are used in the development of neural cuff electrodes, implantable neurostimulation devices, and in electrically-active wound healing substrates. We identified some of the more recent developments in biocompatible, electroconductive materials that are elastic or at least flexible (see Table 1.1).

Electroconductive materials used in these biocompatible constructs included carbon-based materials, polyaniline fibers, and PEDOT, as well as the incorporation of protocols in which doping agents are applied to materials. As shown in Table 1.1, the electroconductivity or resistivity listed varies substantially from construct to construct, due to the materials and processing techniques used. Carbon-based materials, namely single and multi-walled carbon nanotubes and nanoparticles, were found to be the most popular electroconductive material used.[10, 13, 24, 32, 34, 39] Carbon-based materials are often used as a component of neural electrodes, and have become increasingly popular in biomedical devices since their preparation became standardized in 1991.[121-125] Certain carbon-based materials have a lower percolation threshold than others, influencing conductivity and giving them a wide range of potential uses.[126,127] They are particularly interesting as an alternative electroconductive material compared to the more commonly used TiN, Pt, and IrOx.[119] The primary issues with carbon-based materials are

related to biocompatibility and mechanical properties. Although they have been shown to promote neural differentiation and simulate neural cell growth, many carbon-based products have shown biocompatibility-based issues.[128-132] This is particularly related to the size of the material, as with nanotubes, and the synthesis process, which can result in cytotoxicity.[133-135] Carbon-based products of various types were considered in the development of our work, but eventually ruled out because of these issues and their impact on the elasticity of the construct.

PEDOT is another increasingly popular electroconductive material. It is a water-dispersable polymer that can easily be blended with other polymers or electroconductive materials.[136-138] It too has been used in neural electrodes and neural cell culture, and has provided positive results both alone and as a composite.[139-142] However, PEDOT has shown mixed results in the literature. PEDOT electrodes have formed cracks and undergone delamination, resulting in issues related to stability and preventing its use in clinical products. Another issue related to the use of PEDOT is that it requires the addition of a dopant (typically poly(styrene sulphonate)). The addition of such dopants have historically shown to increase biocompatibility-related issues.[143, 144] Different PEDOT processing and dopants have resulted in improved effects on both counts. PEDOT was explored throughout the course of this thesis due to the promising results our group has had using this material as an electroconductive substrate.[140] It was not, however, chosen as the final material for our construct.

C2020322P6 is a cross-linked polymeric platinum paste with a solids content between 85.5 and 86.5% and resistivity of 0.32 Ohm/sq, produced by the Gwent Group (SunChemical®). This product was specifically designed for low temperature systems and to be cured onto polymeric substrates. Like other Gwent polymeric products, C2020322P6 platinum paste is screen printable and can be used to create electrochemical sensors. However, unlike other similar materials (e.g., Gwent platinum paste C2010309P3 and C2011004P5), the C2020322P6 platinum paste is well-suited to soft materials and can be cured at low heat.[154]

This material is consequently fairly unique; there are currently no publications discussing its use. The most similar material utilized is Gwent C2050804P9, a platinum polymer paste also suited to low temperatures and capable of being cured on a wide range of polymeric materials. There are minimal differences between these two products; however, the C2050804P9 platinum polymer paste has a slightly lower conductivity and more polymer trapped between particles of the platinum, resulting in a rougher texture when applied to surfaces.

Table 1.1: Biocompatible Electroconductive and Piezoelectric Elastomer Constructs

Study	Polymer	Maximum Functional or at Break Elongation	Storage or Young's Modulus	Conductive or Piezoelectric Material	Maximum Conductivity/ Resistivity
Super Stretchable Electroactive Elastomer Formation Driven by Aniline Trimer Self-Assembly[10]	PEG2k-AT6-TMP	1643%	3.8 - 7.7 MPa	Polyaniline nanofibers, nanosized carbon black	$8.2 \cdot 10^{-6}$ to 0.1 S/cm
Electromechanically Responsive Liquid Crystal Elastomer Nanocomposites for Active Cell Culture[13]	Liquid crystal elastomers	35%	2.1 - 8.1 kN	Carbon black nanoparticles	0.2 – 38.5 Ω · m
Carbon Nanotube-Coated Silicone as a Flexible and Electrically Conductive Biomedical Material[24]	Silicone	Tested up to 20%		Single and multiwall carbon nanotubes	0.86 to 1.5×10^{3} kΩ/sq
Development of a Regenerative Peripheral Nerve Interface for Control of a Neuroprosthetic Limb[30]	Silicone			PEDOT	
A Conductive Composite Nanomaterial with Biocompatible Matrix and Multilayer Carbon Nanotubes[32]	Carboxy-methylcellulose matrix and flexible polymers			Multiwall carbon nanotubes	~1.2 - 4 · 10^{4} S/m
Silicone Substrate with Collagen and Carbon Nanotubes Exposed to Pulsed Current for MSC Osteodifferentiation[34]	PDMS, Silicone			Carbon nanotubes	760 – 827 Ω
Simple and Cost-Effective Method of Highly Conductive and Elastic Carbon Nanotube/Polydimethylsiloxane Composite for Wearable Electronics[39]	PDMS	25 - 110%	2 - 4 MPa	Carbon nanotubes	2.03 - 5225 Ω /sq
Synthesis and Characterization of Conductive, Biodegradable, Elastomeric Polyurethanes for Biomedical Applications[41]	Conductive Polyurethane	75 - 728%	3.1 - 17.9 MPa	Doped with camphorsulfonic acid	$2.7 \cdot 10^{-10}$ - 7.3 · 10^{-5} S/cm

To date, this polymeric platinum has only been discussed in two publications: It has been utilized to create electrochemical biosensors to monitor oxidative stress during embryo development and to produce flexible chloride sensors, which can be used for various biomedical, environmental and food-related purposes.[155, 156]

Polymers used in these biocompatible constructs included silicone, PDMS, liquid crystal elastomers, polyurethane, and PLLA:PEG copolymers. The most popular polymer was found to be silicone-based.[24, 30, 34, 39] Given the ease of manipulation of silicone-based substrates, these polymers are often the material of choice for biological and perdurable artificial skins, wound healing substrates, and components of implantable medical devices, such as neural arrays, catheters, and slow-release birth control, such as the Implanon.[145-149]

The use of artificial skin in medicine dates back to the 1970s, with the Yannas-Burke group trialling the first biological artificial skin in 1979.[150] This artificial skin substrate was a porous, biodegradable matrix made of animal collagen and glycosaminoglycan molecules that encouraged cell growth, combined with a silicone based cover. This created a new dermis that allowed gas permeation and mitigated infection, providing a rough temporary substitute for the epidermis. This artificial skin led to the commercial product Silastic, as well as various other artificial skin products including Matriderm, Integra, Dermagraft, and Myskin.[151-153]

From a materials perspective, all of these products are, notably, very much unlike those presented in Tables 1.1 and 1.2, as they are degradable and focus primarily on an elastomer layer, rather than any stimulatory component. This is the primary rationale that separates our work from that of most biodegradable hydrogels, which are typically utilized to promote wound healing or to improve the adherence of skin grafts.[159] Furthermore, these materials are often tailored to the growth of fibroblast and keratinocyte-type cells, rather than complete skin with the potential for long-term growth, including the integration of vascularization and neural components. Although there are obviously a multitude of material constructs that can be used in the creation of skin substrates (see Table 1.2), the majority of these have not been assessed using the same methodologies as our own construct.

1.3.6 Summary of Electroconductive and/or Pressure-Sensitive Elastomer Constructs

Not all electroconductive elastomers are created equally. Many do not have the same features as our construct. Specifically we aimed to produce a construct with elastic mechanical properties, high tensile strength, conductivity, piezoelectricity, and biocompatibility. Table 1.2, which summarizes the properties of other similar constructs to the one aimed to be developed on this thesis, compiles recent electroconductive elastomers that have been designed with biomedical purposes in mind. In cases where the attribute is not listed, this aspect of the construct has not yet been assessed.

This table shows that in many cases, the overall research approach is similar although the ultimate design and explicit purpose differ. Most notably, at the time this work was started, most of the constructs listed in Table 1.2 had not yet been created. Out of the 42 electroconductive and piezoelectric elastomer constructs in Table 1.2, only eight have been assessed in cell culture scenarios and validated for biocompatibility.

It should also be noted that certain constructs are not made of entirely biocompatible materials. For instance, PANi (polyaniline), used in the construct of Yu et al., releases cytotoxic impurities (e.g., ammonium persulfate).[45] However, this may not make this polymer unusable in biocompatible contexts, as it is often doped, reducing the extent of the cytotoxicity; or produced as a core layer within nanofibers, which prevents any released impurities from reaching the cells.[157] In stasis, the latter solution may result in a functional biocompatible construct; yet in motion, there is the potential for degradation of the external layer over time, which may result in cytotoxicity.

Out of these biocompatible constructs, the maximum functional elongation or at break elongation percentages have been assessed for only three.[10, 39, 41] This is noteworthy since elastomers are typically characterized as materials with elongation values between one hundred and several thousand percent.[46] While it is easy enough to create blended materials (i.e., mixing carbon nanotubes into rubber), increases in electroconductivity typically result in decreases in elasticity.

Finally, out of the remaining three constructs, two can be considered perdurable, like our construct.[10, 39] The remaining third construct is biodegradable.[41] Perdurability was not listed in this chart as the degradation rates of the constructs in Table 1.2 were not commented on unless one of their established attributes was biodegradability.

In summary, based on our review of existing publications, there are only two electroconductive elastomers that have comparable properties to the construct created in this thesis: those of Chen et al and Kim et al. Both utilize carbon-based materials as their primary electroconductive material and are extremely soft, with moduli comparable to skin. However, the functional properties between the two differ otherwise, with elongation at break values that are over ten-fold apart. Kim et al.'s construct, with the lower elongation at break value, was designed for wearable electronics. In comparison, Chen et al.'s construct, with an elongation at break value in the thousands, was developed for soft tissue engineering.

Table 1.2: A Summary of Electroconductive and/or Pressure-Sensitive Elastomer Constructs (Part 1/4)

Study	Polymer	Maximum Functional or at Break Elongation	Storage or Young's Modulus	Conductive or Piezoelectric Material	Maximum Conductivity/ Resistivity	Bio-compatible
1. Study of Two Types of Sensors of Static Forces—a Piezoelectric Sensor and a Piezoelectric Elastomer Sensor[4]	Electroconductive rubber		$0.98 \cdot 10^{11}$ MPa	Brass plates PZT4M	Changes based on volume of rubber	
2. Liquid Single Crystal Elastomer/Conducting Polymer Bilayer Composite Actuator: Modelling and Experiments[5]	Liquid Single Crystal Elastomer	30 – 50%	2.8 GPa	PEDOT:PSS	Actuates based on conductive layer thickness	
3. Investigation of Electroconductive Films Composed of Polyvinyl Alcohol and Graphitized Carbon Black[6]	Polyvinyl alcohol	Changes based on polymer to carbon ratio		Graphitized carbon black	10^{-2} - $10^{7}\ \Omega$	
4. Characterization of Thermoplastic Elastomers Based Composites Doped with Carbon Black[7]	Kraton G1645 (styrene-b-ethylbutylene-b-styrene)	1800 - 2475%	8 - 14 MPa	Carbon black	$6.1 - 9.5 \cdot 10^{-4}$ S/m	
5. Study of the Reinforcing Mechanism and Strain Sensing in a Carbon Black Filled Elastomer[8]	Poly(styrene-co-butadiene)	60% was the maximum tested	Varies based on carbon content	Carbon black	10^{-2} - 10^{-14} S/cm based on carbon content	
6. Relationship Between Conductivity and Stress–Strain Curve of Electroconductive Composite with SBR or Polycaprolactone Matrices[9]	Poly(styrene-co-butadiene) or Polycaprolactone	≤ 650%		Carbon black and super-conductive carbon black	1.4 - 14 S/m	
7. Super Stretchable Electroactive Elastomer Formation Driven by Aniline Trimer Self-Assembly[10]	PEG2k-AT6-TMP	1643%	3.8 - 7.7 MPa	Polyaniline nanofibers, nanosized carbon black	$8.2 \cdot 10^{-6}$ to 0.1 S/cm	Yes
8. Dielectric and Microwave Properties of Elastomer Composites Loaded with Carbon–Silica Hybrid Fillers[11]	Natural rubber SVR 10			Carbon black and doping agents	$2.2 \cdot 10^{3}$ - $1.2 \cdot 10^{13}\ \Omega \cdot$ m	
9. Superhydrophobic and Electroconductive Carbon Nanotube-Fluorinated Acrylic Copolymer Nanocomposites from Emulsions[12]	Fluorinated acrylic copolymer Capstone ST-100			Multi-walled carbon nanotubes	25 S/m	
10. Electromechanically Responsive Liquid Crystal Elastomer Nanocomposites for Active Cell Culture[13]	Liquid crystal elastomers	Tested up to 35%	2.1 - 8.1 kN	Carbon black nanoparticles	0.2 – 38.5 Ω · m	Yes
11. Reduced Graphene Oxide/Hydroxylated Styrene–Butadiene–Styrene Tri-Block Copolymer Electroconductive Nanocomposites: Preparation and Properties[14]	Styrene-butadiene-styrene	318 - 632%	2.32 -7.48 MPa	Reduced graphene oxide	1.3 S/m	
12. Simultaneous Improvement in Both Electrical Conductivity and Toughness of Polyamide 6 Nanocomposites Filled with Elastomer and Carbon Black Particles[15]	Polyamide 6	63-311%	0.85 - 1.11 GPa	Carbon black	7.1×10^{-6} S/m	

Table 1.2: A Summary of Electroconductive and/or Pressure-Sensitive Elastomer Constructs (Part 2/4)

	Study	Polymer	Maximum Functional or at Break Elongation	Storage or Young's Modulus	Conductive or Piezoelectric Material	Maximum Conductivity/ Resistivity	Bio-compatible
13.	Effect of Small Additions of Carbon Nanotubes on the Electrical Conductivity of Polyurethane Elastomer[16]	Polyurethane		≤30 MPa	Single wall carbon nanotubes	Varies based on carbon concentration/ temperature	
14.	Fabrication and Evaluation of the Novel Elastomer Based Nanocomposite with Pressure Sensing Function[17]	Silicone	≤200%		Carbon-Silica	$1.62 \cdot 10^{-1}$ to $5 \cdot 10^{14}\ \Omega \cdot$ cm	
15.	Electroconductive Composites from Polystyrene Block Copolymers and Cu–Alumina Filler[18]	Polystyrene block copolymers	17%	50 - 150 MPa	Cu–Al_2O_3	$4.35 \cdot 10^{-16}$ to $7.7 \cdot 10^{-5}$ S/cm	
16.	Hybrid Nanocomposites of Thermoplastic Elastomer and Carbon Nanoadditives for Electromagnetic Shielding[19]	Poly (styrene-*b*-ethylene-ran-butylene-*b*-styrene)			Graphene nanoplatelets and carbon nanotubes	$1.2 \cdot 10^{-17}$ to 2.2 S/cm	
17.	Continuously Producible Ultrasensitive Wearable Strain Sensor Assembled with Three-Dimensional Interpenetrating Ag Nanowires/Polyolefin Elastomer Nanofibrous Composite Yarn[20]	Polyolefin elastomer nanofibrous yarn	~575%	No change in modulus after nanowire addition	Ag nanowires	10 Ω	
18.	Design and Fabrication of Soft Artificial Skin Using Embedded Microchannels and Liquid Conductors[21]	Silicone rubber	Failure begins at 250%	63 kPa	Eutectic gallium-indium	2.5 – 3.1 Ω at rest	
19.	Polyisoprene-Nanostructured Carbon Composite – A Soft Alternative for Pressure Sensor Application[22]	Polyisoprene			Carbon black	10^5 to $10^{-1}\ \Omega \cdot$ m	
20.	Conductivity and Mechanical Properties of Composites Based on MWCNTs and Styrene-Butadiene-Styrene Block™ Copolymers[23]	Styrene-butadiene-styrene		16.3 – 94.1 MPa	Multiwall carbon nanotubes	10^{-4} to 1.6 S/cm	
21.	Carbon Nanotube-Coated Silicone as a Flexible and Electrically Conductive Biomedical Material[24]	Silicone	Tested up to 20%		Single and multiwall carbon nanotubes	0.86 to 1.5×10^3 kΩ/sq	Yes
22.	Electrically Conducting Polyaniline-PBMA Composite Films Obtained by Extrusion[25]	Poly(*n*-butyl methacrylate) - polyaniline			Doped with dodecyl-benzene sulfonic acid	$2 \cdot 10^{-2}$ - $1 \cdot 10^{-9}$ S/cm	
23.	Electro-Conductive Sensors and Heating Elements Based on Conductive Polymer Composites[26]	Cotton yarn; polyethylene; polyamide; latex			Carbon black	0.1 - 3.6 kΩ · cm; varies based on carbon content	
24.	Electrical Properties of Flexible Pressure Sensitive Chezacarb/Silicone Rubber Nanocomposites[27]	Silicone/PDMS			Carbon black and natural graphite	10^3 - $10^5\ \Omega \cdot$ m	
25.	Carbon Nanotube-Based Thermoplastic Polyurethane-Poly(methyl Methacrylate) Nanocomposites for Pressure Sensing Applications[28]	Polyurethane-poly(methyl methacrylate)			Multiwalled carbon nanotubes		

Table 1.2: A Summary of Electroconductive and/or Pressure-Sensitive Elastomer Constructs (Part 3/4)

	Study	Polymer	Maximum Functional or at Break Elongation	Storage or Young's Modulus	Conductive or Piezoelectric Material	Maximum Conductivity/ Resistivity	Bio-compatible
26.	Single-Walled Carbon Nanotube/Silicone Rubber Composites for Compliant Electrodes[29]	Silicone	Tested up to 300%	0.399 -4.6 MPa	Single walled carbon nanotubes; ionic liquid	18 - 63 S/cm	
27.	Development of a Regenerative Peripheral Nerve Interface for Control of a Neuroprosthetic Limb[30]	Silicone			PEDOT		Yes
28.	Electrical, Mechanical and Piezo-Resistive Behaviour of a Polyaniline/Poly(*n*-butyl Methacrylate) Composite[31]	Polyaniline-poly(*n*-butyl methacrylate)	50 - 250%	60 - 140 MPa	Doped with n-dodecyl-benzene-sulfonic acid	$10^3 – 10^9\ \Omega$ /sq	
29.	A Conductive Composite Nanomaterial with Biocompatible Matrix and Multilayer Carbon Nanotubes[32]	Carboxy-methylcellulose matrix and flexible polymers			Multiwall carbon nanotubes	~1.2 - $4 \cdot 10^4$ S/m	Yes
30.	Piezoresistive Behavior Study on Finger-Sensing Silicone Rubber/Graphite Nanosheet Nanocomposites[33]	Silicone rubber			Graphite nanosheets	Piezoresistive under low pressure	
31.	Silicone Substrate with Collagen and Carbon Nanotubes Exposed to Pulsed Current for MSC Osteodifferentiation[34]	PDMS, Silicone			Carbon nanotubes	760 – 827 Ω	Yes
32.	An Ultra-Sensitive Resistive Pressure Sensor Based on Hollow-Sphere Microstructure Induced Elasticity in Conducting Polymer Film.[35]	Polypyrrole		Low elastic modulus changing with compression	Doped with phytic acid	0.5 S/cm	
33.	Electrical Properties of PPy-Coated Conductive Fabrics for Human Joint Motion Monitoring[36]	Polypyrrole	Tested up to 25%		Doped with 97% Anthraquinone-2-sulfonic acid sodium salt Monohydrate; oxidized with 98% iron(III) chloride (FeCl3) hexahydrate	0.67- 3.83 kΩ	
34.	A Supramolecular Biomimetic Skin Combining a Wide Spectrum of Mechanical Properties and Multiple Sensory Capabilities[37]	Acrylic acid and 3-dimethyl (methacryloyl oxyethyl) ammonium propane sulfonate	10,000%	≤ 5 KPa		$\geq 2 \cdot 10^{-5}$ S/cm	
35.	Strain and Damage Monitoring in SBR Nanocomposites Under Cyclic Loading[38]	Styrene-Butadiene Rubber	≥ 300%	1.5 - 12.8 MPa	Carbon black and carbon nanotubes	10^{-2} - 10^{-15} S/cm	

Table 1.2: A Summary of Electroconductive and/or Pressure-Sensitive Elastomer Constructs (Part 4/4)

	Study	Polymer	Maximum Functional or at Break Elongation	Storage or Young's Modulus	Conductive or Piezoelectric Material	Maximum Conductivity/ Resistivity	Bio-compatible
36.	Simple and Cost-Effective Method of Highly Conductive and Elastic Carbon Nanotube/Polydimethylsiloxane Composite for Wearable Electronics[39]	PDMS	25 - 110%	2 - 4 MPa	Carbon nanotubes	2.03 - 5225 Ω /sq	Yes
37.	Enhanced Electrical Conductivity and Mechanical Property of SBS/Graphene Nanocomposite[40]	Styrene-butadiene-styrene		10.5 -23.8 MPa	Graphene oxide	10^{-12} to 1.64 · 10^{-2} S/m	
38.	Synthesis and Characterization of Conductive, Biodegradable, Elastomeric Polyurethanes for Biomedical Applications[41]	Conductive Polyurethane	75 - 728%	3.1 - 17.9 MPa	Doped with camphor-sulfonic acid	$2.7 \cdot 10^{-10}$ - $7.3 \cdot 10^{-5}$ S/cm	Yes
39.	Electronic Properties of Transparent Conductive Films of PEDOT:PSS on Stretchable Substrates[42]	PDMS	30 - 200%		PEDOT:PSS	100 - 550 S/cm	
40.	3D-Stacked Carbon Composites Employing Networked Electrical Intra-Pathways for Direct-Printable, Extremely Stretchable Conductors[43]	Polystyrene–poly isoprene-polystyrene	Assessed up to 300%	2.1 KPa	Ni nano-particles and reduced graphene oxide	2.1 - 6 S/cm	
41.	Highly Sensitive, Stretchable, and Wash-Durable Strain Sensor Based on Ultrathin Conductive Layer@Polyurethane Yarn for Tiny Motion Monitoring[44]	Polyurethane			Carbon black	≤ 6.04 S/cm	
42.	Patterned, Highly Stretchable and Conductive Nanofibrous PANI/PVDF Strain Sensors Based on Electrospinning and *in situ* Polymerization[45]	Polyaniline	22% for recovery of strain; max of 110%		PVDF	Pressure-related conductivity	

1.4 References

1. Abraira, Victoria E., and David D. Ginty. "The sensory neurons of touch." *Neuron* 79.4 (2013): 618-639.
2. Gardner, E. P. "Touch. Encyclopedia of life sciences." (2010).
3. Ray, Partha Pratim. "Channel modeling of human somatosensory nanonetwork: Body discriminative touch and proprioception perspective." *arxiv preprint arxiv:1406.3693*(2014).
4. Georgiev, Nikola. "Study of two types of sensors of static forces-a piezoelectric sensor and a piezoelectric elastomer sensor." *Techsys 2017* (2017).
5. Greco, Francesco, et al. "Liquid single crystal elastomer/conducting polymer bilayer composite actuator: modelling and experiments." *Soft Matter* 9.47 (2013): 11405-11416.
6. Barkauskas, Jurgis, and Aušra Vinslovait. "Investigation of electroconductive films composed of polyvinyl alcohol and graphitized carbon black." *Materials research bulletin* 38.8 (2003): 1437-1447.
7. Latko, Paulina, Aleksandra Bogucka, and Anna Boczkowska. "Characterization of thermoplastic elastomers based composites doped with carbon black." *Int J Mech Eng Autom*2 (2015): 171-176.
8. Georgousis, G., et al. "Study of the reinforcing mechanism and strain sensing in a carbon black filled elastomer." *Composites Part B: Engineering* 80 (2015): 20-26.
9. Krajči, Juraj, Zdenko Špitálský, and Ivan Chodák. "Relationship between conductivity and stress–strain curve of electroconductive composite with SBR or polycaprolactone matrices." *European Polymer Journal* 55 (2014): 135-143.
10. Chen, Jing, et al. "Super stretchable electroactive elastomer formation driven by aniline trimer self-assembly." *Chemistry of Materials* 27.16 (2015): 5668-5677.
11. Al-Ghamdi, Ahmed A., et al. "Dielectric and microwave properties of elastomer composites loaded with carbon–silica hybrid fillers." *Journal of Applied Polymer Science* 133.7 (2016).
12. Bayer, Ilker S., Adam Steele, and Eric Loth. "Superhydrophobic and electroconductive carbon nanotube-fluorinated acrylic copolymer nanocomposites from emulsions." *Chemical engineering journal* 221 (2013): 522-530.
13. Agrawal, Aditya, et al. "Electromechanically Responsive Liquid Crystal Elastomer Nanocomposites for Active Cell Culture." *ACS Macro Letters* 5.12 (2016): 1386-1390.
14. Xiong, Yuanqin, et al. "Reduced graphene oxide/hydroxylated styrene–butadiene–styrene tri-block copolymer electroconductive nanocomposites: Preparation and properties." *Materials Science and Engineering: B* 177.14 (2012): 1163-1169.
15. Hu, Juan, et al. "Simultaneous improvement in both electrical conductivity and toughness of polyamide 6 nanocomposites filled with elastomer and carbon black particles." *Industrial & Engineering Chemistry Research* 53.6 (2014): 2270-2276.
16. Novikov, G. F., et al. "Effect of small additions of carbon nanotubes on the electrical conductivity of polyurethane elastomer." *Russian Journal of Physical Chemistry A* 88.10 (2014): 1790-1794.
17. Han, Youn Gyu, et al. "Fabrication and evaluation of the novel elastomer based nanocomposite with pressure sensing function." *Materials science forum*. Vol. 544. Trans Tech Publications, 2007.
18. Nadeem, QuratulAin, et al. "Electroconductive Composites from Polystyrene Block Copolymers and Cu–Alumina Filler." *Materials* 9.12 (2016): 989.

19. Kuester, Scheyla, et al. "Hybrid nanocomposites of thermoplastic elastomer and carbon nanoadditives for electromagnetic shielding." *European Polymer Journal* 88 (2017): 328-339.
20. Zhong, Weibing, et al. "Continuously Producible Ultrasensitive Wearable Strain Sensor Assembled with Three-Dimensional Interpenetrating Ag Nanowires/Polyolefin Elastomer Nanofibrous Composite Yarn." *ACS applied materials & interfaces* 9.48 (2017): 42058-42066.
21. Park, Yong-Lae, Bor-Rong Chen, and Robert J. Wood. "Design and fabrication of soft artificial skin using embedded microchannels and liquid conductors." *IEEE Sensors Journal*12.8 (2012): 2711-2718.
22. Zavickis, Juris, et al. "Polyisoprene-nanostructured carbon composite–A soft alternative for pressure sensor application." *Sensors and Actuators A: Physical* 171.1 (2011): 38-42.
23. Pedroni, Lucas G., et al. "Conductivity and mechanical properties of composites based on MWCNTs and styrene-butadiene-styrene block™ copolymers." *Journal of applied polymer science* 112.6 (2009): 3241-3248.
24. Matsuoka, Makoto, et al. "Carbon nanotube-coated silicone as a flexible and electrically conductive biomedical material." *Materials Science and Engineering: C* 32.3 (2012): 574-580.
25. Castillo-Ortega, M. M., et al. "Electrically conducting polyaniline-PBMA composite films obtained by extrusion." *Journal of applied polymer science* 89.1 (2003): 179-183.
26. Koncar, V., et al. "Electro-conductive sensors and heating elements based on conductive polymer composites." *International Journal of Clothing Science and Technology*21.2/3 (2009): 82-92.
27. Zevri, L., et al. "Electrical properties of flexible pressure sensitive chezacarb/silicone rubber nanocomposites." *Nanoscience and nanotechnology*, 13 (2013)
28. Imran, Syed Muhammad, et al. "Carbon nanotube-based thermoplastic polyurethane-poly (methyl methacrylate) nanocomposites for pressure sensing applications." *Polymer Engineering & Science* 56.9 (2016): 1031-1036.
29. Kim, Tae Ann, et al. "Single-walled carbon nanotube/silicone rubber composites for compliant electrodes." *Carbon* 50.2 (2012): 444-449.
30. Urbanchek, Melanie G., et al. "Development of a regenerative peripheral nerve interface for control of a neuroprosthetic limb." *BioMed Research International* 2016 (2016).
31. Del Castillo-Castro, T., M. M. Castillo-Ortega, and P. J. Herrera-Franco. "Electrical, mechanical and piezo-resistive behavior of a polyaniline/poly (n-butyl methacrylate) composite." *Composites Part A: Applied Science and Manufacturing* 40.10 (2009): 1573-1579.
32. Ichkitidze, L. P., et al. "A Conductive Composite Nanomaterial with Biocompatible Matrix and Multilayer Carbon Nanotubes." *Biomedical Engineering* 47.2 (2013): 68-72.
33. Chen, Ling, G. H. Chen, and Liang Lu. "Piezoresistive behavior study on finger-sensing silicone rubber/graphite nanosheet nanocomposites." *Advanced Functional Materials*17.6 (2007): 898-904.
34. Jamal, Daniyal, and Roche C. de Guzman. "Silicone substrate with collagen and carbon nanotubes exposed to pulsed current for MSC osteodifferentiation." *International journal of biomaterials* 2017 (2017).
35. Pan, Lijia, et al. "An ultra-sensitive resistive pressure sensor based on hollow-sphere microstructure induced elasticity in conducting polymer film." *Nature communications* 5 (2014): 3002.

36. Jiyong, Hu, et al. "Electrical properties of PPy-coated conductive fabrics for human joint motion monitoring." *Autex Research Journal* 16.1 (2016): 7-12.
37. Lei, Zhouyue, and Peiyi Wu. "A supramolecular biomimetic skin combining a wide spectrum of mechanical properties and multiple sensory capabilities." *Nature communications* 9.1 (2018): 1134.
38. Georgousis, G., et al. "Strain and damage monitoring in SBR nanocomposites under cyclic loading." *Composites Part B: Engineering* 131 (2017): 50-61.
39. Kim, Jeong Hun, et al. "Simple and cost-effective method of highly conductive and elastic carbon nanotube/polydimethylsiloxane composite for wearable electronics." *Scientific reports* 8.1 (2018): 1375.
40. Li, Hui, et al. "Enhanced electrical conductivity and mechanical property of SBS/graphene nanocomposite." *Journal of Polymer Research* 21.5 (2014): 456.
41. Xu, Cancan, et al. "Synthesis and characterization of conductive, biodegradable, elastomeric polyurethanes for biomedical applications." *Journal of Biomedical Materials Research Part A* 104.9 (2016): 2305-2314.
42. Lipomi, Darren J., et al. "Electronic properties of transparent conductive films of PEDOT: PSS on stretchable substrates." *Chemistry of Materials* 24.2 (2012): 373-382.
43. Chae, Changju, et al. "3D-Stacked Carbon Composites Employing Networked Electrical Intra-Pathways for Direct-Printable, Extremely Stretchable Conductors." *ACS applied materials &interfaces* 7.7 (2015): 4109-4117.
44. Wu, Xiaodong, et al. "Highly sensitive, stretchable, and wash-durable strain sensor based on ultrathin conductive layer@ polyurethane yarn for tiny motion monitoring." *ACS applied materials & interfaces* 8.15 (2016): 9936-9945.
45. Yu, Gui-Feng, et al. "Patterned, highly stretchable and conductive nanofibrous PANI/PVDF strain sensors based on electrospinning and in situ polymerization." *Nanoscale* 8.5 (2016): 2944-2950.
46. Ray, Dipa, ed. *Biocomposites for High-Performance Applications: Current Barriers and Future Needs Towards Industrial Development*. Woodhead Publishing, 2017.
47. Concannon, Matthew J. "Tendon and Nerve Surgery in the Hand: A Third Decade." *Plastic and Reconstructive Surgery*102.3 (1998): 916.
48. Busse, Daniela, et al. "A synthetic sandalwood odorant induces wound-healing processes in human keratinocytes via the olfactory receptor OR2AT4." *Journal of investigative dermatology* 134.11 (2014): 2823-2832.
49. Denda, Mitsuhiro, et al. "Epidermal keratinocytes as the forefront of the sensory system." *Experimental dermatology*16.3 (2007): 157-161.
50. Ang, Gina C. "History of skin transplantation." *Clinics in Dermatology* 23.4 (2005): 320-324.
51. Hauben, Daniel Joseph, A. Baruchin, and A. Mahler. "On the histroy of the free skin graft." *Annals of plastic surgery* 9.3 (1982): 242-245.
52. Hauben, Daniel Joseph, A. Baruchin, and A. Mahler. "On the histroy of the free skin graft." *Annals of plastic surgery* 9.3 (1982): 242-245.
53. Alolabi, Noor, Haley Augustine, and Achilles Thoma. "Hand transplantation&58; current challenges and future prospects." *Transplant Research and Risk Management* 55.1 (2016): 23-29.

54. Jones, Jon W., et al. "Successful hand transplantation—one-year follow-up." *New England Journal of Medicine* 343.7 (2000): 468-473.
55. Shores, Jaimie T. "Recipient screening and selection: who is the right candidate for hand transplantation." *Hand clinics* 27.4 (2011): 539-543.
56. Amirlak, Bardia, et al. "Creating a hand transplant program." *Clinics in plastic surgery* 34.2 (2007): 279-289.
57. Bueno, Ericka, et al. "Rehabilitation following hand transplantation." *Hand* 9.1 (2014): 9-15.
58. Juma, A., D. Oudit, and M. Ellabban. "Patterns of sensory and autonomic reinnervation of long-standing myocutaneous microvascular flaps and split-skin grafts applied to fascial beds." *Canadian Journal of Plastic Surgery* 13.1 (2005): 16-22.
59. English, Kathleen B., et al. "Functional innervation of cultured skin grafts." *Journal of investigative dermatology* 99.2 (1992).
60. Raspopovic, Stanisa, et al. "Restoring natural sensory feedback in real-time bidirectional hand prostheses." *Science translational medicine* 6.222 (2014): 222ra19-222ra19.
61. Ortiz-Catalan, Max, Bo Håkansson, and Rickard Brånemark. "An osseointegrated human-machine gateway for long-term sensory feedback and motor control of artificial limbs." *Science translational medicine* 6.257 (2014): 257re6-257re6.
62. Dhillon, G. S., et al. "Effects of short-term training on sensory and motor function in severed nerves of long-term human amputees." *Journal of neurophysiology* 93.5 (2005): 2625-2633.
63. Tan, Daniel W., et al. "A neural interface provides long-term stable natural touch perception." *Science translational medicine* 6.257 (2014): 257ra138-257ra138.
64. Burke, John F., et al. "Successful use of a physiologically acceptable artificial skin in the treatment of extensive burn injury." *Annals of surgery* 194.4 (1981): 413.
65. Gravante, G., et al. "A randomized trial comparing ReCell® system of epidermal cells delivery versus classic skin grafts for the treatment of deep partial thickness burns." *Burns* 33.8 (2007): 966-972.
66. Plettig, Jörn, et al. "Active wound dressing with artificial capillaries for temporary wound irrigation and skin cell supply." *Artificial organs* 36.4 (2012): 446-449.
67. Lumelsky, Vladimir J., Michael S. Shur, and Sigurd Wagner. "Sensitive skin." *IEEE Sensors Journal* 1.1 (2001): 41-51.
68. Kim, Jaemin, et al. "Stretchable silicon nanoribbon electronics for skin prosthesis." *Nature communications* 5 (2014): 5747.
69. Wu, Wenzhuo, Xiaonan Wen, and Zhong Lin Wang. "Taxel-addressable matrix of vertical-nanowire piezotronic transistors for active/adaptive tactile imaging." *Science* (2013): 1234855.
70. Someya, Takao, et al. "Conformable, flexible, large-area networks of pressure and thermal sensors with organic transistor active matrixes." *Proceedings of the National Academy of Sciences* 102.35 (2005): 12321-12325.
71. Trung, Tran Quang, et al. "Transparent and flexible organic field-effect transistor for multi-modal sensing." *Organic Electronics* 13.4 (2012): 533-540.

72. Graz, Ingrid, et al. "Flexible active-matrix cells with selectively poled bifunctional polymer-ceramic nanocomposite for pressure and temperature sensing skin." *Journal of Applied Physics* 106.3 (2009): 034503.
73. Di Giacomo, Raffaele, et al. "Biomimetic temperature sensing layer for artificial skins." *arXiv preprint arXiv:1512.01161*(2015).
74. Tee, Benjamin CK, et al. "An electrically and mechanically self-healing composite with pressure-and flexion-sensitive properties for electronic skin applications." *Nature nanotechnology* 7.12 (2012): 825.
75. Hammock, Mallory L., et al. "25th anniversary article: the evolution of electronic skin (e-skin): a brief history, design considerations, and recent progress." *Advanced materials* 25.42 (2013): 5997-6038.
76. Xu, Sheng, et al. "Stretchable batteries with self-similar serpentine interconnects and integrated wireless recharging systems." *Nature communications* 4 (2013): 1543.
77. Jeon, Jin, Han-Bo-Ram Lee, and Zhenan Bao. "Flexible wireless temperature sensors based on Ni microparticle-filled binary polymer composites." *Advanced Materials* 25.6 (2013): 850-855.
78. Mannsfeld, Stefan CB, et al. "Highly sensitive flexible pressure sensors with microstructured rubber dielectric layers." *Nature materials* 9.10 (2010): 859.
79. Craig, A. D. "Interoception: the sense of the physiological condition of the body." *Current opinion in neurobiology* 13.4 (2003): 500-505.
80. Proske, Uwe, and Simon C. Gandevia. "The proprioceptive senses: their roles in signaling body shape, body position and movement, and muscle force." *Physiological reviews* 92.4 (2012): 1651-1697.
81. Muscolino, J. E. "kinesiology: The skeletal system and muscle function, Mosby Elsevier, St." (2006).
82. Cox, James J., et al. "An SCN9A channelopathy causes congenital inability to experience pain." *Nature* 444.7121 (2006): 894.
83. Smith, Jonathan K., et al. "Ethical considerations in elective amputation after traumatic peripheral nerve injuries." *Neurology: Clinical Practice* 4.4 (2014): 280-286.
84. Beekwilder, J. P., and T. Beems. "Overview of the clinical applications of vagus nerve stimulation." *Journal of clinical neurophysiology* 27.2 (2010): 130-138.
85. Fried, Itzhak. "Brain stimulation in Alzheimer's disease." *Journal of Alzheimer's Disease* 54.2 (2016): 789-791.
86. Barbanti, Piero, et al. "Non-invasive vagus nerve stimulation for acute treatment of high-frequency and chronic migraine: an open-label study." *The journal of headache and pain* 16.1 (2015): 61.
87. Thakral, Gaurav, et al. "Electrical stimulation to accelerate wound healing." *Diabetic foot & ankle* 4.1 (2013): 22081.
88. Gater Jr, David R., et al. "Functional electrical stimulation therapies after spinal cord injury." *NeuroRehabilitation* 28.3 (2011): 231-248.
89. Stocum, David L., and Jo Ann Cameron. "Looking proximally and distally: 100 years of limb regeneration and beyond." *Developmental Dynamics* 240.5 (2011): 943-968.
90. Yun, Maximina H., Phillip B. Gates, and Jeremy P. Brockes. "Regulation of p53 is critical for vertebrate limb regeneration." *Proceedings of the National Academy of Sciences* (2013): 201310519.

91. Godwin, James W., Alexander R. Pinto, and Nadia A. Rosenthal. "Macrophages are required for adult salamander limb regeneration." *Proceedings of the National Academy of Sciences* 110.23 (2013): 9415-9420.
92. Becker, Robert O., and Joseph A. Spadaro. "Electrical stimulation of partial limb regeneration in mammals." *Bulletin of the New York Academy of Medicine* 48.4 (1972): 627.
93. Li, Chunyi, et al. "Deer antler–a novel model for studying organ regeneration in mammals." *The international journal of biochemistry & cell biology* 56 (2014): 111-122.
94. Tai, Guangping, Michael Tai, and Min Zhao. "Electrically stimulated cell migration and its contribution to wound healing." *Burns & trauma* 6.1 (2018): 20.
95. Zhao M, Pu J, Forrester JV, McCaig CD. Membrane lipids, EGF receptors, and intracellular signals co-localize and are polarized in epithelial cells moving directionally in a physiological electric field. FASEB J. 2002;16:857–9.
96. Fang KS, Ionides E, Oster G, Nuccitelli R, Isseroff RR. Epidermal growth factor receptor relocalization and kinase activity are necessary for directional migration of keratinocytes in DC electric fields. J Cell Sci. 1999;112:1967–78.
97. Kloth, Luther C., and Jeffrey A. Feedar. "Acceleration of wound healing with high voltage, monophasic, pulsed current." *Physical Therapy* 68.4 (1988): 503-508.
98. Feedar, Jeffrey A., Luther C. Kloth, and Gary D. Gentzkow. "Chronic dermal ulcer healing enhanced with monophasic pulsed electrical stimulation." *Physical Therapy* 71.9 (1991): 639-649.
99. Kloth, Luther C. "Electrical stimulation for wound healing: a review of evidence from in vitro studies, animal experiments, and clinical trials." *The international journal of lower extremity wounds* 4.1 (2005): 23-44
100. Nair, Harikrishna KR. "Microcurrent as an adjunct therapy to accelerate chronic wound healing and reduce patient pain." Journal of wound care 27.5 (2018): 296-306.
101. Kim, Hosan, et al. "An overview of the efficacy of a next generation electroceutical wound care device." *Military medicine* 181.suppl_5 (2016): 184-190.
102. Clegg, John P., and Julian F. Guest. "Modelling the cost-utility of bio-electric stimulation therapy compared to standard care in the treatment of elderly patients with chronic non-healing wounds in the UK." *Current medical research and opinion* 23.4 (2007): 871-883.
103. Wirsing, Peter G., et al. "Wireless micro current stimulation–an innovative electrical stimulation method for the treatment of patients with leg and diabetic foot ulcers." *International wound journal* 12.6 (2015): 693-698.
104. Deer, Timothy R., et al. "International neuromodulation society critical assessment: guideline review of implantable neurostimulation devices." *Neuromodulation: Technology at the Neural Interface* 17.7 (2014): 678-685.
105. Charleston, W. V., et al. "Intracranial neurostimulation for pain control: a review." *Pain Physician* 13 (2010): 157-165.
106. Davis, Nick J., and Martijn Van Koningsbruggen. "'"Non-invasive" brain stimulation is not non-invasive." *Frontiers in systems neuroscience* 7 (2013): 76.

107. Chang, Chun-Hung, Hsien-Yuan Lane, and Chieh-Hsin Lin. "Brain Stimulation in Alzheimer's Disease." *Frontiers in psychiatry* 9 (2018): 201.
108. Sabbah, Hani N. "Electrical vagus nerve stimulation for the treatment of chronic heart failure." *Cleveland Clinic journal of medicine* 78.0 1 (2011).
109. Ogbonnaya, Sunny, and Chandrasekaran Kaliaperumal. "Vagal nerve stimulator: evolving trends." *Journal of natural science, biology, and medicine* 4.1 (2013): 8.
110. Uthman, B. M., et al. "Effectiveness of vagus nerve stimulation in epilepsy patients A 12-year observation." *Neurology* 63.6 (2004): 1124-1126.
111. Beekwilder, J. P., and T. Beems. "Overview of the clinical applications of vagus nerve stimulation." *Journal of clinical neurophysiology* 27.2 (2010): 130-138.
112. Nesbitt, Alexander D., et al. "Initial use of a novel noninvasive vagus nerve stimulator for cluster headache treatment." *Neurology* 84.12 (2015): 1249-1253.
113. Fried, Itzhak. "Brain stimulation in Alzheimer's disease." *Journal of Alzheimer's Disease* 54.2 (2016): 789-791.
114. Bonaz, Bruno. "Is-there a place for vagus nerve stimulation in inflammatory bowel diseases?." *Bioelectronic Medicine*4.1 (2018): 4.
115. Kirchner, A., et al. "Left vagus nerve stimulation suppresses experimentally induced pain." *Neurology* 55.8 (2000): 1167-1171.
116. Moens, Maarten, et al. "Return to Work of Patients Treated With Spinal Cord Stimulation for Chronic Pain: A Systematic Review and Meta-Analysis." *Neuromodulation: Technology at the Neural Interface* (2018).
117. Grahn, Peter J., et al. "Enabling task-specific volitional motor functions via spinal cord neuromodulation in a human with paraplegia." *Mayo Clinic Proceedings*. Vol. 92. No. 4. Elsevier, 2017.
118. Tronstad, Christian, et al. "A study on electrode gels for skin conductance measurements." *Physiological measurement* 31.10 (2010): 1395.
119. Cogan, Stuart F. "Neural stimulation and recording electrodes." *Annu. Rev. Biomed. Eng.* 10 (2008): 275-309.
120. Clippinger, Frank W. "A sensory feedback system for an upper-limb amputation prosthesis." *Bulletin of Pusthetics Research Fall 1974* (1974): 247-258.
121. Dhillon, G. S., et al. "Effects of short-term training on sensory and motor function in severed nerves of long-term human amputees." *Journal of neurophysiology* 93.5 (2005): 2625-2633.
122. Iijima, Sumio. "Helical microtubules of graphitic carbon." nature 354.6348 (1991): 56.
123. Lu, Fushen, et al. "Advances in bioapplications of carbon nanotubes." Advanced Materials 21.2 (2009): 139-152.
124. Keefer, Edward W., et al. "Carbon nanotube coating improves neuronal recordings." Nature nanotechnology 3.7 (2008): 434.
125. Wang, Ke, et al. "Neural stimulation with a carbon nanotube microelectrode array." *Nano letters* 6.9 (2006): 2043-2048.
126. Li, Jing, et al. "Correlations between percolation threshold, dispersion state, and aspect ratio of carbon nanotubes." Advanced Functional Materials 17.16 (2007): 3207-3215.

127. Zeng, Xiaomei, et al. "Characteristics of the electrical percolation in carbon nanotubes/polymer nanocomposites." The Journal of Physical Chemistry C 115.44 (2011): 21685-21690.
128. Keefer, Edward W., et al. "Carbon nanotube coating improves neuronal recordings." Nature nanotechnology 3.7 (2008): 434.
129. Matsumoto, K., et al. "Stimulation of neuronal neurite outgrowth using functionalized carbon nanotubes." Nanotechnology 21.11 (2010): 115101.
130. Mattson, Mark P., Robert C. Haddon, and Apparao M. Rao. "Molecular functionalization of carbon nanotubes and use as substrates for neuronal growth." Journal of Molecular Neuroscience 14.3 (2000): 175-182.
131. Hu, Hui, et al. "Polyethyleneimine functionalized single-walled carbon nanotubes as a substrate for neuronal growth." The Journal of Physical Chemistry B 109.10 (2005): 4285-4289.
132. Hu, Hui, et al. "Chemically functionalized carbon nanotubes as substrates for neuronal growth." Nano letters 4.3 (2004): 507-511.
133. Porter, Alexandra E., et al. "Direct imaging of single-walled carbon nanotubes in cells." Nature nanotechnology 2.11 (2007): 713.
134. Lacerda, Lara, et al. "Carbon nanotubes as nanomedicines: from toxicology to pharmacology." Advanced drug delivery reviews 58.14 (2006): 1460-1470.
135. Patlolla, Anita, Brionna Knighten, and Paul Tchounwou. "Multi-walled carbon nanotubes induce cytotoxicity, genotoxicity and apoptosis in normal human dermal fibroblast cells." Ethnicity & disease 20.1 Suppl 1 (2010): S1.
136. Xiao, Yinghong, et al. "Electrochemical polymerization of poly (hydroxymethylated-3, 4-ethylenedioxythiophene)(PEDOT-MeOH) on multichannel neural probes." Sensors and Actuators B: Chemical 99.2-3 (2004): 437-443.
137. Abidian, Mohammad Reza, et al. "Interfacing conducting polymer nanotubes with the central nervous system: chronic neural recording using poly (3, 4-ethylenedioxythiophene) nanotubes." *Advanced Materials*21.37 (2009): 3764-3770.
138. Cui, Xinyan, and David C. Martin. "Electrochemical deposition and characterization of poly (3, 4-ethylenedioxythiophene) on neural microelectrode arrays." Sensors and Actuators B: Chemical 89.1-2 (2003): 92-102.
139. Richardson-Burns, Sarah M., et al. "Polymerization of the conducting polymer poly (3, 4-ethylenedioxythiophene)(PEDOT) around living neural cells." Biomaterials 28.8 (2007): 1539-1552.
140. Pires, Filipa, et al. "Neural stem cell differentiation by electrical stimulation using a cross-linked PEDOT substrate: expanding the use of biocompatible conjugated conductive polymers for neural tissue engineering." Biochimica et Biophysica Acta (BBA)-General Subjects 1850.6 (2015): 1158-1168.
141. Luo, Xiliang, et al. "Highly stable carbon nanotube doped poly (3, 4-ethylenedioxythiophene) for chronic neural stimulation." Biomaterials 32.24 (2011): 5551-5557.
142. Lu, Yi, et al. "Electrodeposited polypyrrole/carbon nanotubes composite films electrodes for neural interfaces." Biomaterials 31.19 (2010): 5169-5181.
143. Collazos-Castro, Jorge E., et al. "Bioelectrochemical control of neural cell development on conducting polymers." Biomaterials 31.35 (2010): 9244-9255.

144. Asplund, Maria, Tobias Nyberg, and Olle Inganäs. "Electroactive polymers for neural interfaces." Polymer Chemistry 1.9 (2010): 1374-1391.
145. Yang, Junyan, and David C. Martin. "Microporous conducting polymers on neural microelectrode arrays: I Electrochemical deposition." *Sensors and actuators B: Chemical* 101.1-2 (2004): 133-142.
146. Major, Ian, Evert Fuenmayor, and Christopher McConville. "The production of solid dosage forms from non-degradable polymers." *Current pharmaceutical design* 22.19 (2016): 2738-2760.
147. Yu, Betty, et al. "An elastic second skin." *Nature materials*15.8 (2016): 911.
148. Choi, Won Mook, et al. "Biaxially stretchable "wavy" silicon nanomembranes." *Nano Letters* 7.6 (2007): 1655-1663.
149. Chortos, Alex, Jia Liu, and Zhenan Bao. "Pursuing prosthetic electronic skin." *Nature materials* 15.9 (2016): 937.
150. Yannas, I. V., et al. "Progress in design of an artificial skin." *Federation Proceedings*. Vol. 38. No. 3. 9650 Rockville Pike, Bethesda, Md 20814-3998: Federation Amer Soc Exp Biol, 1979.
151. Chua, Alvin Wen Choong, et al. "Skin tissue engineering advances in severe burns: review and therapeutic applications." *Burns & trauma* 4.1 (2016): 3.
152. Cheshire, Perdita A., et al. "Artificial dermal templates: A comparative study of NovoSorb™ Biodegradable Temporising Matrix (BTM) and Integra® Dermal Regeneration Template (DRT)." *Burns* 42.5 (2016): 1088-1096.
153. Abu-Faraj, Ziad O., ed. *Handbook of research on biomedical engineering education and advanced bioengineering learning: interdisciplinary concepts: interdisciplinary concepts*. Vol. 2. IGI Global, 2012.
154. Gwent Group: Advanced Material Systems, "Overview of the range of our Products" http://www.gwent.org/gem_paste_overview.html
155. Cunha-Silva, Hugo, and M. Julia Arcos-Martinez. "Development of a selective chloride sensing platform using a screen-printed platinum electrode." *Talanta* 195 (2019): 771-777.
156. Gómez-Mingot, Maria, et al. "Electrochemical devices for monitoring biomarkers in embryo development." *Electrochimica Acta* 140 (2014): 42-48.
157. Kašpárková, Věra, et al. "Exploring the Critical Factors Limiting Polyaniline Biocompatibility." *Polymers* 11.2 (2019): 362.
158. Gestos, Adrian, et al. "Tensile testing of individual glassy, rubbery and hydrogel electrospun polymer nanofibres to high strain using the atomic force microscope." *Polymer Testing* 32.4 (2013): 655-664.
159. Choi, J. S., et al. "Hydrogel-impregnated dressings for graft fixation: a case series." *Journal of wound care* 24.7 (2015): 326-328.

CHAPTER 2.
MATERIALS AND METHODOLOGY

2.1. Outline

The materials in this section are separated by characteristic, then by methodology. Tables 2.1, 2.2, and 2.3 separate polymeric materials based on factors such as conjugation, conductivity and mechanical properties. Section 2.2.2 further elaborates on flexible polymers (some of which are conductive), while 2.2.3 expands on elastic polymers. Section 2.2.4 discusses electroconductive materials, while 2.2.5 expands on organic materials that were utilized.

Section 2.3 discusses the various methodologies used to process these polymers, including spin coating, drop casting, and electrospinning. Section 2.4 expands upon the electroconductive processes, such as electrodeposition and thermal evaporation. In Section 2.5, you can find the details on the creation of the complete, three-layered constructs.

In the following sections, 2.7 through 2.10, analyses of the individual polymers and the complete constructs are discussed. These include mechanical, conductivity, mechanoelectrical and piezoelectric analyses of the polymers. These sections are elaborated upon in Chapter 3 (mechanical), Chapter 4 (electrical conductivity, piezoelectric, and mechanoelectrical analyses), and Chapter 5 (cellular tests).

2.2. Polymers, Organic Materials, and Solvents

2.2.1 Selected Polymers and Solvents Used for Their Dissolution

Various polymers were selected for their established biocompatibility, flexibility/elasticity, and perdurable properties. Polymers and solvents used to prepare casting solutions for further electrospun meshes or films preparation are listed in Tables 2.2.1, 2.2.2, and 2.23. Details on casting solutions preparation are given on Sections 2.2.2 and 2.2.3, where polymers are grouped according withbeing described as a flexible or an elastic material.

Table 2.1: Conductive/Piezoelectric Polymers Assessed for Electrospinning

Polymer	Solvent	Young's Modulus	Notable Properties
Polyimide (PI)  Aromatic heterocyclic Linear	DMF DMAc	2.23-2.55 GPa [2]	Dielectric constant values (ε) range between 2.78 - 3.48; conductivity is easily modifiable.[3]
Poly Methyl Methacrylate (PMMA) 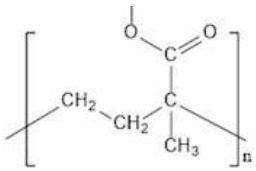	DMF DMAc DMF:Acetone Chloroform:DMF	Nanofiber: 136 MPa; Solid: 3 GPa[7]	10^{-11} S/cm[8]
Poly [(vinylidenefluoride) -co-trifluoro ethylene] 70:30 (P(VDF-TrFE)) 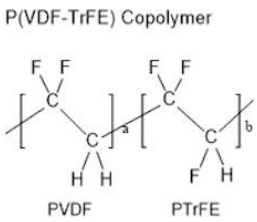	DMAC:Acetone DMF:Acetone	1.2 GPa[9]	Piezoelectric
Polyacrilonitrile (PAN) 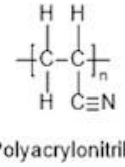	DMF	7.8-9.5 GPa[10]	Cross-linking or cyclization required for perdurability. Insulator unless treated [11, 12]
Polyvinyl Pyrrolidone (PVP) 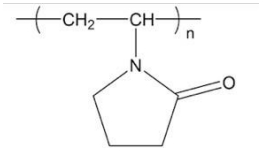	DMF Ethanol	2.433 GPa; value highly influenced by molecular weight.[13]	Insulating properties in large amounts; conductivity is primarily determined by thermal activation.

Table 2.2: Insulating Polymers Assessed for Electrospun Mesh Creation

Polymer	Solvent	Young's Modulus	Notable Properties
Polysulfone (PSu) 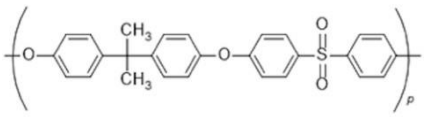	DMF THF DMAc:Acetone	1538.7 MPa[19]	Flexible Insulator; additional treatment required for perdurability.
Polyisoprene 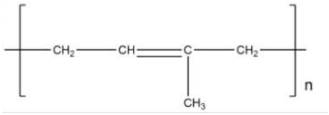	THF Chloroform	N/A (Liquid)	Elastic Insulator
Polybutadiene 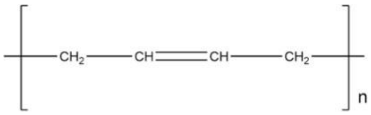	Toluene	1.2 MPa[15]	Elastic Insulator
Poly (styrene-isoprene-styrene) (SIS) 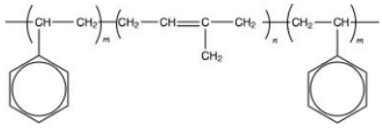	THF	21 MPa[17]	Elastic Insulator, Manufactured as Kraton D1161PT (SIS)
Poly (styrene-butadiene-styrene) (SBS) 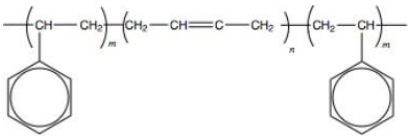	THF	32 MPa[17]	Elastic Insulator; Manufactured as Kraton D1152ES (SBS)
Poly (styrene-isobutylene-styrene) (SIBS) 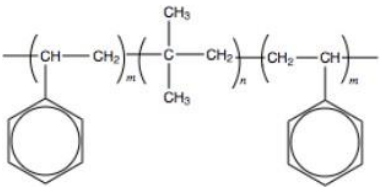	DMF THF Chloroform	0.044-0.181 GPa[18]	Elastic Insulator, Manufactured as Kaneka (SIBS)

Table 2.3: Conjugated Conductive Polymers

Polymer	Solvent	Perdurability Treatment Required?	Young's Modulus	Conductivity
Poly 3,4-ethylene dioxythiophene (PEDOT) + Polystyrene Sulfonate (PSS) 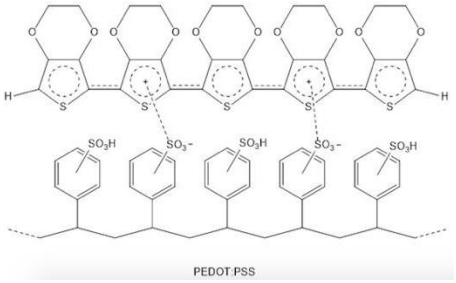	Water-based solvents	Crosslinking required	2 GPa[20]	Variable depending on heating, solvents, crosslinking, etc.[21]
Poly (3-hexylthiophene -2,5-diyl) (P3HT) 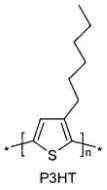	Chloroform	No	N/A (Liquid)	6.675×10^{-5} S/cm when not doped; 0.34 S/cm when doped.[22]
Polypyrrole (PPy) 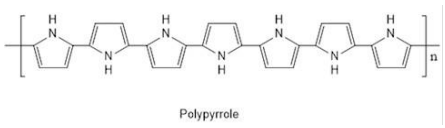	Chloroform m-Cresol	No	1.2 and 3.2 GPa[23]	1005 S/cm; influenced by mechanical stressors [24]

*See Table 2.1 for flexible conductive polymers (e.g., PAN and PI)

2.2.2 Flexible Polymers and Preparation of Casting Solutions

Polyimide (PI)

Polyimide (Evonik, Leizing P84) was mixed with DMF (Acros Organics) or Dimethylacetamide (DMAc) at concentrations between 10-20 wt% by dissolving the polymer in solutions overnight with the assistance of magnetic stir bars. Both planar sheets and electrospun fibres were created from this protocol. This polymer is further discussed in Ch. 3.

Poly(methyl methacrylate) (PMMA)

Poly(methyl methacrylate) (Sigma Alrich) was mixed at concentrations between 10-20 wt% with Tetrahydrofuran (THF) (Carlo Erba, Dasti Group Reagents SAS), DMF (Acros Organics), or THF:DMF and at a 1:1 ratio. In all cases, magnetic stir bars were used to create a homogenous solution. DMF was found the be the easiest solvent to work with, and electrospun

fibres and planar sheets were created from this protocol. This polymer is further discussed in Chapter 3.

Poly(vinylidenefluoride-co-trifluoroethylene) (P(VDF-TrFE))

Poly(vinylidenefluoride-co-trifluoroethylene), known as (P(VDF-TrFE)) (Piezotech-Arkema, 70:30 copolymer ratio) is a piezoelectric polymer. A total of 3.6g of P(VDF-TrFE) was dissolved in a mixture of 8.2mL Dimethylformamide (DMF) (Acros Organics), and 8.2 mL Acetone (Valente roberio.ida). The mixture was heated at 40^{o}C for 4 hours while mixed with a magnetic stir bar to make a homogenous solution. Both planar sheets and electrospun fibres were created from this protocol. This polymer is further discussed in Chapter 3.

Polyacrylonitrile (PAN)

Polyacrylonitrile (Sigma Aldrich) was created at a 6-15wt% range in DMF (Acros Organics). The solution was stirred overnight at room temperature, then heated the following day for 2-4 hours at 80^{o}C to improve solution homogeneity. Electrospun fibers were created from this protocol. This polymer is further discussed in Chapter 3.

Polyvinylpyrrolidone (PVP)

PVP (Sigma Aldrich), with a molecular weight of 1,300,000, was dissolved in pure ethanol or a mixture of ethanol and dimethylformamide or chloroform at a ratio of 60:40. Concentration of PVP solutions were made between 5-30%. All polymer solutions were stirred for 24 hours before being used to create electrospun fibers. This polymer is further discussed in Chapter 3.

Polysulfone (PSU)

Polysulfone was mixed at 20 wt% PSU (Mw 26,000, Aldrich, USA) was prepared in DMF (Acros Organics) or THF (Carlo Erba, Dasti Group Reagents SAS):DMF at a 1:1 ratio. Magnetic stir bars were used to create a homogenous solution. Electrospun fibres were created from this protocol. This polymer is further discussed in Chapter 3.

2.2.3 Elastic Polymers and Preparation of Casting Solutions

Polyisoprene

Polyisoprene (Mw 38,000; Sigma-Aldrich) is an elastomer in liquid format that was blended with Kraton D1152ES (SBS) at concentrations of 5-20 wt%. Kraton D1152ES (SBS) was prepared as stated above and the appropriate amount of polyisoprene was mixed into it, resulting in final concentrations of 10 wt% for Kraton D1152ES (SBS) and 5 wt%, 10 wt%, 15 wt% and 20 wt% of polyisoprene. This polymer is further discussed in Chapter 3.

Poly(butadiene)

Poly(butadiene) (Mw 200,000; Polysciences) is a rubber block that was mixed with THF using a magnetic stir bar until a viscous liquid was formed, then mixed with liquid solutions of Kraton D1152ES (SBS). This yielded final concentrations of 10 wt% for Kraton D1152ES (SBS) and 10 wt% of poly(butadiene). Tetrahydrofuran (THF; Carlo Erba, Dasti Group Reagents SAS), Dimethylformamide (DMF; Acros Organics), and Acetone (Valente roberio.ida) were used to dissolve the polymers and make planar sheets or electrospun fibers. All reagents were analytical grade and used without further purification. This polymer is further discussed in Chapter 3.

Poly (styrene-isoprene-styrene): Kraton D1161PT (SIS)

Kraton D1161PT (SIS) (also known as SIS) is a styrene-isoprene-styrene block copolymer with 15 \% PS and a molecular weight of 207,000-237,000 (Kraton Polymers). This polymer was blended with THF (Carlo Erba, Dasti Group Reagents SAS) at 5-20 wt% concentrations by stirring for 12-24 hours. This polymer was cast into sheets and is further discussed in Chapter 3.

Poly (styrene-butadiene-styrene): Kraton D1152ES (SBS)

Kraton D1152ES (SBS) (also known as SBS) a styrene-butadiene-styrene block copolymer with 30 \% PS and a molecular weight of 122,000 (Kraton Polymers). This polymer was blended with THF (Carlo Erba, Dasti Group Reagents SAS) at 5-20 wt% concentrations by

stirring for 12-24 hours. Iron(III) p-toluenesulfonate hexahydrate (Mw 677.52; Aldrich) was used at concentrations of 5-25 wt% to enhance conductivity of electrospun Kraton D1152ES (SBS) solutions. This polymer was cast into sheets and electrospun when mixed with Iron (III) p-toluenesulfonate hexahydrate, and is further discussed in Chapter 3.

Kaneka SIBSTAR™ 102T and 062M

SIBSTAR is a styrene-isobutylene-styrene block copolymer with approximately 22 \% styrene content (Kaneka Belgium N.V.). Blends of 062T (Mw. unknown) and 062M (Mw. 35,000) were created at a 1:1 ratio at 5-20 wt% concentrations with THF (Carlo Erba, Dasti Group Reagents SAS) by stirring for 12-24 hours. This polymer was cast into sheets and is further discussed in Chapter 3.

2.2.4 Electroconductive Materials

Electroconductive Flexible Polymers

Electroconductive flexible conductive materials are listed in table 2.1. The details for polymeric materials are provided in section 2.2.2. Electroconductive polymers include Polyimide (PI), Poly(methyl methacrylate) (PMMA), Poly(vinylidenefluoride-co- trifluoroethylene) (P(VDF-TrFE)), Polyacrylonitrile (PAN), and Polyvinylpyrrolidone (PVP). In several cases, however, these materials are only conductive after specific treatments – particularly thermal treatments – and large amounts are likely to act as insulators.

Conjugated Electroconductive Polymers

Poly 3,4-ethylenedioxythiophene (PEDOT) + PSS, Polypyrrole (PPy), and Poly(3-hexylthi ophene-2,5-diyl) (P3HT) are all liquid polymers that can be blended with more viscous polymers in order to increase conductivity and facilitate electrospinning, or can be spin coated as surface coatings. Similarly, Gwent polymeric pastes are miscible with specific solvents and select polymers but cannot be used independently given their viscosity and liquid state. Platinum polymer paste (C2020322P6) from the Gwent Group is a cross-linked, screen printable paste. The platinum paste can be diluted with Gwent diluent (S2030203D1) or used as it is.

Conjugated electroconductive polymers were available as pre-prepared solutions that could be modified using specific solvents and methods, such as thermal treatments, based on their individual properties and miscibility. Details on these conjugated polymers are shown in Table **2.3.** Further details on the spin coating or other processing for these polymers are listed later on this chapter, in section 2.4.2, with results detailed in Chapter 4. None of these polymers were successfully electrospun, but further details on the attempted protocols are provided in the appendix.

Iridium Oxide

Irdium oxide (IrOx) solutions were prepared as reported by Cruz et al. and Petit et al.[31, 32] In short, solutions of iridium (III) chloride (IrCl3·xH2O, Sigma-Aldrich, 206245 reg) were made using milliQ water, oxalic acid (H2C2O4·2H2O, Sigma-Aldrich, 99%) and potassium carbonate (K2CO3, Pro-bys, 99%). These solutions were used for electrodeposition and blending with other polymers. Alternatively, iridium (III) chloride alone was blended with other water soluble polymers (e.g., PVP), and used for electrospinning. These protocols are detailed further in section 2.4.2, with results detailed in Chapter 4.

Carbon-Based Materials

Functionalized single-walled carbon nanotubes (SWCNTs-COOH, <90%, D 1-2 n, L 5-30 μm; Nanostructured & Amorphous Materials, Inc.), with a COOH content of 2.59-2.87%, carbon nanotube ink (Sigma Aldirch), Kish graphite coarse powder, Graphene oxide (GO), and N-doped graphene are all utilized in Chapter 4. Further details on these materials can be found in the section on electroconductive materials (section 2.4.3).

2.2.5 Organic Materials

Porcine skin was obtained from freshly slaughtered pigs within 12 hours of death. Portions of skin were harvested from ankle joints and the skin surrounding the auricular muscles. Samples were all used within 72 hours of the estimated time of death.

2.3. Polymeric Material Deposition Methodologies (Chapter 3)

2.3.1 Preparation and Cleaning of Substrates for Cast Samples

Two basic types of substrates for casting samples were used: Commercially available glass and Indium Tin Oxide (ITO) covered glass. Prior to spin coating, substrates were cleaned to remove any contaminants from the surface as such impurities can lead to short-circuited devices and induce behavioural irregularities. Materials were cleaned in different ways:

- ITO substrates used in spin coating were ultrasonic cleaned with several solvents. First, distilled water with a few drops of non-ionic detergent was used for 15 minutes. Then, to remove the detergent, the substrates were rinsed thoroughly with distilled water. The remaining water was then eliminated by immersing ITO covered glasses into HPLC grade acetone (270725, Sigma Aldrich) for 10 minutes. Finally, glasses were dipped in 2-propanol alcohol HPLC for 5 minutes and blow dried with a N2 gun.

- The cleaning process for glass substrates used in spin coating was identical to that of ITO covered glass, with the exception that instead of starting the process with ionic-detergent aqueous mixture for 15 minutes, piranha solution (50% H2SO4 + 50% H2O2) was used for 20 minutes. This procedure makes the surface very hydrophilic. In cases where this was undesirable, glasses were washed with de-ionized water and boiled for 30 minutes.

- For drop casting, petri dishes and glass plates were soaked in bleach to remove any previous polymeric residue, then washed with soap and water.

2.3.2 Defined-Area Drop Casting of Elastomers

Drop casting involves pouring or dropping solution into a substrate and allowing spontaneous solvent evaporation to create a film. This type of procedure is simple and can create variable thicknesses of films based on the solution concentration. However, the thickness can be somewhat difficult to control and poor uniformity may be an issue for certain polymer-solvent mixtures. Solvent evaporation rates and film morphology can be controlled by heating the substrate. Drop casting was performed for elastomers Kraton D1161PT (SIS), Kraton

D1152ES (SBS), Kraton D1152ES (SBS)-polyisoprene, and Kaneka SiBS 062M/062T. The procedures followed are described below:

- 10% weight solutions of Kraton D1161PT (SIS) was prepared in THF.
- 10% weight solutions of Kraton D1152ES (SBS) was prepared in THF.
- A 10% weight blend of Kaneka SiBS 062M and 062T (50:50 \% weight) was prepared in DMF.

Samples were mixed at ambient temperature for 12-24 hours using a magnetic stir bar. Solutions were poured into petri dishes (60-150 mm x 15 mm) to create planar sheets of these polymers. Polymer sheets were prepared at either ambient temperature or at 37ºC under vacuum for 12-24 hours. Polymers were then extracted from petri dishes and left to air dry for a further 24 hours in order to promote the creation of uniform polymers and reduce retention of solvent. At this stage, polymers were cut into sizes suited to individualized tests; all polymer samples were between 0.7 and 1 millimeter in thickness.

- Kraton D1152ES (SBS)-polyisoprene blends solutions were prepared by thoroughly mixing polyisoprene (polyisoprene, cis; average Mw 38,000, Sigma Aldrich) in 10 % weight solutions of previously prepared Kraton D1152ES (SBS) in THF.

- This yielded polyisoprene final concentrations of 2.5, 10, 15, and 20% weight. It was not feasible to produce samples greater than 25 % weight as the viscous consistency of polyisoprene prevented solidification of the samples. Samples were mixed for 12 hours with a magnetic stir bar, then drop cast into petri dishes (60-150 mm x 15 mm). Samples were prepared at 37ºC under vacuum for 12-24 hours, extracted from petri dishes, and left to air dry for a further 24 hours in order to promote the creation of uniform polymers and reduce retention of solvent. All polymer samples were between 0.7 and 1 millimeter in thickness.

Elastomer and elastomer blend films obtained after casting were further heated from ambient temperature to assess the effect of heating procedure on mechanical properties and polymer uniformity. This secondary step was done for mechanical tests detailed in Chapter 3. The procedures followed were:

- 37ºC for 12-24 hours, then heated to 80ºC, remaining at 80ºC at 30 minutes.
- 37ºC for 12-24 hours, then heated to 80ºC, remaining at 80ºC at 30 minutes. Temperature was then increased to 145ºC - 150ºC and remained at this temperature range for 30 minutes.

In both cases, samples were then left at ambient temperature for 24 hours, extracted from petri dishes, and allowed to rest for a further 24-48 hours before further tests were performed.

2.3.3 Tape Casting (Casting Knife) of P(VDF-TrFE)

Casting knives work by moving a blade on a stationary substrate to create a large, uniform piece of material. In this process, a liquid is placed on a substrate beyond the doctor blade. A constant relative movement is established between the blade and the substrate, and the liquid is spread on the substrate to form a thin sheet that results in a film once it has dried. Thickness is determined based on the height of the wet layer, surface tension, wetting, viscosity, and coating speed. This technique is optimal when producing sheets of material as minimal material wastage occurs. The equation for calculation of thickness during the casting process is:

$$Film\ Thickness \propto \beta\ \frac{\rho_{sol}}{\rho_{film}} h_0\ (1 + \frac{h_0^2 \Delta P}{6\mu UL})$$

Equation 2.1: Equation for Calculation of Thickness During the Drop Casting Process. Where U = blade speed, μ = fluid viscosity, L = channel length, ρ = density, h_0 = blade height, and ΔP = slurry pressure head.[25]

Tape casting was used to preparation of P(VDF-TrFE) as follows: P(VDF-TrFE) (Copolymer P(VDF-TrFE 70:30; Piezotech Arkema)) was prepared in DMF: acetone (50:50 % weight) at concentrations of 18% wt by heating the mixture at 40ºC for 4 hours to promote solution homogeneity. Films were cast at ambient temperature using custom made casting knives to produce films of 250 μm and 400 μm. Once cast, films were placed on top of an autoclave to

accelerate solvent evaporation and promote film homogeneity.

2.3.4 Spin Coating

Spin coating, a technique utilized since the beginning of the 20th century, is a simple, cheap, solution-based deposition technique that can be used with both inorganic and organic solutions. This process enables the creation of films with reproducible thickness to be obtained, covering flat substrates with areas up to (ø ≥ 30 cm). Applications of spin coating include paint or protective coatings of planar, industrial products. This can be used to protect products against corrosion, UV light, humidity and abrasion. Spin coating can also be used to coat materials for optical data mass storage and create microelectronics.

The spin-coating process can be divided into four steps: deposition, spin-up, spin-off, and evaporation. The first three stages occur sequentially, while the evaporation step occurs throughout the process, predominantly at the end.[26, 27] Figure 2.1. shows a representation of the spin-coating process.

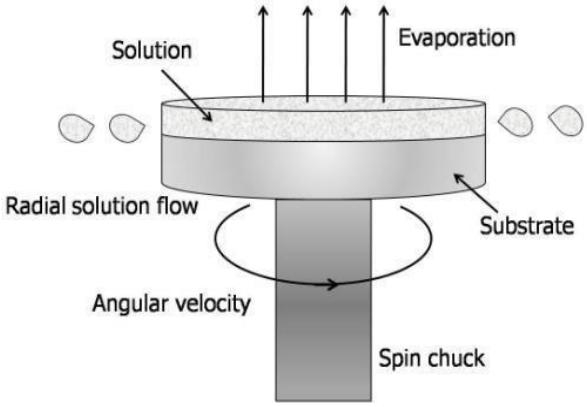

Figure 2.1: Schematic of the Spin Coating Process. Where a solution is spread on the substrate due to centrifugal force. During this, evaporation of the solvent occurs. These two processes lead to a thin film being uniformly deposited on the substrate's surface.

Deposition: The substrate is placed on the spin chuck and the solution is dispersed over it. Dispersion can be done using a pipette, nozzle, or spraying the solution onto the surface. During this step, the substrate can be static or rotating at low angular velocity. The most important requirement is for the solution to wet the surface completely, or incomplete coverage may occur. To prevent this, excess coating solution is typically dispensed on the substrate.[26]

Spin-up: In the second stage, the substrate is rapidly accelerated up to the final angular velocity, configured by the user. The spin speed is measured in rotations per minute (rpm). Most of the solution is expelled from the substrate surface due to centripetal acceleration.

Spin-off: In this step, the substrate is rotating at the final speed. The solution continues to be spread over the substrate, thinning the film due to centrifugal force. When enough solvent has evaporated, the viscosity of the solution increases and the spread ceases.[26, 27]

Evaporation: In this step, thinning occurs due to evaporation of the remaining solvent when it is absorbed into the atmosphere. If significant evaporation occurs too quickly, a solid skin forms on the fluid surface. This impedes the evaporation of solvent trapped under this skin, leading to coating defects.[27]

Film thickness decreases with lower concentrations and viscosity and more rapid angular velocity.[26] The choice of the solvent is important: solvents with higher volatility will result in thicker films at a given initial concentration and viscosity, but too much volatility may result in non-uniformities.

The amount of solution initially deposited on the substrate, deposition rate of the solution, history of rotational acceleration prior to the final acceleration, and total spin time have limited or no effects. The main disadvantages are that this technique is designed solely for flat substrates, and that product may be wasted excessively during the spin-up stage. This technique can also be sensitive to the physical properties of the solution and can be sensitive to factors such as temperature, airflow velocity, relative humidity, and thermal surroundings for the evaporation component of the procedure.

Due to these facts, to obtain reproducible polymer films, it is necessary to have a fixed set of operational conditions for a given spin-coating apparatus and solvent/solute. Each individual protocol is detailed in the subsections below.

Flexible Spin Coated Polymers (PI, PAN, PMMA, P(VDF-TrFE))

Spin coating was used to deposit polymers on substrates and test their electroconductivity independently of elastomeric substrates. Polyimide, PAN, PMMA, P(VDF-TrFE), and PEDOT:PSS were all created using this methodology.

These polymer casting solutions (as described in section 2.2.2) were spin coated (Spin-Coater KW-4A, Chemat Technology) on glass slides at 1500-1800 rpm (30-60 seconds). When required, the obtained polymeric films were annealed at temperatures between 80-150°. Films with ~90μm thickness were obtained. The annealing process removed any residual traces of organic solvents on the polymeric films.

Electroconductive Spin Coated Polymers (PEDOT:PSS, P3HT, and PPY))

Coating ITO glass with PEDOT:PSS (poly(3,4-ethylenedioxythiophene):poly(styrene sulfonic acid) reduces electrical shortages, improving the function of the produced materials. PEDOT:PSS was therefore spin-coated on pre-patterned ITO covered glasses at 1800 rpm (rotations per minute) over a period of 30 to 60 seconds. Then the films were then baked at 120ºC for 10 min at normal atmosphere to remove the remaining water.

The PEDOT:PSS water dispersion used in this thesis was purchased from Bayer AG, Baytron P AI 4083 (≈ 1.5% w/w). PEDOT alone was prepared by adding 0.03 M PEDOT (483028, Sigma-Aldrich, 97%), 0.01 M of K_2CO_3 (584087, Sigma-Aldrich, 99%) and $H_2C_2O_4 \cdot 2H_2O$ (247537, Sigma-Aldrich, 99%) until a pH of 8 was achieved.

P3HT (445703, Sigma Aldrich) and PPy (482552, Sigma Aldrich) were obtained as pre-prepared solutions. The deposition of these materials was performed in the same manner to PEDOT:PSS but at 1500 rpm, with the same annealing procedure post spin-coating.

Spin coating of both flexible and electroconductive materials were performed in order to collect preliminary data for this thesis. Although this technique was fundamental to this work, spin coating was not utilized for the research that was ultimately analysed over the course of this work. Spin coating data can, consequently, primarily be found in the appendix.

2.3.5 Electrospinning (PI, PANI, PMMA, P(VDF-TrFE), PAN, PSU, Kraton D1152ES (SBS), PVP, PVP/IrO2)

Electrospinning is one of the main methodologies used for this project. This technique is a method of producing nanofibers from a large variety of materials (polymers, composites, ceramics, etc.) in an easy, cost effective, versatile manner. An electrospinning apparatus generally contains three basic components: a capillary tube with a needle or pipette, a high-power voltage supply, and a metal collector or a target. The capillary tube and target are held at a precise distance, while the polymeric solution is forced through the syringe pump to the needle. A schematic representation of this process is shown in Figure 2.2.

When the repulsive electrostatic force overcomes the surface tension, pendant drops are formed. This is followed by the Taylor cone, a conical protrusion, once a critical voltage has been applied to the system. From this cone emerges a continuous jet directed towards the collector. As such, the jet reaches the collector, the solvent evaporates, and drypolymer fibers at nanoscale dimensions are deposited on the surface and collected as an interconnected web of fibers.[28, 29]

Polymer electrospinning can be done in two different ways, horizontally and vertically, as shown in the schematic below. Horizontal electrospinning is shown on the top of the figure, with vertical electrospinning shown on the bottom. The vertical method was used for the creation of all flexible polymers, but the horizontal method was the preferred use when electrospinning elastomers in order to reduce beading that often forms within scaffolds.

The home-made used electrospinning setup consists of a high voltage power supply (Glassman High Voltage, Inc., Series EL, Model PS/EL40P01), a syringe pump (KDS Scientific, Model KDS Legato 210), and a teflon tube which connects a syringe (VWR, Henke Sass Wolf) to a needle (EFD International, Inc., Needle Valve Dispense Tip Kit). Needles of various inner diameters were used. Different electrospinning parameters as well as different collectors were used to obtain random and aligned nanofibers. Random fibers were obtained using a flat, rounded copper plate, while aligned fibers were obtained using two parallel rectangular stainless steel plates with a gap of 2.5 cm.

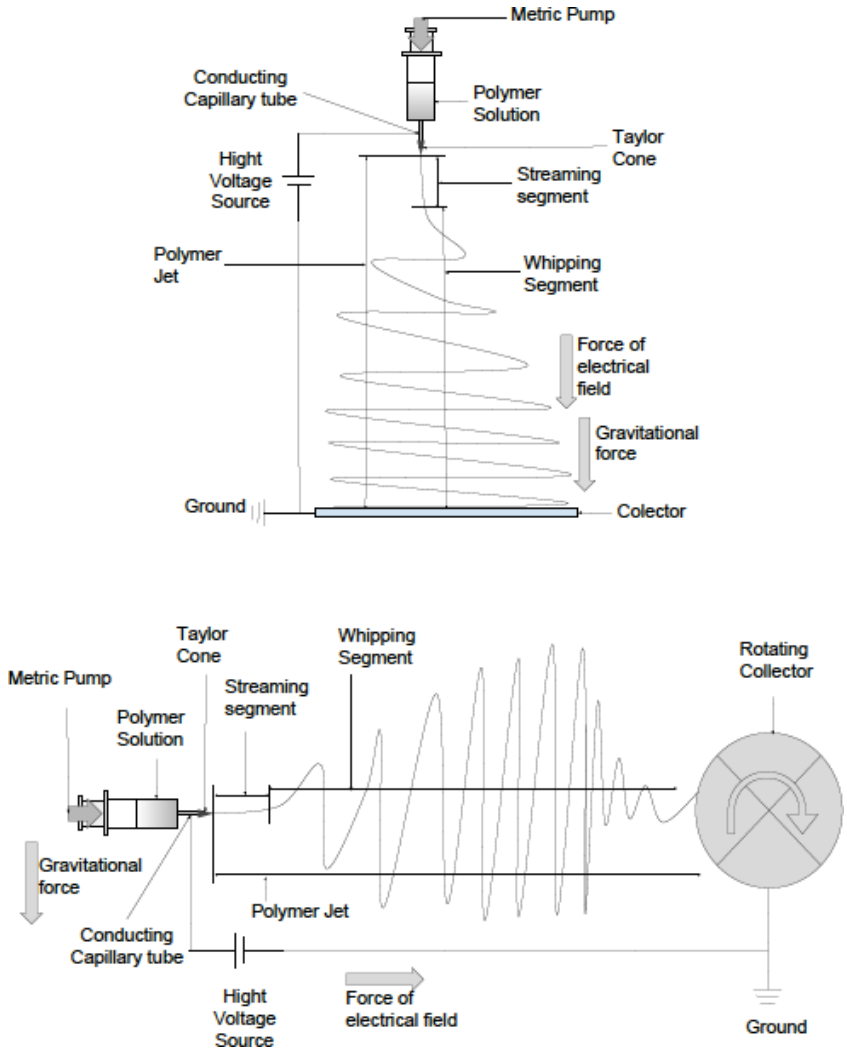

Figure 2.2: Schematic of Vertical (A) and Horizontal (B) Electrospinning. Created by Rolando Matos, PhD candidate at the University of Surrey

Electrospinning was successfully applied to:

- Polyimide (PI), Poly(methyl methacrylate) (PMMA), Poly(vinylidenefluoride-co-trifluoroethylene) (P(VDF-TrFE)), Polyacrylonitrile (PAN), Polysulfone (PSU), Polyvinylpyrrolidone (PVP) and Poly (styrene-butadiene-styrene) (SBS, Kraton D1152ES (SBS)), as described in Tables 2.1 and 2.2
- PVP-IrO2 mixture

Electrospinning of the following materials was unsuccessful:

- Polyaniline (PANI)
- Poly(phenylene oxide) (PPO)
- Kraton D1161PT (SIS)
- Kaneka SIBSTAR^{TM} 102T:062M (SIBS)

The unsuccessful polymers are detailed further in the appendix. The applied electrospinning parameters used for the polymers that were successfully electrospun are detailed below.

Polyimide

Solutions of polyimide, prepared as described before for film casting, were electrospun vertically (Figure 2.2A). The viscous polymer was loaded into a syringe equipped with a 0.80 mm (inner diameter) stainless steel gauge needle connected to a high voltage power supply (Glassman High voltage Inc., PS/EL40P01.0-22). Voltage provided ranged between 15-25 kV. The ground collector was a fixed copper plate at a distance of 17 cm. The solution was supplied with use of a syringe pump (NE-300, New Era Pump System, Inc.) at a feed rate of 0.1 μL/min. Collection was always performed at a relative humidity at 25% or less.

Poly(methyl methacrylate) (PMMA)

Solutions of Poly(methyl methacrylate), prepared as described before for film casting, were electrospun vertically (Figure 2.2A) and delivered using a syringe pump (KD Scientific, Legato 210) at a feed rate of 17 ul/min. A stainless steel needle (Nordson EFD, inner diameter 0.25mm and external diameter 0.52mm) was used as an electrode, and the ground collector was a fixed copper plate. A high voltage was exerted between the nozzle and the collector to generate a Taylor cone using a power supplier (Glassman High voltage Inc., PS/EL40P01.0-22). The applied voltage was 20 kV, and the nozzle-to-collector distance was 25 cm.

Poly(vinylidenefluoride-co-trifluoroethylene) (P(VDF-TrFE))

Solutions of P(VDF-TrFE), prepared as described before for film casting, were electrospun vertically (Figure 2.2A) and delivered using a syringe pump (KD Scientific, Legato 210) at a feed rate of 4000 nL/min. A stainless steel needle (Nordson EFD, inner diameter 0.25mm and external diameter 0.52mm) was used as an electrode, and the ground collector was a fixed copper plate. A high voltage was exerted between the nozzle and the collector to generate a Taylor cone using a power supplier (Glassman High voltage Inc., PS/EL40P01.0-22). The applied voltage was 15-20 kV, and the nozzle-to-collector distance varied from 15 to 20 mm.

Polyacrylonitrile (PAN)

Solutions of Polyacrylonitrile, prepared as described before for film casting, were briefly warmed and electrospun vertically (Figure 2.2A) and delivered using a syringe pump (KD Scientific, Legato 210) at a feed rate of 0.5 mL/h through an 18-gauge stainless steel needle. The needle was connected to a high voltage power supply (Glassman High voltage Inc., PS/EL40P01.0-22) with voltage provided between 15-30 kV. The distance between the plate and needle was 25 cm. Collection was always performed at a relative humidity at 35% or less.

Polysulfone (PSU)

Solutions of PSU, prepared as described before for film casting, were electrospun vertically (Figure 2.2A) and delivered using a syringe pump (KD Scientific, Legato 210) at a feed rate of **1.5** ml/h. The polymer was loaded into a syringe equipped with a 0.60 mm (inner diameter) stainless steel gauge needle connected to a high voltage power supply (Glassman High voltage Inc., PS/EL40P01.0-22). Voltage was provided at 15 kV. The distance between the plate and needle was 20 cm.

Polyvinylpyrrolidone (PVP) and IrOX-PVP

Solutions of PVP, prepared as described before for film casting to concentrations between 10-15%, were electrospun vertically and delivered using a syringe pump (KD Scientific, Legato

210) at a feed rate of 2 ml/hr. PVP solutions were spun at 7.5 to 15 kV using a needle with an inside diameter of 0.5 mm at a distance of 20cm from needle to collector.

Iridium oxide solutions, prepared as detailed in section 2.3.2, were mixed with previously prepared solutions of PVP (as detailed in section 2.2.2) at ratios of 1:2 to 1:5. Solutions were mixed overnight, and allowed to evaporate somewhat for a further 24 hours. Electrospinning parameters used were the same. Fibers were dried for 2 hours at 80^{o}C, and a further hour at 500^{o}C if removal of PVP was required.

Kraton D1152ES (SBS) (Poly (styrene-butadiene-styrene)

Solutions of SBS (Kraton D1152ES (SBS)) and Iron(III) p-toluenesulfonate hexahydrate (Mw 677.52; Aldrich) were dissolved in THF at respective concentrations of between 5 to 15% weight and 20 to 40 % weight mixing prepared THF solutions of Kraton D1152ES (SBS) and Iron(III) p-toluenesulfonate hexahydrate. The Kraton D1152ES (SBS) and Iron(III) p-toluenesulfonate hexahydrate solutions were electrospun horizontally (Figure 2.2B.) and delivered using a syringe pump (KD Scientific, Legato 210) at a feed rate of 1500nL/min. A stainless steel needle (Nordson EFD, inner diameter 0.1 mm and external diameter 0.24 mm) was used as nozzle. The ground collector was either a fixed copper plate or a rotating drum. The rotating drum with 8 cm diameter moved at 200 revolutions per minute. A high voltage was exerted between the nozzle and the collector using a power supplier (Glassman High voltage Inc., PS/EL40P01.0-22). The applied voltage for copper plate collection was 20-35 kV, and the nozzle-to-collector distance varied from 15 to 25 mm. The applied voltage for the rotating drum was 15-25 kV, and the nozzle to collector distance varied from 20 to 35mm. As this was a novel protocol that was created for the purposes of this thesis, images of this polymer are detailed in the results section.

2.3.6 Dip Coating (Elastomers on PEDOT:PSS, P3HT, and PPY)

Dip coating allows for substrates to be dipped into a solution and withdrawn at a controlled speed, resulting in single or multiple layers of coatings. Thickness is determined by the balance of forces at the liquid-substrate interface, as stated in the Landau and Levich equation.[30] Elastomers were used as the substrate being dip coated into liquid-state electroconductive

polymers such as PEDOT:PSS, P3HT, and PPY. Dip coating was also used as a method to create elastomers in shaped formats, rather than planar sheets or fibrous forms. In such cases, elastomers were cast onto glass substrates (e.g., test tubes), which are detailed in the appendix.

2.4. Preparation and Electrical Characterization of Electrical Materials (Chapter 4)

2.4.1 Iridium Oxide Synthesis With and Without Oxalate

IrOx pre-deposition solutions were prepared as reported by Cruz et al. and Petit et al.[31, 32] A solution 4 mM of iridium (III) chloride ($IrCl_3 \cdot xH_2O$, Sigma-Aldrich, 206245 reg) in 50 mL of milliQ water was prepared. Oxalic acid ($H_2C_2O_4 \cdot 2H_2O$, Sigma-Aldrich, 99%) was subsequently added up to a concentration of 20 mM. Potassium carbonate was then added (K_2CO_3, Pro-bys, 99%) up to 0.1 M and the pH was adjusted to 10. The prepared solution was aged for 4 days at 37°C to promote slow hydrolysis. It was kept in refrigeration after this period until use. To prepare non-oxalate pre-deposition solutions, the procedure is identical besides for the addition of oxalic acid.

Iridium Oxide Electrodepostion

Electrodeposition is a method used to deposit a conductive material onto a substrate. Typically, the substrate is an electrode and the conductive material be deposited is in a pre-deposition solution state, containing the reduced/oxidized precursor, or other species that will get involved in secondary electrode reactions. Modulation of intensity and potential control the final thickness, homogeneity and microstructure of the coatings. Here, potentiodynamic deposition was used for deposition of iridium oxide.

Potentiodynamic deposition uses repetitive pulsed or triangular potential signals to cause the potential of the working electrode to sweep back and forth between a designated value range. The working electrode current may be measured during the potential scan in dynamic potential voltammetries. The potential drives the reactions related to the working electrode, with the current proportional to the reaction rate. Typical iridium oxide (IrOx) electrodeposition curves are shown in Figure 2.3.

The potentiodynamic depositions done in this thesis did not utilize stirred solutions. Therefore, the system current was limited by the diffusion of reactants to the electrode surface, as shown in the I vs E voltammograms (Figure 2.3. When the potential is increased until the voltage value is large enough for a redox reaction, the current increases to a maximum value. It then decreases for the depletion of the reactive species near the surface, yielding its characteristic wave. An identical cathodic wave will appear in the reduction direction if the process is reversible, but secondary reactions and/or the structural reorganization of the solid synthesized typically make the process irreversible.

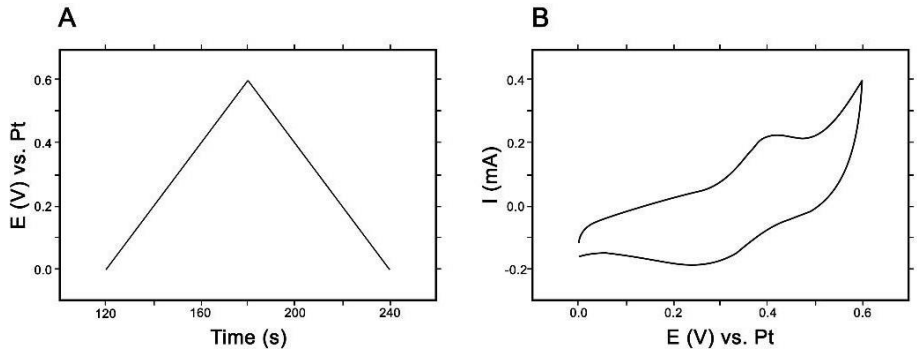

Figure 2.3: Potentiodynamic Deposition of IrOx Coatings. A) Triangular potential excitation sweep and B) Voltammogram (intensity vs potential curve) sourced from UAB's Casañ-Pastor Lab.[34]

Iridium oxide anodic electrodeposition was firstly presented by Petit et al., who used a constant current technique.[32] These techniques are typically used when a unique crystallization process exists and there is no interference from other chemical reactions. However, the Casan-Pastor group at the University Autonoma de Barcelona demonstrated that potentiodynamic synthesis methods result in more homogeneous film microstructures with improved adhesion to Pt-coated substrates.[33] All IrOx depositions were done in accordance with their improved techniques.

A schematic representation of the electrochemical cell used in the electrodeposition process is shown in Figure 2.4 A glass recipient is filled with the aqueous pre-deposition solution and three electrodes are immersed. The counter-electrode used was platinum foil, while the pseudo-reference electrode is a platinum wire (both from Goodfellow, 99%). Use of a conventional reference electrode (like Ag/AgCl) as reference instead a Pt wire was dismissed in accordance to the Casan-Pastor method. Use of platinum as pseudo-reference electrode has been previously reported, yielding similar potentials to Ag/AgCl reference electrodes.[34]

The working electrode where the sample was deposited was a transparent soda-lime glass slide (76x25 mm2 AFORA) covered with 5 nm of titanium (as adhesion film) and 12 nm of platinum for control samples. Experimental samples utilized samples of elastomeric polymers coated with Gwent polymeric platinum or electrodeposited platinum. For all the hybrid coatings, the size of the substrate and the counter-electrode used was smaller, around 38x12 mm^2. The Ti-Pt deposition was carried out by vacuum thermal evaporation in the Optical Laboratory of the Universidad Autónoma de Barcelona. This procedure is further detailed below under section 2.4.3. The thickness of the metallic layers was controlled by a sensing quartz microbalance. To increase crystallinity, homogeneity and conductivity, glass substrates were heated 4 hours at 450ºC before use as electrodes. Elastomeric samples were not heated.

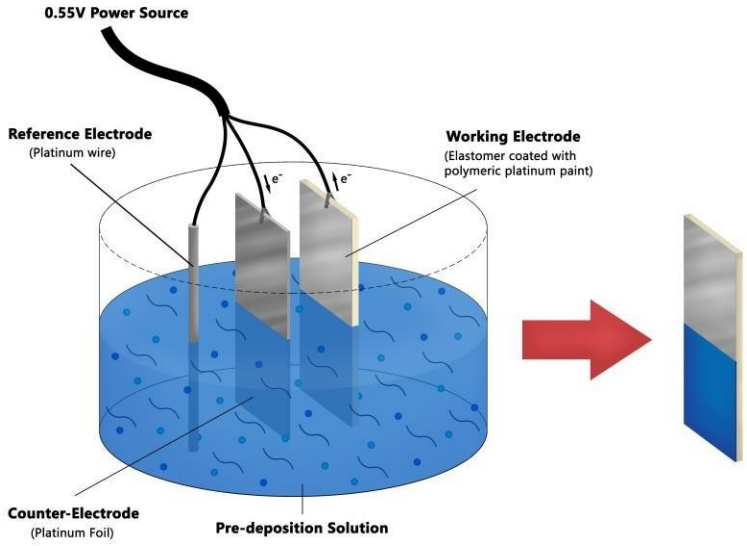

Figure 2.4: Representation of the IrOx Electrodeposition Process. The three-electrode system used during IrOx electrodeposition and cyclic voltammetry.

To ensure maximum reproducibility and electric field homogeneity, working and counter electrodes have the same dimensions. Separation between electrodes was kept constant at 1 cm. The equipment used for electrochemical deposition of the coatings was a VMP3 potentiostat/galvanostat from Biologics Science Instruments. Electrodeposition was performed at a scan rate of 10 mV/s and switching potentials of open circuit potential - 0.55 V. The number of cycles used during the synthesis determines the final thickness of the coating and was done at a minimum of 50 cycles. After synthesis, coatings were washed with distilled water and dried in air until further use.

Iridium Oxide Electrospinning

Iridium oxide cannot be electrospun on its own; it can be combined with a solvent and secondary polymer and then electrospun, however. Typical compatible polymers are those which can be dissolved in ethanol and other water-based solvents. Iridium oxide-PVP electrospinning was detailed in section 2.3.5.

2.4.2 Surface-Coated Electroconductive Materials on Elastomers

Thermally Evaporated Materials (Gold, Titanium, and Platinum)

Thermal evaporation is a simple, affordable method of evaporating materials with low melting points and depositing them onto selected substrates. This technique was used due to the reduced change of damage to the substrate surface, as substrate heating throughout the deposition process can be minimal (>100 ºC).[35] However, the density of the deposited films can be variable and not uniform. This technique is illustrated in figure 2.5.

After the substrate and the materials to be evaporated are inserted inside the bell jar, a vacuum is made. The vacuum pressure (typically 10^{-2} to 10^{-6} torr), prevents a reaction from occurring between the evaporated material and atmosphere.[36-38] Consequently, at these pressures, evaporated atoms travel in straight line towards the substrate: the most straightforward direction they can follow.

The material to be deposited is placed in a tungsten, tantalum, or molybedum wire source connected to two electrodes. In this case, the deposited material was heated via an electrical current that passed through a tungsten filament (Joule effect). Materials such as these are used because of their high melting points and vapor pressure at the evaporation temperature.[36] Deposition rate and thickness of the evaporated substance as it reaches the substrate are controlled by sensing quartz microbalance.

In the current work, Gold, titanium, and platinum were deposited onto either control glass substrates or elastomers (Kaneka SIBSTAR™) using thermal evaporation. Samples were made

using the Edwards Coating System E306A or the thermal evaporator of the glovebox system MBraun MB 200B at the Optical Laboratory of the UAB.

- In the case of glass, substrates were heated for four hours at 450ºC to improve deposition homogeneity, following thermal evaporation.
- In the case of deposition on elastomer substrates (Kaneka SIBSTA™), thermal evaporation was performed as on glass, but for a reduced period of time (around 1 hour).

In both cases, the evaporator used had a surrounding atmosphere with very low O2 and H2O content (< 0.3 ppm).

This technique was also used as the method for:

- Creating electrodes used in potentiodynamic deposition of IrO2 on elastomers (Kaneka SIBSTAR™), which are discussed in Chapter 4.
- Coating samples for further conductivity analysis and imaging analysis (i.e., SEM), which is discussed in Chapter 4.

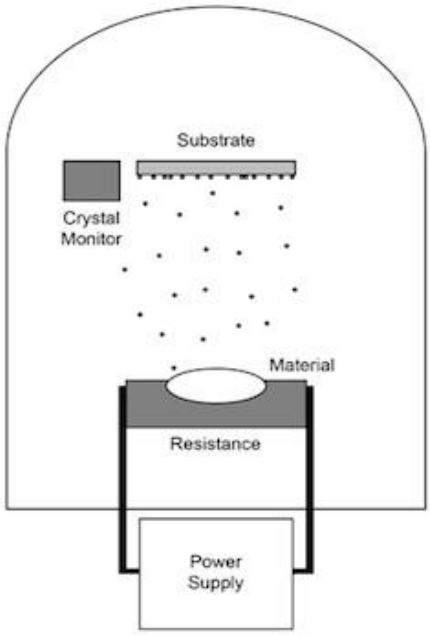

Figure 2.5: Schematic of Thermal Evaporation Deposition. The material to be deposited and the substrate are placed in a chamber under high vacuum. After the material to be deposited has been heated, the evaporated material reaches the substrate and condenses. Film deposition rate and thickness are controlled by a quartz crystal monitor.

Sp(2) Carbon Materials Blended With Elastomers

Carbon Nanotubes: Functionalized single-walled carbon nanotubes (SWCNTs-COOH, <90%, D 1-2 n, L 5-30 μm; Nanostructured & Amorphous Materials, Inc.), with a COOH content of 2.59-2.87%, were mixed with various pure solvents (THF, DMF, Ethanol) until they had been dissolved, then blended with flexible polymers and elastomers (10 % wt Polyimide, 10% wt Kaneka SIBS) at various concentrations (5, 10, 15, 20, and 25% wt). The electroconductivity of overall material constructs was assessed and is detailed in Chapter 4.

Graphite: Graphite utilized was previously prepared by UAB-ICMAB group members in the Casan-Pastor laboratory. Kish graphite coarse powder (100 mesh, 0.15 mm), provided by Nanomagnetics Ltd, was oxidized following the method described in the article of G. Tobias et al. by treating the graphite with nitric acid (HNO3, Fisher Chemical, 65%) [39]. Around 200 mg of graphite was added to a round-bottomed flask with 100 mL of 3 MHNO3 and refluxed at 130ºC during 45 hours in order to ensure the mild oxidation. Then, the mixture was filtered with a 0.2 μm Millipore polycarbonate membrane and rinsed with distilled water until pH=7. The black powder is then dried in air. Quantification of functional groups was performed by X-Ray Photoelectron Spectroscopy (XPS) on pre- and after-treated graphite, yielding an atomic relation O/C around 0.08. Graphite was then blended with flexible polymers (10% wt Polyimide, 10% wt Kaneka SIBS) at various concentrations (5, 10, 15, 20, and 25% wt). The electroconductivity of overall material constructs was assessed and is detailed in Chapter 4.

Graphene and Graphene-N: Graphene oxide (GO) was previously prepared by ICMAB group of Carbon Nanomaterials and Inorganic Nanostructures using the Hummers method and was characterized by termogravimetric analysis (TGA) showing around 20 wt (%) of functionalized groups[40]. N-doped graphene was obtained by ammonolysis of the previously prepared GO. Nitrogen content was also studied by TGA and the results show a 20 wt (%) of functionalization (including nitrogen and oxygen species). Graphene oxide was then blended with flexible polymers and elastomers (10 % wt Polyimide, 10% wt Kaneka SIBS) at various concentrations (5, 10, 15, 20, and 25% wt) and the electroconductivity of the overall material was assessed.

Painted Materials (Polymeric Platinum, Silver, Carbon Nanotube Pastes)

Various materials were painted onto elastomeric substrates as the simplest approach to apply electrical materials. These materials were considered in an attempt to compare the uniformity of paste-based materials versus their thermally evaporated counterparts. Specifically, electroconductive pastes were utilized; namely:

- Polymeric platinum paste (Gwent, C2020322P6)
- Silver paste (Gwent, C2080415P2)
- Carbon nanotube conductive ink (Sigma Aldrich, 792462)

All of these pastes were individually applied to elastomeric substrates using a palette knife in order to evenly distribute the paste across the substrate. Rapid drying processes at high temperatures (80-150 ^{o}C) were found to improve homogeneity and adherence.

2.5 Preparation of the Three Layered Construct (Chapters 3, 4, and 5)

The preparation of the three-layered construct is detailed throughout Chapters 3, 4, and 5. In summary, this construct required the following steps:

1. Elastomeric polymers (namely Kaneka SIBS, Kraton D1152ES (SBS), Kraton D1161PT (SIS) were drop cast as previously described in section 2.3.2. Substrates created were transparent.

2. Electroconductive elastomers were produced as previously described in step 1, then made electroconductive by applying polymeric platinum (Gwent) as described in section 2.4.3. Samples were heated from room temperature to 80 ^{o}C at ramp heat. A secondary step could also be performed, heating from 80 ^{o}C to 140 ^{o}C at ramp heat. The overall heating process comprised of both steps lasted for a total of 2 hours.

3. Piezoelectric, electroconductive elastomers were produced as previously described in #2. However, aligned or random electrospun P(VDF-TrFE), created as detailed in section 2.3.5, was applied while polymeric platinum remained wet. The ramp-based

heat-treating process that is described in step 2 was subsequently completed, allowing the polymeric platinum to act as both an adhesive and electrode base for the piezoelectric polymer.

2.6 Electrical Characterization Methods (Chapter 4)

2.6.1 Electrical Conductivity Analysis

Multimeter measurements of resistance (in ohms) were initially taken to measure the approximate conductivity of the samples. These allowed for the conductivity of samples to be performed before more in-depth electroconductivity analyses were performed. They also allowed for validation of the electrical conductivity set-ups detailed below, and used in cell culture.

Electrical conductivity reported was assessed by four-point probe method, using an in-house built setup as depicted in the schematic below and a conductivity measurement system using Keithley 4200 Semiconductor Characterization System (4200-SCS). IV curves were taken from 5 different spots in each sample, the slopes averaged and then used to calculate overall electroconductivity. Thickness was measured using a Dektak 3.21 Profilometer.

All samples utilized gold coating prior to testing. Four gold strips 40-50 nm in thickness were deposited on each sample through thermal evaporation using Edwards Coating System E306A. For the in-house set up tests, each probe (typically in the form of a copper wire) was attached to the gold contacts using adhesive silver paste (Figure 2.6B). A DC current source was applied between the outermost electrodes (1 and 4, Figure 2.6A). Values of 0.1, 0.2, 0.5, 1.0, 2.0 and 5.0 μA were applied in both directions by inverting the signal, while corresponding voltage values were measured between electrodes 2 and 3. Least squares regression analysis in Microscoft Excel was used to find the Resistance (R) of the material, given by the linear relation:

$$\mathrm{R} = \frac{v}{i}\ [\Omega]$$

Equation 2.2: The Linear Relation Used to Find the Resistance (R) of the Material.

The electrical resistivity ρ is related to the resistance as shown below:

$$R = \rho \frac{l}{S} \Leftrightarrow \rho = R \frac{S}{l} [\Omega . \text{cm}]$$

Equation 2.3: Electrical Resistivity ρ as Related to Resistance.

Where l is the length of the piece of the material, in this case, the distance between gold contacts, and S is the cross-sectional area of the film, that is, the product of the film thickness by the width. Finally, electrical conductivity σ is defined as the reciprocal of resistivity:

$$\sigma = 1\rho [\Omega^{-1} . cm^{-1} \text{ or } \text{S/cm}]$$

Equation 2.4: Electrical Conductivity.

An alternative four point probe system was also used to confirm results. Four 50nm stripes of gold (thermal evaporation using an Edwards Coating System E 306A) were deposited on each sample to improve the electrical contact. Resistance was evaluated using the Keithley 4200 Semiconductor Characterization System (4200-SCS). IV curves were taken from 5 different spots in each sample, slopes were averaged, and overall electroconductivity was calculated based on these results. Thickness was measured using a Dektak 3.21 Profilometer.

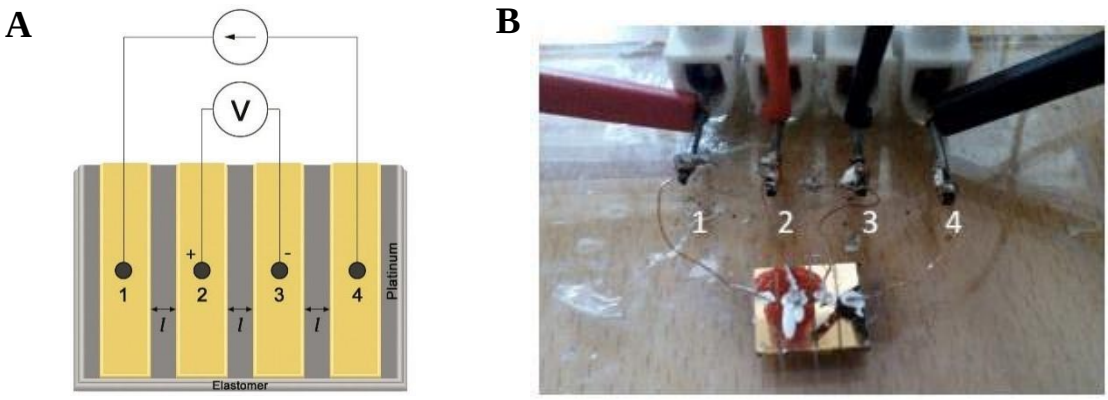

Figure 2.6: Representation of the 4-Point Probe Method. Schematic representation of the 4-point probe method (A) and assembly of 4-point probe method in-house set up from the Morgado Lab of Instituto Superior Tecnico (B), depicting the four gold contacts, showing connections of each probe with silver paste.

2.6.2 Potentiostat Electrochemical Impedance Spectroscopy (EIS)

Electrochemical Impedance Spectroscopy (EIS) was performed at open circuit potential (OCP) over the frequency range of 10 kHz−10 mHz with a potential amplitude of 0.05 V using an AUTOLAB-302N potentiostat/galvanostat. Levels of potassium and sodium in the blood typically vary from 3.5-5.2 mM and 135-145 mM, respectively. Potassium can be found at 2-fold higher concentrations in intracellular regions than outside the membrane, whereas it is the opposite for sodium ions. EIS spectra were collected after samples had been immersed in solutions of PBS for 24-72 hours. Fresh PBS was used during the EIS data collection process. These results can be found in Chapter 4.

2.7. Mechanical Assessments (Chapter 3)

2.7.1 Tensile Deformation Assessment

Tensile deformation experiments were performed in a TA-Instruments DMA Q800 apparatus. These tests were performed at the Universitat Politècnica de Catalunya under the guidance of Dr. Eloi Pineda. Pieces of polymer (namely, P(VDF-TrFE), SIS Kraton D1161PT (SIS), SBS Kraton D1152ES (SBS), and SBS-Polyisoprene blends) and porcine skin samples were subjected to a constant strain rate of 10% per min=1.67×10^{-3} s^{-1} at ambient temperature. In both cases, a 10 mm area was considered as the effective area of mechanical tests. The nominal stress was estimated as the applied force divided by the initial cross section area of the samples. Strain was calculated as $(L-L_0)/L_0$, where L was the length and L_0 was the original length.

The Young's Modulus was calculated as the value of stress over strain. Young's Moduli of elastic materials were computed as the average value of the stress to strain ratio from 0 to 12.5%, that is, the range of maximum elevation of the curve. Flexible polymers, that is, P(VDF-TrFE) fibres and sheets, had similar curves and the Young’s modulus were computed from 0 to 20 \%. As skin has a J-curve, a very different stress-strain curve compared to the elastomers, two Young's Moduli were calculated: the elastic modulus and the deformation modulus. The elastic modulus was calculated at the curved incline at the start of the "J" shape, between 5 and 20% strain, while the deformation modulus calculated the “J” shape’s incline, between 35 to 60%.

2.7.2 Fatigue Analysis

The same machinery used in section 2.7.1 was utilized to perform mechanical fatigue analysis on the aforementioned polymers and skin. The resistance under cyclic deformation was assessed by tensile oscillation tests at ambient temperature. The force cycles were applied at 10 Hz and with a stress ratio (maximum stress / minimum stress) R = 0.111.

In order to compare the resistance of the different polymeric and skin samples under similar conditions of varying strain the tests were performed controlling the strain amplitude. All of the materials were tested at three separate strain amplitudes: 2.5, 5, and 10%. This corresponds to strain rates in the order of 0.1 to 1 s^{-1}. The maximum length of the tests were 150 hours each, corresponding to 5.4 times 10^6 cycles. Three cyclic deformation tests were performed for each amplitude and material.

2.7.3 Elongation at Break Analysis

Mechanical properties were evaluated using a universal testing machine (Zwick GmbH & Co., model Z2.5/TN1S) with integrated testing software (testXpert, Zwick). Samples of P(VDF-TrFE), SBS Kraton D1152ES (SBS), and SBS-Polyisoprene blends used for the test stress−strain assays consist of rectangular specimens with dimensions of 20 mm by 3 mm, with approximately 1mm thickness. The initial grip separation was set at 10 mm, and the cross-head speed was 800 mm/min. These tests were performed at the Universitat Politècnica de Catalunya in the lab of Dr. Carlos Aleman.

2.7.4 Electromechanical Characterization

Electromechanical assessments were performed using the same machinery detailed in section 2.7.3, along with a customized electroconductivity capture set-up utilizing a two point probe and soft electrode clamps. Samples of P(VDF-TrFE), SBS Kraton D1152ES (SBS), and SBS-Polyisoprene blends were measured in stasis and at set points of elongation. Samples dimensions were between 20 mm by 3 mm, with approximately 1mm thickness. The initial grip separation was set at 10 mm. Cross-head speed was 800 mm/min.

2.8. Piezoelectric Characterization of P(VDF-TrFE) (Chapter 4)

P(VDF-TrFE) is notable as this polymer was processed in planar form, random electrospun format and aligned electrospun format, as has been detailed in previous sections (i.e., 2.3.5). The primary format of this polymer that was fully analysed was electrospun in either random or aligned format. These polymers were assessed both independently and in conjunction with other layers.

2.8.1 P(VDF-TrFE) Phase Assessment & Fourier Transformation Infared Spectroscopy

FTIR analysis was performed using the Perkin Elmer FTIR-ATR 4000-400 series with ZnSe accessory. The spectra were collected in the range 1600–200 cm^{-1} with a resolution of 4 cm^{-1} and 30 scans. The spectra were collected for electrospun fibrous sheets and drop cast samples of similar thickness. Omnic acquisition software was used, and data was analysed further using PeakFit. Samples were assessed in various states: not heated, ramp heat treatment to 80^{o}C over a total period of one hour or 90 minutes, and ramp heat treatment to 140^{o}C over a period of one hour or 90 minutes. Fibrous samples were all measured in transmittance mode; planar, drop cast samples were measured in reflectance mode.

2.8.2 P(VDF-TrFE) Piezoelectric Functionality and Validation

Piezoelectric response tests of P(VDF-TrFE) electrospun membranes and complete constructs. An experimental assembly was prepared (Universitat Politècnica de Catalunya by Lama S.B.C., Estrany F., Casellas F.), as depicted below, based on a hermetic and pressurized pneumatic circuit at about 0.4 - 0.5 bar relative pressure. This was modulated with a pressure reducer and measured with a precision gauge connected in bypass. The picture shows the pressurized pneumatic circuit.

The pneumatic pressurized circuit connects the sample to be tested in derivation with a previously calibrated pressure sensor, the pneumatic pulse generator which functions manually, and with the receiver of the response signal of the piezoelectric and pressure sensor, a Freescale Semiconductor, model MPX4250AP (NXP Semiconductors, Manifold Absolute

Pressure). This consists of a data acquisition module (National Instruments, NI USB-6001) connected to a computer, that utilizes the LabView program (National Instruments) for monitoring and recording the signals of the pressure sensor and the piezoelectric membrane.

Figure 2.7 shows the connections made in the assembly to perform the tests. The sample support consists of a small wooden board supported by screws on which the membrane is located. This is hermetically fitted with the pressurized pneumatic circuit through a metal clamp, as shown in the photo. The complete hermetic fit between the head and membrane is ensured by a small O-ring.

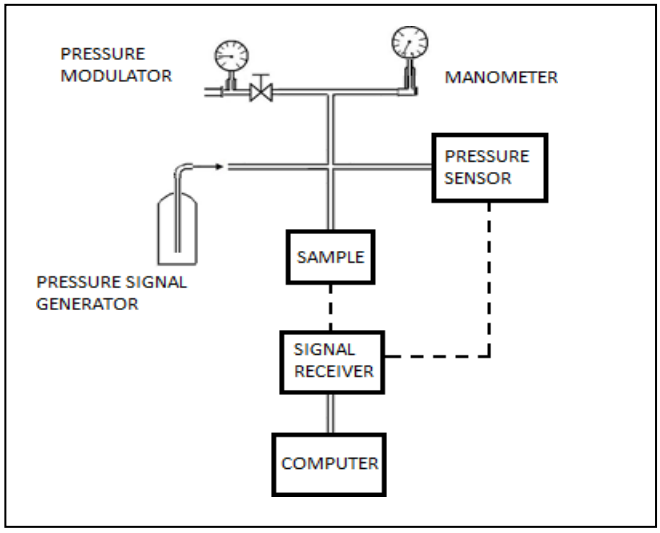

Figure 2.7: Depiction of the Pressurized Pneumatic Circuit and System

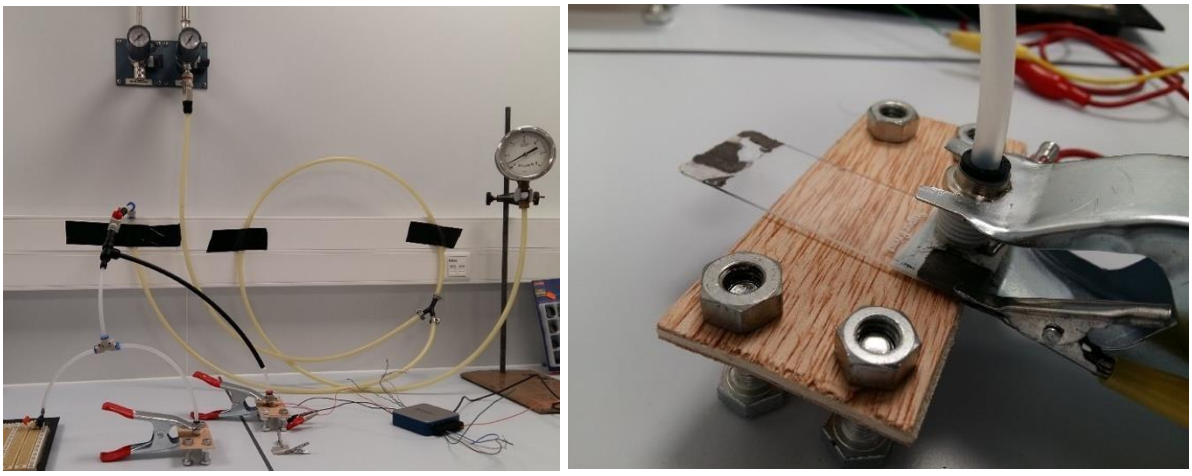

Figure 2.8: Assembly of the Pressurized Pneumatic Circuit. Assembly scheme of the pneumatic circuit, showing A) Bourdon type precision manometer (right), and B) The manually generated signal of the piezoelectric, generated by creating pressure at approximate one-second intervals (left).

2.9. Cultured Cells, Media, Substrates and Analysis (Chapter 5)

2.9.1 Cell Culture Supports

Cell Culture Scaffolds: Creation of Complete Constructs

Three types of constructs were used in cell culture to create elastomeric, electroconductive elastomeric, and piezoelectric, electroconductive elastomeric substrates. These substrates (made of the polymers SBS-Kraton D1152ES (SBS), polyisoprene and P(VDF-TrFE)) were created individually, as detailed in section 2.3.5. Electroconductive substrates and three-layered piezoelectric substrates were created, as detailed in section 2.5. Conductivity and piezoelectricity-related analysis of these substrates are detailed in Chapter 4.

All samples were sterilized with 70% ethanol for 12-24 hours, then sterilized with UV for a further 24 to 48 hour period prior to use. Further details on cell culture related analyses can be found in Chapter 5.

3D-Printed Wells for Sample Cell Culture

Custom-made 3D printed holding samples wells were used for cell culture. Such wells allow cell culture with media on prepared samples, while integrating the sample as an isolated component of an electrical circuit. The wells were designed using a CAD software following the drawings previously established within the group [not published]. The original drawings were modified as the original wells were found to be prone to leakage, causing oxidation and resulting in contamination and cell death. This was due to the presence of copper wiring used as the electrodes.

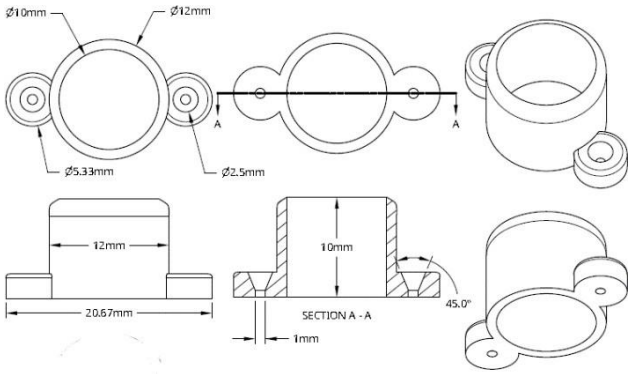

Figure 2.9: Customized Wells

The new wells had secondary, exterior wells on each side to prevent the electrodes from coming into any direct contact with potential leakage. The 3D-printed wells were created using FDM via Makerbot Makerware Type II according to the setting parameters shown in Table 2.4. Two commercial filaments were used: Transparent PET (t-glase, Taulman 3D148) and conductive PLA (cPLA – ProtoPasta conductive PLA, ProtoPlant149). The height and inner diameter of the wells were made at 1 cm, resulting in a cell culture area of about 0.875 cm^2, approximate to that of 48-well plate. All the wells used were a minimum of 20mm length by width. The wells design was further optimized to contain a working volume of about 500 uL of cell medium, with a maximum capacity of 785 uL of fluid. The sides of the wells used in this second design also include supports which serve to affix copper wires used during electrical experiments.

All wells were coated with PDMS prepared using Sylgard® 184 Silicone Elastomer Kit (Dow Corning) to avoid media leakage. The desired amount of elastomer to curing agent were combined in a 1:10 weight proportion. The two were mixed together for one minute using a stirrer, and set down in a desiccator under vacuum for 30 minutes to degass. A small amount of PDMS was then poured onto a 3D-printed cylindrical mold placed on a clean glassware, and the PDMS was thermally crosslinked at 95^oC for 15 minutes, forming the bottom of the PDMS case. The scaffold was then placed inside the mould with a weight on top, PDMS was poured around the scaffold and left overnight for crosslinking at room temperature. Once this procedure was complete, surgical glue was used to attach scaffold wells to scaffolds which had been produced as previously detailed in section 2.7.1.

Table 2.4: Settings for Wells Created on Makerbot Makerware Type II

Parameter	Setting Value
Layer Height	0.40 mm
Extruder Nozzle Diameter	0.40 mm
Right Extruder (PET)	232ºC
Left Extruder (cPLA)	210ºC
Build Plate	70ºC
Speed while Extruding	10 mm/s

The settings used to create both types of wells are detailed in the Table 2.4. Low extrusion speeds (i.e., 10 mm/s) were required to print parts with small, detailed, dimensions, which are present in the newly created wells. Increased time was consequently needed for filament layer cooling.

2.9.2 Cell Types, Media, and Basic Cell Culture Protocols

A variety of cells have been used for the experiments in this thesis, namely: L929 fibroblasts, human and rat keratinocytes, ReN cells, Schwann cells and human and rat dorsal root ganglion cells. Fibroblasts, keratinocytes and neural cells are all considered to be essential components of a somatosensory system model. These cell types were used throughout this thesis as we wanted to look at cells that were optimal for creating a somatosensory system model. L929 fibroblasts and ReN cells were used as the cell lines primarily used to establish cell culture parameters on scaffolds.

L929 Fibroblasts and Fibroblast Assays

Fibroblast media was prepared as DMEM (Life Technologies) with 20% FBS (Gibco, 10082147) and 1% Anti-Anti (Gibco, 15240062). Cells were extracted from cryopreservation and quickly thawed at 37ºC in a water bath. Vials of cells were diluted in 5 to 10 millilitres of media, and centrifuged at 1250 rpm for seven minutes at room temperature. The resulting supernatant was discarded and pellet was re-suspended in 1mL of media. Cells were counted and cultured on tissue culture plates as detailed in Table 2.5. These values were utilized when plating cells on polymeric substrates, as well, as these would vary in size between 0.95 and 9.4 cm^2. Cells were seeded at varying densities ranging between 3,000 to 10,000 cells per cm^2.

Cells extracted from cryopreservation were typically seeded at 3,000 cells per cm^2, cultivated until they reached 80 to 90% confluency, and passaged into other flasks, as described in Table 2.6, or for use in other assays. In some cases, cells were cryopreserved to create further cell banks, which is detailed later on in this section.

`Table 2.5: Cell Cultivation Standards

Cell Culture System	Deposition Area (cm^2)	Volume Of Media (mL)
T-175	175	20 (30-52.5)
T-75	75	10 (15-22.5)
T-25	25	5 (5-7.5)
6 well plate	9.4	2
12 well plate	3.83	2
24 well plate	1.88	1
48 well plate	0.95	0.5
96 well plate	0.32	0.15

Fibroblast Cell Counting

Counting of cells was performed by pipetting 10uL of Trypan-Blue into 96 well-plates according to the desired number of measurements. 10uL of the mixture was transferred into a Newbauer chamber and the number of viable (and/or not) cells present per quadrants, according to the total cells present, was calculated as follows:

$$\frac{Cells}{mL} = \frac{Total\ Cell\ Number\ counted}{Number\ of\ quadrants}\ x\ (dilution\ factor)\ x\ (2x10^4)$$

Equation 2.5: Number of viable cells present per quadrant

Fibroblast Cell Passaging

In order to passage cells, media was removed from cells and cells were washed with PBS twice. Trypsin was then pipetted into flasks according to size, as detailed in Table 2.6. Plates were placed in the incubator at 37ºC and 5%CO_2 for seven minutes. Trypsin was neutralized by applying twice the volume of DMEM-based fibroblast media (detailed above) to trypsin in the cell suspension. Neutralised medium was placed into a falcon tube, and was verified that there were no further attached cells remaining in the original flasks. This suspension was centrifuged at 1250 rpm for seven minutes, the resulting supernatant was discarded, and the cell pellet was resuspended in media. Cells were counted (as previously detailed) and plated at 3,000 cells per

cm^2 for both commercial plates and, considering lower adhesion rates, at 3,000 to 10,000 cells per cm^2 on the materials prepared (unless otherwise specified). Cell culture plates were then placed it an incubator (37ºC, 5% CO_2).

Table 2.6: Cell Passaging Standards

Cell Culture System	Volume Trypsin (0.05%) In mL
T-175	7
T-75	4
T-25	2
T-12.5	2
6 well plate	1
12 well plate	0.7
24 well plate	0.3 – 0.4
48 well plate	0.1-0.05
96 well plate	0.01 – 0.02

Fibroblast Cryopreservation

Trypsinized cells (as created in the cell passaging protocol prior) were resuspended in 10 (v/v)% dimethyl sulfoxide (DMSO) cryopreservation medium (900uL per 100-200uL of cells). Each vial had a minimum of $1x10^6$ cells. Cryopreservation medium is kept on ice throughout the process. Vials were cooled at an optimal rate of 1ºC/min until -80ºC was reached, then transferred to liquid nitrogen for long term storage.[41]

ReN Cells

ReN cell VM human neural progenitor cells were obtained from Millipore. ReN cells were derived from the ventral mesencephalon region of human fetal brain and immortalized by retroviral transduction with v-myc oncogene. Cell doubling time is typically between 20 to 30 hours. These cells can be differentiated *in vitro* electrophysiologically to astrocytes, neurons, and other cells.[41] Unless otherwise stated, basic protocols such as cell counting, passaging, and cryopreservation were identical to those of fibroblasts.

ReN Cell Media

Media used for ReN cells is known as N2 media. N2 media is composed of DMEM, glutamax, glucose, N2 supplement, pen-strep, and insulin. The shelf life for this media is one month, so media was made regularly in small volumes. If made to a volume of 100 millilitres, the media proportions are as follows:

Table 2.7: N2 Media

Ingredient	Volume (mL)
DMEM + Glutamax	97.40
Glucose (1.6 g/L)	1.60
N2 Supplement (1%)	1.00
Pen-Strep (1%)	1.00
Insulin (20ug/mL)	0.08

During cell culture, passaging, and expansion of REN cells, N2 media is mixed with two cofactors: EGF and FGF. 90uL of N2 media is added to every 10uL of each cofactor. Once mixed, these working solutions have a shelf life of 7 days. Cofactor B27 is also used, but does not require any additional N2 media dilution and has a 15-day shelf life.

In order to stimulate differentiation in REN cells, N2 media without cofactors is mixed with B27 Neural Differentiation media to create N2-B27 Media. To create this media, equal parts of N2 Media and B27 Neural Differentiation media are mixed together. When made at a volume of 100 millilitres, B27 media is created as follows:

Table 2.8: B27 Neural Differentiation Media

Ingredient	Volume (mL)
Neurobasal Media	96.50
B27 Supplement 1%	2.00
L-Glutamine 2mM	1.00
Pen/Strep 0,50%	0.05

ReN Cell Culture Substrate Preparation

ReN cells are kept in standard tissue culture flasks pre-coated with L-orthonine solution prior to plating. L-orthonine solutions in flasks and are incubated at 37ºC for 30 minutes to 2 hours. After this period, the excess of L-orthonine solution was removed and the flask was washed

with PBS. PBS was removed and replaced with Laminin solution at a concentration of 10-20ug/mL of PBS. Laminin solution was left in flasks for 2h at 37ºC or overnight at 4ºC. The excess of Laminin solution was then removed from plates and ReN cells were seeded onto flasks and cultured in either N2 or N2-B27 media. This protocol was applied not only cell culture flaks but all substrates, including polymeric ones.

ReN Cell Thawing and Expansion

Prior to use in experiments, cells were thawed and cultured for at least one passage. This allows them to recover from the thawing process, allowing them to return to the normal cell cycle, and prevents delayed-onset apoptosis. A great proportion of cells suffer from apoptosis post-thawing, which occurs due to the activation of the caspase cascade or changes in mitochondrial permeability caused by free radicals in the cytoplasm, causing a leakage of cytochrome C.[42, 43]

Thawed ReN cells were taken out of cryopreservation and rapidly, briefly heated in a 37 ºC water bath. The cell mixture was then resuspended in N2 media without cofactors, then centrifuged at 1000 rpm for three minutes. Supernatant was discarded, and cells were resuspended in N2 medium supplemented with growth factors. Cells were then seeded onto the previously coated flasks. ReN cells were plated at a density of 20,000 cells/cm2 for confluency in two to three days or 50,000-100,000 cells/cm^2 for confluency in one day. Freshly plated ReN cells had media changed on the first day after plating and every two days after.

ReN Cell Passaging

ReN cells were passaged using accutase. ReN cells were passaged by removing media from the flask containing cells, washing cells with PBS, and adding accutase to the flask of cells. Accutase was left in the flask at 37ºC for 7 minutes. Accutase was neutralized by using double the volume of N2 media without added cofactors. The cell suspension was then centrifuged at 1,000 rpm for 3 minutes. Supernatant was removed and the pellet was resuspended in the appropriate media. ReN cells being expanded were plated with N2 media co-factors EGF, FGF, and B27; differentiated ReN cells were plated with N2-B27 media.

ReN Cell Cryopreservation

ReN cells were cryopreserved in the same manner as fibroblasts, but at a density of $1.5-3\times10^5$ cells per vial.

Human Dorsal Root Ganglion (hDRG) Cells

Media for hDRG Cells

Media for human dorsal root ganglion cells is composed primarily of neurobasal media (Gibco Cat 21103-049). When made to a volume of a half a litre, 10 mls of B-27 (Gibco Cat 17504-044), 5 mls of supplement N-2 (Gibco Cat 17502-048), 7.5 mls of FBS, 5 mls of Pen/Strep, and 5 mls of Glutamax are added. Cells are cultured in this media until differentiation of cells is required. Media was always pre-warmed prior to use with cells.

Short term differentiation media is used for experiments done within 48 hours after the start of differentiation. Short term differentiation can be induced by adding the following growth factors to culture media: 0.125uM Forskolin (Sigma), 0.25mg/ml dibutyl-cyclic-AMP (Sigma), 25 ng/ml human NGF (Sigma), 25 ng/ml human BDNF (Sigma), 25 ng/ml Activin A (Prospec), and 25 ng/ml GRO (Peprotech).

For longer differentiation experiments, differentiation media should be mixed with Schwann cell supernatant at a 2:1 ratio. Long-term differentiation media should initially contain a final concentration of 75 uM of forskolin. Differentiation of cells should occur within 24 hours of the change in media, and neurite retraction may occur after 36 hours due to forskolin. After 48 hours, replaced media should contain 100 uM forskolin. Cells that become unresponsive to forskolin need to be subcloned. This occurs with multiple passages and long-term culture.

Culturing Cryopreserved hDRG Cells

Cryopreserved cells are rapidly thawed in a 37^{o}C water bath. 10mls of pre-warmed DRG medium are added to the contents of each cryovial, and spun at 1000 rpm (200 RCF) for 5 minutes. Supernatant was decanted and the pellet resuspended in an appropriate volume of pre-

warmed culture medium. Cells were plated and incubated as normal, with adhesion beginning within one hour. Neurite outgrowth normally begins within two to three hours. DRGs double within 24 hours and were passaged before 80% confluency and at minimum 50% confluency.

Passaging of hDRG Cells

Cells in culture that had grown to 70-80% confluency were washed three times with pre-warmed PBS. PBS was removed and 0.05% Trypsin-EDTA was added for one to two minutes to detach cells. Cells were then resuspended in double to triple the amount of complete culture medium to neutralize the trypsin solution. The solution was spun at 1000 rpm (200 RCF) for 5 minutes, and cells were plated appropriately. Flasks were swirled to ensure even distribution of cells.

Subcloning of hDRG Cells

100 to 200 cells were seeded per T-75 flask and allowed to grow into colonies of 50-100 cell groups. Before cloning, cells were covered with 3mls of 0.05% trypsin. A glass capillary tube connected to rubber tubing was used to create a gentle vacuum. Each clone was extracted and transferred to 24 well plate well. Cell colonies were grown to approximately 60% of confluency and passaged, splitting the quantity of cells in half. Cells were then allowed to grow to 70% confluency, then susceptibility to forskolin was assessed. Clones with higher differentiation rates grow more slowly, hence smaller colonies are desirable. One "good" clone is identifiable in every 60 to 100 clones. This clone should be expanded into T-75 flasks and cryofrozen.

Cryopreservation of hDRG Cells

Cells to be cryopreserved were trypsinized in the same manner as if they were being passaged. They were then counted and centrifuged at 150xg for 10 minutes. The supernatant was removed and resuspended in freezing medium made of 10% DMSO, 80% DRG culture medium, and 10% FBS. 1mL of freezing medium was used per 1-5x10^6 cells. Cells in cryovials were kept on ice for approximately 30 minutes, then transferred to a -80C freezer for 24 hours before being stored in liquid nitrogen long term.

Human Keratinocyte Cells (hKeratinocyte or HEKa-APF)

hKeratinocyte Cell Media

EpiLife Medium was supplemented with Supplement S7 prior to use. One 500 ml bottle of medium is appropriate per 5 ml vial of supplement. Medium with supplement is usable for a period of one month. No components of media or other products were pre-warmed.

hKeratinocyte Substrate Preparation

Tissue culture dishes and other substrates used for hKeratinocyte cell culture were coated with Cascade Biologics's Coating Matrix Kit (Cat. no. R-011-K). Dilution Medium (Cat. no. R-012-50) was added to each flask to coat the complete surface. Coating Matrix (Cat. no. R-011-05) was then directly added to the dilution medium in each flask. Flasks were capped, swirled gently, and incubated for 30 minutes at room temperature. Excess coating matrix-dilution medium was removed from each flask before use. Unused flasks were stored at 4C for short periods of time.

hKeratinocyte Cell Thawing and Expansion

Human keratinocyte cells were thawed in 37C water baths. Cell concentrations were created at 1.25 x 10^4 viable cells/ml, and plated into tissue culture flasks or scaffolds. Media was changed after 24-36 hours, and every subsequent 48 hours until 50% confluency was reached. Between 50-80%, media was changed every 24 hours and should be passaged as they reach densities closer to 80%. Cell cultures seeded at 2.5×10^3 cells/cm^2 typically reach 80% confluency within 5-7 days.

hKeratinocyte Cell Passaging

Cells to be passaged have their culture medium removed, and Trypsin-EDTA is added to each flask. Flasks are incubated for 10-18 minutes at room temperature until cells have become completely rounded. 3 mls of defined trypsin inhibitor was added to each flask to neutralize the trypsin, and cells were moved to a sterile tube. A further 3 mls were added to each flask to

remove any remaining cells. The solution was then centrifuged at 180 x g for seven minutes. Supernatant was discarded, and the cell pellet was resuspended in 4 mls of cell culture media. Cells were seeded onto new culture vessels at a density of 2.5 x 10^3 cells/cm^2.

hKeratinocyte Cell Cryopreservation

Cells were cryopreserved in the same manner as fibroblasts, taking into account the different centrifugation speeds required. Vials were frozen down to contain 5×10^5 cells each.

Human Schwann Cells

Human Schwann Cell Media

Schwann cell media is composed primarily of high glucose DMEM (Gibco 11965-092). DMEM is then supplemented with 0.2% Glucose (Gibco 15023-021), 2mM L-Glutamine (Gibco 25030-081), 10% FBS (Sigma F4135), 2uM Forskolin (Sigma F6886), and 100 units/ml penicillin G sodium &100 µg/ml streptomycin (Gibco 15140). Media was always pre-warmed prior to use with cells.

Culturing Human Schwann Cells

Human Schwann cells taken out of cryopreservation should be rapidly thawed in a 37C water bath. Cells are mixed with warmed HSC medium and spun at 1000 rpm for 10 minutes. The supernatant was decanted and the pellet resuspended before plating. Adherence begins approximately 1 hour after plating and cells double in about 24 hours. Cell cultures should be split every 2–4 days as cell cultures reach 70–80% confluency.

Passaging Human Schwann Cells

HSC cells to be passaged are rinsed three times with PBS. 0.05% Trypsin-EDTA was added to each flask for one to two minutes to detach cells (monitor under microscope). Digestion of cells is stopped through resuspension in double the amount of HSC media. Cells are then plated and swirled to ensure even distribution of cells.

Cryopreservation of Human Schwann Cells

HSC cells that had been previously trypsinized, as in the passaging process, were resuspended in freezing medium so that the concentration was no more than $5x10^6$ cells/mL. Freezing medium consists of 10% DMSO, 70% HSCs culture medium, and 20% FBS. 1mL is required for every $2\text{-}5x10^6$ cells. Cells in freezing medium are kept at -20C for one or two hours, then transferred to 80C for 24 hours. Cells are subsequently transferred to liquid nitrogen for long term storage.

Keratinocyte-Dorsal Root Ganglion Cell Culture

Co-culture of keratinocytes and dorsal root ganglion cells was done to create an optimal somatosensory system cell culture model.

Human Keratinocyte-Dorsal Root Ganglion Co-Culture

Co-culture of human keratinocyte and DRG cells was initially attempted in the same way as rat keratinocyte-dorsal root ganglion cells. Dishes and scaffolds were pre-coated with Coating Matrix kits at room temperature for 30 minutes to 2 hours. Coating Matrix was always removed before plating cells.

Keratinocytes were cultured at 1,000,000 cells per well in 6 well plates. Epilife medium supplemented with S7 and antibiotics, as previously detailed, was used for the culture of these keratinocytes. After one hour to confirm adhesion of keratinocytes, DRG neurons were added to the cell culture at 50,000 cells per well. Media was removed within 24 hours and replaced with fresh media, then changed every 48 hours thereafter. Neuronal outgrowth was apparent within one day. Confluency and neuronal outgrowth was observable, but DRG population viability was less than expected following plating. Keratinocyte proliferation was apparent in contrast to slower-growing DRG populations. For this reason, a second media type was tested using a 2:1 ratio of Epilife media to DRG media (previously listed). This media promoted keratinocyte and DRG proliferation at a more even rate, encouraging improved DRG adhesion in the initial plating process. Cultures of up to two week periods were grown successfully with

balanced keratinocyte-DRG populations. Tissue formation was present as early as 10 days into the culture. Co-cultures were able to be passaged for several months without issue.

Fibroblast, Keratinocyte, Dorsal Root Ganglion, Schwann Cell Co-Culture

Following human keratinocytes and DRG co-culture, a more elaborate somatosensory system co-culture was attempted. Fibroblasts, keratinocytes, DRGs, and Schwann cells were combined to create a second somatosensory system model. In addition to this, other relevant co-culture controls were assessed to confirm that the appropriate media and ratios of cells were being combined in the final model for long term cellular growth.

Table 2.9: Somatosensory System Co-Cultures

Full Somatosensory Co-Culture	Fibroblast, Keratinocyte, Dorsal Root Ganglion, and Schwann Cell Co-Culture		
Other Partial Co-Cultures Assessed	Fibroblast-Keratinocyte		
	Fibroblast-DRG	Keratinocyte-DRG	
	Fibroblast-Schwann	Keratinocyte-Schwann	DRG-Schwann

As in the previous co-culture, Keratinocytes were cultured at 1,000,000 cells per well in 6 well plates. A 2:1 ratio of Epilife media to DRG media was used. After one hour to confirm adhesion of keratinocytes, DRG neurons were added to the cell culture at 50,000 cells per well, Schwann cells were added at 25,000 cells per well, and Fibroblasts were added at 25,000 cells per well. Media was removed within 24 hours and replaced with fresh media, then changed every 48 hours thereafter. Neuronal outgrowth was apparent within one day. Confluency and neuronal outgrowth was observable, and Schwann cells seemed to regulate and mediate overall growth of cells in the population, particularly fibroblasts. Fibroblasts, Keratinocytes, DRGs, and Schwann cells proliferated in respective rates of rapidly to slowly when co-cultured together, all cell types were able to coexist for periods of up to two weeks before passaging was necessary. The formation of cellular structures were observable within 36 hours. Tissue formation was present as early as 10 days into the culture. Co-cultures were able to be passaged for several months without issue.

2.9.3 ISO Standard Cytotoxicity Assays

Direct and indirect contact cytotoxicity assays were performed in vitro according to ISO 10993-5:2009(E) guidelines for biomedical devices in order to assess the biocompatibility of materials using the L929 mouse fibroblast cell line (L929 cell line, DSMZ Germany). The table shown depicts the quantities of materials required to accurately perform the assays.

All L929 fibroblasts used in these experiments were cultured in Eagle's Modified Dulbecco's Medium (DMEM, Gibco) supplemented with 10% (v/v) of fetal bovine serum (FBS, Gibco) and 1% penicillin–streptomycin antibiotics solution (Gibco, Life Technologies) and incubated (37 ºC, 5% CO_2, fully humidified).

Table 2.10: Summary of ISO 10993-5:2009(E) Guidelines for Cytotoxicity Assays

Thickness (mm)	Extraction Ratio (Surface Area or Mass/Volume)	Example Materials
< 0.5	6 cm^2/ml	Films, Sheets, Tubing Wall
0.5-1.0	3 cm^2/ml	Tubing Wall, Slab, Moulded Item
> 1.0	3cm^2/ml	Larger Moulded Items
> 1.0	1.25 cm^2/ml	Elastomeric Closures
Irregularly Shaped Solids	0.2 g/ml	Powder, Pellets, Foam, Non-Absorbent Moulded Items
Irregular, Porous, Low Density Materials	0.1 g/ml	Membranes, Textiles
There are no standardized methods for testing absorbents or hydrocolloids. Instead, the volume of extraction is determined for each 0.1g or 1.0 cm^2 of material. This volume is added to each extraction mixture.		

Preparation of Materials for Cytoxicity Tests

Material specimens were glued to microscope slide glass coverslips using sterile FDA-approved biocompatible glue (Silastic® medical adhesive silicone, type A). Samples were allowed to dry for at least 12 hours and prior to use in experiments hydrated in 1% penicillin–streptomycin antibiotics solution (Life Technologies) in Phosphate Buffer Solution (PBS, Gibco). Samples were sterilized by 24 hours of UV exposure followed by 24 hours immersion on 10% penicillin–streptomycin antibiotics solution (Life Technologies) in Phosphate Buffer Solution (PBS, Gibco). All operations were carried out in laminar flow chambers.

Indirect Contact Assays

For indirect contact assays, triplicates for each material were placed on 6-well plates (Falcon®, BD Biosciences) containing 2 mL of culture medium and kept in an incubator (37 °C, 5 \% CO2, fully humidified) for 24 hours. The liquid extracts were used to cultivate the L929 fibroblasts, seeded in 24-well plate (Falcon®, BD Biosciences) at an initial density of 8×10^4 cells/cm^2 for 24 h. Media incubated in tissue culture polystyrene incubated with sterile glass coverslips were used as a negative control, and a piece of latex glove (toxic) was used as positive control. Cell metabolic activity was quantified after 24 hours cultures using MTT, i.e. (3-(4,5-Dimethylthiazol-2-yl)-2,5-Diphenyltetrazolium Bromide), and measuring absorbance at 570 nm using the MTT kit (Thermofisher) as per manufacturer instructions. Absorbance for the negative control was reported at 100%; all other values were calculated respectively.

Direct Contact Assays

Direct contact assays were performed by placing test materials on the top of L929 fibroblast cultures in 24-well plates. Cells were cultured at $1.5x10^5$ per cm^2 and kept in an incubator (37 °C, 5 \% CO2, fully humidified) for 24 hours. After the incubation period, cells were observed under an inverted fluorescence microscope in order to qualitatively evaluate whether cells were confluent or a halo of inhibition at cell material interface was formed. This experiment was extended for a further 24 hours (a total of 48 hours), at which time the cells were imaged again. All cells were observed under an inverted fluorescence microscope (Leica DMI 3000B, Germany) in order to qualitatively evaluate if they are confluent or formed a halo of inhibition. Microscopy is detailed in a later section.

Alamar Blue Assay (24 well-plate)

Alamar (100uL) stock solution was diluted in DMEM 10% FBS not MSC (900uL). Medium was removed from cell culture plates, and 700 uL of the Alamar-media solution was added to each plate. Plates were incubated for two hours at 37ºC. 200 uL from each well were transferred to 96 well black, flat bottomed plates in triplicate, where fluorescence was read. Emission was set at 560nm and reading at 590nm, with variable Gain). Using pre-made calibration curves, total cell number was determined.

2.9.4 Cell Fixation and Staining

Mammalian Cell Fixation and Permeabilization

Prior to staining with immunofluorescent markers, cells were fixed and dehydrated. In order to do this, media was removed and cells were washed twice with PBS. After removal of PBS, each sample was immersed in either 4% paraformaldehyde, a combined solution of 2% paraformaldehyde and 2.5% glutaraldehyde, or 6% BSA in PBS at 37°C. The fixation time for samples ranged between 5 and 45 minutes at ambient temperature. Protocols varied due to scaffold sensitivity and staining types. Following fixation, fixed cells were washed twice with PBS. If no experiments were being planned immediately following this procedure, cells were left in the fridge immersed in PBS, or PBS-azide. Immunoblotting or other types of cell staining were performed thereafter.

Staining of Fixed Cells

Fixed mammalian cells should be washed with PBS, then incubated with 10% goat serum mixed in PBS-triton and PBS-azide for one hour. Certain stains, such as Nissl, are not able to be used with goat serum, and did not undergo this process. Non-immunocytochemistry cell staining was done with stains such as Phalloidin, Nissl, and DAPI. Phalloidin and Nissl (0.5 mg/mL) were diluted in PBS (1:200); DAPI was diluted at 3:200 and incubated for 1 hour and 5 minutes, respectively. Cells were then washed twice with PBS, and left in PBS until imaging.

Immunocytochemistry

Following cell permeabilization, primary antibodies were then added to cells and left overnight at 4C. Cells were then washed three times with PBS. Subsequent incubation was done with light-sensitive secondary antibodies for two hours at 4C. Washes with PBS were done three times, and a final counterstaining with Hoescht 33342 (2ug/ml; Sigma) was done for two minutes. A final three washes were done with distilled H20. PBS glycerol can be added as mounting media to prevent fading of antibody for long-term storage; coverslips should be applied and samples should be sealed with transparent nail varnish. Stained cells were visualized under a fluorescence microscop (Leica DMI 3000B), using the software Nikon-

AcT1, as is detailed later on in the section on fluorescence microscopy. The primary and secondary antibody stains used are detailed below.

Table 2.11: Antibodies Used in Immunocytochemistry

Primary Antibodies	**Type**	**Source**	**Dilution**
Anti-TUJ1	Mouse IgG	Covance	1:4000
Beta-Tubulin III	Mouse IgG	Covance	1:1000
GFAP	Mouse IgG/Rabbit IgG	Millipore	1:100
Secondary Antibodies			
Anti-Alexa 546 (red)	Goat Anti-Mouse IgG	Life Technologies	1:400/1:500
Anti-Alexa 546 (red)	Goat Anti-Mouse IgG	Life Technologies	1:400/1:500
Anti-Alexa 488 (green)	Goat Anti-Rabbit IgG	Life Technologies	1:400/1:500

Cell Dehydration

Following cell fixation (or fixation, permeabilization, and staining), solutions of either ethanol or isopropanol were prepared at concentration of 20%, 40%, 60%, 80%, 90% and 96%. Following the aforementioned fixation protocol, any PBS was removed from cells and replaced with the 20% solution. This solution was allowed to remain on cells for 30 minutes, then removed, and replaced with the 40% solution. This process was repeated with each solution in increasing order. After completion of the 96% solution incubation, cells were allowed to dry in a desiccator/fume hood at room temperature as slowly as possible. Cells can them be taken to SEM for imaging.

Live-Dead Cell Staining

Live-Dead Staining using the LIVE/DEAD® Viability/Cytotoxicity Assay Kit, containing Calcein AM and Ethidium homodimer-1. This kit simultaneously determines live and dead cells intracellular esterase activity and plasma membrane integrity. This assay has been utilized to quantify apoptotic cell death and cell-mediated cytotoxicity.[44, 45]

Cells to be stained are first washed with PBS, then calcein diluted in PBS to create a 2uM working solution was applied to cells and incubated for approximately 30 minutes. A 4 uM EthD-1 solution was created and added directly to the solution and cells. Cells can be imaged immediately or mounted on slides, sealed with fingernail polish, and subsequently imaged.

Calcein is imaged as green fluorescence in live cells (ex/em ~495 nm/~515 nm). EthD-1 binds to nucleic acids, producing red fluorescence in dead cells (ex/em ~495 nm/~635 nm).

Live Cell Staining (Cell-Specific Trackers)

Cell Tracker Fluorescent Probe

Cell tracker dye was dissolved in DMSO to a final concentration of 10 mM. Stock solutions were made to a final working concentration of 0.5–25 μM in serum-free medium. Media on cell culture was removed, cells were washed with PBS, and cell tracker diluted in media was applied. Incubation was done for 15-45 minutes, then media with dye was removed and regular cell culture medium was applied to the cells. All images were taken within two to three hours following the initial staining.

NeuroTrace Fluorescent Nissl Stain

Nissl stains can be used to identify high protein synthesis found in the rough endoplasmic reticulum of neuronal perikarya and dendrites, thereby identifying neuronal cells. Nissl staining can be performed on live and fixed tissue. Cells were repeatedly washed with PBS for ten minutes, and neurotrace stain was diluted 20- to 300-fold in PBS. Incubation was left for 20-30 minutes. Stain was then removed, and cells were washed three times over a period of ten minutes in PBS. All images were taken within two to three hours following the initial staining.

Alkaline Phosphatase Live Stain

Alkaline Phosphatase is a stem cell stain that differentially stains pluripotent stem cells (PSCs). Stock solutions of alkaline phosphatase (AP) were diluted at 1 uL for each 0.5 mL of medium or PBS. Growth medium in cultures is removed and solutions are washed twice with culture medium. AP stains are prepared in culture medium, applied to cells, and incubated for 20-30 minutes. Cells were then washed twice with media to reduce the background signal. All images were taken within two to three hours following the initial staining.

2.9.5 Cell Culture and Culture in Electrical Fields

Mammalian Adhesion Assays

Material specimens were glued to microscope slide glass coverslips using sterile FDA-approved biocompatible glue (Silastic® medical adhesive silicone, type A). Samples were allowed to dry for at least 12 hours and prior to use in experiments hydrated in 1 \% penicillin–streptomycin antibiotics solution (Life Technologies) in Phosphate Buffer Solution (PBS PBS, Gibco). Samples were sterilized by 24 hours of UV exposure followed by 24 hours immersion on 10 \% penicillin–streptomycin antibiotics solution (Life Technologies) in Phosphate Buffer Solution (PBS, Gibco). All operations were carried out in laminar chambers.

Adhesion assays were performed using the L929 mouse fibroblast cell line (L929 cell line, DSMZ Germany). L929 fibroblasts were cultured in Eagle's Modified Dulbecco's Medium (DMEM, Gibco) supplemented with 10 \% (v/v) of fetal bovine serum (FBS, Gibco) and 1 \% penicillin–streptomycin antibiotics solution (Gibco, Life Technologies) and incubated (37 ºC, 5% CO_2, fully humidified). Cells were seeded directly onto scaffolds and allowed to adhere for a period of 8 days, then stained with fluorescent markers and imaged.

Variations of adhesion assays were performed over a duration of 3-14 days using Fibroblast, ReN, Schwann, Dorsal Root Ganglion, and Keratinocyte cells.

Mammalian Electrical Field Scaffold Set-up

Previously prepared 3D-printed scaffold wells that had been coated with PDMS and glued to scaffolds were prepared by attaching copper wires to each well-scaffold substrate. Copper wires with a diameter of 0.35 mm were used to connect the electrical scaffolds to the electrodes from the electrical set-up. The tips of all copper wires were dipped in acetic acid before attaching them to scaffolds in order to remove the insulating enamel and improve conductivity. Copper wires were then connected to scaffolds by gluing the tips to the scaffolds using conductive silver paste (Electrodag 1415, Agar Scientific). All scaffolds were again sterilized as previously detailed after attachment of any wires.

Mammalian Electrical Field Experimental Set-up

The setup for electrical field experiments is shown below. The equivalent circuit is a simple voltage divider where the scaffolds, represented as resistors, are connected in series with a rheostat. The circuit shows how the connection from the voltage source positive terminal to the scaffolds (node 1) and from these to the rheostat (node 2) is made via cables connected to the samples. The cables enter the incubator and are connected to scaffolds via copper wires. The rheostat is connected to the grounded negative terminal of the voltage source.

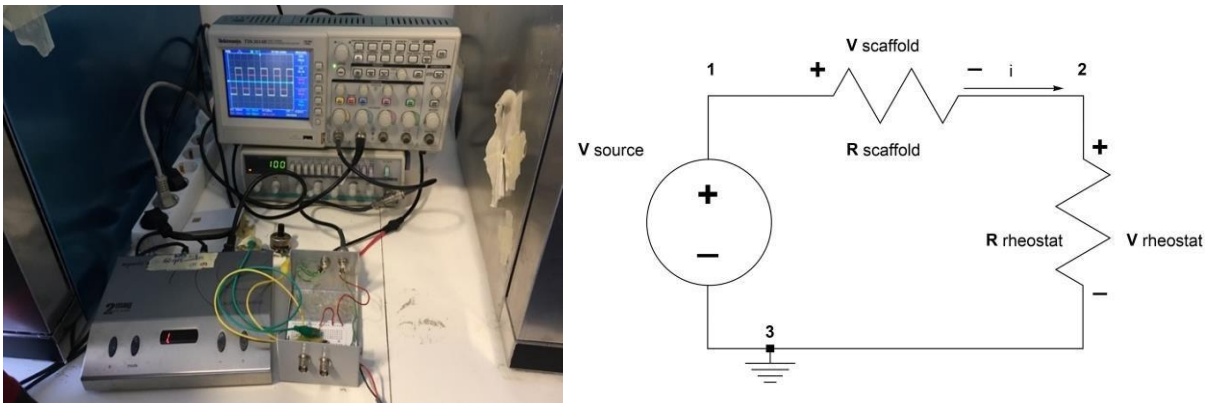

Figure 2.10: Experimental Setup for the Electrical Field Experiments. A) "Electrical Setup" kept next to the cell incubator, composed of a voltage source, oscilloscope, rheostat and a circuit board that maintains the circuit; (B) Schematic of the circuit.

The rheostat indirectly measures scaffold voltage (Vscaffold), the difference between the source (Vsource) and rheostat voltage (Vrheostat) which are measured at the oscilloscope. This method is useful as it prevents contamination from probes connected directly to scaffolds. The rheostat also acts as an alternative method to adjust scaffold voltage by making the resistance value alterable. The scaffold resistance (Rscaffold) is measured with a multimeter before connecting them to the rest of the circuit. By knowing the resistance, the scaffold voltage was necessary to obtain a desired current value. Voltage can be adjusted to the desired value by adjusting the source or rheostat resistance.

Mammalian Electrical Field Culture and Expansion

Previously prepared scaffolds with 3D-printed wells and copper wires that had been sterilized as previously stated were pre-coated as required for each cell type. Cells were then seeded onto scaffolds with a density of 30 000 cells/cm^2 using the expansion culture medium. Cells were expanded in a manner similar to the methods used in previous studies.[46] An AC Electric Field

was applied as a voltage quadratic pulse of 100 Hz over four consecutive days after seeding. Culture medium was changed every 48 hours. After four days, cells were stained and imaged through SEM or confocal imaging.

Mammalian Electrical Field Differentiation

The differentiation protocol used is similar to that conducted by Pires et al.[46] Cells were first expanded as previously detailed, and the AC electric field was applied over days intermittently 12-hour "on" and 12-hour "off" sequence. Media was changed ever 48 hours. After seven days, cells were stained and imaged through SEM or confocal imaging.

2.10 Microscopy and Other Assessments of the Construct (Chapter 5)

2.10.1 Fluorescence Microscopy Imaging

All bright-field and fluorescence images were taken using the Leica® DMI 3000B microscope, Nikon® DXM 1200F digital camera and Nikon® AcT1 software. As previously detailed in the staining section, Hoescht or DAPI (Sigma), with a maximum excitation at 340 nm and fluorescence emission maximum at 488 nm, were used to stain cellular nuclei. Phalloidin (Sigma) was done at excitation of 540-545 nm; fluorescence emission maximum at 570-573 nm and stained with the TRITC excitation filter. Antibody staining done with Alexa Fluor-546 (Life Technologies) had a maximum excitation at 556 nm; fluorescence emission maximum at 573 nm and was imaged using a TRITC filter. Antibody staining done with Fluor-488 (Life Technologies) had a maximum excitation at 490 nm; fluorescence emission maximum at 525 nm and were imaged with a FITC excitation filter.[47-50]

2.10.2 Scanning Electron Microscopy (SEM)

Prior to SEM analysis, samples with cells were fixed with glutaraldehyde 1.5% (v/v) in PBS at 37°C for 1 hour. The samples were washed three times with PBS and afterwards the samples were immersed in ethanol solutions at different concentrations, 25, 50, 75, and 99% for 30 min each at 37 °C. Before the observation of the substrates they were coated with a 30 nm Au/Pd layer using a Polaron model E5100 coater (Quorum Technologies). Images were obtained

using a Field Emission Gun Scanning Electron Microscope (FEG-SEM) (JEOL, JSM-7001F model).

2.10.3 Confocal Microscopy

Samples from adhesion and proliferation assays were imaged with a laser scanning confocal microscope (Leica TCS-SP5) equipped with a continuous Ar-ion laser (Multi-line LASOSs LGK 7872 ML05) and a Ti:sapphire laser (Spectra-Physics Mai Tai BB, 710–990 nm, 100 fs, 82 MHz). A 63x 1.2 N.A. water immersion objective was used (HCX PL APO CS 63.0x 1.20WATERUV). Prior to imaging, samples with cells were stained with Alkaline Phosphatase (Thermofisher) for one hour in PBS. Samples were not fixed, and were imaged live due to dye uptake by the scaffolds resulting in excessive autofluorescence when fixed. Resulting images were processed using Image J software.

2.10.4 Energy-dispersive X-ray spectroscopy (EDX)

EDX was used to perform elemental analyses of coated substrates. The technique utilises emitted X-Rays to analyses atoms irradiated by electron beams. As each element has an unique atomic structure, identifiable peaks on its X-ray spectrum can be obtained. The equipment utilized is the same as detailed in the SEM section. Voltages of 5-30kV and high vacuum conditions were used.

2.10.5 Atomic Force Microscopy (AFM)

AFM in dynamic mode was performed using a Pico Plus Molecular Imaging microscope and 10 nm sized silicone tips. The cantilever strength used was approximately 40 N/m and resonance frequency was 170 kHz. Various images were taken throughout different areas of the sample in order to subsequently analyse the roughness and grain size. Roughness value can be calculated using the following equation:

$$S_q = \sqrt{\frac{1}{A} \iint_A z^2(x,y)\,dx\,dy}$$

Equation 2.6: Roughness Value

2.10.6 Contact Angle

Contact angle was measured to assess the hydrophobicity of the materials used in cell culture, namely Kraton D1152ES (SBS). Kraton D1152ES (SBS) coated with Gwent polymeric platinum, and P(VDF-TrFE). Contact angle was defined as the angle formed between a drop of liquid and the surface of the substrate, as shown below. The sessile drop profile method was used. Contact angle was assessed with either the Kruss DSA25B goniometer and Drop Shape Analysis 4 Software by measuring the tangent angle at the three-phase contact point (Figure 2.11), or the Pocket Goniometer PG2 model. The bigger the angle, the larger the hydrophobic surface. Hydrophobicity was defined as $\theta > 90^{o}$.

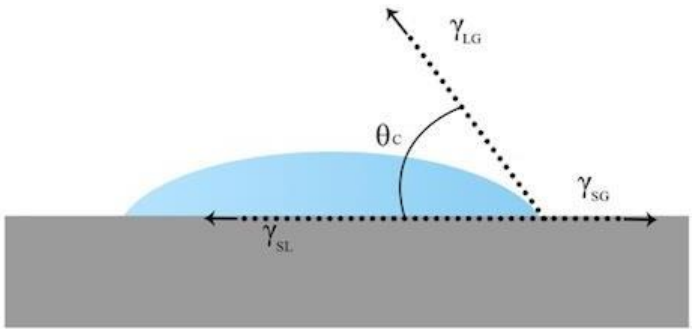

Figure 2.11: Schematic of Contact Angle Methodology. Contact angle (θC) of liquid droplets can be measured at the three-phase (solid, liquid, and gaseous) contact point. The solid-liquid interfacial tension is defined as γSL, liquid surface tension is γLG, and solid-vapour interfacial tension as γSG.

2.11 References:

1. Yao, Jian, Cees WM Bastiaansen, and Ton Peijs. "High strength and high modulus electrospun nanofibers." *Fibers* 2.2 (2014): 158-186.
2. Chang, Wen-Yang, Te-Hua Fang, and Yu-Cheng Lin. "Physical characteristics of polyimide films for flexible sensors." *Applied Physics A* 92.3 (2008): 693.
3. Chisca, Stefan, et al. "Dielectric and conduction properties of polyimide films." *Semiconductor Conference (CAS), 2011 International*. Vol. 2. IEEE, 2011.
4. Li W, Wan M. Porous polyaniline films with high conductivity. Synthetic metals. 1998 Jan 30;92(2):121-6.
5. Yang, Jiping, et al. "Polyaniline/polypropylene film composites with high electric conductivity and good mechanical properties." *Journal of applied polymer science* 56.7 (1995): 831-836.
6. Hammo, Shamil M. "Effect of Acidic Dopants properties on the Electrical Conductivity of Poly aniline." *Tikrit Journal of Pure Science* 17.2 (2012): 76-78.
7. Grabbert, Niels, et al. "Mechanical properties of individual composite poly (methyl-methacrylate)-multiwalled carbon nanotubes nanofibers." *IOP Conference Series: Materials Science and Engineering*. Vol. 64. No. 1. IOP Publishing, 2014.
8. Coelho, Paulo Henrique da Silva Leite, et al. "Electrical percolation, morphological and dispersion properties of MWCNT/PMMA nanocomposites." Materials Research 17 (2014): 127-132.
9. Malmonge, Luiz Francisco, et al. "Thermal and mechanical properties of PVDF/PANI blends." Materials Research 13.4 (2010): 465-470.
10. Mikolajczyk, Teresa, et al. "Strength properties of polyacrylonitrile (PAN) fibres modified with carbon nanotubes with respect to their porous and supramolecular structure." *Fibres & Textiles in Eastern Europe* 17.6 (2009): 13-20.
11. Jacquemin, J. L., A. Ardalan, and G. Bordure. "Electrical conductivity and dielectric constant of heat-treated polyacrylonitrile in an AC regime." *Journal of Non-Crystalline Solids* 28.2 (1978): 249-257.
12. Teoh, H., P. D. Metz, and W. G. Wilhelm. "Electrical conductivity of pyrolyzed polyacrylonitrile." *Molecular Crystals and Liquid Crystals* 83.1 (1982): 297-306.
13. Chen, Wei, et al. "Improved polyvinylpyrrolidone microneedle arrays with non-stoichiometric cyclodextrin." *Journal of Materials Chemistry B* 2.12 (2014): 1699-1705.
14. Tsui, C. P., et al. "Prediction for debonding damage process of glass beads-reinforced modified polyphenylene oxide under simple shear." *Journal of materials processing technology*167.2-3 (2005): 429-437.
15. Sadhu, Susmita, and Anil K. Bhowmick. "Preparation and properties of nanocomposites based on acrylonitrile–butadiene rubber, styrene–butadiene rubber, and polybutadiene rubber." *Journal of Polymer Science Part B: Polymer Physics* 42.9 (2004): 1573-1585.
16. Armani, Deniz, Chang Liu, and Narayan Aluru. "Re-configurable fluid circuits by PDMS elastomer micromachining." *Micro Electro Mechanical Systems, 1999. MEMS'99. Twelfth IEEE International Conference on*. IEEE, 1999.
17. Kraton Performance Polymers, Inc. Kraton: The Global Connection for Polymer and Compound Solutions Product and Application Guide. Kraton Performance Polymers, Inc., 2014, www.kraton.com.

18. Suleiman, David, et al. "Mechanical and chemical properties of poly (styrene-isobutylene-styrene) block copolymers: Effect of sulfonation and counter ion substitution." *Journal of Applied Polymer Science* 131.11 (2014).
19. Linares, A., and J. L. Acosta. "Structural characterization of polymer blends based on polysulfones." *Journal of applied polymer science* 92.5 (2004): 3030-3039.
20. Tahk, Dongha, Hong H. Lee, and Dahl-Young Khang. "Elastic moduli of organic electronic materials by the buckling method." *Macromolecules* 42.18 (2009): 7079-7083.
21. Vosgueritchian, Michael, Darren J. Lipomi, and Zhenan Bao. "Highly conductive and transparent PEDOT: PSS films with a fluorosurfactant for stretchable and flexible transparent electrodes." *Advanced functional materials* 22.2 (2012): 421-428.
22. Kuila, Biplab K., and Arun K. Nandi. "Physical, mechanical, and conductivity properties of poly (3-hexylthiophene)− montmorillonite clay nanocomposites produced by the solvent casting method." *Macromolecules* 37.23 (2004): 8577-8584.
23. Cuenot S, Demoustier-Champagne S, Nysten B. Elastic modulus of polypyrrole nanotubes. Physical Review Letters. 2000 Aug 21;85(8):1690.
24. Osagawara, M., et al. "Enhancement of electrical conductivity of polypyrrole by stretching." *Synthetic metals* 14.1-2 (1986): 61-69.
25. Chou, Ye T., Ya T. Ko, and Man F. Yan. "Fluid flow model for ceramic tape casting." *Journal of the American Ceramic Society* 70.10 (1987): C-280.
26. Norrman, K., A. Ghanbari-Siahkali, and N. B. Larsen. "6 Studies of spin-coated polymer films." *Annual Reports Section" C"(Physical Chemistry)* 101 (2005): 174-201.
27. Luurtsema, Gregory A. *Spin coating for rectangular substrates*. Berkeley: University of California, 1997.
28. Teo, Wee E., and Seeram Ramakrishna. "A review on electrospinning design and nanofibre assemblies." *Nanotechnology* 17.14 (2006): R89.
29. Pham, Quynh P., Upma Sharma, and Antonios G. Mikos. "Electrospinning of polymeric nanofibers for tissue engineering applications: a review." *Tissue engineering* 12.5 (2006): 1197-1211.
30. Schwartz, L., and L. White. "Modelling of the dip-coating process." (1994).
31. Cruz, A. M., et al. "Iridium oxohydroxide, a significant member in the family of iridium oxides. Stoichiometry, characterization, and implications in bioelectrodes." *The Journal of Physical Chemistry C* 116.8 (2012): 5155-5168.
32. Petit, Michel A., and Vincent Plichon. "Anodic electrodeposition of iridium oxide films." *Journal of Electroanalytical Chemistry* 444.2 (1998): 247-252.
33. Cruz Rodríguez, Ana Milena. *Obtaining and characterization of electroactive materials for neuronal growth support* . Universitat Autònoma de Barcelona, 2011.
34. Kasem, By Kasem K., and Stephanie Jones. "Platinum as a reference electrode in electrochemical measurements." *Platinum Metals Review* 52.2 (2008): 100-106.
35. Bourne Jr, Henry C., L. George Chow, and David S. Bartran. "Deposition Temperature of Evaporated Permalloy Films." *Journal of Vacuum Science and Technology* 8.5 (1971): 619-621.
36. Levy, F. "Film Growth and Epitaxy: Methods." (2014).

37. Shinar, J., R. Shinar, and R. J. Groarke. "An overview of organic light-emitting diodes and their applications." (2014).
38. Wasa, Kiyotaka, Makoto Kitabatake, and Hideaki Adachi. *Thin film materials technology: sputtering of control compound materials*. Springer Science & Business Media, 2004.
39. Tobias, Gerard, et al. "Enhanced sidewall functionalization of single-wall carbon nanotubes using nitric acid." *Journal of nanoscience and nanotechnology* 9.10 (2009): 6072-6077.
40. Hummers Jr, William S., and Richard E. Offeman. "Preparation of graphitic oxide." *Journal of the american chemical society* 80.6 (1958): 1339-1339.
41. Hunt, Charles J. "Cryopreservation of human stem cells for clinical application: a review." *Transfusion Medicine and Hemotherapy* 38.2 (2011): 107-123.
42. Baust, John M., Robert Van Buskirk, and John G. Baust. "Cell viability improves following inhibition of cryopreservation-induced apoptosis." *In Vitro Cellular & Developmental Biology-Animal* 36.4 (2000): 262-270.
43. ReNcell VM Human Neural Progenitor Cell Line. at <https://www.merckmillipore.com/PT/en/product/ReNcell-VM-Human-Neural-Progenitor-Cell-LIne,MM_NF-SCC008?bd=1> (accessed May 1, 2018).
44. Weil, M., et al. "Constitutive expression of the machinery for programmed cell death." *The Journal of Cell Biology* 133.5 (1996): 1053-1059.
45. Papadopoulos, Nikolaos G., et al. "An improved fluorescence assay for the determination of lymphocyte-mediated cytotoxicity using flow cytometry." *Journal of immunological methods* 177.1-2 (1994): 101-111.
46. Pires, Filipa, et al. "Neural stem cell differentiation by electrical stimulation using a cross-linked PEDOT substrate: expanding the use of biocompatible conjugated conductive polymers for neural tissue engineering." *Biochimica et Biophysica Acta (BBA)-General Subjects* 1850.6 (2015): 1158-1168.
47. DAPI for nucleic acid staining | Sigma-Aldrich. at <http://www.sigmaaldrich.com/catalog/product/sigma/d9542?lang=pt&region=PT> (accessed May 1, 2018).
48. Phalloidin–Tetramethylrhodamine B isothiocyanate Phalloidin from Amanita phalloides | Sigma-Aldrich. at <http://www.sigmaaldrich.com/catalog/product/sigma/p1951?lang=pt&region=PT> (accessed May 1, 2018).
49. Alexa Fluor® 546 dye. at <https://www.thermofisher.com/pt/en/home/life-science/cell-analysis/fluorophores/alexa-fluor-546.html> (accessed May 1, 2018).
50. Alexa Fluor® 488 dye. at <https://www.thermofisher.com/pt/en/home/life-science/

CHAPTER 3.
MECHANICAL ASSESSMENT OF SELECTED POLYMERS AND THE COMPLETE CONSTRUCT

3.1. Outline

This chapter explores the use of flexible and elastic polymers that can be used in the development of second skin substrates. The introduction discusses the mechanical properties of skin compared to the substrates designed to mimic skin. It also elaborates upon the uses of flexible versus elastic materials, their properties and mechanical limitations.

The results are divided in 4 sections. The first section, 3.3.1 discusses one of our primary hypotheses: If it is possible to get a electrospun mesh of flexible materials to behave in a mechanically comparable manner to skin; i.e., the electrospun mesh would provide increased elastic properties compared to films or blocks of material used. Flexible polymers in this section were preferentially treated through electrospinning methods in order to decrease their Young's modulus values. Elastomeric polymers, which are more difficult to electrospin, were preferentially treated through drop casting methods. At this stage, a preliminary assessment was made. The majority of electrospun meshes that had been created were found to lack either robustness or true elastic behaviour. Consequently, the combinations of conditions used and materials selected in this work refute the initial hypothesis: It was not possible to produce a robust, elastic, electrospun mesh using flexible materials. Nonetheless, this work produced P(VDF-TrFE) electrospun fibers, useful as piezoelectrics, which are discussed in this chapter as well as in chapters 4 and 5.

The second section, 3.3.2, discusses the initial assessment of elastic alkene-styrene copolymers, which were prepared as films. Fibers were made of some of these polymers to mimic skin structure. Electrospinning was attempted on elastomeric polymers as well, but was not deemed a necessity due to their mechanical properties in planar form. In addition to electrospinning flexible materials, a new protocol was developed for the electrospinning of elastomer styrene-butadine-styrene (Kraton D1152ES (SBS)). Notably, this protocol requires the addition of iron (III) p-toluenesulfonate to make the spinning solution conductive enough to respond to the applied electrical field and obtain fibers. The mechanical properties of both planar and electrospun elastic materials were compared against skin.

Due to the variable influence of processing on polymers, we provide SEM analysis of the materials produced in the two first subsections. We initially manually assessed the mechanical

properties of polymers, particularly in respect to the analysis of mechanical changes that occurred over time (e.g., dehydration-related changes to mechanical properties). These sections detail the process that was undertaken in the selection of finding polymers suitable as second skin substrates.

The third section, 3.3.3, is focused on the quantitative assessment of alkene-styrene polymers. The mechanical and biocompatibility properties of silicone and other elastomers are well established. Similarly, the commercial alkene-styrene based materials chosen for these experiments had been previously tested to ISO standards. However, we created blended materials and nanostructured variants that were entirely novel and had unknown properties. The Young's moduli, stress-strain curves and fatigue properties for all of these materials were determined.

Finally, the fourth and concluding section, 3.3.4, assessed porcine skin alongside our selected polymers to validate the materials' performance. To our knowledge, this is the first analysis directly comparing mammalian skin to polymers in order to optimize second skin creation.

3.2. Introduction

3.2.1 The Mechanical Properties of Skin vs. Skin Substrates

Skin, well known as the largest organ of the body, is composed of stratum corneum, epidermis, dermis, and hypodermis.[1] The functions of skin range from thermoregulation to protection against pathogens and physical injury. Skin is particularly unique because it has both exceptional mechanical strength and viscoelastic properties. This auto-regulated organ hasthe capacity to contort and reform repeatedly while remaining resistant to tear. It's well-established, non-homogenous, anisotropic, viscoelastic properties affect various fields, including cosmetology, dermatology, cosmetic surgery, and pharmacology.[2-4] The mechanical properties of skin are of particular concern to medical professionals that manage skin wounding, such as when grafting burns or treating the complex ulcerations that occur to diabetics.[4, 5] Despite this, the complexities of skin's mechanical properties remain poorly understood.

On a microscopic level, skin deformation involves straightening bundles of tightly wound collagen. Their conformation elongates and changes orientation toward the direction of the applied force. Meanwhile, stretched fibres of elastin and the interfibrillar matrix act as load bearers. Collagen fibres subsequently begin to bend. Shear stress of these fibres results in a higher young's modulus than elastin, responsible for skin's mechanical resistance and stiffness. Deformation ends with collagen fibres acting as even stronger load bearers-- with stress appearing proportional to strain.[4] Experimentally, skin shows good extensibility when affected by small forces. However, as the forces increase it becomes much stiffer, giving rise to the established stress and strain 'J-curve'.[6, 7] This unique curve can be divided into three parts, all of which are ascribed to the fibrillary and amorphous microstructure of the dermis—the same component that the skin owes its unique strength and viscoelasticity to.[4]

Mimicking skin is particularly challenging from a materials perspective; the unique non-homogenous, anisotropic, viscoelastic properties of skin make it difficult to replicate.[8] Polymers used for the creation of artificial and second skin substrates must exhibit a high degree of elasticity, rather than the flexibility required for muscle and skeletal tissue engineering. The ideal skin substitute would be made of perdurable materials or be self-healing, as well as biocompatible. It should also have a low young's modulus while simultaneously having a high strength capacity that promotes fatigue-resistance. In particular, the creep capacity and recovery of skin are remarkable attributes that make it difficult to replicate. A variety of polymers can replicate one or a few of skin's interesting properties, but no single polymer can yet exactly replicate all of them. Currently, two main types of bioengineered skin substitutes exist: artificial skins and second skins, which may also be referred to as electronic skins.

Artificial skin substrates promote skin regeneration. The first artificial skin was created in 1979.[9] This artificial skin substrate was a porous, biodegradable matrix made of animal collagen and glycosaminoglycan molecules that encouraged cell growth. Combined with a silicone based cover, this artificial skin created a new dermis that allowed gas permeation and mitigated infection, providing a rough temporary substitute for the epidermis. Artificial skin substrates today are based on the same principle-- they are typically biodegradable and are replaced by the extracellular matrix as natural tissue regenerates. Polymers used for skin grafts,

such as poly(lactide-co-glycolide), are the biodegradable support structures typically used in current artificial skin development.[10]

Unlike artificial skin, second skin substrates tend to be perdurable, non-implantable materials. They are typically designed for cosmetic applications or integration with prosthetics and robotic artificial sensors to further the integration of human-machine interfaces.[11, 12] Second skin substrates attempt to mimic the aesthetic, sensorial, or mechanical properties of mammalian skin. Ideally, second skins have the capacity to regenerate or are perdurable. Artificial skin products are often made of elastomers, particularly silicone-based and alkene-styrene-based co-polymers.[12-14] Such products include MIT's elastic second skin and Stanford's organic electronic skin.[14, 15]

The mechanical properties of skin have viscoelastic, anisotropic properties that can be assessed through a variety of methods. The most accurate assessments are done *in vivo,* which allows *in situ* measurements of skin to be taken. However, this doesn't allow for exact comparisons with synthetic materials, whether these are for high-compression, spacesuit-related wearables or artificial skin substrates.[9, 48]

In the 1980s, a variety of studies attempted to determine the Young's modulus of human skin. The values obtained varied between $2x10^4$ N/m^2 to $1.8xl0^7$ N/m^2 as a parameter that increases with age.[49] Teams using different methods to compare the Young's modulus of skin *in vivo* found dramatically different results. A study was published in 1980 yielding an elastic modulus of $4.2xl0^5$ N/m^2 that increases with age. A comparable study was published in 1989 resulting in an elastic modulus of $11.2xl0^5$ N/m^2, with a 20% increase in this value after the seventh decade.[49] In contrast, a study by Vogel et al found that a child's elasticity modulus was, on average, 70 N/mm^2 (MPa), while an elderly adult's elasticity modulus averaged at 60 N/mm^2.[50]

Variations in the Young's modulus of mammalian skin will always be the norm due to differences in experimental conditions. However, beyond use of different methodologies, variations in results can be obtained due to harvesting different skin sites in subjects of varying ages, leading to a difference in the nature and amplitude of the deformations. Given these differences in methodology, region studied, subject age, and other influential factors, we determined that a direct comparison of skin and our chosen polymers was essential. We decided

to use porcine skin as we needed to utilize fresh skin from a reproducible subject group to compare to our polymers.

Recent studies have confirmed the low stiffness of human skin (Young's modulus ca. 0.3–1.0 MPa).[51] Although other studies state that porcine skin is equivalent to human skin, values of porcine skin in the literature tend to be somewhat higher, presenting as 2.5 ± 2.1 MPa for the cranial abdominal region of porcine foetuses and 1.85 ± 0.85 MPa for the thoracic limb region.[52] However, the same study showed that the conventional Young's moduli for these region-specific samples were different, with the cranial abdominal region presenting a Young's modulus of 4.02 ± 3.81 MPa and the thoracic limb region a value of 7.68 ± 3.96 MPa.[52] Our interests in skin were related to regions that experience constant mobility and fatigue, such as joints. As such, our selected porcine samples are notably different to those studied; we selected ankle joints and lower auriculae skin samples.

3.2.2 Flexible vs. Elastic Materials

Flexible and elastomeric materials are frequently used for biomedical purposes. Flexible polymers are often blended with a range of other materials — from metals to other polymers. Certain flexible materials are capable of dual functionality, acting as conductors, piezoelectrics or other sensors. Elastomers, on the other hand, are most well-established as insulators and wearables. Their purposes may be limited if they are too soft. When blended with other materials, elastomers often lose their unique mechanical properties.

Natural elastomeric materials, like skin, have a much wider range of properties than their synthetic counterparts. The aim of this chapter was to identify biocompatible, perdurable, flexible and elastic materials with comparable mechanical properties to skin. Our ultimate goal was to create a material construct that would mimic skin's properties on even a nanoscale level.

We began our research by attempting to create an electrospun meshes for flexible materials. Flexible and elastic polymers can be easily differentiated through their different stress and strain capacities. These can be assessed through the calculation of the Young's modulus. However, the mechanical properties of polymers is modifiable. Both Young's modulus and the

shape of stress-strain curves can be altered by producing polymers at different thicknesses or processing them into different nanoscale or microscale structures.

For example, solid Poly(methyl-methacrylate) (PMMA) has a Young's modulus of 3 GPa in its solid state. However, its Young's modulus is as low as 136 MPa when processed into nanofibrous form.[16] This is a 22-fold difference. Similarly, Polyvinyl Pyrrolidone (PVP) has a Young's modulus of 2.433 GPa in planar form, though this value can vary substantially due to molecular weight.[17, 34] PVP's Young's modulus can decrease to values between 8.8 and 40.8 MPa in nanofibrous form. The exact value is not only determined by the polymer's molecular weight, but due to the chosen solvent.

Given the dramatic changes in mechanical properties that can occur through processing flexible materials, we selected a range of polymers to be prepared as electrospun meshes. We preferentially selected flexible polymers with electroconductive properties. This was important as solution conductivity is essential for the creation of nanofibers through techniques such as electrospinning.

We selected biocompatible polymers with Young's modulus values of less than 10 GPa in planar form and assessed their capacity to be used as a component of skin substrates. Polysulfone (PSu), with a Young's modulus of 1.539 GPa, and Poly [(vinylidenefluoride)-co-trifluoro ethylene] 70:30 (P(VDF-TrFE)), which has a Young's modulus of 1.2 GPa and were the most flexible materials selected.[23, 27] Polyacrilonitrile (PAN), with a planar Young's modulus between 7.8 and 9.5 GPa, was the least flexible material chosen.[28] These polymers, along with polymers Polyimide (PI), PMMA, and PVP, were processed through the techniques such as electrospinning, drop casting, and spin coating.

Similar to our chosen biocompatible, perdurable, flexible polymers, selected elastomers were copolymers we believed were capable of mimicking the complex mechanical properties of skin. We sought out elastomers that could mimic the mechanical properties of the dermis, specifically those with the potential to be used as substrates for subdermal implants. We focused on alkene-styrene copolymers, which may be flexible or elastic depending on the nature of the additional monomers used. These copolymers are easy to modify and process in different structures, giving them the potential to be used in a wide range of biomedical

devices.[40-42] However, selecting these polymers was also advantageous given their potential novelty. There are only around a dozen publications detailing the use of electrospun alkene-styrene based polymers.[5, 76-83] Thus far, electrospun alkene-styrene polymers include styrene-isoprene-styrene (SIS), styrene-butadiene-styrene (SBS), styrene–ethylene/butylene–styrene (SEBS), and poly(styrene-β-isobutylene-β-styrene) (SIBS). The properties for these various flexible and elastic polymers were previously summarised in Chapter 2.

3.2.3 Uses for Bioengineered Flexible Materials

Flexible polymers, namely our selected polymers PMMA, PVP, PI, PAN, PSu and P(VDF-TrFE), are all commonly used as bioengineered and biomedical materials.[61] Once processed into electrospun fibers, the uses of these flexible materials multiply. Most studies focus on creating blends of polymers, which have tailor-made properties specifically suited for biomedical purposes. Notably, blends of polymers does not only refer to polymer-polymer blends, but other materials blended into polymers. For instance, PMMA, PI and other polymers are commonly blended with carbon nanotubes to enhance conductivity and modify the mechanical properties of the nanofibers.[62]

Polyaniline (PANi)-PAN blends, for instance, have been utilized as substrates that support the expansion and differentiation of skeletal muscle cells.[63] Similarly, polycaprolactone (PCL)-PVP blends have been used as degradable scaffolds for tissue engineering.[64] However, there are several variables that can influence the properties of blended polymers, including the different solvents chosen and ratios at which these polymers are blended. This allows blended materials to have a range of different properties and uses. PCL-PVP, for instance, can also be used as an antimicrobial and drug delivery system.[65]

It's rare to find untreated individual flexible materials used in the literature. Even when a polymer has been used on its own, it has often been modified in a specific manner. For instance, it's unlikely to see only electrospun polyacrylonitrile, but rather also surface functionalized PAN nanofibers that are engineered. Such surface functionalized electrospun fibers have been used as filters that can support the removal of both bacteria and viruses from water.[66]

The one exception to this may be P(VDF-TrFE). As a flexible piezoelectric, this polymer can be used on its own for bone tissue regeneration, energy harvesting, robotics, or lab-on-chip devices.[67, 68] However, this polymer is still likely to be blended: There are several patents using P(VDF-TrFE) blended with other polymers, like PLLA (poly-L-lactic acid), for regenerative medicine purposes.[69-71]

You'll note that none of these perdurable polymers has applications that are greatly relevant to skin. With the exception of P(VDF-TrFE) and PVP, which both have wound healing applications, softer, biodegradable materials are usually considered more suitable as scaffolds for skin.[68, 72] Collagen, gelatin, chitosan, cellulose, silk and other natural polymers are typically considered to be more suitable electrospun substrates, though synthetic, water-soluble, biodegradable polymers like poly(vinyl alcohol) (PVA) or poly(ε-caprolactone) (PCL) are also commonly utilized.[72] However, all of these materials are degradable and unsuitable for our purposes.

This specifically resulted in a search for perdurable polymers with similar Young's moduli to electrospun PCL or PCL blends, which range from 21.42 to 82.08 MPa. Average elongation at break values for PCL and PCL blends range between 24 and 158.54%. These values closely resemble those of skin, which is estimated to have a Young's Modulus between 2.9 and 150 MPa and an elongation at break value that ranges between 17 and 207 percent.[73] Ideally, our chosen material would have a Young's modulus on the lower end of the scale, with a much higher elongation at break value, given our desire to create a material with perdurable properties and construct that expresses minimal amounts of hysteresis. This required us to extend our search into elastomeric materials, specifically assessing thermoplastic elastomers.

3.2.4 Uses for Bioengineered Thermoplastic Elastomers

At the time that this work was being elaborated, medical grade elastomers like butadiene rubber, ethylene-propylene, polyisoprene, silicone rubber, styrene-butadiene rubber (SBR), and urethane elastomers were all already commonly used in biomedical devices.[74] Certain copolymers, such as poly(styrene)-b-poly(DL-lactide) (PS-PDLLA), were even being assessed as potential drug delivery systems.[75] Such materials are typically processed by tape casting or

molding; the elasticity and lack of conductivity of produced solutions makes them difficult to produce in nano-structured or micro-structured conformations.

Alkene-styrene polymers were considered to be particularly interesting to us as even planar cast materials were elastic, yet strong. Reported Young's moduli ranged from 6 to 32 MPa, with elongation at break values between 630 and 1,300%.[35-39] Various different alkene-styrene copolymers had also been electrospun – but in very few studies.[5, 76-83] Given the limited mechanical information available comparing planar versus electrospun elastomers, research into the use of alkene-styrene copolymers was particularly intriguing as there was substantial opportunity for novelty.

For example, styrene–ethylene/butylene–styrene (SEBS) had also been electrospun in several studies. However, these triblock copolymers were often blended with at least small amounts of other polymers, including polyaniline (PANi) doped with camphorsulfonic acid (CSA) and poly(ethylene oxide)-b-poly(propylene oxide)-b-poly(ethylene oxide) (PEO-PPO-PEO), as well as materials, like carbon nanotubes, that could help increase the conductivity of the solution.[76-78]

While these polymers have an average Young's moduli in the range of 23 to 31 MPa in planar form, they have fairly low elongation at break percentages compared to other alkene-styrene polymers (500 to 800%).[79] Comparatively, styrene-isoprene-styrene (SIS) and styrene–butadiene–styrene (SBS) polymers have Young's moduli in the same range (21 MPa and 32 MPa, respectively), but have higher elongation at break values that range between 900 and 1,300 percent.[35-39]

In theory, these materials would provide us with suitable potential substrates. However, combining an only moderately strong material with flexible or conductive additives, which have the potential to increase the Young's moduli and change the shape of the stress-strain curve, can produce a final material with dramatically different properties. A paper published during the duration of this work listed the Young's moduli of SEBS as ranging between 9 and 46 MPa, with elongation at break values between 585 and 1173%. These values varied primarily based on the directionality and alignment of electrospun nanofibers and the

integration of carbon nanotubes, allowing nanofibrous mats to be created as tissue scaffolds with tailor-made mechanical properties.[82]

Similarly, styrene-isoprene-styrene has been blended with polystyrene to produce electrospun fibers that have modifiable mechanical properties, ranging from 0.5 to 50 MPa, with 80 to 1,400% elongation at break values.[46] Notably, when electrospun alone, SIS produces Young's modulus values between 0.01 to 0.215 MPa and elongation at break values ranging between 412 and 1711%.[83] These materials are currently being explored for proton exchange applications.

Styrene–butadiene–styrene has been electrospun for nearly two decades [5], but papers featuring this polymer are few and far between. To date, fibers have only been prepared as a pure solution twice; other papers that discuss the production of fibers have used additives to enhance conductivity such as triazolinedione cross-linkers and carbon nanotubes.[5, 80-82] Alone, SBS fibers have a Young's modulus ranging between 0.03 and 0.23 MPa, with elongation at break values between 333 and 442%. Carbon nanotube-SBS mixtures have slightly higher Young's moduli ranging between 0.17 to 0.29 MPa, but variable elongation at break values, which range from 327 to 1480%. In cases towards the latter end of the spectrum, mechanical properties have consequently been heavily modified by these additives.[5, 80, 81] These various SBS nanofibers have been used for membrane distillation, filtration, and as a component of structural reinforcements. SBS also has the potential to be used for tissue engineering purposes.[82]

Finally, Poly(styrene-β-isobutylene-β-styrene) has been explored through the work of Lim et al and Liu et al.[43, 44] A thesis submitted by another member of Liu's lab, Gestos A., reported that pure SIBS fibers had a Young's modulus of 59 ±27 MPa, while planar SIBS had a modulus of 3 MPa.[84] Notably, SIBS is the most extensively tested elastomer out of all alkene-styrene polymers in terms of biocompatibility, as it is already clinically approved for use as a coating on the TAXUS coronary stent.[44]

Given the promising but limited data on this polymer, we selected SIBS, along with the less well-researched SIS and SBS, as the primary potential alternatives to the flexible materials that had been selected. Our ultimate goal was to produce perdurable, highly flexible or elastomeric nanofibers to integrate into our final construct.

3.3. Results

3.3.1 Preliminary Assessment of Flexible Polymers for Skin Substrate Creation

We began by assessing flexible polymers, namely all the polymers reported on table 2.1: polyimide (PI), polyaniline (PANi), poly methyl methacrylate (PMMA), polyacrylonitrile (PAN), Poly [(vinylidenefluoride)-co-trifluoro ethylene (P(VDF-TrFE)); and also three polymers reported in table 2.2: polyvinyl pyrrolidone (PVP), polysulfone (PSU) and polyphenylene oxide (PPO). We attempted to create fully miscible solutions, cast membranes, and then create electrospun fibers for each polymer.

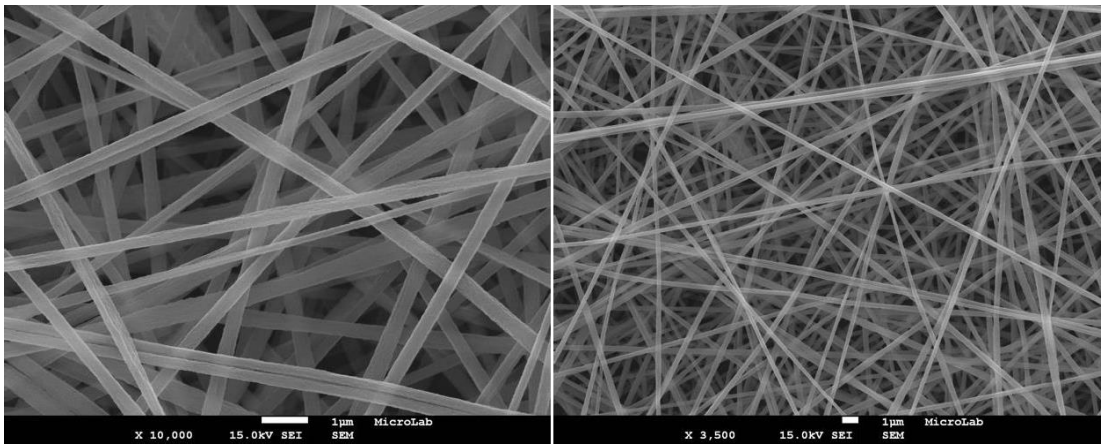

Figure 3.1: Polyimide. Average Fiber Diameter: 0.299 µm

Polyimide was assessed as it has been used in flexible sensors.[24] Its dielectric constant ranges between 2.78 - 3.48 and it has easily modifiable conductivity.[29] Polyimide was electrospun at 15%wt in DMF and DMAc. Both aligned and random fibers were created, as well as films. With a reported Young's modulus of 2.23-2.55 GPa, we selected PI in the hopes that its mechanical properties would be elastic in nanofibrous form.[24] Despite electrospinning, PI was not found suitable for our purposes.

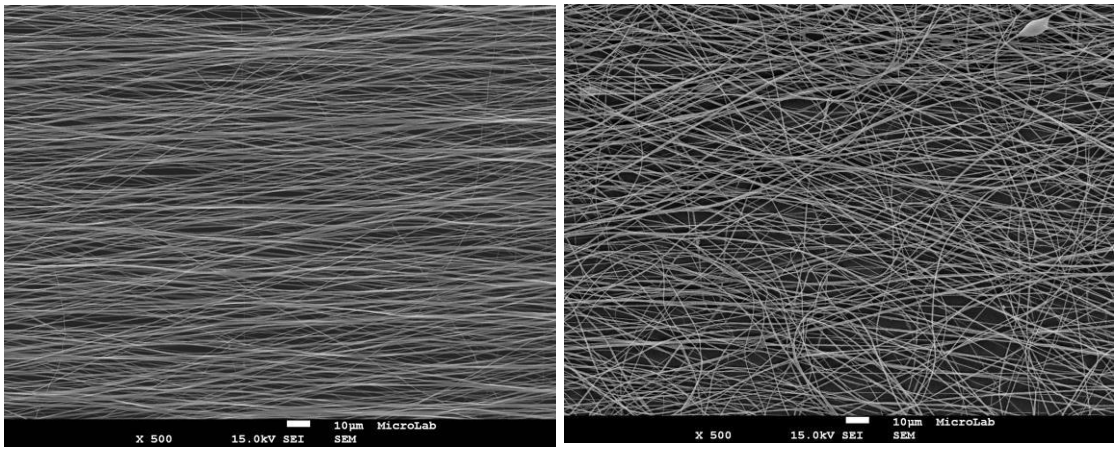

Figure 3.2: Poly(methyl-methacrylate). Average Fiber Diameter: 0.763 µm

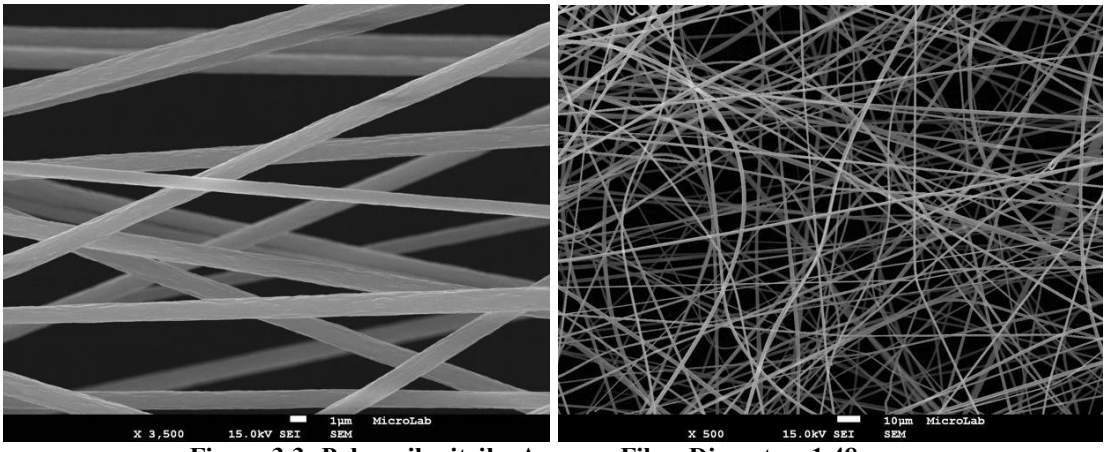

Figure 3.3: Polyacrilonitrile. Average Fiber Diameter: 1.48 µm

Poly (methyl-methacrylate) (PMMA) has minimal electroconductivity and was selected as it can be easily combined with electroconductive substrates.[16, 30] PMMA at 10%wt in DMF was electrospun. Both aligned and random fibers were able to be created. PMMA fibers produced were fluffy, and were capable of being stored in water for long periods of time without losing their structure. Notably, PMMA fibers retain water and are consequently liable to swelling. Polyacrilonitrile, like PMMA, can be easily combined with electroconductive substrates.[28] However, unlike PMMA, PAN was unable to be stored in water. This polymer was supposedly perdurable. However, we found that pristine PAN disintegrated in water. In the literature, this polymer is typically treated in several ways, including cyclization and gamma irradiation. We attempted to cross-link PAN via γ irradiation, using a protocol similar to that of Liu et al.[85] However, while this procedure allowed PAN fibers to retain their integrity, they altered their mechanical properties. PAN fibers were also found to lose alignment after storage in liquid, complicating use in cell culture.

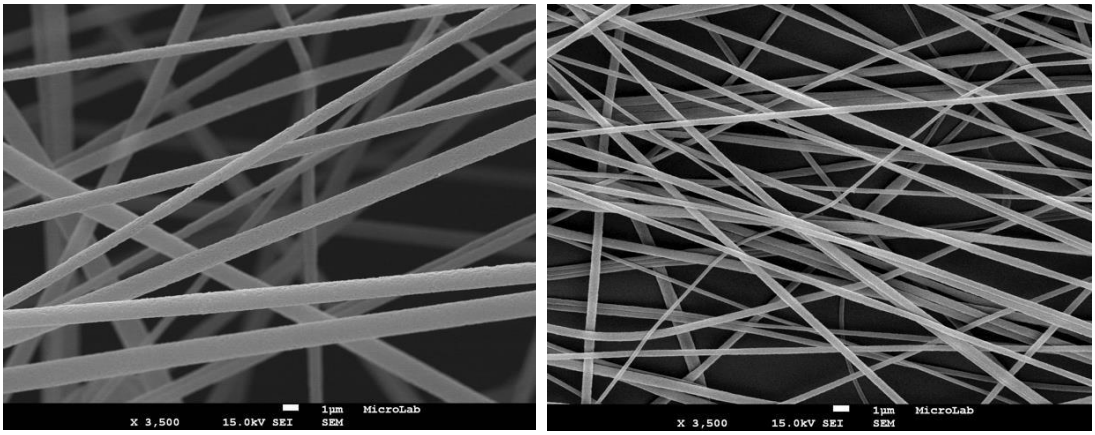

Figure 3.4: Polysulfone. Average Fiber Diameter: 0.485 µm

Polysulfone is a durable, transparent polymer that has been used in tissue engineering applications.[31-33] We were capable of producing electrospun PSU fibers, but only in random conformations. Despite the reported modulus of 1,538.7 MPa, this polymer proved to be difficult to electrospin.[23] Notably, this polymer was found to have a lower Young's modulus after storage in liquid.[31] Unfortunately, the resulting electrospun mesh that was produced was not sufficiently elastic for uses related to skin.

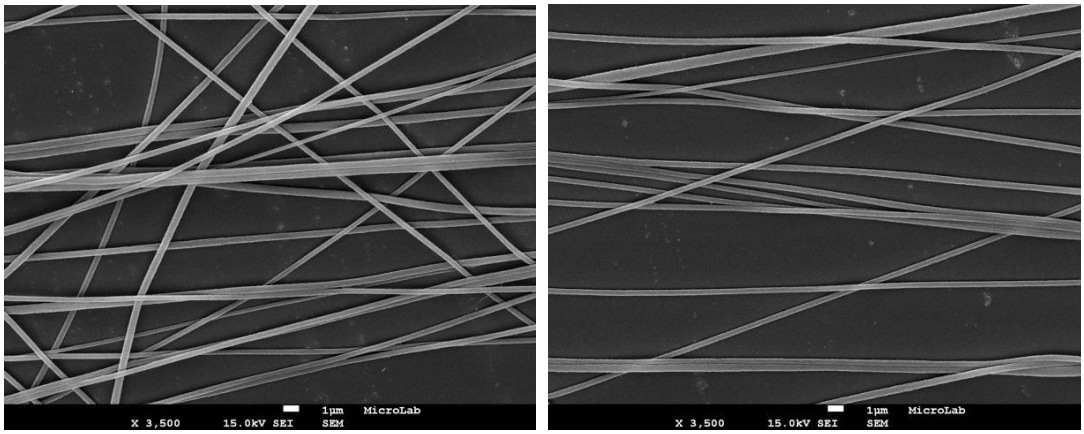

Figure 3.5: Polyvinyl Pyrrolidone. Average Fiber Diameter: 0.413 µm

Polyvinyl Pyrrolidone is a flexible polymer that has been used in cosmetic and medical products. PVP can be made at a range of different molecular weights and is miscible in various types of solvents — both of which can dramatically influence mechanical properties and the way in which the polymer can be processed.[17, 34] We were able to electrospin this polymer with ease, and continued working with it in order to create PVP-IrOx fibers. This process is detailed later on in this chapter.

P(VDF-TrFE), a piezoelectric polymer, was the easiest polymer to work with. Due to its natural charge, P(VDF-TrFE) can be easily processed into nanostructured configurations. Examples of aligned and random P(VDF-TrFE) fibers are shown in Figure 3.6. The way it is processed, as well as the annealing or poling process applied to the final product, can irreversibly change the material: namely, its phase, mechanical properties, piezoelectric functionality. P(VDF-TrFE) is reported a flexible and not elastomeric material.[9] As such, it lacks the mechanical properties desired and we determined it could not be used as the sole component of our construct. We chose to utilize it as the pressure-sensitive layer (detailed in Chapter 4).

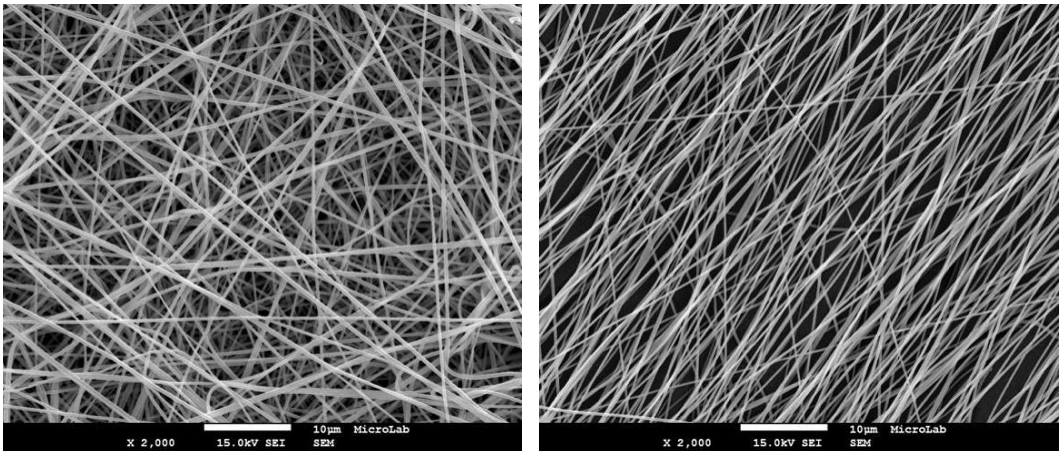

Figure 3.6: Electrospun Poly[(vinylidenefluoride-co-trifluoroethylene] (P(VDF-TrFE)). Average Fiber Diameter: Random Fibers: 0.43 µm; Aligned Fibers: 0.329 µm

In addition to the polymers that were successfully electrospun, we attempted to produce fibers from two other flexible polymers: polyaniline (PANi) and polyphenylene oxide (PPO). Electrospun fibers were not successfully created from either of these polymers; PPO proved soluble in both chlorobenzene and DMF but could only be cast in planar form. Alone, PANi was not soluble in chloroform, and the alternative, m-cresol, was determined inappropriate for biocompatible use. The polymers that were successfully electrospun were measured; averages of 30 were taken. The averaged values are listed in Table 3.1, alongside reported ranges of diameters from the literature.[86-91] As expected, these electrospun fibers are all sub-micron in diameter, though not technically nanofibers, as these averages are, for the most part, greater than 300 nm.[92, 93]

Given the preliminary nature of this data and the amount of polymers we had selected. We developed a ranking system to determine how to quantify and value these results. The ranking system was determined as detailed in Table 3.2. For each scale, we gave polymers a value. The final value is summarized in Table 3.3.

Table 3.1: Diameters of Electrospun Flexible Polymers [86-91]

Polymer	Reported Diameters (nm)	Average Diameters of Fibers (nm)
Polyimide (PI)	50 - 300	299
Poly Methyl Methacrylate (PMMA)	200 - 400	763
Poly [(vinylidenefluoride) -co-trifluoro ethylene] 70:30 (P(VDF-TrFE))	90 - 860	329 (aligned) 430 (random)
Polyacrilonitrile (PAN)	25 - 325	
Polyvinyl Pyrrolidone (PVP)	200 - 400	413
Polysulfone (PSu)	350 – 450	485

The results of this ranking system allowed us to discard certain polymers immediately: namely PANi and PPO, which we had experienced difficulty processing. Similarly, PAN was discarded due to the secondary step required to prevent degradation and the loss of flexibility resulting from this procedure. Although PSu had produced highly flexible and potentially elastic fibers, the difficulty processing them compared to other polymers and notable inability to produce aligned fibers allowed us to discard this polymer, as well. Finally, PI and PMMA were some of the easiest polymers to work with – yet simply inadequate for our needs.

Table 3.2: Ranking System for Preliminary Evaluation of Flexible Polymers

Scale to Determine Flexibility: 0. Could not be electrospun 1. Breaks when bent 2. Breaks when stretched 3. Deforms when minimally stretched 4. Deforms when substantially stretched 5. Akin to PDMS rubber	**Scale to Determine Processability:** 1. Complex procedure required for miscibility 2. Easily miscible in at least one solvent 3. Easily miscible in multiple solvents or combination of solvents 4. Easily miscible in multiple solvents and blended with other polymers or electroconductive materials
Scale to Determine Degradation 1. Degrades in water or cell culture media without further treatments 2. Degrades in ethanol 3. Does not degrade in water, media or ethanol	**Scale to Determine Value of Polymer:** 1. No conductivity or piezoelectricity 2. Low conductivity or minimal piezoelectricity 3. Highly conductive or piezoelectric

Table 3.3: Flexible Polymers Assessed for Electrospun Mesh Creation

Polymer	Solvent	Reported Young's Modulus	Ranking From Preliminary Assessment Scale
Polyimide (PI)	DMF DMAc	2.23-2.55 GPa [2]	11
Polyaniline (PANi)	m-Cresol Chloroform	1.5-2.2 GPa[4,5]	7
Poly Methyl Methacrylate (PMMA)	DMF DMAc DMF:Acetone Chloroform:DMF	Nanofiber: 136 MPa; Solid: 3 GPa[7]	11
Poly [(vinylidenefluoride) -co-trifluoro ethylene] 70:30 (P(VDF-TrFE))	DMAC:Acetone DMF:Acetone	1.2 GPa [9]	14
Polyacrilonitrile (PAN) 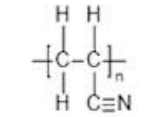 Polyacrylonitrile	DMF	7.8-9.5 GPa[10]	8
Polyvinyl Pyrrolidone (PVP)	DMF Ethanol	2.433 GPa; variable due to molecular weight.[13]	12
Poly(phenylene oxide)	Chlorobenzene DMF	2.7 GPa[14]	4

Polysulfone (PSu)	DMF THF DMAc:Acetone	1538.7 MPa[19]	10
			
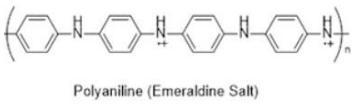 Polyaniline (Emeraldine Salt)			
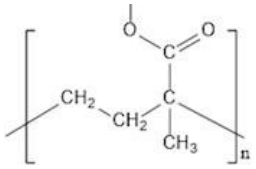 P(VDF-TrFE) Copolymer 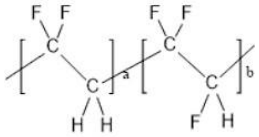 PVDF PTrFE			
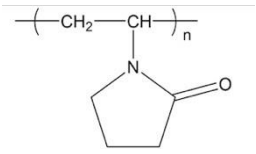			
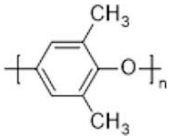			
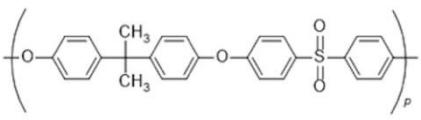			

The remaining polymers, PVP and P(VDF-TrFE), were retained as they allowed us the most ease in continuing our experiments. P(VDF-TrFE) was originally considered as a stand-alone material, but ultimately was deemed unsuitable due to the rapid fatigue that this material experiences, a phenomenon detailed later on in this chapter. However, electrospun fibers of this polymer were deemed suitable for a different purpose: as piezoelectric pressure sensors. Nanofibers of P(VDF-TrFE) are particularly ideal for this purpose; Ico et al. has described the improvement in piezoelectric functionality and simultaneous increase in Young's modulus in accordance with a 10-fold decrease in fiber diameters (from 860 to 90 nm). Piezoelectric functionality of this polymer is further detailed in Chapter 4.

Similarly, work with PVP was continued, but not as the construct's base layer. This polymer was utilized in various strategies to develop electroconductive substrates that can be used in the full construct. This polymer was combined with iridium oxide, the synthesis of which is described in Chapter 4. Similarly, the novel protocol for PVP-IrOx is detailed in Chapter 4.

3.3.2 Initial Assessment and Processing of Elastic Polymers for Skin Substrate Creation

Following the results of our preliminary assessment of flexible materials, we chose to focus on thermoplastic elastomers. Out of the various elastic materials that were considered, we focused on styrene-based diblock or triblock polymers, with butadiene, butylene, and/or isoprene. We selected these polymers due to their reported mechanical properties (in certain cases available for both planar and fibrous forms). The reported properties of these planar materials is detailed alongside the reported Young's modulus for nanofibers in Table 3.4.

In addition, we considered the use of additional polymers, namely polybutadiene and PDMS, as well as additives such as conductive paints, carbon nanotubes and iron (III) p-toluenesulfonate, to incorporate into these polymers in order to facilitate their processing. Initially, we wanted to mimic the complex geometries that naturally exist in skin. Therefore we also attempt to electrospun the selected elastomers. However, elastic materials can be difficult to process using electrospinning and other similar techniques. Kaneka poly(styrene-β-isobutylene-β-styrene) products have been successfully electrospun in fibrous meshes as have Kraton products, including poly(styrene-butadiene-styrene) and poly(styrene-isoprene-styrene) polymers.[43-47]

Table 3.4: Reported Properties of Selected Alkene-Styrene Copolymers[35-39, 82-84, 94]

Polymer	Structure	Molecular weight (g/mol)	Styrene content (%)	Tensile Strength (MPa)	300% Modulus (MPa)	Elongation at Break %	Young's Modulus of Similar Nanofibers (MPa)
Kraton D1161PT (SIS)	Styrene-Isoprene-Styrene block copolymer with 15% PS and 19% diblock.	207,000-237,000	13.5 to 16.5	21	0.9	1,300	0.01 to 0.215 MPa
Kraton D1152ES (SBS)	Styrene-Butadiene-Styrene block copolymer with 30% PS and 15% diblock	122,000	28.5 to 30.5	32	2.8	900	0.03 to 0.23 MPa
Kaneka SIBSTAR 062M		35,000	22.5% styrene	6	0.4	760	59 ±27 MPa
Kaneka SIBSTAR 062T		Non disclosed	23% styrene	10.9	0.66	630	14.2 MPa

We were not able to create clean electrospun Kaneka poly(styrene-β-isobutylene-β-styrene) products 062M or 062T, despite applying the previously created protocols by Lim et al, Liu et al, and Gestos et al. However, these notably utilized a different manufacturer's poly(styrene-β-isobutylene-β-styrene) which may have had a differing styrene content. Our attempt to electrospin poly(styrene-β-isobutylene-β-styrene) followed the work of Liu et al, who utilized iron (III) p-toluenesulfonate to to facilitate SIBS electrospinning.[44] Examples of these attempts are shown in Figure 3.7, which shows electrospun Kaneka 062M SIBS as random fibers with beading (top right, left), alongside microscale-sized droplets (bottom left) and larger droplet structures (bottom right).

The beaded structures that formed were actually able to create sputtered films. However, the formation of these beads could produce larger beads during long deposition processes. This made us reluctant to proceed further due to concerns about the potential effects these beads would have on the mechanical properties of our fibrous mats, as well as issues with reproducibility.[101] Beading is also known for being able to interfere with cellular

proliferation.[95] Although beading can often be resolved, these various issues resulted in us abandoning attempts to process Kaneka SIBS products into nanostructured conformations.

Despite the challenges we faced with Kaneka 062M and 062T (SIBS), we were able to modify the protocol developed by Liu et al for the creation of Kraton D1152ES (SBS) Poly(styrene-butadiene-styrene) electrospun meshes. Like with Kaneka 062M and 062T Poly(styrene-β-isobutylene-β-styrene), the high hydrophobicity and elasticity of this polymer made it particularly challenging to consistently obtain nanofibers by electrospinning, rather than droplets. This was expected when electrospinning all elastomers, given that this processing technique typically requires a solution with some conductance.

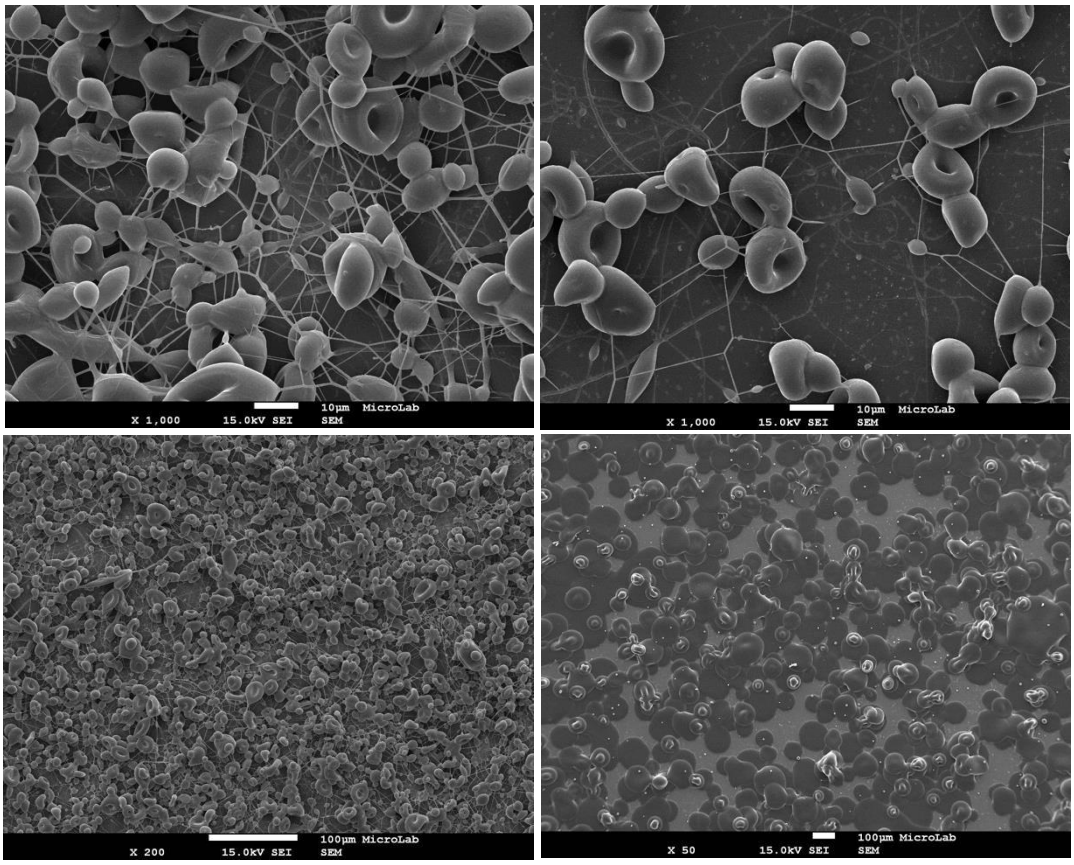

Figure 3.7: Electrospun Kaneka Poly(styrene-β-isobutylene-β-styrene) in Chloroform. Average Fiber Diameter: 1.89µm; Bubble Diameter: 11.06 µm

The product data for Kraton's D1152ES lists this material as a butadiene-based block copolymer that is composed of 30% polystyrene and 15% diblock, while the D1161PT polymer is an isoprene-based block copolymer composed of 15% polystyrene and 19% diblock. Both of these options are quite similar to SIBS in structure, and are additionally translucent and elastic, with potential uses in similar applications. Our initial comparison of these polymers

found that Kraton D1152ES (SBS) was easier to work with compared to Kraton D1161PT (SIS) and Kaneka SIBS. Using the same scaling system listed in Table 3.1, we ranked these polymers as 13, 12, and 11, respectively. Given the fact that the mechanical properties of all three polymers were fairly comparable when planar sheets were assessed manually, we chose to continue with the assessment of all three in planar form but continue our attempts of electrospinning on only Kraton D1152ES (SBS).

We attempted to electrospin Kraton D1152ES (SBS), initially experiencing similar issues as we had with Kaneka 062M and 062T SIBS. However, we discovered that environmental factors were a major component in the reproducibility and quality of our results. Environmental controls were not in place surrounding the electrospinning set-up, resulting in highly variable temperatures ranging from 19 to 29^{o}C and humidity levels ranging between 13 and 42%. The lower end of the spectrum for both temperature and humidity positively affected the production of Kraton D1152ES (SBS) substantially, yielding fibrous structures (Figures 3.8-3.12).

Electrospinning of Kraton D1152ES (SBS) with additional Iron (III) p-toluenesulfonate was attempted to increase the electroconductivity of the solution and thereby increase the electrospinnability of the fibers. We found that, along with variables of temperature and humidity, fibrous structures were also partially regulated by the concentration of Iron (III) p-toluenesulfonate. We considered this additive to be particularly ideal for our purposes as it had been shown to have no negative effects on neural cells in the experiments of Liu et al, unlike other electroconductive materials.[44]

When Iron (III) p-toluenesulfonate was added in amounts between 1-8%, Kraton D1152ES (SBS) showed minimal to no improvement in structure. The conformation of these fibers was highly irregular and unpredictable and primarily controlled by external factors such as temperature and humidity. However, higher concentrations (between 15-30% wt) of iron (III) p-toluenesulfonate improved electrospinning of Kraton D1152ES (SBS) substantially.

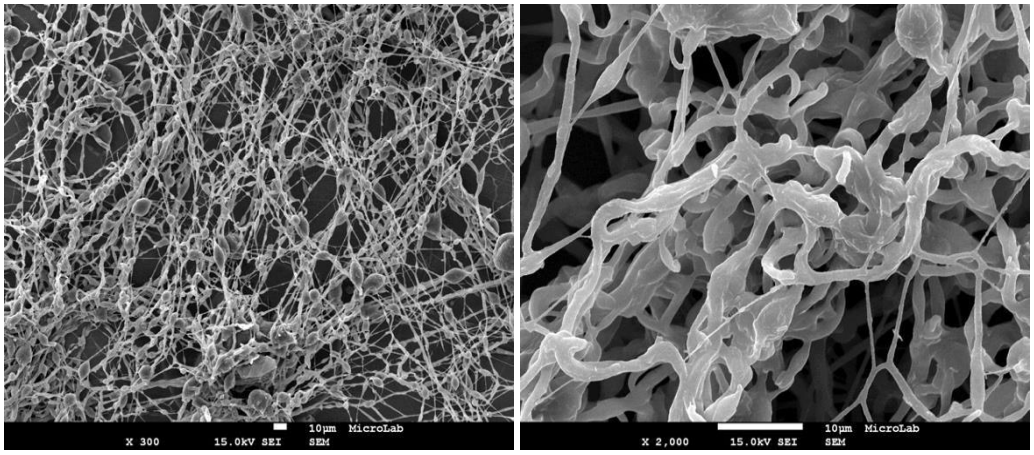

Figure 3.8: 1%wt Iron (III) p-toluenesulfonate and 10%wt Kraton D1152ES (SBS). Fiber Diameter: 1.28 to 3.04 µm

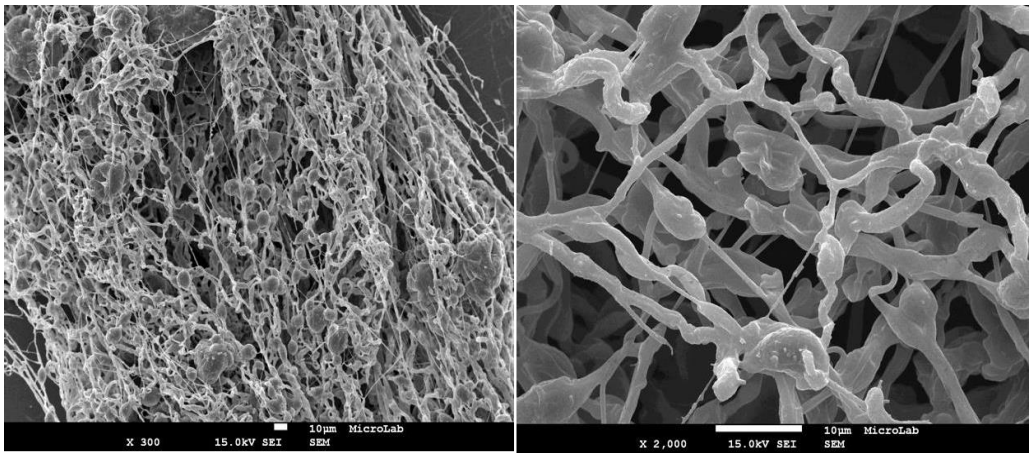

Figure 3.9: 10%wt Iron (III) p-toluenesulfonate and 10%wt Kraton D1152ES (SBS). Fiber Diameter: 1.26 to 2.13 µm

Finally, solvents also can impact the electrospinnability of a solution. As such, both THF and chloroform were tested. Figure 3.8 and 3.9 show the production of Kraton D1152ES (SBS) (SBS) fibers with minimal amounts of iron (III) p-toluenesulfonate. Fibers produced are curly, with some amount of beading. Comparatively, fibers with higher concentrations of iron (III) p-toluenesulfonate, as in Figure 3.10, did not have similar structures. However, high levels of Iron (III) p-toluenesulfonate resulted in fibers that became brittle immediately after electrospinning (data not shown). Iron (III) p-toluenesulfonate at concentrations at 20% wt or higher were deemed to alter the elastomeric properties of SBS.

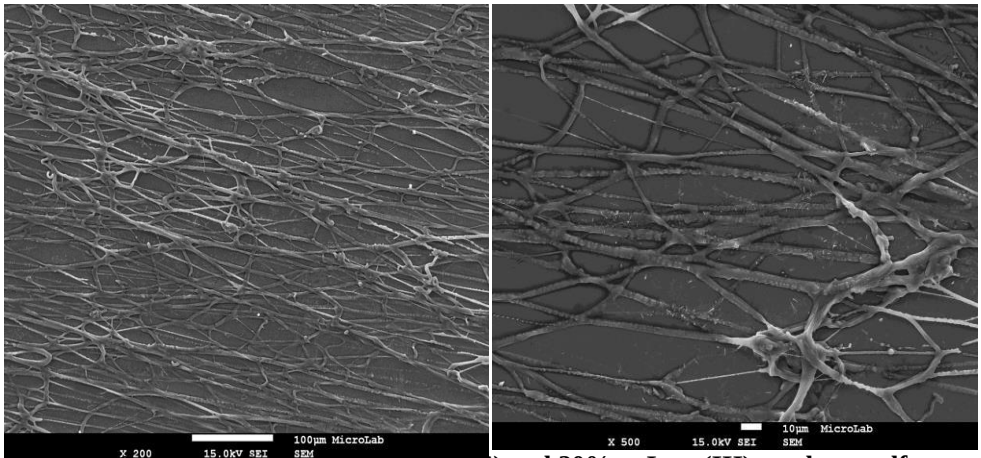

Figure 3.10: 10%wt Kraton D1152ES (SBS) and 20%wt Iron (III) p-toluenesulfonate. Fiber Diameter: 3.25 to 4.64 µm

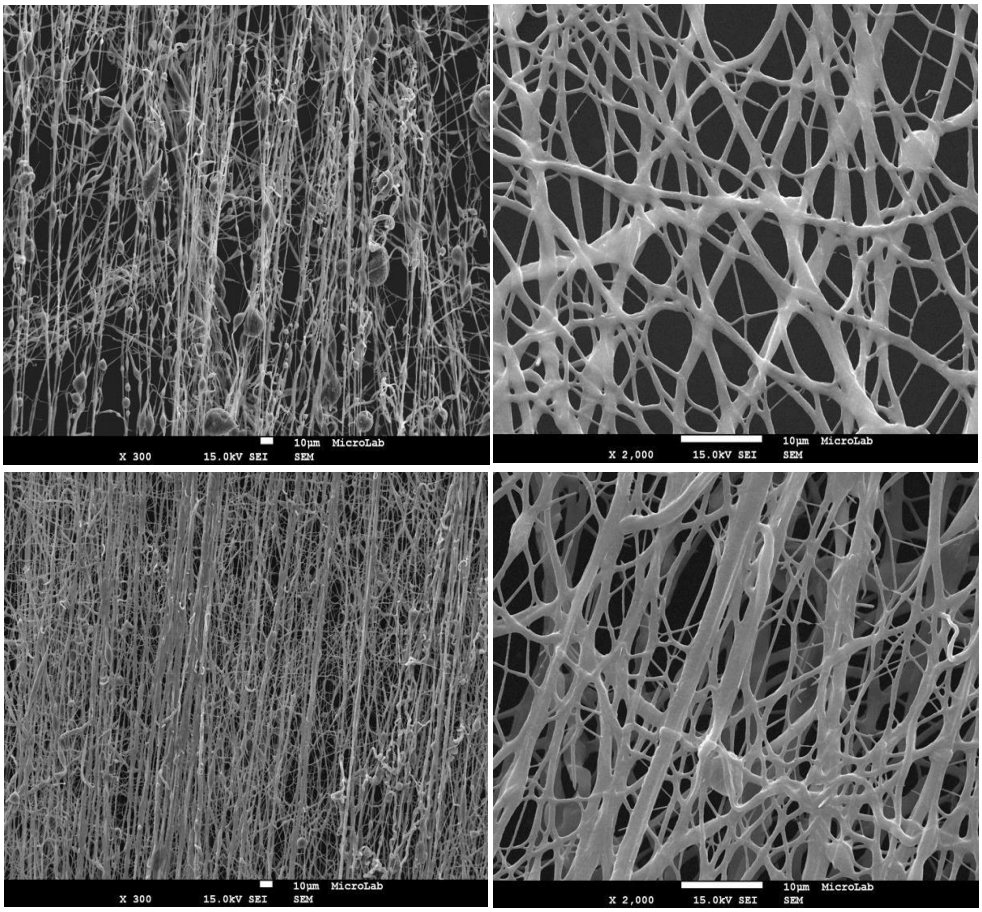

Figure 3.11: 10%wt Kraton D1152ES (SBS) and 16.5% wt Iron (III) p-toluenesulfonate Produced Using THF (top) and Chloroform (bottom). Average Diameter of THF Fibers: 1.78 µm (left) and 1.04 µm (right). Average Diameter of Chloroform Fibers: 2.84 µm (left) and 0.830 µm (right)

Nanofibrous conformation and mechanical properties were found to be optimal in the mixture of 16.5%wt Iron (III) p-toluenesulfonate with 10%wt Kraton D1152ES (SBS). As shown in Figures 3.11, this concentration allows for defined fibers. The elastomeric properties of

Kraton D1152ES (SBS) caused webbing and fibers of irregular sizes in both cases. At this stage, we found that while we were able to obtain more homogenous fibers in terms of size with THF, we were able to obtain better alignment of fibers when using chloroform. Other images can be found in the appendix. Notably, these fibers most resemble those of styrene-isoprene-styrene created by Feng et al.[43, 86]

Table 3.5: Elastomers Assessed for Electrospun Mesh Creation

Polymer	Solvent	Repored Young's Modulus	Observation of the current study
Polyisoprene 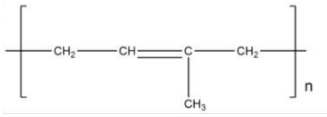	THF Chloroform	N/A (Liquid)	Only usable as an additive and for planar/cast materials
Polybutadiene 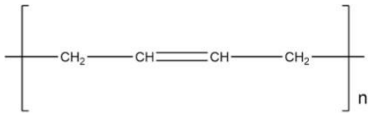	Toluene	1.2 MPa(15)	Only usable as an additive and for planar/cast materials
Poly (dimethylsiloxane) (PDMS) 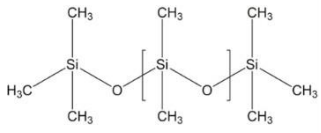	DMF THF	3.6-8.7 x 10^5 Pa (varies based on mixing ratio)(16)	Not miscible with other elastic polymers being assessed
Poly (styrene-isoprene-styrene) (SIS) 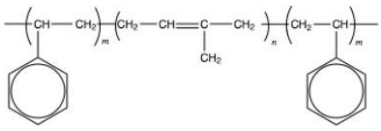	THF	21 MPa(17)	Electrospinning not attempted; ranking of 11
Poly (styrene-butadiene- styrene) (SBS) 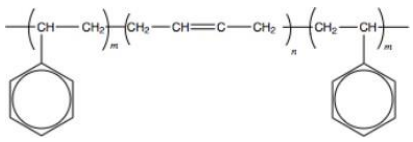	THF	32 MPa(17)	Electrospinning attempted unsuccessfully, ranking of 12
Poly (styrene-isobutylene-styrene) (SIBS) 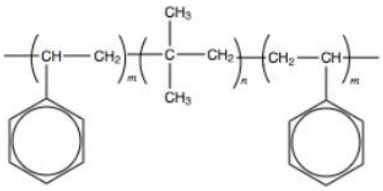	DMF THF Chloroform	0.044-0.181 GPa(18)	Electrospinning successful, ranking of 13

Over long durations, iron (III) p-toluenesulfonate induced dehydration of the fibers and breakage. This was evident in samples with over 20%wt iron (III) p-toluenesulfonate as it occurred rapidly. This led us to monitor our other samples produced with this additive. After two or more months in storage, even samples with low iron (III) p-toluenesulfonate

concentrations would become brittle and consequently unusable. Further analysis of these polymers degradation at this time was not feasible due to complete breakdown of the scaffold. At this stage, rehydration also proved impossible. Henceforth, only freshly prepared Kraton D1152ES (SBS) blended iron (III) p-toluenesulfonate samples were used when assessing mechanical properties. Notably, we experienced no issues with pure Kraton D1152ES (SBS).

We also attempted to create polymer blends with Kraton D1152ES (SBS) and polyisoprene or polybutadiene for electrospinning purposes. These were much less successful than the pure polymer or solution mixed with Iron (III) p-toluenesulfonate, and could only be made as membranes. These polymers were created through drop casting or casting knife methodologies and are detailed and analysed further in the following section. Concluding remarks regarding the preliminary assessment of our elastomers is summarized in Table 3.5.

Having successfully created elastic and flexible nanofibers, mechanical testing was performed on planar and electrospun Kraton D1152ES (SBS) SBS alongside planar and electrospun P(VDF-TrFE). This included an assessment of the Young's modulus, stress-strain curves, fatigue properties, and elongation at break, which are detailed in the subsequent sections (3.3.3 and 3.3.4).

3.3.3 Tensile Deformation of Skin and Polymers

The ranking system designed for preliminary assessment allowed us to easily identify polymers that we thought would have suitable properties for the creation of our final construct. We ultimately selected the vast majority of our elastomeric materials, alongside flexible piezoelectric P(VDF-TrFE), in order to perform more quantitative tests of these materials' mechanical properties. Of course, our interest was not only standard attributes, such as Young's modulus, strength or fatigue. We specifically wanted to understand these polymers in comparison to skin.

We consequently chose to compare skin samples with various elastomers, namely: Kraton D1152ES (SBS), polyisoprene mixed with Kraton D1152ES (SBS), polybutadiene mixed with Kraton D1152ES (SBS), Kraton D1161PT (SIS), and Kaneka SIBS. Given the ease of working with Kraton D1152ES (SBS), we chose to study it in electrospun format, as a pristine

membrane, and as a membrane mixed with other elastomers (polyisoprene and polybutadiene) in films prepared through drop casting.

We additionally heated samples to 37ºC, 80ºC, and 150ºC to assess the influence of heat treatments on the polymer's mechanical properties. Heat treatments were not necessarily relevant for the elastomers themselves, but needed to be assessed as components of the multi-layered construct required further heat processing or annealing. Subsequent heat treatments and material annealing have the potential to induce polymer rearrangements resulting in altered mechanical properties.

We additionally selected P(VDF-TrFE) as a flexible polymer to analyse comparatively with our synthetic elastomers from Table 3.2, and porcine skin. This polymer has interesting piezeoelectric properties that would be useful to integrate in our final construct and is easy to electrospin, resulting in the production of robust fiber meshes. P(VDF-TrFE) was also selected as it was able to provide us with information on the mechanical differences between flexible and elastic materials used in second skin development, acting as a type of negative control. It also allowed us to further our understanding of planar and flexible electrospun materials and their mechanical differences. We specifically analysed uniform, dense mats of P(VDF-TrFE) nanofibers, as well as planar sheets produced using a casting-knife processing.

Our tensile deformation assessment of these materials includes the traditional overview based on Young's moduli data: A standard parameter in the mechanical characterization of materials. However, due to the complexity of the materials we were assessing, stress-strain curves were also used to assess the mechanical properties of these materials. This approach allowed us to make a suitable identification and selection of materials suitable for second skin applications.

Young's Moduli for Elastomers, Flexible Polymers and Skin

Human skin has a reported Young's modulus that ranges from 0.03 MPa to 150 MPa.[50, 51, 73] Comparatively, porcine skin has a reported Young's modulus between 1.85 ± 0.85 and 7.68 ± 3.96 MPa.[52] Both human and porcine skin have dramatically different moduli depending on the age of the subject that the samples came from, the age of the samples tested if these samples were *ex vivo*, and the parameters used to take these measurements. As porcine skin is

considered to be comparable to human skin, we considered that fresh porcine skin from joint areas would give us the closest possible data to the moduli and stress-strain curves we were attempting to replicate.

Figure 3.12 shows the Young's moduli for Kraton D1152ES (SBS), Kraton D1152ES (SBS) blended with polyisoprene, Kraton D1152ES (SBS) blended with polybutadiene, Kraton D1161PT (SIS), P(VDF-TrFE). It also shows both elastic and deformation moduli for skin. These moduli are computed from the soft region of the J-curve and rigid region of the J-curve, respectively. The values for the elastic and deformation Young's moduli of pig skin, shown in pink in Figure 3.12, are on the lower end of those shown in previous studies.[52] However, this is within the norm as our selected auricular and joint regions are also notably different to those typically studied. Our selection has focused on areas of the body that move with frequency, thereby increasing the likelihood of lower Young's moduli.

Polymers were prepared by drop casting methodology unless otherwise identified as electrospun fibers. The resulting membranes were prepared at different temperatures. Temperature is well known to deform elastomers and change their properties, sometimes irreversibly, though the exact impact it has will depend on the polymer and the increase in temperature.[96] We found that at low heat, the homogeneity of polymer films improved. We therefore assessed Kraton D1152ES (SBS) at room temperature, 37^{o}C, 80^{o}C, and 150^{o}C, all shown in red in Figure 3.13. We found that between 37^{o}C and 150^{o}C, there were minimal changes in modulus values. Kraton D1152ES (SBS) processed at room temperature was found to have nearly double the Young's modulus value, as can be seen in Figure 3.12.

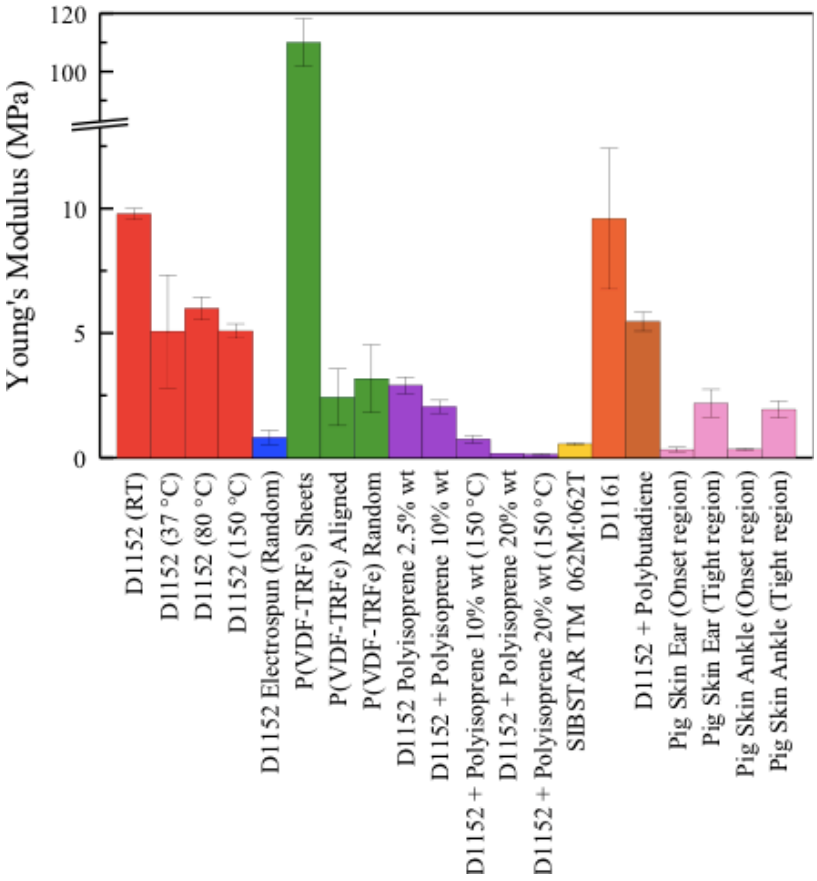

Figure 3.12: Young's Moduli of Skin, Flexible Materials, and Elastomers. From left to right, depicting the Young's modulus values of Kraton D1152ES (SBS) at room temperature, 37°C, 80°C, and 150°C, and electrospun Kraton D1152ES (SBS). P(VDF-TrFE) is similarly assessed in planar form, as well as aligned and random electrospun fibers. Drop cast sheets of blended Kraton D1152ES (SBS) and polyisoprene at concentrations of 2.5, 10, and 20%, as heated 10 and 20% blends. A 50:50 blend of planar Kaneka SIBSTAR 062M and 062T, Kraton D1151PT, and blend of Kraton D1152ES (SBS) and polybutadiene are the final polymers shown. Finally, values for porcine skin (auricular and ankle joint regions) are shown.

Comparatively, unheated electrospun Kraton D1152ES (SBS) has a value that is 10-fold lower than the planar processed material. Young's modulus value is more than other pure electrospun SBS or SIS, but far less than the reported values for SIBS.[82-84, 94] The Young's modulus for this sample is shown in dark blue in Figure 3.13. Its modulus is substantially smaller than the drop cast samples, as is expected from nanofibrous samples. In theory, complex, nanofibrous geometry of an electrospun elastomer should be able to mimic mechanical properties similar to that of skin. In terms of Young's modulus value, electrospun Kraton D1152ES (SBS) has a median value between the moduli of porcine auriculae and ankle joints.

Kraton D1152ES (SBS) blends with 2.5%, 10%, and 20% polyisoprene and 10% polybutadiene were created. These were created with the aim of obtaining a softer material. Polyisoprene is the main component of natural rubber and polybutadiene is well-known for its elastomeric

properties. We chose to assess these samples blended with polyisoprene at two temperatures, 37ºC and 150ºC. Their Young's moduli are shown in purple in Figure 3.13. As little as 2.5% of polyisoprene was shown to reduce the moduli of Kraton D1152ES (SBS) by half, while heating was able to reduce the moduli of the blends with 10% and 20% polyisoprene even further. 10% and 20% blends yielded Young's moduli values equivalent or less than those of skin. In contrast, the 10% polybutadiene blend, shown in brown in Figure 3.12, was created at room temperature. Its modulus is equivalent to the heated pure Kraton D1152ES (SBS) samples, implying that the addition of polybutadiene is an alternative method of reducing the Young's modulus of this material.

The remaining elastomers we tested, Kraton D1161PT (SIS) and Kaneka SIBSTAR™ 062M:062T, are shown in Figure 3.12 in orange and yellow, respectively. These elastomers have properties and structure similar to that of styrene-butadiene co-polymer Kraton D1152ES (SBS), yet had the highest and lowest Young's modulus values of any pure polymer tested. The value for Kaneka SIBSTAR™ 062M:062T is in line with the values reported by Gestos et al.[84] Notably, the value of Kaneka SIBS is equivalent to several Kaneka D1152ES (SBS)-polyisoprene blends and skin.

Finally, P(VDF-TrFE), shown in green in Figure 3.13, was created in three conformations: Flat sheets, random fiber meshes, and aligned fiber meshes. These results provided an example of the Young's modulus of a flexible material, supporting our hypothesis that electrospinning could produce nanofiber meshes with much lower moduli compared to those of the same materials in planar form. In this case, we saw a 50-fold reduction in the Young's modulus of planar and electrospun P(VDF-TrFE). However, despite this dramatic reduction, the electrospun meshes of P(VDF-TrFE) had substantially higher moduli than those of several elastomers, including Kaneka SIBSTAR™ 062M:062T, electrospun Kraton D1152ES (SBS), and planar Kraton D1152ES (SBS)-polyisoprene blends.

Nonetheless, the fibrous random and aligned P(VDF-TrFE) meshes were both in the range of skin and had equivalent moduli values to several elastomers. This is not only in the case of our own results on porcine skin, but other results that have reported the Young's moduli to be in the range of 1.85 ± 0.85 and 7.68 ± 3.96 MPa.[52] Given that the Young's Modulus of skin is also reported to be between 0.03 and 150 MPa,[50,51,73] there is no reason to believe that

nanofibers of P(VDF-TrFE) could not be used as a skin-based substrate, given our findings. This highlighted the impact that nanostructured conformations can make on a material, allowing comparisons between this flexible polymer, the complex fibrous structure of skin, and the aforementioned elastomers.

Although Young's modulus is typically used as the gold standard in measurements of flexibility or elasticity, both the shape of the curve and fatigue properties of the material are equally valid factors in determining comparability to skin. Continuing on in our analysis, we assessed the variable curvature presented during shear stress.

Stress-Strain Curves of Elastomers, Flexible Polymers, and Skin

Flexible and elastic polymers have markedly different stress-strain curves. Elasticity is an intrinsic property defining the ability to sustain and recover from strain, which arises directly from the stress-strain curves characterizing the intrinsic mechanical response of each material. Flexibility, however, is a characteristic dependent not only on the material's properties but on its shape and aspect ratio, i.e. the thickness-to-length ratio. Stiffer but still flexible conformations of such materials can sustain bending and compression. However, many elastic polymers are too soft when produced in very thin geometries, at least for the same purposes that one would use the same polymer for in bulk form.[97]

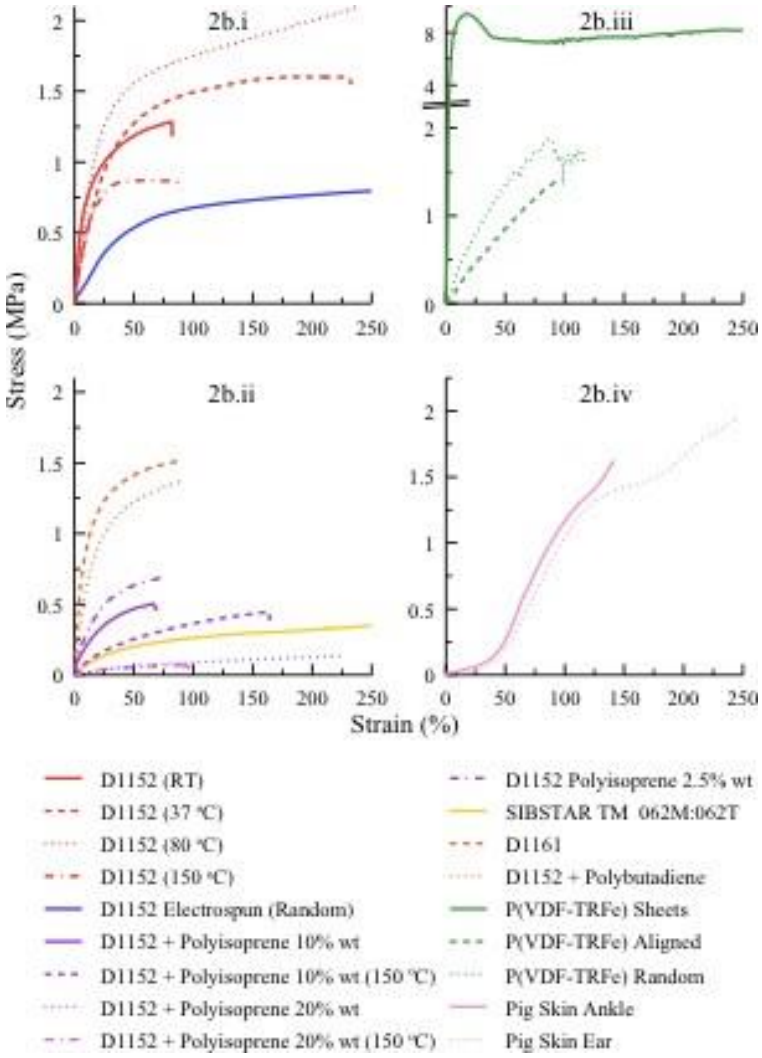

Figure 3.13: Stress-Strain Curves Skin, Flexible Materials, and Elastomers. Top left: Stress-strain curves for Kraton D1152ES (SBS) at room temperature, 37ºC, 80ºC, and 150ºC, and electrospun Kraton D1152ES (SBS). Top right: Stress-strain curves for P(VDF-TrFE) in planar form, as well as aligned and random electrospun fibers. Bottom left: Drop cast sheets of blended Kraton D1152ES (SBS) and polyisoprene at concentrations of 2.5, 10, and 20%, as heated 10 and 20% blends. A 50:50 blend of planar Kaneka SIBSTAR 062M and 062T, Kraton D1151PT, and blend of Kraton D1152ES (SBS) and polybutadiene are also shown. Bottom right: Porcine skin (auricular and ankle joint regions). Curves reaching the maximum of the axis did not fail within the machine's range.

The elastomers assessed have properties and structure which are similar to one another. We aimed to produce these elastomers under as many of the same conditions possible in order to minimize variables. In theory, they should all yield highly similar results. However, heat treatments and processing through electrospinning have still produced notable differences. The stress strain curves in Figure 3.13 show how seemingly similar materials are in fact comparatively softer or weaker than each other. For instance, electrospun Kraton D1152ES (SBS) had a Young's modulus most comparable to Kaneka SIBSTAR™ 062M:062T and

planar Kraton D1152ES (SBS) blended with 10% polyisoprene. Figure 3.13 highlights how none of these have produced comparable stress-strain curves to one another.

Kraton D1152ES (SBS) blends 10%, and 20% polyisoprene, listed in purple in Figure 3.13 (2b.ii) as before, had Young's moduli values that were similar or less than those of skin. However, their stress-strain curves show them to have different mechanic responses. By the same principle, electrospun Kraton D1152ES (SBS) (blue, 2b.i) and planar Kaneka SIBS (yellow, 2b.ii) also have elastic moduli values similar to the ones of skin. Their stress-strain curves show that they are able to withstand a higher percentage of strain, but are not able to handle a comparable amount of stress compared to skin. While Young's moduli are listed as the standard valuation of a material, these stress-strain curves show that despite similar moduli, none of our preferred materials are comparable to skin.

In contrast, planar P(VDF-TrFE), shown in green in Figure 3.14 (2b.iii) had an exceptionally high Young's modulus. As a flexible material, this was to be expected. Its stress-strain curve shows that it is a much stronger material than skin or any other polymers we assessed. However, this material is susceptible to rapid permanent deformation. In contrast, the aligned and random nanofibers are able to undergo recoverable deformation for much longer, and consequently start their stress-strain curves in a manner much more similar to skin. However, the strain percentage they are capable of is much less.

Some flexible polymers can express a considerable extent of elastic (recoverable) deformation, while retaining a relatively high Young's modulus at the onset region of the stress-strain curve. P(VDF-TrFE) is complex material given that the higher the Young's modulus, the better the piezoelectric function.[90] Similarly, nanofibers may be processed into other confirmations, such as coils (not attempted in this study), which can also affect both piezoelectric function and mechanical properties.[98] Given our intentions for this material, these are all factors to be highly conscious of. Our current results show that nanofibers of this flexible polymer are highly similar to skin. However, any modifications to the material for further enhancement of function could impact the mechanical aspect of this material substantially. On a similar note, the strain percentage of our P(VDF-TrFE) nanofibers are similar to ankle joints, but not the auricular region. For optimal use of this material as an implantable, the exact region of skin would need to be assessed for compatibility with this polymer's mechanical properties. Lack of this data

has the potential to result in early device failure given the lower strain percentage of P(VDF-TrFE) compared to our and other reported data on porcine skin.[52]

Although stress-strain curves are certainly important, the deformation and fatigue properties of these materials is equally so, as well. Fatigue is not only measured manually or cyclically; it can be estimated by the shape of a stress-strain curve used to calculate Young's moduli. While it is possible to obtain Young's moduli comparable to skin for flexible materials, these materials experience rapid permanent deformation. This ultimately means that while the produced elongation at break values may be comparable, material fatigue and overall mechanical properties are incomparable to skin.

Additionally, the degree of crystallinity, the glass transition temperature (above or below the working temperature), pre-stressing treatments, and other factors all have a direct incidence in the stress-strain behaviour, especially for flexible materials which are less likely to return to their original state.[53, 90, 92, 97] S-shaped and J-shaped curves are common; the latter is usually associated with pre-stressed materials but is also traditionally found in skin. While P(VDF-TrFE) follows a similar curve to porcine skin in our data, it would be unable to replicate these results repeatedly whilst remaining a functional piezoelectric material. From the results shown in Figure 3.13 (2b.i, ii, and iii), none of our chosen materials have the J-shaped curve present in skin. Obtaining materials with intrinsic J curves is challenging, but these curves may be found in pre-stressed materials and fibrous materials. In contrast to P(VDF-TrFE), this means that elastomers may produce J-shaped curves when measured following repeated stress.

Figure 3.13 (2b.iv) shows the traditional J-shaped curve that can be expected when assessing the mechanical properties of the dermis. Skin's anisotropic characteristics are often remarked upon. The first region of the J-curve corresponds to the low modulus resulting from streamlined collagen, while stretched elastin fibres strain against the gel ground substance. The second region of the curve results from organized, cross-linked collagen fibres bending. The stress strain behaviour is a result of the shear of those fibres against the skin ground substance. The third region, where the curve becomes linear again, corresponds to the final alignment of collagen fibres with one another in the direction of applied force. This is, notably, the region used to estimation of the larger Young's modulus, the deformation modulus. Here, skin stiffens at increasingly higher stress until it eventually breaks. The second and third regions are

responsible for the load bearing properties of the skin tissue, and skin is normally under tension *in vivo*. The complexity skin's curve is why both elastic and deformation Young's moduli values were listed in Figure 3.12.

A given rubbery material, including those used in this study, can be pre-stressed and then assessed to promote constructs with J-shaped shear-stress behaviours. However, such a procedure may compromise fatigue resistance and decrease overall elasticity. Alternatively, processing materials as fibrous or porous structures, which can be created through electrospinning, wet spinning, or gas foaming, may result in J-shaped curves. This is because the stress initially acts upon only the soft matrix, but after some time, fibres align in the direction of the stress and the entire matrix is pulled against the force, stiffening the fibres. While this is not the case for our electrospun or planar materials, understanding the differences between J and S shaped curves is essential for a complete understanding of material mechanical properties. In this case, assessing the variable curvature presented during shear stress — particularly, the point of skin's deformation in J shaped curves — allowed us to determine which polymeric materials were capable of withstanding the same amount of force as skin.

In conclusion, the results of Figure 3.13 show us that few materials have the strength of skin, easily eliminating all of the polymers we assessed except for Kraton D1152ES (SBS), shown in red in Figure 3.13 (2b.i). Only this polymer would be able to be considered perdurable in the context of skin-related applications. The combination of results shows us that the low heat treatment applied to this polymer is able to lower its Young's modulus without significantly impacting its strength. While it does not possess skin's traditional J-shape, it can withstand comparable stress and strain. Further tests related to pre-stressing of the material may produce a material that more directly mimics skin or other natural elastomers. Interestingly, P(VDF-TrFE) fibers, which have a similar Young's modulus to skin, can also withstand comparable stress. Unfortunately, the limited strain capacity of P(VDF-TrFE) means that this material would have to either be further modified for use as a stand-alone material or that nanofibers could act as a different and non-essential component of the construct. We continued our analysis of this polymer with the idea of optimizing its use for further tests in Chapter 4.

Elongation at Break Properties of Selected Elastomers and Flexible Polymers

To better understand our stress-strain results, particularly those of the polymers capable of withstanding a level of stress similar to skin, elongation at break points were assessed. We did not assess skin here because it only bends in standardized ways, according to the movement of limbs, joints, or when making facial expressions. Also, skin possesses regenerative capacity; if it were to stretch to the point of tearing or even breaking, skin would grow anew.

Figure 3.13 shows that Kraton D1152ES (SBS), Kraton D1161PT (SIS) and P(VDF-TrFE) are capable of withstanding stress similar to skin, but only Kraton D1152ES (SBS) can withstand the same amount of strain. The point of failure for Kraton D1152ES (SBS) was able to surpass that of the machine, unlike skin and the other polymers tested. In contrast, Kraton D1152ES (SBS) blended with polyisoprene was capable of withstanding strain in variable amounts, and lacked the strength to withstand comparable stress to skin or pure Kraton D1152ES (SBS). We consequently selected heated and unheated Kraton D1152ES (SBS), Kraton D1152ES (SBS) + 10% polyisoprene, and Kraton D1152ES (SBS) + 20% polyisoprene to analyse in further elongation at break assessments.

We did not list P(VDF-TrFE) in this figure because it suffers from a fatigue and deformation that makes its deformation and break point different to the elastomers. It would be inappropriate to list a material that is not of the same thickness or structure alongside these planar polymers due. However, in our studies, we found that the elongation at break percentage for P(VDF-TrFE) films was 828%. The elongation at break percentage for P(VDF-TrFE) fibers was 279%. The complete compilation of this data can be found in the appendix.

P(VDF-TrFE) is a flexible polymer that does not break easily, but deforms substantially and it is reported to lose its piezoelectric capacity when subjected to excess mechanical strain.[53] In our own experiments, we observed that P(VDF-TrFE) films deformed permanently prior to even 50% elongation; at its "break" point, its deformation was 5-6 times its original size. Such deformations are to be expected. Singh et al has shown how even minimal, repeated mechanical stressors can cause mechanical fatigue of P(VDF-TrFE).[53] This mechanical phenomenon is perhaps best described by Lam et al, whose work describes the elastic-plastic deformation stages that this flexible polymer undergoes, even in nanofibrous form.[99] According to Lam et

al, this deformation process occurs first with the yielding region at 45% strain, followed by a yielding stage between 60 to 200% strain, then a third stage leading to between 200 and 327%.[99] Notably, this work also reported that annealed polymers have a substantially reduced elongation at break that is only 44%.[99] We did not measure the mechanical properties of P(VDF-TrFE), but our fibers' elongation at break values are in line with these.

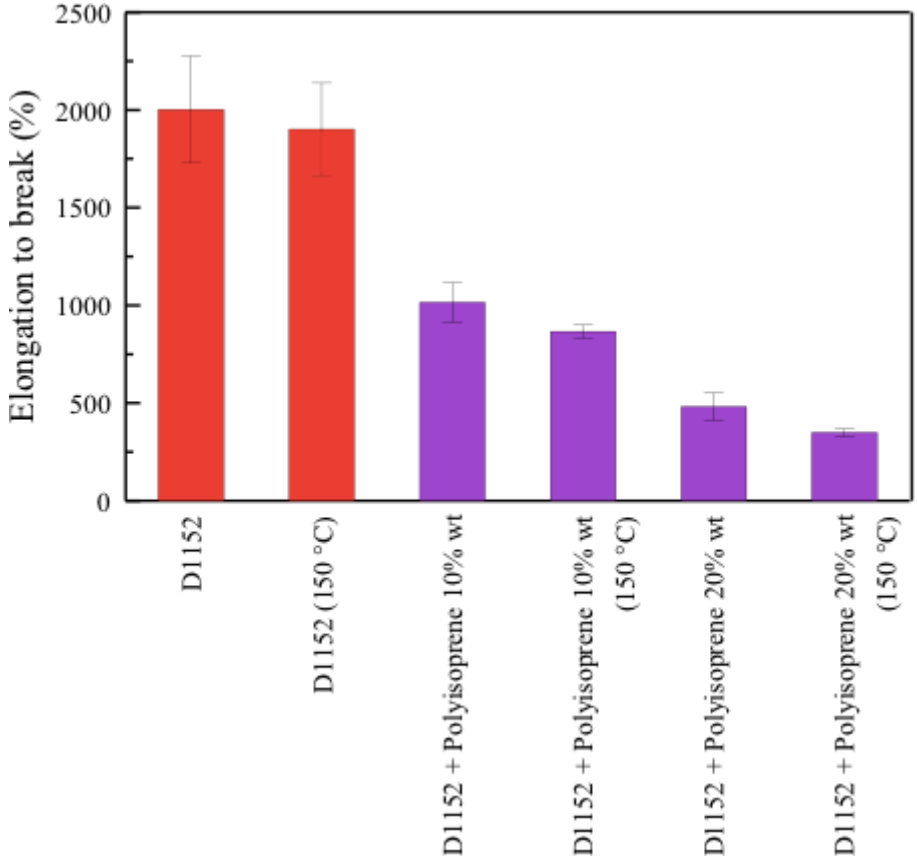

Figure 3.14: Elongation at Break Percentages of Elastomeric Polymers. Elongation at break values for Kraton D1152ES (SBS) in red, and Kraton D1152ES (SBS) blended with polyisoprene in purple.

Elongation at break points in Figure 3.14 show that Kraton D1152ES (SBS) is capable of remarkable elongation. It can stretch 2-4 $_{\text{times}}$ as much as polyisoprene blends, different stressors notwithstanding. Despite stretching to 2225%, Kraton D1152ES (SBS) showed permanent deformation of no more than 50% of its original size (data not shown). This elongation at break result was unexpected, as Kraton product specifications state D1152 (SBS) is capable of a maximum elongation of up to 900%. However, differences in solvent, weight to volume concentration, and equipment are all potential determining factors in these results.

Polyisoprene blends were capable of elongations between 300-900% as shown in Figure 3.14, with exact elongations dependant on the percentage of polyisoprene. Permanent deformations (data not shown) for these samples occurred much earlier compared to those for Kraton D1152ES (SBS). Nontheless, these deformations were minor in comparison to the deformations experienced by P(VDF-TrFE). This may be reflective of the lack of capacity to elongate as much as D1152, and consequently relative, reduced deformation. Deformation data can be found in the appendix.

Earlier in this chapter, the elongation at break value of skin was reported to range between 17 and 207 percent.[73] In theory, any of these polymers could be used as biomaterials for skin based on our reported elongation-at-break data. Given the stress-strain curves, it is unlikely that polyisoprene blends would be appropriate as implantables within any region with substantial repeated mobility (i.e., joints) due to their inability to withstand a comparable amount of strength. However, the elongation at break data was higher than skin for all polyisoprene blends. While it may not be an ideal perdurable polymer, polyisoprene blends may consequently be well-suited as components of wearables and soft electrodes.

Analysis of Young's Moduli, Stress-Strain Curves and Elongation at Break Data

Like biological skin, any artificial or second skin will mostly operate under fairly constant, variable amounts of stress. Thus, materials that make up such products must exhibit a similar robustness to skin. The ideal material should be able to be stretched under significant stress with high applied forces, and be able to bear higher loads without deforming or breaking. As such, candidate materials used in the replication of skin must have both high elasticity and relatively high fatigue resistance in order to avoid permanent deformations or fracture.

Considering Young's modulus alone, Kaneka SIBS, Kraton D1152ES (SBS) polyisoprene blends, and electrospun Kraton D1152ES (SBS) are interesting candidates. All of these exhibit a value between the elastic and deformation moduli of skin. However, in a subsequent analysis considering the overall range of the stress-strain curves for selected polymers, these materials are shown to be either softer (Kaneka SIBS, Kraton D1152ES (SBS) polyisoprene blends, and electrospun Kraton D1152ES (SBS), or simply less resistant to failure (Kraton D1161PT (SIS) and Kraton D1152ES (SBS) polybutadiene blends) than skin. Most materials assessed failed

before 100% strain, while porcine joint skin reaches nearly 150% and skin surrounding ear musculature reaches 250%. The elongation at break analysis confirmed this, showing decreasing elongation at break percentages based on increasing amounts of polyisoprene and heat treatment.

The results from Figures 3.12, 3.13, and 3.14 show the remarkable impact of processing on the mechanical properties of elastomers. The Young's moduli, tensile strength, and elongation at break obtained for the elastomer sheets and electrospun fibres examined in this work differ substantially from those reported for poly[styrene-β-(ethylene-co-butylene)-β-styrene] processed as membranes for electrodialysis (thickness: 100-150 μm) or as membranes for dielectric elastomer actuators (thickness: 94 ± 29 μm).[54, 55]

Skin has a variable ultimate strain percentage in different mammals, making it difficult to mimic. In humans, this value may be as high as 207%,[73] but our own data on porcine skin yields values as high as 250%. Considering this, as well the stress skin is capable of withstanding, planar Kraton D1152ES (SBS) is the only material with comparable Young's modulus values and stress-strain curves. Nonetheless, like all the other polymeric materials tested in this study, Kraton D1152ES (SBS) does not present an identical stress-strain curve to skin. Additionally, its load-bearing capacity is only comparable when it is cured at relatively low temperatures (ideally 37ºC). In contrast, heated Kraton D1152ES (SBS) fails much earlier, and electrospun Kraton D1152ES (SBS) presents much lower load bearing properties. However, the latter possesses variable quantities of iron (III) p-toluenesulfonate hexahydrate, which can alter these properties substantially.

Technically, a material such as electrospun P(VDF-TrFE) may perform perfectly adequately compared to human skin. Indeed, the Young's moduli of electrospun P(VDF-TrFE) fibres are more similar to those of porcine skin, while films present a very high Young's modulus capable of briefly withstanding strongly applied forces. Unfortunately, these stress-strain curves also show that flexible electrospun P(VDF-TrFE) experiences creep, material deformities, and partial breakage at relatively low strain compared to porcine skin samples. P(VDF-TrFE) copolymers typically have Young's moduli of approximately 1.5 GPa when made in films; comparatively, fibrous structures may have Young's modulus values anywhere between 6.0 and 340 MPa, tensile strengths below 3 MPa.[57, 58, 56, 99, 100] As such, this material was expected

to mimic skin's properties to some extent. While the results reported in the literature for films may vary from our own (likely due to the extreme thinness of our films) the electrospun values are indeed in the expected range. As with mammalian skin, these values can be highly variable due to thickness, heat processing (if necessary for optimization of ferroelectric properties), and various other factors. The differences between P(VDF-TrFE) constructs illustrates how crucial macroscopic design is when defining mechanical properties.

Kraton D1152ES (SBS) has been engineered in a particular way that could be an ideal second skin substitute. Although the shape of the stress-strain curves of the material compared to those of skin are of a different type, planar D1152 is capable of resisting comparatively high amounts of stress and easily can withstand great strain — greater than skin, even under repeated duress. The main difference between these materials is that, unlike skin, it does not undergo a J-shaped curve of deformation, which is the cause of its larger Young's modulus. Its elongation at break data also implies that it has the capacity for a lifespan that far surpasses *ex vivo* skin; a particularly important trait as D1152 possesses no regenerative capacity. When considering materials for second skin substitute purposes, repetitive stress and strain must be considered as most polymers are not self-healing. Human joint movements range from a minimum of 60^{o} to a maximum of 140^{o} degrees, found in wrist extension and elbow flexion, respectively.[59] Meanwhile, skin has an age dependent ultimate strain percentage that ranges from 75% in neonates to 60% in the elderly.[60] In comparison to parts of the body capable of undergoing regular, repeated strain, nerves, which act as a viscoelastic material, stretch approximately 15% in situ, and are capable of stretching up to 40% before reaching the plastic region of permanent deformation.[59] The typical load-elongation and stress-strain curves for peripheral nerve in a digit can be seen in Figure 3.15.

It is notable that viscoelastic materials, including nerves and skin, have variable stiffness that changes when elongation occurs rapidly rather than slowly.[59] Studies of rabbit tibial nerves have shown that maximum elongation can range between 38.5% to 55.7%, based simply on the rate of elongation.[59] This implies that viscoelastic materials exhibit reduced abilities to tolerate elongation when elongated rapidly. As such, elongation rate plays a major role in deformation and hysteresis. Our own materials were elongated at the maximum rate possible, implying that the results in Figure 3.14 may in fact be the lowest maximum elongation rates achievable. Although the maximum elongation has been established; repeated, regular strain is

a more important metric for biomedical materials. In the body, this is done an infinite number of times—meaning that the fatigue properties of our selected materials are essential to our assessment. Our fatigue analysis of skin and polymers is detailed in the next section.

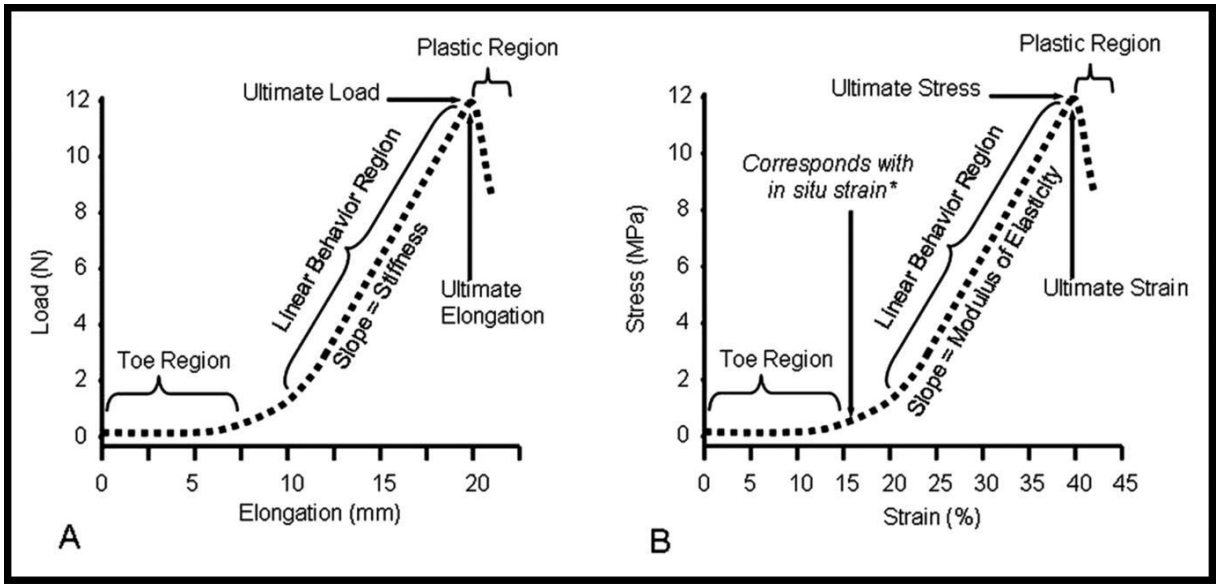

Figure 3.15: Load-Elongation and Stress-Strain Curves for Peripheral Nerve in a Digit. Taken from the *Structure and Biomechanics of Peripheral Nerves: Nerve Responses to Physical Stresses and Implications for Physical Therapist Practice*. Phys Ther. 2006;86(1):92-109. Copyright Oxford University Press [59]

3.3.4 Comparative Analysis of Skin and Elastomers through Fatigue Assessment

Fatigue resistance of flexible and elastic polymers is highly dependent on test conditions. The failure process throughout repeated deformation cycles will change enormously for different test modes (tension or flexion) and sample shapes. In tensile conditions, the magnitude of average stress during a fatigue test and its corresponding position in the stress-strain curve is a critical factor. The presence of simultaneous creep and physical aging also have to be taken into account. The large variety of factors influencing fatigue resistance makes specific fatigue tests mimicking potential working conditions essential for assessing material durability in real applications.

As previously mentioned, selection of a second skin substrate requires one of two properties: regeneration, or such a long lifespan where regeneration is not needed. Since the assessed polymers are all subject to mechanical fatigue and consequent points of ultimate strain, it is extremely important for their mechanical properties to be capable of long term use, through

several cycles of deformation as reflected in fatigue assays. As shown in Figure 3.16, the strain amplitude of the pig skin ankle and ear show failure at or prior to 10 thousand cycles when subjected to an amplitude around 2.5%, while they can sustain up to 10^5-10^6 cycles at very low amplitudes of around 0.5%.

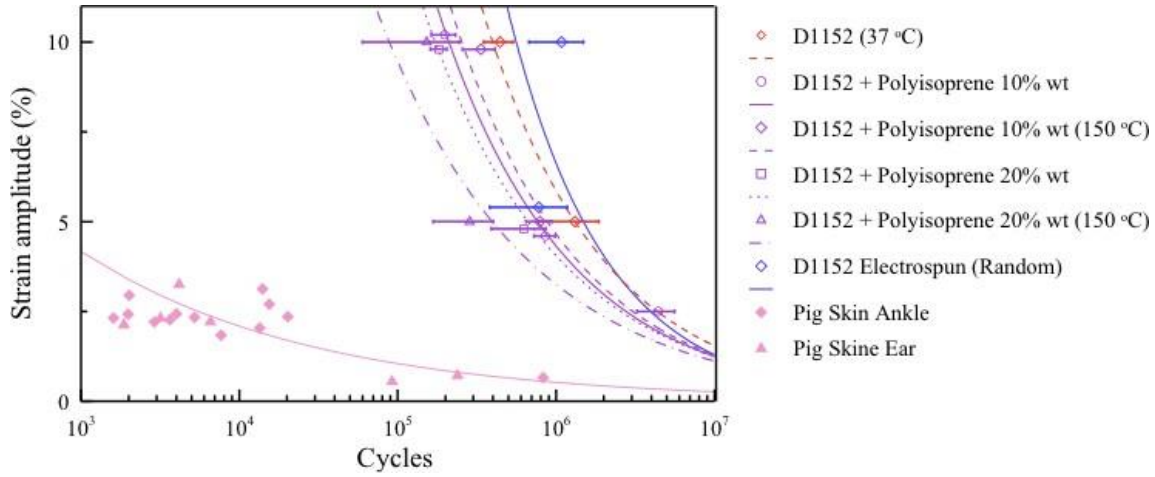

Figure 3.16: Fatigue Analysis of Elastomers and *Ex Vivo* Skin. Fatigue analysis of Kraton D1152ES (SBS) in red, Kraton D1152ES (SBS) blends with polyisoprene in purple, electrospun Kraton D1152ES (SBS) in blue, and porcine skin in pink .

In Figure 3.16, the number of cycles to failure are shown as a function of strain amplitude in tensile fatigue tests. The error bars correspond to the average of absolute deviations from the mean value. The lines shown are best fits between the three different strain oscillation amplitudes, ε, and the number of cycles to failure, *N*, assuming: $\varepsilon = aN^{-b}$ behaviour (based on the Coffin-Manson relation). The amplitudes of strain were fixed at 2.5%, 5%, and 10%. The small vertical displacements in polymeric materials are fictive displacements to better visualize the data. At 2.5%, most materials did not reach a point of failure during the tests. In such cases, amplitude data is not shown, but specific values can be visualized in Table 3.3. Because of the differences in strain amplitude skin was capable of handling, porcine skin is displayed as individual test results instead of an average value. This is done with the aim of visualizing the overall dispersion obtained.

The fatigue behaviours of the various synthetic materials are fairly similar within each strain amplitude. When subjected to deformation cycles of 5% and 10% amplitude, they fail within 10^5 to $2x10^6$ cycles. On the other hand, in tests performed at 2.5%, most samples did not reach a point of failure. Fatigue tests are very dependent on non-controllable sample characteristics like micro-cracks or density inhomogeneity. As such, a great quantity of tests at varied amplitudes are necessary to fully determine the fatigue behaviour of these materials.

Table 3.6: Strain Amplitude & Cycles to Failure of Elastomers

Material	Strain amplitude	Cycles to Failure
D1152 37 ^{o}C	2.5%	$>5\times10^{6}$
	5.0%	1.3×10^{6}
	10%	4.4×10^{5}
D1152 + Polyisoprene 10% wt	2.5%	4.0×10^{6}
	5.0%	8.5×10^{5}
	10%	2.0×10^{5}
D1152 + Polyisoprene 10% wt (150 ^{o}C)	2.5%	$>5\times10^{6}$
	5.0%	7.9×10^{5}
	10%	3.3×10^{5}
D1152 + Polyisoprene 20% wt	2.5%	$>5\times10^{6}$
	5.0%	6.3×10^{5}
	10%	1.8×10^{5}
D1152 + Polyisoprene 20% wt (150 ^{o}C)	2.5%	$>5\times10^{6}$
	5.0%	2.8×10^{5}
	10%	1.5×10^{5}
D1152 Electrospun (Random)	2.5%	$>5\times10^{6}$
	5.0%	7.8×10^{5}
	10%	1.1×10^{6}

The main tendency observed in these fatigue tests is that samples containing polyisoprene show a reduction of fatigue resistance compared to planar, heat-treated Kraton D1152ES (SBS) and Electrospun Kraton D1152ES (SBS). This is consistent with our assumptions based on the elongation at break data previously shown. Regardless, all synthetic materials show fatigue resistance orders of magnitude higher than the skin samples for all amplitudes tested. Based on stress-strain curves, we suspected that polyisoprene blended samples would not be capable of the same amount of strain as skin. However, our fatigue tests show that this is not the case. Here, skin is incapable of withstanding strain greater than 2.5%. Given that the ultimate strain of human skin can be up to 207%, this can be assumed to be due to the *ex vivo* nature of these tests.[73] As skin possesses regenerative capacities *in vivo*, the fatigue capacity of these polymers is extremely promising given that our polymers are non-regenerative synthetic materials.

3.4 Conclusions

Our work in this chapter focused on the mechanical properties of a wide range of polymers and polymer blends. In the context of a perdurable polymer capable of mimicking the properties of skin, Kraton D1152ES (SBS) is capable of undergoing large amounts of stress and strain that surpass those found in the body, even those of the dermis. It is additionally capable of withstanding large amounts of mechanical fatigue, like many elastomers, only deforming after undergoing substantial elongation. This study provides the basis of information required for creating products that can be implanted or worn long-term. Not all the materials tested are suitable as substitutes for artificial skin as their fatigue properties are inadequate for this application, and skin's viscoelastic, anisotropic characteristics are quite challenging to replicate. However, the other polymers tested undoubtedly have other potential uses, such as in soft electrodes, other types of biomedical devices, or wearables.

As skin is capable of regeneration, an extensive assessment of fatigue would likely involve deformation tests focused on mimicking the anisotropic properties of skin affixed to a body, to understand whether these materials could be used as wearables or in similar contexts. Our own research could be furthered by performing fatigue tests in a humidified environment, preventing dehydration-based fatigue failure, which occurred to skin in this study at an accelerated rate. Similarly, electrospun materials experience changes to their mechanical properties after long periods of time or prolonged exposure to air; a humidified environment during testing would almost certainly influence results. In summary, this work shows that Kraton D1152ES (SBS) is an elastomer with easily modifiable mechanical properties when combined with other polymers, such as polyisoprene, or additives, such as iron(III) p-toluenesulfonate hexahydrate. It has distinct promise for use in a variety of fields.

3.5 References

1. Abellan, Marie-Angèle, Hassan Zahouani, and Jean-Michel Bergheau. "Contribution to the determination of in vivo mechanical characteristics of human skin by indentation test." *Computational and mathematical methods in medicine* 2013 (2013).
2. Edwards, Christopher, and Ronald Marks. "Evaluation of biomechanical properties of human skin." *Clinics in dermatology* 13.4 (1995): 375-380.
3. Pailler-Mattei, C., et al. "Rheological behaviour of reconstructed skin." *journal of the mechanical behavior of biomedical materials* 37 (2014): 251-263.
4. Nicolle, Stéphane, et al. "New regime in the mechanical behavior of skin: strain-softening occurring before strain-hardening." *Journal of the mechanical behavior of biomedical materials* 69 (2017): 98-106.
5. Gerhardt, L-C., et al. "Skin–textile friction and skin elasticity in young and aged persons." *Skin Research and Technology* 15.3 (2009): 288-298.
6. Ottenio, Mélanie, et al. "Strain rate and anisotropy effects on the tensile failure characteristics of human skin." *Journal of the mechanical behavior of biomedical materials* 41 (2015): 241-250.
7. Jor, Jessica WY, et al. "Estimating material parameters of a structurally based constitutive relation for skin mechanics." *Biomechanics and modeling in mechanobiology* 10.5 (2011): 767-778.
8. Mahmud, Jamaluddin, et al. "A parametric study and simulations in quantifying human skin hyperelastic parameters." *Procedia Engineering* 41 (2012): 1580-1586.
9. Yannas, I. V., et al. "Progress in design of an artificial skin." *Federation Proceedings*. Vol. 38. No. 3. 9650 Rockville Pike, Bethesda, Md 20814-3998: Federation Amer Soc Exp Biol, 1979.
10. Ulery, Bret D., Lakshmi S. Nair, and Cato T. Laurencin. "Biomedical applications of biodegradable polymers." *Journal of polymer science Part B: polymer physics* 49.12 (2011): 832-864.
11. Kim, Jaemin, et al. "Stretchable silicon nanoribbon electronics for skin prosthesis." *Nature communications* 5 (2014): 5747.
12. Chortos, Alex, Jia Liu, and Zhenan Bao. "Pursuing prosthetic electronic skin." *Nature materials* 15.9 (2016): 937.
13. Choi, Won Mook, et al. "Biaxially stretchable "wavy" silicon nanomembranes." *Nano Letters* 7.6 (2007): 1655-1663.
14. Yu, Betty, et al. "An elastic second skin." *Nature materials*15.8 (2016): 911.
15. Tee, Benjamin C-K., et al. "A skin-inspired organic digital mechanoreceptor." *Science* 350.6258 (2015): 313-316.
16. Grabbert, Niels, et al. "Mechanical properties of individual composite poly (methyl-methacrylate)-multiwalled carbon nanotubes nanofibers." *IOP Conference Series: Materials Science and Engineering*. Vol. 64. No. 1. IOP Publishing, 2014.
17. Chen, Wei, et al. "Improved polyvinylpyrrolidone microneedle arrays with non-stoichiometric cyclodextrin." *Journal of Materials Chemistry B* 2.12 (2014): 1699-1705.
18. Tsui, C. P., et al. "Prediction for debonding damage process of glass beads-reinforced modified polyphenylene oxide under simple shear." *Journal of materials processing technology*167.2-3 (2005): 429-437.

19. Sadhu, Susmita, and Anil K. Bhowmick. "Preparation and properties of nanocomposites based on acrylonitrile–butadiene rubber, styrene–butadiene rubber, and polybutadiene rubber." *Journal of Polymer Science Part B: Polymer Physics* 42.9 (2004): 1573-1585.
20. Armani, Deniz, Chang Liu, and Narayan Aluru. "Re-configurable fluid circuits by PDMS elastomer micromachining." *Micro Electro Mechanical Systems, 1999. MEMS'99. Twelfth IEEE International Conference on*. IEEE, 1999.
21. Kraton Performance Polymers, Inc. Kraton: The Global Connection for Polymer and Compound Solutions Product and Application Guide. Kraton Performance Polymers, Inc., 2014, www.kraton.com.
22. Suleiman, David, et al. "Mechanical and chemical properties of poly (styrene-isobutylene-styrene) block copolymers: Effect of sulfonation and counter ion substitution." *Journal of Applied Polymer Science* 131.11 (2014).
23. Linares, A., and J. L. Acosta. "Structural characterization of polymer blends based on polysulfones." *Journal of applied polymer science* 92.5 (2004): 3030-3039.
24. Chang, Wen-Yang, Te-Hua Fang, and Yu-Cheng Lin. "Physical characteristics of polyimide films for flexible sensors." *Applied Physics A* 92.3 (2008): 693.
25. Li W, Wan M. Porous polyaniline films with high conductivity. Synthetic metals. 1998 Jan 30;92(2):121-6.
26. Yang, Jiping, et al. "Polyaniline/polypropylene film composites with high electric conductivity and good mechanical properties." *Journal of applied polymer science* 56.7 (1995): 831-836.
27. Malmonge, Luiz Francisco, et al. "Thermal and mechanical properties of PVDF/PANI blends." Materials Research 13.4 (2010): 465-470.
28. Mikolajczyk, Teresa, et al. "Strength properties of polyacrylonitrile (PAN) fibres modified with carbon nanotubes with respect to their porous and supramolecular structure." *Fibres & Textiles in Eastern Europe* 17.6 (2009): 13-20.
29. Chisca, Stefan, et al. "Dielectric and conduction properties of polyimide films." *Semiconductor Conference (CAS), 2011 International*. Vol. 2. IEEE, 2011.
30. Coelho, Paulo Henrique da Silva Leite, et al. "Electrical percolation, morphological and dispersion properties of MWCNT/PMMA nanocomposites." Materials Research 17 (2014): 127-132.
31. DeMeuse, M. T. "Polysulfones as a reinforcement in high temperature polymer blends." *High Temperature Polymer Blends*. 2014. 165-173.
32. Gohil, S. V., et al. "Polymers and composites for orthopedic applications." *Materials for Bone Disorders*. 2017. 349-403.
33. McKeen, Laurence W. *Permeability properties of plastics and elastomers*. William Andrew, 2016.
34. Núñez, Carla Nathaly Villacís, et al. "Effect of organic solvents in morphology and mechanical properties of electrospun polyvinylpyrrolidone fibers." *Congreso de Ciencia y Tecnología ESPE*. Vol. 13. No. 1. 2018.
35. Kraton.com: http://docs.kraton.com/pdfDocuments/20091105084144234664 58.PDF
36. Joly, Gert, and Jaak L. Moerenhout. "Styrenic block copolymer compositions to be used for the manufacture of transparent, gel free films." U.S. Patent No. 7,838,598. 23 Nov. 2010.

37. Liu, Yuxia, Charles W. Paul, and Peter D. Palasz. "Optically clear hot melt adhesives and uses thereof." U.S. Patent Application No. 15/426,214.
38. http://docs.kraton.com/pdfDocuments/200910280744097346616 6.PDF
39. Bertoldi, S., et al. "Innovative polymers for TMD rehabilitation devices." *J Dent App* 1.6 (2014): 119-123.
40. Ranade, Shrirang V., Robert E. Richard, and Michael N. Helmus. "Styrenic block copolymers for biomaterial and drug delivery applications." *Acta Biomaterialia* 1.1 (2005): 137-144.
41. Ohara, Kazumasa, and Tsuyoshi Mihayashi. "Catheter tube and catheter comprising the tube." U.S. Patent No. 7,998,124. 16 Aug. 2011.
42. Burlot, Delphine, Paul Lassalle, and Laurent Lalet. "Adhesive composition and element for attaching to human skin." U.S. Patent Application No. 15/884,981.
43. Lim, Goy Teck, et al. "Highly hydrophobic electrospun fiber mats from polyisobutylene-based thermoplastic elastomers." *Biomacromolecules* 12.5 (2011): 1795-1799.
44. Yong Liu, Xiao Liu, Jun Chen, Kerry J. Gilmore and Gordon G. Wallace "3D Bio-nanofibrous PPy/SIBS mats as platforms for cell culturing" Chem. Commun., 2008, 3729-3731
45. Zhou, Hua, et al. "Electrospun fibrous membranes with super-large-strain electric superhydrophobicity." *Scientific reports* 5 (2015): 15863.
46. Feng, Shuqin, and Xinyuan Shen. "Electrospinning and Mechanical Properties of Polystyrene and Styrene-Isoprene-Styrene Block Copolymer Blend Nanofibres." *Journal of Macromolecular Science, Part B* 49.2 (2010): 345-354.
47. Fong, Hao, and Darrell H. Reneker. "Elastomeric nanofibers of styrene–butadiene–styrene triblock copolymer." *Journal of Polymer Science Part B: Polymer Physics* 37.24 (1999): 3488-3493.
48. Holschuh, Bradley, Edward Obropta, and Dava Newman. "Low spring index NiTi coil actuators for use in active compression garments." *IEEE/ASME Transactions on Mechatronics* 20.3 (2015): 1264-1277.
49. Escoffier, Catherine, et al. "Age-related mechanical properties of human skin: an in vivo study." *Journal of Investigative Dermatology* 93.3 (1989).
50. Vogel, H. G. "Age dependence of mechanical and biochemical properties of human skin. II: Hysteresis, relaxation, creep and repeated strain experiments." *Bioengineering and the skin* 3.2 (1987): 141-176.
51. Shergold, Oliver A., Norman A. Fleck, and Darren Radford. "The uniaxial stress versus strain response of pig skin and silicone rubber at low and high strain rates." *International Journal of Impact Engineering* 32.9 (2006): 1384-1402.
52. Żak, Malgorzata., et al. "Determination of the mechanical properties of the skin of pig foetuses with respect to its structure." *Acta of Bioengineering and Biomechanics*13.2 (2011): 37-43.
53. Singh, Deepa, and Ashish Garg. "The combined effect of mechanical strain and electric field cycling on the ferroelectric performance of P (VDF-TrFE) thin films on flexible substrates and underlying mechanisms." *Physical Chemistry Chemical Physics* 18.42 (2016): 29478-29485.
54. Pérez-Madrigal, Maria M., et al. "Enhanced dielectric performance of a block copolymer-polythiophene nanocomposite." *Journal of Polymer Science Part B: Polymer Physics* 54.18 (2016): 1896-1905.

55. Müller, Franciélli, et al. "New sulfonated polystyrene and styrene–ethylene/butylene–styrene block copolymers for applications in electrodialysis." *The Journal of Physical Chemistry B* 116.38 (2012): 11767-11779.
56. Yao, Jian, Cees WM Bastiaansen, and Ton Peijs. "High strength and high modulus electrospun nanofibers." *Fibers* 2.2 (2014): 158-186.
57. Fang, F., S. C. Shan, and W. Yang. "A multipeak phenomenon of magnetoelectric coupling in Terfenol-D/P (VDF-TrFE)/Terfenol-D laminates." *Journal of Applied Physics*108.10 (2010): 104505.
58. Bhavanasi, Venkateswarlu, et al. "Enhanced piezoelectric energy harvesting performance of flexible PVDF-TrFE bilayer films with graphene oxide." *ACS applied materials & interfaces*8.1 (2015): 521-529.
59. Topp, Kimberly S., and Benjamin S. Boyd. "Structure and biomechanics of peripheral nerves: nerve responses to physical stresses and implications for physical therapist practice." *Physical therapy* 86.1 (2006): 92-109.
60. Pawlaczyk, Mariola, Monika Lelonkiewicz, and Michał Wieczorowski. "Age-dependent biomechanical properties of the skin." *Advances in Dermatology and Allergology/Postępy Dermatologii i Alergologii* 30.5 (2013): 302.
61. Pham, Quynh P., Upma Sharma, and Antonios G. Mikos. "Electrospinning of polymeric nanofibers for tissue engineering applications: a review." *Tissue engineering* 12.5 (2006): 1197-1211.
62. Arash, B., Q. Wang, and V. K. Varadan. "Mechanical properties of carbon nanotube/polymer composites." *Scientific reports* 4 (2014): 6479.
63. Hosseinzadeh, Simzar, et al. "The nanofibrous PAN-PANi scaffold as an efficient substrate for skeletal muscle differentiation using satellite cells." *Bioprocess and biosystems engineering* 39.7 (2016): 1163-1172.
64. Kim, Gyeong-Man, et al. "Electrospinning of PCL/PVP blends for tissue engineering scaffolds." *Journal of Materials Science: Materials in Medicine* 24.6 (2013): 1425-1442.
65. Pilehvar-Soltanahmadi, Younes, et al. "An overview on application of natural substances incorporated with electrospun nanofibrous scaffolds to development of innovative wound dressings." *Mini reviews in medicinal chemistry* 18.5 (2018): 414-427.
66. Ma, Hongyang, Benjamin S. Hsiao, and Benjamin Chu. "Functionalized electrospun nanofibrous microfiltration membranes for removal of bacteria and viruses." *Journal of membrane science* 452 (2014): 446-452.
67. Beringer, Laura T., et al. "An electrospun PVDF-TrFe fiber sensor platform for biological applications." *Sensors and Actuators A: Physical* 222 (2015): 293-300.
68. Tandon, Biranche, Jonny J. Blaker, and Sarah H. Cartmell. "Piezoelectric materials as stimulatory biomedical materials and scaffolds for bone repair." *Acta biomaterialia* 73 (2018): 1-20.
69. Guo, Hong-Feng, et al. "Piezoelectric PU/PVDF electrospun scaffolds for wound healing applications." *Colloids and Surfaces B: Biointerfaces* 96 (2012): 29-36.
70. Arinzeh, Treena L., Norbert Weber, and Michael Jaffe. "Electrospun electroactive polymers for regenerative medicine applications." U.S. Patent Application No. 10/052,412.

71. Kang, Guo-dong, and Yi-ming Cao. "Application and modification of poly (vinylidene fluoride)(PVDF) membranes–a review." *Journal of membrane science* 463 (2014): 145-165.
72. Wang, Jing, and Maike Windbergs. "Functional electrospun fibers for the treatment of human skin wounds." *European Journal of Pharmaceutics and Biopharmaceutics* 119 (2017): 283-299.
73. Dias, J. R., P. L. Granja, and P. J. Bártolo. "Advances in electrospun skin substitutes." *Progress in Materials Science* 84 (2016): 314-334.
74. Szycher, Michael. *High performance biomaterials: a complete guide to medical and pharmceutical applications*. Routledge, 2017.
75. Lee, Jae-Young, et al. "Poly (styrene)-b-poly (DL-lactide) copolymer-based nanoparticles for anticancer drug delivery." *International journal of nanomedicine* 9 (2014): 2803.
76. Ribeiro, S., et al. "Electrospun styrene–butadiene–styrene elastomer copolymers for tissue engineering applications: effect of butadiene/styrene ratio, block structure, hydrogenation and carbon nanotube loading on physical properties and cytotoxicity." *Composites Part B: Engineering* 67 (2014): 30-38.
77. Müller, Franciélli, et al. "New sulfonated polystyrene and styrene–ethylene/butylene–styrene block copolymers for applications in electrodialysis." *The Journal of Physical Chemistry B* 116.38 (2012): 11767-11779.
78. Kurusu, Rafael S., and Nicole R. Demarquette. "Wetting of hydrophilic electrospun mats produced by blending SEBS with PEO–PPO–PEO copolymers of different molecular weight." *Langmuir* 32.7 (2016): 1846-1853.
79. Kraton.com: "Kraton™ Polymers for Oil Modification: Versatile Solutions for Synthetic and Natural Based Oils." https://kraton.com/products/pdf/General%20Oil%20Gels.pdf
80. Duong, Hung Cong, et al. "A novel electrospun, hydrophobic, and elastomeric styrene-butadiene-styrene membrane for membrane distillation applications." *Journal of membrane science* 549 (2018): 420-427.
81. van der Heijden, Sam, et al. "Novel composite materials with tunable delamination resistance using functionalizable electrospun SBS fibers." *Composite Structures* 159 (2017): 12-20.
82. Ribeiro, S., et al. "Electrospun styrene–butadiene–styrene elastomer copolymers for tissue engineering applications: effect of butadiene/styrene ratio, block structure, hydrogenation and carbon nanotube loading on physical properties and cytotoxicity." *Composites Part B: Engineering* 67 (2014): 30-38.
83. Feng, Shu-Qin, et al. "Studies on the electrospun submicron fibers of SIS and its mechanical properties." *Journal of applied polymer science* 114.3 (2009): 1580-1586.
84. Gestos, Adrian, et al. "Tensile testing of individual glassy, rubbery and hydrogel electrospun polymer nanofibres to high strain using the atomic force microscope." *Polymer Testing* 32.4 (2013): 655-664.
85. Liu, Weihua, et al. "Radiation-induced crosslinking of polyacrylonitrile fibers and the subsequent regulative effect on the preoxidation process." *Radiation Physics and Chemistry* 81.6 (2012): 622-627.
86. Ding, Yichun, et al. "Electrospun polyimide nanofibers and their applications." *Progress in Polymer Science* 61 (2016): 67-103.
87. Yuan, Xiaoyan, et al. "Morphology of ultrafine polysulfone fibers prepared by electrospinning." Polymer international 53.11 (2004): 1704-1710.
88. Ding, Yichun, et al. "Electrospun polyimide nanofibers and their applications." *Progress in Polymer Science* 61 (2016): 67-103.

89. Liu, Ying, et al. "Effects of fiber orientation and diameter on the behavior of human dermal fibroblasts on electrospun PMMA scaffolds." *Journal of Biomedical Materials Research Part A: An Official Journal of The Society for Biomaterials, The Japanese Society for Biomaterials, and The Australian Society for Biomaterials and the Korean Society for Biomaterials* 90.4 (2009): 1092-1106.
90. Ico, Gerardo, et al. "Size-dependent piezoelectric and mechanical properties of electrospun P (VDF-TrFE) nanofibers for enhanced energy harvesting." *Journal of Materials Chemistry A* 4.6 (2016): 2293-2304.
91. He, Xiuli, et al. "Electrospun PVP fibers and gas sensing properties of PVP/36 YX LiTaO3 SAW device." *Sensors and Actuators B: Chemical* 145.2 (2010): 674-679.
92. Yuan, H., Q. Zhou, and Y. Zhang. "Improving fiber alignment during electrospinning." *Electrospun Nanofibers*. Woodhead Publishing, 2017. 125-147.
93. Rahmani, Shahrzad, Mehdi Rafizadeh, and Framarz Afshar Taromi. "Statistical analysis of nanofibers alignment in magnetic-field-assisted electrospinning including an alignment percentage formula." *Journal of Applied Polymer Science* 131.23 (2014).
94. Granero, A. J., Wagner, P., Wagner, K., Razal, J. M., Wallace, G. G., & in het Panhuis, M. (2011). Highly Stretchable Conducting SIBS-P3HT Fibers. Advanced Functional Materials, 21(5), 955–962. doi:10.1002/adfm.201001460
95. Rabionet, Marc, et al. "Electrospinning PCL scaffolds manufacture for three-dimensional breast cancer cell culture." *Polymers* 9.8 (2017): 328.
96. Le, Hong Hai, et al. "Time dependent deformation behavior of thermoplastic elastomers." *Polymer* 44.16 (2003): 4589-4597.
97. Ao, Zhimin, and Sean Li. "Temperature-and thickness-dependent elastic moduli of polymer thin films." *Nanoscale research letters* 6.1 (2011): 243.
98. Baniasadi, Mahmoud, et al. "High-performance coils and yarns of polymeric piezoelectric nanofibers." *ACS applied materials & interfaces* 7.9 (2015): 5358-5366.
99. Lam, Tu-Ngoc, et al. "Tuning mechanical properties of electrospun piezoelectric nanofibers by heat treatment." *Materialia* (2019): 100461.
100. Jiang, Yonggang, et al. "Aligned P (VDF-TrFE) nanofibers for enhanced piezoelectric directional strain sensing." Polymers 10.4 (2018): 364.
101. Lu, Jian-Wei, et al. "Electrospinning of sodium alginate with poly (ethylene oxide)." Polymer 47.23 (2006): 8026-8031.

CHAPTER 4. ELECTROCONDUCTIVE, ELECTROMECHANICAL, AND PIEZOELECTRIC BEHAVIOR OF THE CONSTRUCT

4.1 Outline

The mechanical results previously detailed in Chapter 3 allowed us to identify which elastomers were best suited for uses in wearables and perdurable implantables. However, the nature of this work necessitates an electroconductive component. This essentially means that this chapter focuses on the creation and validation of soft electrodes which can have added piezoelectric functionality. We begin with the identification of other soft electroconductive and piezoelectric constructs, discussed in Section 4.2. This section discusses the properties of these constructs, as well as the challenges of maintaining electroconductive or piezoelectric function alongside functional elastomeric properties. We go on to discuss the initial materials considered.

Section 4.3 includes our preliminary assessment of these materials, with a focus on those able to adhere successfully to our selected elastomers, producing sufficient conductivity for the first time. Here we specifically discuss the development of our first soft electrodes: Kaneka SIBSTAR^{TM} (SIBS) with thermally evaporated platinum, thermally evaporated gold, painted silver, and thermally evaporated platinum with electrodeposited iridium oxide. These are all functional two layered constructs that can serve as soft electrodes in further research. The creation of the latter combination, SIBS-platinum-IrOx, is a novel electrode that has not been previously reported in the literature. Following these results, these electroconductive materials are analysed in attempt to understand how they may respond to repeated stress and strain. We were able to obtain an alternative cross-linked polymeric platinum that we believed would be well-suited for biomedical purposes. This platinum acted as both a conductive and adherent surface. This allowed us to create soft electrode surfaces not only of elastomers and platinum, but customizable soft, piezoelectric electrodes, detailed in section 4.4.

In Sections 4.5, 4.6, and 4.7 we analyse the functionality of the complete construct. This includes both the electrical properties and electromechanical properties, which include the determination of Young's modulus, fatigue and electromechanical fatigue. Section 4.8 focuses on a piezoelectric analysis of the construct, through both FTIR and piezoelectric function. This and the final section conclude our validation on the creation of an elastomeric, conductive, piezoelectric construct with easily customizable properties.

4.2. Introduction

4.2.1 Electroconductive Materials Used in Biocompatible Devices

Creating an electroconductive elastomer is a conundrum. Electroconductive materials are often flexible, but rarely elastic. Clinically, elastomers substrates are used as insulators for conductive devices. For instance, implanted vagus nerve stimulation therapy utilizes 43 centimeter long silicone, platinum, and iridium-based devices with resistances ranging between 120 to 250 Ω.[1] Implantable extra- and intra-muscular and/or extra- and intra-neural electrodes also often involve electroconductive elastomers.[2,3] However, traditionally, the more elastic a material, the less conductive — and vice versa. More often than not, such products and other electroconductive elastomers lose most of their elastomeric properties in the production process, which has been discussed in previous chapters.

In Table 4.1, 41 electroconductive or piezoelectric elastomer constructs were identified as similar products to the electroconductive elastomer we aimed to create. From these constructs, three had noteworthy elastic properties, with elongation at break points above 1600%. Mixtures of PEG2k-AT6-TMP, polyaniline, and carbon black had conductivity ranging from $8.2 \cdot 10^{-6}$ to 0.1 S/cm.[10] Styrene-β-ethylbutylene-β-styrene (Kraton G1645) blended with carbon black had conductivity values in a similar range: $6.1 - 9.5 \cdot 10^{-4}$ S/m.[7] Most interesting was acrylic acid and 3-dimethyl (methacryloyloxyethyl) ammonium propane sulfonate, which had the highest elongation at break value of 10,000% and conductivity of $\geq 2 \cdot 10^{-5}$ S/cm.[37] In brief, we found electroconductive elastomers with elongation at break values higher than 1600% had conductivities no higher than 0.1 S/cm.

As elongation at break values were reduced, higher conductivities were reported. A further eight studies reported electroconductive elastomers with elongation at break values over 300%. On the lower end of the spectrum, the conductivity of styrene-butadiene rubber, carbon black, and carbon nanotube-based constructs ranged between $10^{-2} - 10^{-15}$ S/cm.[38] This number jumped to 1.3 S/cm with the combination of reduced graphene oxide and hydroxylated styrene–butadiene–styrene that had elongation at break values of ≥ 300%.[14] This was a more than ten-fold increase compared to the previously mentioned PEG2k-AT6-TMP, polyaniline, and carbon black blend with a maximum conductivity of 0.1 S/cm.[10] Polystyrene–polyisoprene-

polystyrene mixed with Ni nanoparticles and reduced graphene oxide showed an even higher conductivity range between 2.1 - 6 S/cm.[43] Finally, blends created using poly(styrene-co-butadiene) or polycaprolactone and carbon black had conductivity values in the range of 1.4 - 14 S/m.[9] Therefore, according to the literature on electroconductive elastomers similar to our own selected polymers, we could expect a conductivity ranging between $6.1 \cdot 10^{-4}$ S/m and 14 S/m.

The remaining four polymers with elongation at break values higher than 300% pursued substantially different approaches to us. Conductive polyurethane doped with camphorsulfonic acid had conductivity values ranging between $2.7 \cdot 10^{-10}$ - $7.3 \cdot 10^{-5}$ S/cm.[41] Polyamide 6 filled with elastomers and carbon black had a conductivity of 7.1×10^{-6} S/m.[15] Notably, its elongation at break values ranged between 63 - 311%.[15] Polyolefin elastomer nanofibrous yarn and Ag nanowires had a reported resistivity of 10 Ω.[20] Finally, silicone, single walled carbon nanotubes, and ionic liquid had one of the highest conductivities with values ranging between 18 - 63 S/cm.[29] Interestingly, this final construct was only tested up to 300%-- we can only assume that the elongation at break value is similar.

Five more conductive constructs were identified: These had elongation at break values between 100% and 250%. Conductive nanofibrous PANI/PVDF strain sensors were created, but their precise conductivity value was not listed.[45] Silicone-Carbon nanocomposites had resistivity values ranging between $1.62 \cdot 10^{-1}$ to $5 \cdot 10^{14}$ Ω · cm , which result in an equivalent conductivity value range of $5 \cdot 10^{-15}$ to 6.1728 S/cm.[17] Similarly, PDMS-Carbon nanotubes had aresistivity range of 2.03 - 5225 Ω /sq.[39] Silicone rubber and eutectic gallium-indium stated resistivity values of 2.5 – 3.1 Ω at rest and that failure begins at 250%, but listed no defined elongation at break point.[21] Finally, conductive films of PEDOT:PSS on PDMS had the highest conductivity ranging between 100 - 550 S/cm.[42] With elongation at break points between 50-200%, this final construct gives the maximum conductivity listed for any electroconductive elastomer we encountered in the literature. The remaining studies that were identified had no elongation at break values or electromechanical data listed.

Table 4.1: A Summary of Soft Electroconductive and/or Pressure-Sensitive Constructs (1/5)

Study	Polymer	Maximum Functional or at Break Elongation	Storage or Young's Modulus	Conductive or Piezoelectric Material	Maximum Conductivity/ Resistivity	Bio-compatible
Study of two types of sensors of static forces—a piezoelectric sensor and a piezoelectric elastomer sensor[4]	Electroconductive rubber		0.98 $\cdot 10^{11}$ MPa	Brass plates PZT4M	Changes based on volume of rubber	
Liquid single crystal elastomer/conducting polymer bilayer composite actuator: modelling and experiments[5]	Liquid Single Crystal Elastomer	30 – 50%	2.8 GPa	PEDOT:PSS	Actuates based on conductive layer thickness	
Investigation of electroconductive films composed of polyvinyl alcohol and graphitized carbon black[6]	Polyvinyl alcohol	Changes based on polymer to carbon ratio		Graphitized carbon black	10^{-2} - 10^{7} Ω	
Characterization of Thermoplastic Elastomers Based Composites Doped with Carbon Black[7]	Kraton G1645 (styrene-b-ethylbutylene-b-styrene)	1800 - 2475%	8 - 14 MPa	Carbon black	6.1 - 9.5 $\cdot 10^{-4}$ S/m	
Study of the reinforcing mechanism and strain sensing in a carbon black filled elastomer[8]	Poly(styrene-co-butadiene)	60% was the maximum tested	Varies based on carbon content	Carbon black	10^{-2} - 10^{-14} S/cm based on carbon content	
Relationship between conductivity and stress–strain curve of electroconductive composite with SBR or polycaprolactone matrices[9]	Poly(styrene-co-butadiene) or Polycaprolactone	≤ 650%		Carbon black and super-conductive carbon black	1.4 - 14 S/m	
Super Stretchable Electroactive Elastomer Formation Driven by Aniline Trimer Self-Assembly[10]	PEG2k-AT6-TMP	1643%	3.8 - 7.7 MPa	Polyaniline nanofibers, nanosized carbon black	$8.2 \cdot 10^{-6}$ to 0.1 S/cm	Yes
Dielectric and microwave properties of elastomer composites loaded with carbon–silica hybrid fillers[11]	Natural rubber SVR 10			Carbon black and doping agents	$2.2 \cdot 10^{3}$ - $1.2 \cdot 10^{13}$ Ω · m	

Table 4.1: A Summary of Soft Electroconductive and/or Pressure-Sensitive Constructs (2/5)

Electromechanically Responsive Liquid Crystal Elastomer Nanocomposites for Active Cell Culture[13]	Liquid crystal elastomers	Tested up to 35%	2.1 - 8.1 kN	Carbon black nanoparticles	0.2 – 38.5 Ω · m	Yes
Reduced graphene oxide/hydroxylated styrene–butadiene–styrene tri-block copolymer electroconductive nanocomposites: Preparation and properties[14]	Styrene-butadiene-styrene	318 - 632%	2.32 - 7.48 MPa	Reduced graphene oxide	1.3 S/m	
Simultaneous Improvement in Both Electrical Conductivity and Toughness of Polyamide 6 Nanocomposites Filled with Elastomer and Carbon Black Particles[15]	Polyamide 6	63-311%	0.85 - 1.11 GPa	Carbon black	7.1×10^{-6} S/m	
Effect of small additions of carbon nanotubes on the electrical conductivity of polyurethane elastomer[16]	Polyurethane		≤30 MPa	Single wall carbon nanotubes	Varies based on carbon concentration/ temperature	
Fabrication and Evaluation of the Novel Elastomer Based Nanocomposite with Pressure Sensing Function[17]	Silicone	≤200%		Carbon-Silica	$1.62 \cdot 10^{-1}$ to $5 \cdot 10^{14}$ Ω · cm	
Electroconductive Composites from Polystyrene Block Copolymers and Cu–Alumina Filler[18]	Polystyrene block copolymers	17%	50 - 150 MPa	Cu–Al_2O_3	$4.35 \cdot 10^{-16}$ to $7.7 \cdot 10^{-5}$ S/cm	
Hybrid nanocomposites of thermoplastic elastomer and carbon nanoadditives for electromagnetic shielding[19]	Poly (styrene-*b*-ethylene-ran-butylene-*b*-styrene)			Graphene nanoplatelets and carbon nanotubes	$1.2 \cdot 10^{-17}$ to 2.2 S/cm	
Continuously Producible Ultrasensitive Wearable Strain Sensor Assembled with Three-Dimensional Interpenetrating Ag Nanowires/Polyolefin Elastomer Nanofibrous Composite Yarn[20]	Polyolefin elastomer nanofibrous yarn	~575%	No change in modulus after nanowire addition	Ag nanowires	10 Ω	

Table 4.1: A Summary of Soft Electroconductive and/or Pressure-Sensitive Constructs (3/5)

Design and Fabrication of Soft Artificial Skin Using Embedded Microchannels and Liquid Conductors[21]	Silicone rubber	Failure begins at 250%	63 kPa	Eutectic gallium-indium	2.5 – 3.1 Ω at rest	
Polyisoprene-nanostructured carbon composite – A soft alternative for pressure sensor application[22]	Polyisoprene			Carbon black	10^{5} to 10^{-1} Ω · m	
Conductivity and mechanical properties of composites based on MWCNTs and styrene-butadiene-styrene block™ copolymers[23]	Styrene-butadiene-styrene		16.3 – 94.1 MPa	Multiwall carbon nanotubes	10^{-4} to 1.6 S/cm	
Carbon nanotube-coated silicone as a flexible and electrically conductive biomedical material[24]	Silicone	Tested up to 20%		Single and multiwall carbon nanotubes	0.86 to 1.5×10^{3} kΩ/sq	Yes
Electrically conducting polyaniline-PBMA composite films obtained by extrusion[25]	Poly(*n*-butyl methacrylate) - polyaniline			Doped with dodecyl-benzene sulfonic acid	$2 \cdot 10^{-2}$ - $1 \cdot 10^{-9}$ S/cm	
Electro-conductive sensors and heating elements based on conductive polymer composites[26]	Cotton yarn; polyethylene; polyamide; latex			Carbon black	0.1 - 3.6 kΩ · cm; varies based on carbon content	
Electrical properties of flexible pressure sensitive chezacarb/silicone rubber nanocomposites[27]	Silicone/PDMS			Carbon black and natural graphite	10^{3} - 10^{5} Ω · m	
Carbon nanotube-based thermoplastic polyurethane-poly(methyl methacrylate) nanocomposites for pressure sensing applications[28]	Polyurethane-poly(methyl methacrylate)			Multiwalled carbon nanotubes		
Single-walled carbon nanotube/silicone rubber composites for compliant electrodes[29]	Silicone	Tested up to 300%	0.399 - 4.6 MPa	Single walled carbon nanotubes; ionic liquid	18 - 63 S/cm	
Development of a Regenerative Peripheral Nerve Interface for Control of a Neuroprosthetic Limb[30]	Silicone			PEDOT		Yes

Table 4.1: A Summary of Soft Electroconductive and/or Pressure-Sensitive Constructs (4/5)

Electrical, mechanical and piezo-resistive behavior of a polyaniline/poly(*n*-butyl methacrylate) composite[31]	Polyaniline-poly(*n*-butyl methacrylate)	50 - 250%	60 - 140 MPa	Doped with n-dodecyl-benzene-sulfonic acid	$10^3 – 10^9$ Ω /sq	
A Conductive Composite Nanomaterial with Biocompatible Matrix and Multilayer Carbon Nanotubes[32]	Carboxy-methylcellulose matrix and flexible polymers			Multiwall carbon nanotubes	~$1.2 - 4 \cdot 10^4$ S/m	Yes
Piezoresistive Behavior Study on Finger-Sensing Silicone Rubber/Graphite Nanosheet Nanocomposites[33]	Silicone rubber			Graphite nanosheets	Piezoresistive under low pressure	
Silicone Substrate with Collagen and Carbon Nanotubes Exposed to Pulsed Current for MSC Osteodifferentiation[34]	PDMS, Silicone			Carbon nanotubes	760 – 827 Ω	Yes
An ultra-sensitive resistive pressure sensor based on hollow-sphere microstructure induced elasticity in conducting polymer film.[35]	Polypyrrole		Low elastic modulus changing with compression	Doped with phytic acid	0.5 S/cm	
Electrical Properties of PPy-Coated Conductive Fabrics for Human Joint Motion Monitoring[36]	Polypyrrole	Tested up to 25%		Doped with 97% Anthraquinone-2-sulfonic acid sodium salt monohydrate; oxidized with 98% iron(III) chloride (FeCl3) hexahydrate	0.67- 3.83 kΩ	
A supramolecular biomimetic skin combining a wide spectrum of mechanical properties and multiple sensory capabilities[37]	Acrylic acid and 3-dimethyl (methacryloyloxy ethyl) ammonium propane sulfonate	10,000%	≤ 5 KPa		$\geq 2 \cdot 10^{-5}$ S/cm	

Table 4.1: A Summary of Soft Electroconductive and/or Pressure-Sensitive Constructs (5/5)

Strain and damage monitoring in SBR nanocomposites under cyclic loading[38]	Styrene-Butadiene Rubber	≥ 300%	1.5 - 12.8 MPa	Carbon black and carbon nanotubes	10^{-2} - 10^{-15} S/cm	
Simple and cost-effective method of highly conductive and elastic carbon nanotube/polydimethylsiloxane composite for wearable electronics[39]	PDMS	25 - 110%	2 - 4 MPa	Carbon nanotubes	2.03 - 5225 Ω /sq	Yes
Enhanced electrical conductivity and mechanical property of SBS/graphene nanocomposite[40]	Styrene-butadiene-styrene		10.5 - 23.8 MPa	Graphene oxide	10^{-12} to 1.64 · 10^{-2} S/m	
Synthesis and characterization of conductive, biodegradable, elastomeric polyurethanes for biomedical applications[41]	Conductive Polyurethane	75 - 728%	3.1 - 17.9 MPa	Doped with camphor-sulfonic acid	$2.7 \cdot 10^{-10}$ - $7.3 \cdot 10^{-5}$ S/cm	Yes
Electronic Properties of Transparent Conductive Films of PEDOT:PSS on Stretchable Substrates[42]	PDMS	30 - 200%		PEDOT:PSS	100 - 550 S/cm	
3D-Stacked Carbon Composites Employing Networked Electrical Intra-Pathways for Direct-Printable, Extremely Stretchable Conductors[43]	Polystyrene–polyisoprene-polystyrene	Assessed up to 300%	2.1 KPa	Ni nano-particles and reduced graphene oxide	2.1 - 6 S/cm	
Highly Sensitive, Stretchable, and Wash-Durable Strain Sensor Based on Ultrathin Conductive Layer@Polyurethane Yarn for Tiny Motion Monitoring[44]	Polyurethane			Carbon black	≤ 6.04 S/cm	
Patterned, highly stretchable and conductive nanofibrous PANI/PVDF strain sensors based on electrospinning and *in situ* polymerization[45]	Polyaniline	22% for recovery of strain; max of 110%		PVDF	Pressure-related conductivity	

Out of these studies, the creation of PEDOT:PSS on PDMS is particularly noteworthy as it lists one of the highest possible conductivites for an electroconductive elastomer. The stretchable, conductive films produced in this paper are intended as transparent, capacitive pressure sensors

for mechanically-compliant optoelectronic devices.[42] Although PDMS is a recognized elastomeric material, Lipomi et al. reports that the films are only reversibly stretchable up to 30% uniaxial strain.[42] Buckling is evident at as low as 10%, with significant cracks seen at 50%.[42] Conductivity was retained until 188%, with the elongation at break point listed at almost 200%.[42] With such deformations occurring, cyclic loading results in an expected increased resistivity respective to increases in strain percentage. However, resistivity only changes by a factor of five after 1000 stretches.[42] Despite usage of an elastomeric base, the electromechanical fatigue of these films seems more similar to a flexible electrode—but as conductivity retained up to 188%, this remains the most conductive electroconductive elastomer we identified.[42]

This chapter focuses on electroconductivity of our construct—not only for the successful formation of an electroconductive elastomer, but for the creation of one appropriate for biological applications. Seven of the studies identified produced electroconductive elastomers tested in biological settings.[10, 13, 24, 30, 34, 39, 41] Six of these studies were intended for *in vitro* or *in vivo* use, such as mesenchymal stem cell osteo-differentiation, human-machine interface systems for neuroprosthetics, and soft tissue regeneration.[10, 30, 34] Within these studies, conductivity ranged from 0.1 S/cm to $2.7 \cdot 10^{-10}$ S/cm.[10, 41]

The work of Chen et al details the creation of electroconductive elastomers that have some of the highest listed elongation at break values (1643%) and potential electroconductivity values (maximum of 0.1 S/cm) of electroconductive elastomers designed for biological applications.[10] Notably, neither the electromechanical properties of these constructs nor electromechanical fatigue properties are listed. While cytotoxicity was assessed, cells were not subjected to electrical stimulation in this study, leaving the construct's electrical capacity in question. Over half of the studies that assessed biocompatibility only confirmed a lack of cytotoxicity and did not explore electrical or mechanical stimulation of cells on the their chosen materials.[30, 39, 41]

In contrast, liquid crystal elastomer nanocomposite constructs reported conductivity between $5 \cdot 10^{-2}$ and $2.5974 \cdot 10^{-4}$ S/cm, elastic moduli ranging between 2.1 and 8.1 kN, and stable cyclic loading even after 5000 cycles.[13] This paper selected samples with a thermomechanical strain capacity of 22.5% and tested neonatal rat ventricular myocytes under a 40 V AC pulsed electrical signal for 72 hours.[13] Samples were coated with gold and collagen, polystyrene and

collagen, and glutaraldehyde and collagen.[13] The latter two sample types produced substantial increases in viability following stimulation; no major difference was seen between unstimulated and stimulated gold-collagen coated samples.[13] While the conductivity of the samples post polystyrene-collagen and glutaraldehyde-collagen is not listed, samples prior to coating had a resistivity of $1.33 \cdot 10^{-3}$.[13]

Other studies listed a conductivity of $1.1628 \cdot 10^{-5}$ S/cm as appropriate for C2C12 myoblast cells and maximum conductivity of $7 \cdot 10^{-4}$ S/cm for MSC osteodifferentiation.[24, 34] This implies that a final conductivity between $1.1628 \cdot 10^{-5}$ S/cm to $1.3333 \cdot 10^{-3}$ S/cm would be suitable for *in vitro* or *in vivo* devices. This is less than a previous publications from our lab, which used $2.8 \cdot 10^{-3}$ to $1.8 \cdot 10^{-2}$ S/cm and $9.1 \cdot 10^{-4}$ and 0.8 S/cm for neural stem cell cultures.[47, 48] Both studies produced flexible, biocompatible electrodes with the aim of producing scaffolds able to sustain currents with magnitudes of 0.1-100 μA. A substrate capable of producing current of up to 100 μA typically requires a minimum conductivity of around $1 \cdot 10^{-4}$ S/cm.

4.2.2 Design and Development of a Novel Electroconductive Elastomer

We have previously (in Chapter 3) discussed the importance of mechanical properties and our work. We chose to restrict ourselves to electroconductive materials which would produce a similar substrates to those found naturally in the body. For the purposes of our work, we identified that our ideal substrate may require a matrix as low as 1 to 20 kPa. This is in line with a range of natural biological substrates, including brain tissue on the lower end of the spectrum, glial cells in the median range, and myofibroblasts on the upper end of the spectrum.[50, 51] Our desire to create an electroconductive elastomer suitable for the somatosensory system meant that keratinocytes, fibroblasts, and neuronal cells, particularly dorsal root ganglions and Schwann cells, would have to be receptive to the electromechanical stimulation producible by our construct. Considering both electrical conductivity and mechanical properties in tandem was essential to the progression of our work as any construct produced needed to electromechanically suitable for use with somatosensory system cells. We were consequently forced to restrict our choice of conductive materials, particularly avoiding filler materials, as our identified mechanical properties were already higher than those of the soft biological substrates identified.

We hypothesized that we could create a customizable electroconductive elastomer, with an easily alterable conductive layer would be the optimal construct for *in vitro*, *in vivo*, and wearable uses. Given our final intentions for this construct and the range of electroconductivities we discovered were possible when creating an electroconductive elastomer (as shown in Table 4.1), we chose to prioritize not only the creation of an electroconductive elastomer, but a versatile, customizable electroconductive elastomer with modifiable conductivity and minimal elongation values of at least 100%. Values reaching at least 200% (as occur in skin) were considered ideal.

At this stage, PEDOT, PPy, and P3HT were of interest to us because of their electroconductive properties. These electroconductive polymers also had highly desirable mechanical properties compared to filler materials, such as carbon black, and had the potential to enhance the conductivity of our solutions. While they can be blended with other polymers, PEDOT and PPy are water-based. Blending involves directly mixing the material in a solvent using techniques such as ultrasonication, then mixing the solution of polymer using the same method. Our selected elastomers are not water-soluble, which resulted in miscibility-related issues when we attempted to create blended solutions using these polymers.

We subsequently attempted approaches similar to Lipomi et al,[42] while simultaneously assessing use of solid electroconductive materials, such as gold and carbon nanotubes. Such materials can be integrated or deposited using electrodeposition, inkjet printing, or other techniques to create layered structures. We continued our work by assessing combinations of electroconductive polymers and materials, determining the conductivity of the overall construct, and validating the electromechanical properties of our chosen materials, as is as detailed in the next section (4.3).

4.3 Results

4.3.1 Conceptual analysis: Creation of Electroconductive Elastomers and Initial Assessments

Given the resources available to us, we had a substantial number of combinations of materials to test. We came up with 78 different combinations of materials to test, focusing on materials that we could be utilized through both blending and deposition methodology (figure shown in the appendix). Our preferred materials were IrOx, gold, and carbon nanoparticles. The percentages listed refer to the proportion of combinations involving a particular material, regardless of whether they were used in 'layer by layer' or 'blending' approaches.

To assess these 78 combinations, Kaneka SIBSTAR^{TM} 062M:102T was dissolved in THF or chloroform at 10% wt concentrations and combined with a variety of electroconductive materials. Approximate resistivity was assessed. This assessment was done as a rough gauge to understand how each electroconductive material impacted the electromechanical properties of the polymer. A variety of different materials were assessed (detailed in the appendix). With the exception of the polymers (in solution) and carbon fibers, which were a blended material with a resistivity in the range of 2K Ω, all tested materials had the lowest detectable resistivity (in the range of 200 Ω). In many cases, the combinations tested produced resistivity that was not detectable with our machinery, meaning that the elastomer's insulating properties had been dominant. We hypothesized encapsulation was occurring, a phenomenon that we were later able to confirm and is detailed in Chapter 5. Further details on the various combinations tested can be found in the appendix.

Electroconductivity and elasticity are often contradictory terms outside of organic systems. While elasticity is easily achieved with Kaneka SIBSTAR^{TM} 062M:102T, addition of enough electroconductive materials into a solution results in a material that is no longer elastic. Examples of this can be shown in Table 4.2, where electroconductive but brittle materials were created using Kaneka Kaneka SIBSTAR^{TM} 062M:102T and IrOx. In situations where Kaneka SIBSTAR^{TM} 062M:102T has a water-based electroconductive material placed atop it, (e.g., iridium in water), the material was so hydrophobic that it repelled the electroconductive solution and caused the formation of micelles. This contributed to the lack of homogeneity we

found in some of our samples. Initially, surfactants in combination with water-based electroconductive materials were assessed. However, after testing with PSS and sodium stearate failed, we moved on to other promising layer-by-layer approaches.

4.3.2 Experimental Creation of Electroconductive Elastomers and Initial Assessments

In contrast to water-soluble coatings, we found that Kaneka SIBSTAR™ 062M:102T was easily coated with gold and platinum nanoparticles via thermal evaporation. Furthermore, we found that following platinum coating, we were able to electrodeposit IrOx onto Kaneka SIBSTAR™ 062M:102T, as shown in Figure 4.1. Electrodeposition allows for material thickness, homogeneity, and coating microstructure to be controlled through the modulation of intensity and potential. The thermally evaporated platinum, which adheres to the polymer during the thermal evaporation process, acts as a protective coating against the hydrophobic nature of the elastomer, creating a soft electrode that IrOx is able to bind to.

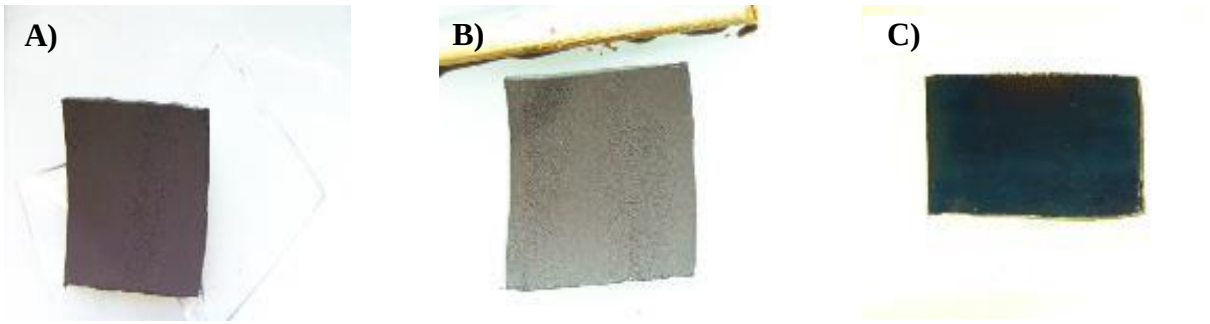

Figure 4.1: Evaluation of the Kaneka SIBSTAR™ + Platinum + IrOx Construct. A) Transparent SIBS prior to treatment (carbon fiber square shown alongside for contrast). B) SIBS following platinum coating through thermal evaporation. C) SIBS and thermally deposited platinum following IrOx electrodeposition. The dark blue tinge is typical.

We chose to explore these results further through use of a platinum paste from the Gwent group. Two types of platinum pastes were assessed: C2050804P9 and C2020322P6. Initially, C2050804P9 was used for our tests as it was readily available to us. However, were able to identify that the cross-linked polymeric platinum paste C2020322P6 was the optimal choice for our construct due to its slightly different properties.

Use of these pastes allowed for more flexibility in the application of the electroconductive material. In particular, heat applied when using pastes could be controlled veryspecifically — a critically influential factor that affects the mechanical properties of the polymers, as detailed

in Chapter 3. The differences between the two platinum paints are listed in Table 4.3 below. Furthermore, we utilized a silver paste provided by Gwent in our initial tests as a proof of concept material. This paste was not biocompatible and was simply used in the process of designing the application process for these materials.

Table 4.3: Gwent Platinum Paints

Paste	Solids Content	Viscosity (Pa.s.)	Resistivity (Ohm/sq)	Curing Temperature (ºC)	Properties
C2050804P9	83-87	14-22	0.59 Ω at 47 µm	80-130	Polymeric platinum
C2020322P6	85.5-86.5	10-15	0.29 Ω at 25 µm	130-180	Crosslinked polymeric platinum

4.3.3 Analysis of Electroconductive Elastomers

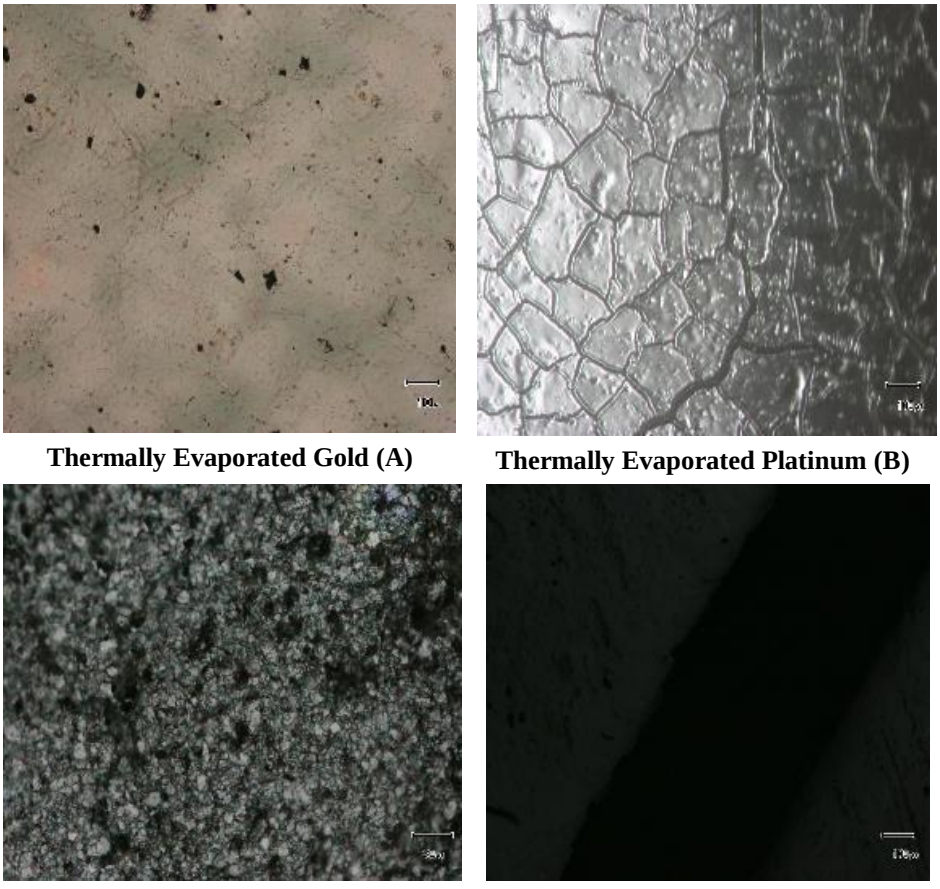

Thermally Evaporated Gold (A) **Thermally Evaporated Platinum (B)**

Silver Paint Atop SIBS (C) **Platinum Paint Atop SIBS (D)**

Figure 4.2: Thermally Evaporated Gold and Platinum and Gwent Silver and Platinum Pastes Atop Kaneka SIBSTAR™ (SIBS)

As we achieved the successful creation of electroconductive elastomers, we proceeded to assess ways to analyse and optimize these results. Confocal microscopy images of platinum, silver, and gold coatings atop Kaneka SIBSTAR™ 062M:102T are shown in Figure 4.2.

As shown, the images are not of particularly good quality as these materials were not transparent. The uneven coatings and textured nature of the thermally evaporated samples is shown in Figure 4.2A and B, particularly in the platinum sample. The Gwent pastes, shown in Figure 4.2C and D, yield a thicker and more even coating. The platinum paste in particular is so dense that imaging through confocal microscopy was impossible. Scanning electron microscopy analysis of silver and platinum paint on Kaneka SIBSTAR™ was also performed. We chose to produce samples, stretch them, then image them for further analysis. Manual stretching was done in a manner that did not perform any material deformation — our intention was merely to understand the impact of mechanical stress on the electroconductive paste.

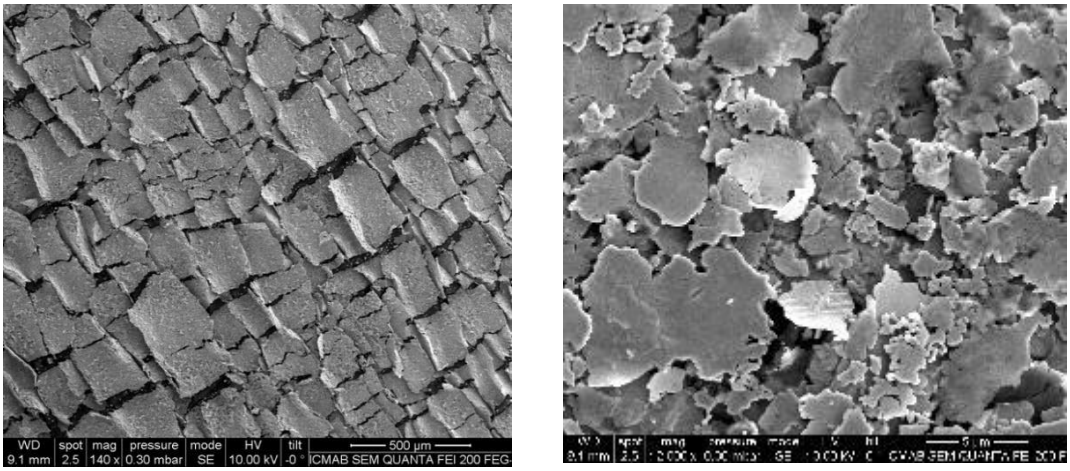

Figure 4.3: SEM of Stretched Silver Paint atop Kaneka SIBS

In our imaging, we were surprised to discover that the morphologies of these paints were dramatically different. Shown in Figure 4.3, the silver paste is flaky, while individual nanoparticles can be seen in the platinum paste in Figure 4.4. The movements of these particles can influence the electromechanical properties of the final construct; while the paint may shift in layers similar to tectonic plates, the nanoparticles cluster and may act in a more flexible manner due to their bonds.

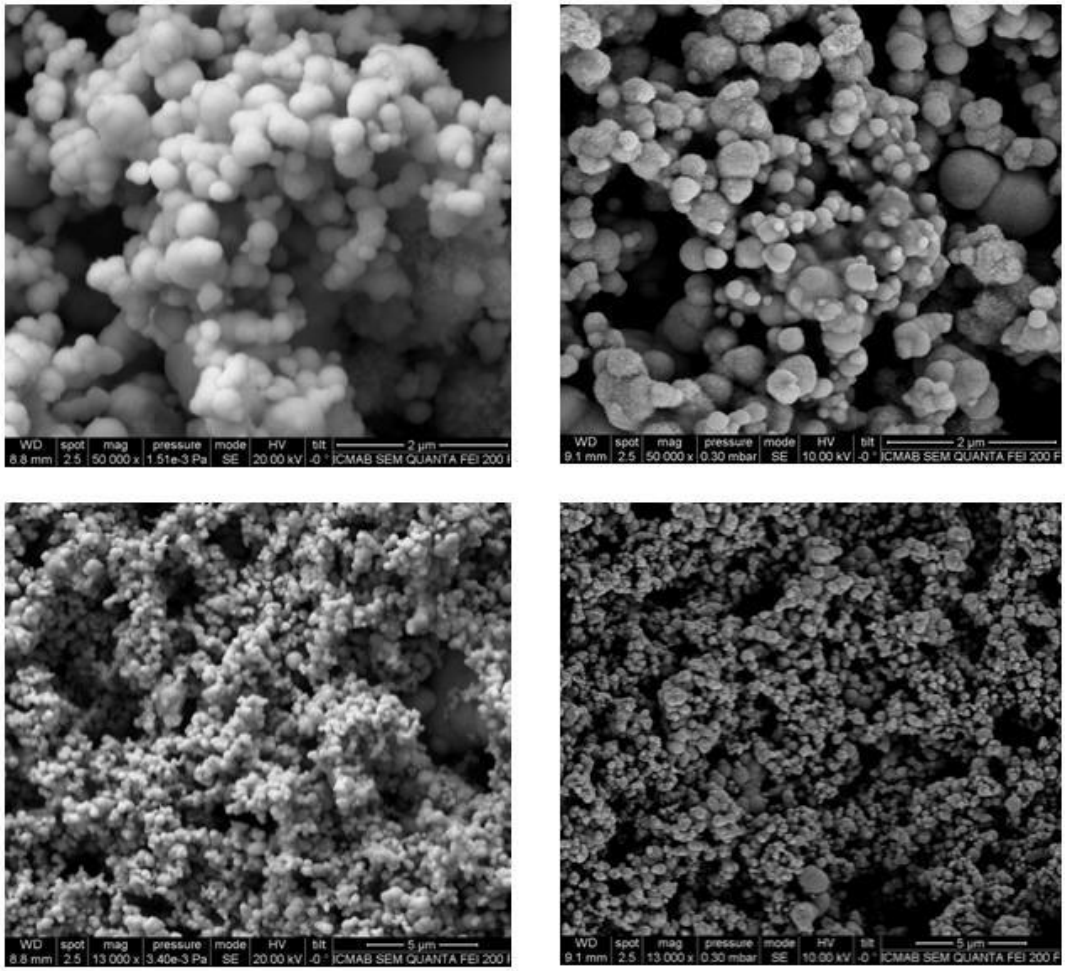

Fig. 4.4: SEM of Platinum Paint atop Kaneka SIBS. Morphological changes of platinum particles following mechanical stress to the elastomer substrate.Unstretched platinum depicted on the left, stretched platinum depicted on the right.

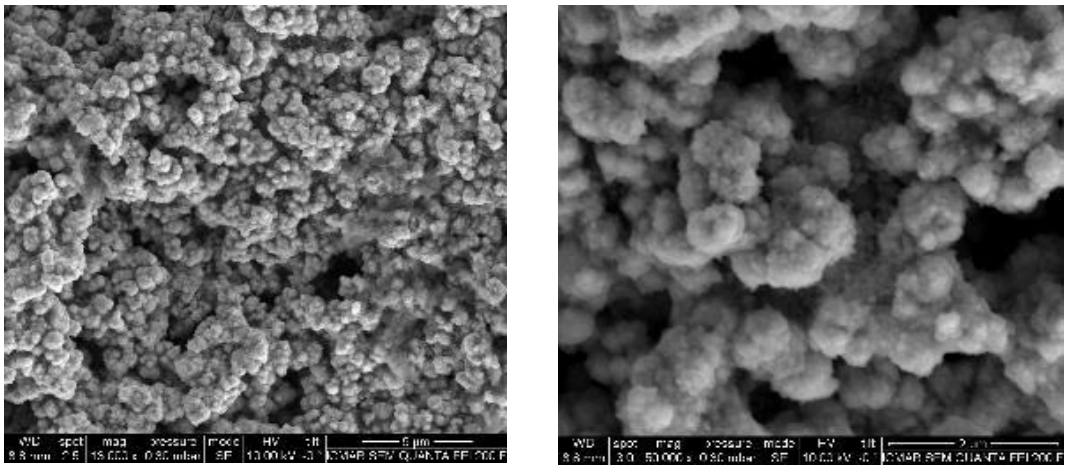

Fig. 4.5: Electrodeposited IrOx and Platinum Paint of Kaneka SIBSTAR™ 062M. Morphological changes of platinum particles following IrOx electrodeposition.

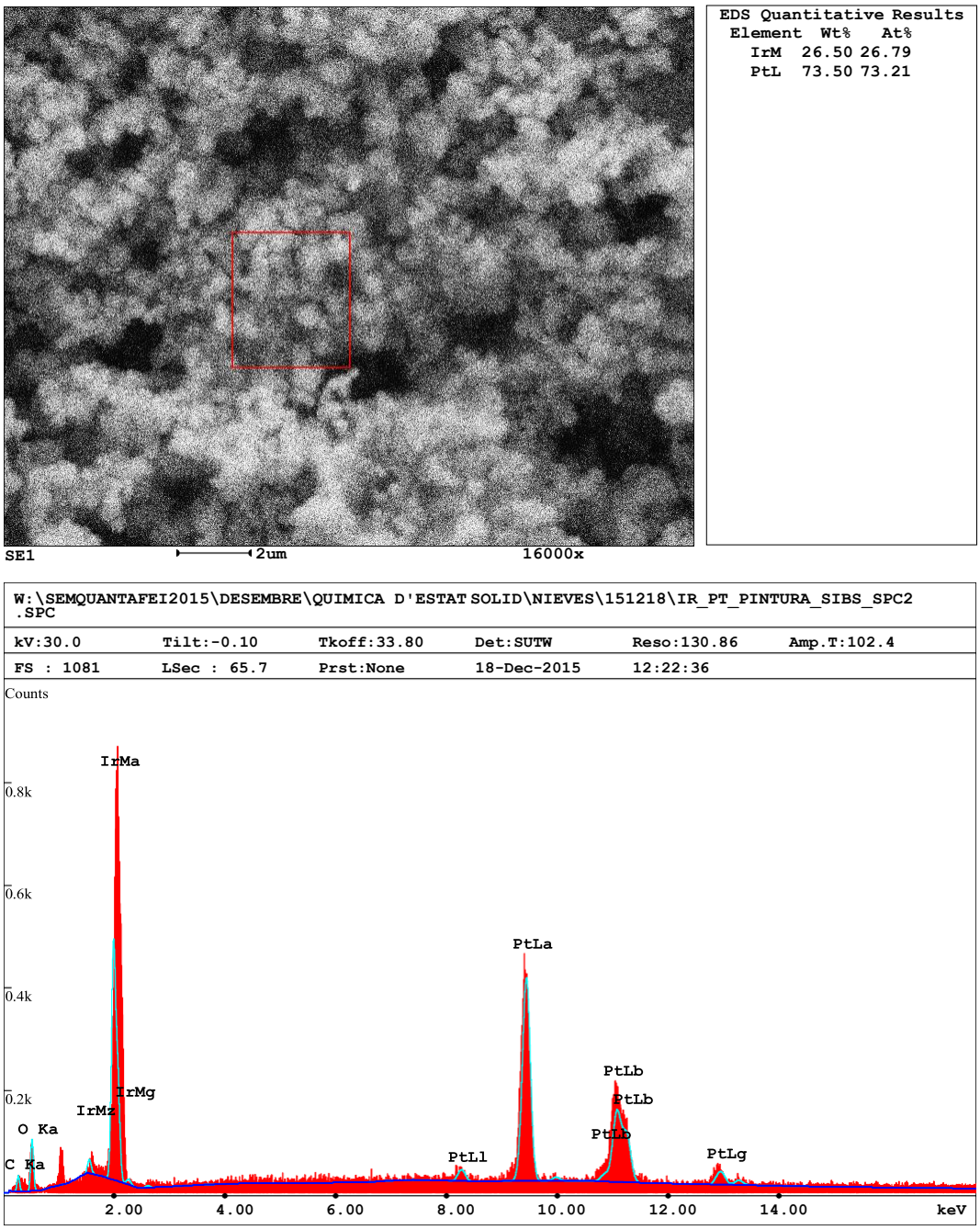

Figure 4.6: EDX Analysis of SIBS, Platinum, and Iridium

We imaged the completed construct of Kaneka SIBSTAR^{TM}, polymeric platinum, and electrodeposited IrOX. As shown in Figure 4.5, the iridium oxide has attached to the platinum. It appears as if the IrOx encapsulates the platinum particles during electrodeposition. We went on to perform energy-dispersive X-ray spectroscopy (EDX) of this sample to confirm IrOx adherence.

As shown in the EDX, the presence of both iridium oxide and platinum is confirmed. The average sample contained approximately 73% polymeric platinum and 26% iridium oxide. Electrodeposition had not previously been performed using polymeric platinum paste. Furthermore, to our knowledge, this method of creating an electroconductive elastomer had not been attempted previously. We believe that this method could be used to create a variety of soft electrodes for biomedical purposes. Additionally, this magnifies the customizable nature of the construct. IrOx and other materials can be added in a controlled fashion, utilizing a set amount of cycles in the electrodeposition process to achieve the desired percentage for the electroconductive elastomer. This minimizes the presence of the base electroconductive material, as well, which can influence cell culture and the success of implanted devices.

Given the ease of using IrOx and its established uses in other biomedical devices, we wished to see if it might be possible to incorporate this substrate into our construct in an alternative way. Iridium oxide solutions, prepared as detailed in Chapter 2 were mixed with previously prepared solutions of PVP at ratios of 1:2 to 1:5. Iridium oxide nanofibers have been previously prepared by Kim et al (2014), but these nanofibers are produced from $IrCl_3$ hydrate with PVP and require a heating at 900^{o}C for two hours.[76] This protocol produced IrOx nanofibers blended with PVP in a way that did not require any such additional steps. The resulting electrospun fibers can be seen in Figure 4.7. If we desired the removal of PVP to produce pure IrOx, we were able to heat fibers for an hour at 500^{o}C.

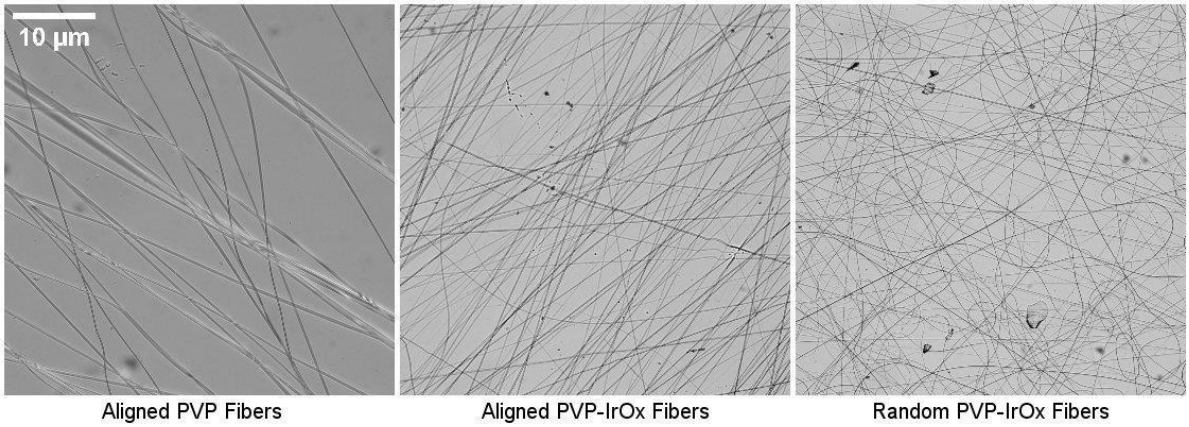

Figure 4.7: Creation of PVP-IrOx Nanofibers. Showing aligned PVP fibers on the far left as controls, aligned PVP-IrOx fibers in the center, and random PVP-IrOx fibers on the far right.

We did not explore the creation of IrOx fibers in further detail. However, we consider this to be a good proof of concept for the creation of a 3D, nanofibrous electroconductive elastomer. Such a construct would ideally utilize electrospun Kraton D1152ES (SBS).

We chose to focus on the use of polymeric platinum for use with our planar polymers. We were able to replicate our previous results using Kraton D1161PT (SIS) and Kraton D1152ES (SBS) without issue. Given the results of mechanical testing shown in Chapter 3, we elected to continue on using planar Kraton D1152ES as our primary elastomer.

4.4 Creation of the Complete Construct

Creation of an electroconductive elastomer was challenging, primarily due to our determination to use an elastomer. The elastomeric properties of our selected polymer constantly caused failure of electroconductive materials, nullifying their properties. Initially, this presented itself as a conflict of interest to our construct — electroconductivity of the construct reduced elastomeric properties, or the insulating properties of the elastomer impeded conductivity. However, we were eventually able to bypass these issues. We assessed the resistivity of these combinations briefly using the two point probe method, then performed a more thorough assessment of conductivity through electrical impedance spectroscopy, which is detailed in section 4.5.

In order to continue validating our results, we needed to ascertain that the electroconductive properties of the construct would neither impede the elastic properties of our elastomer, nor fail immediately when stretched, given that metals do not typically elongate like polymers. The stress and strain and fatigue properties of our materials have been detailed in full in the previous chapter. In sections 4.6 and 4.7, we go on to detail the electromechanical properties of our construct. Finally, section 4.8 details the piezoelectric nature of our construct. The information detailed in this section summarizes the variety of ways a construct such as ours can be made; namely, any additives or specific methodology required. It is important to note that the construct designed is fully customizable, as we go on to prove in further sections. Notably, each polymeric and metal component has to be treated in a different way, and treatments influence mechanical and piezoelectric properties. The different additives or treatments each component requires are detailed in Table 4.3.

As shown in Table 4.3, nearly all components of the construct require heating at a different temperature. As shown in Chapter 3, heat is an important influential factor on the mechanical properties of a polymer. However, regardless of whether processing is occurring through thermal evaporation or heating to optimize cross-linking of the polymer, temperature is essential. As such, any potential electroconductive elastomer created from this table can have variable properties. Most notable is electrospun Kraton D1152, which cannot withstand dehydration and consequently cannot be heat-treated the same way a planar sample can.

Table 4.3: Additives and Treatments Required for Construct Components

Component		Additive	Treatment	Reason
Elastomer (i.e., Kaneka SIBSTAR™ or Kraton D1152ES (SBS))	Planar Cast	None or Isoprene (for increased elasticity)	Heated at 30-40ºC to promote solvent evaporation. Cooled at room temperature for 24h	Curing yields even sheets regardless of thickness and minimizes solvent retention that could affect biocompatibility
	Electrospun	Iron (III) p-toluene-sulfonate	Requires mixing in solvent for 12-24 hours, then further mixing with polymer for homogeneity	Iron (III) p-toluenesulfonate increases electroconductivity of solution, allowing for electrospinning
Metal (i.e., Silver, Gold, or Platinum)	Painted		Curing at 80ºC and/or cross-linking at minimum temperature of 130ºC	Curing allows for paint to dry; cross-linking allows for paint to become biocompatible
	Thermally Evaporated		Thermal evaporation process	Alternative to polymeric pastes
Iridium Oxide	Electrodeposited	None	Solution is prepared and electrodeposited	Promotes controlled adhesion of IrOx
	Dehydration	None	Solution is prepared and combined with metal paste; heated alongside metal paste until evaporated	Alternative to electrodeposition
P(VDF-TrFE)	Planar Cast	None	None, or up to 2 hours of annealing at 80-125ºC	Achievement of optimal ferroelectric state
	Electrospun	None	None, or up to 2 hours of annealing at 80-125ºC	Achievement of optimal ferroelectric state

Creation of an electroconductive elastomer is certainly possible, as any metal paste can air-dry quickly in ambient temperature, but lack of appropriate curing and cross-linking can affect biocompatibility. Equally, P(VDF-TrFE) can have different processing techniques simply based on the manufacturer's treatment process. A secondary annealing process at high temperature would undoubtedly affect any elastomer.

Despite the range of ways a piezoelectric, electroconductive elastomer can be made, we chose to primarily focus on the combination of Kraton D1152, polymeric platinum, and electrospun P(VDF-TrFE). In brief, we created planar sheets of Kraton D1152, applied polymeric platinum paint to the substrate, and adhered electrospun P(VDF-TrFE) fibers using the paint as an electroconductive glue. In order to cross-link the polymeric platinum we heated these constructs to a minimum temperature of 130ºC. The complete methodology for this construct's creation will be summarized in the conclusion of this chapter.

4.5 Analysis of Electroconductive Elastomer and Full Construct

The four point probe method is an established technique for establishing values of conductivity. Elastomers are known insulators. Our first validation was of the insulating properties of the elastomers Kraton D1152 and Kraton D1152 blended with 10% polyisoprene, and P(VDF-TrFE). As expected, these three polymers provided us with negative conductivity values, confirming their resistance. In P(VDF-TrFE), we noticed some outliers on both two-point and four-point probe tests that were conductive. In approximately one tenth of samples, P(VDF-TrFE) samples were conductive. These outliers had conductivity values of 1 S/cm. However, in the majority of cases, conductivity values were negative values (averaging at $0.8x10^{-1}$ S/cm), which is typical of resistive materials. In the literature, conductivity of P(VDF-TrFE) films varies substantially, ranging from $9.5x10^{-5}$ to 10^{-14}. These values typically vary substantially based on the thickness of films produced; thinner films and electrospun mats of P(VDF-TrFE) typically have less resistivity.[71, 73, 74] Our electrospun P(VDF-TrFE) mats had an average thickness of 40 μm.

In Table 4.4, we show the conductivity values of Kraton D1152 coated with polymeric platinum, as well as Kraton D1152 blended with 10% polyisoprene. We wanted to understand the effects of polyisoprene, the primary chemical constituent of natural rubber, from a conductivity perspective. As shown in Table 4.4, the effects were substantial. Conductivity fell from 6 S/cm in Kraton D1152 and platinum samples to 0.6 S/cm in Kraton D1152-polyisoprene and platinum samples. We also wanted to assess the effects of heat on these electroconductive elastomers. As shown, the effect of heating at temperatures as high as 150ºC was also substantial. Kraton D1152 and platinum dropped to a conductivity of 0.1 S/cm, while Kraton

D1152-polyisorpene and platinum fell to 0.3 S/cm. While we knew of the importance of heat on the mechanical properties of P(VDF-TrFE), we were unaware of the impact heat would have on the electroconductive behaviour of our materials.

As such, our final electroconductive elastomer has a conductivity range of 0.1 to 6 S/cm. Conductivity of the previously discussed electroconductive elastomers (Table 4.1) that were used in biological settings ranged from 0.1 S/cm to $2.7 \cdot 10^{-10}$ S/cm.[10, 41] Our lowest results are in line with Chen et al.'s previously discussed PEG2k-AT6-TMP construct, which had an upper range of 0.1 S/cm and was also designed with biological applications in mind.[10] From a conductivity perspective alone, our highest conductivity is similar to polyurethane-carbon black with a listed conductivity of 6.04 S/cm.[44] It is also similar to a very soft polystyrene-polyisoprene-polystyrene elastomer filled with nickel nanoparticles and reduced graphene oxide (maximum conductivity of 2.1 S/cm) and a poly (styrene-β-ethylene-ran-butylene-β-styrene) elastomer containing graphene nanoplatlets and carbon nanotubes (maximum conductivity of 2.2 S/cm). [19, 43] Notably, our chosen alkene-styrene polymer has among the highest conductivity listed. It is notably higher than all similar alkene-styrene blends The maximum conductivity of similar polymers (listed as: polystyrene block copolymers, polyisoprene, styrene-butadiene-styrene, styrene-butadiene rubber, poly(styrene-cobutadiene), poly (styrene-β-ethylene-ran-butylene-β-styrene), and even other Kraton products (i.e., G1645, styrene-β-ethylbutylene-β-styrene)) was 2.2 S/cm.

Finally, we chose to assess the full construct. Given P(VDF-TrFE)'s established behaviour as an insulator, and that this technique assesses the surface conductivity, we were expecting samples to be resistive. As shown in Table 4.4, the conductivity of the complete construct sample was indeed less conductive and in the semi-conducting region. Despite the substantial reduction in conductivity, these values are still in line with those used for MSC osteodifferentiation.[34] They are also in line with the conductivity of flexible materials used by our own team for neural stem cells culture. [47, 48] However, it's important to note that our results and these tests only show surface conductivity. The electrical impedance spectroscopy shown later on in this chapter is capable of determining the ionic conduction mechanism (by creating an Arrhenius plot showing conductivity vs. 1/T).

Table 4.4: Conductivity of Electroconductive Elastomers and Full Construct

Sample	Conductivity (S/cm)	Standard Deviation
D1152 coated with polymeric platinum	6	2
D1152 and 10%wt polyisoprene coated with polymeric platinum	0.6	0.3
D1152 coated with polymeric platinum and heated to 150ºC	0.1	$2x10^{-2}$
D1152 and 10%wt polyisoprene coated with polymeric platinum and heated to 150ºC	0.3	$1x10^{-1}$
D1152 coated with polymeric platinum and P(VDF-TrFE)	6×10^{-4}	

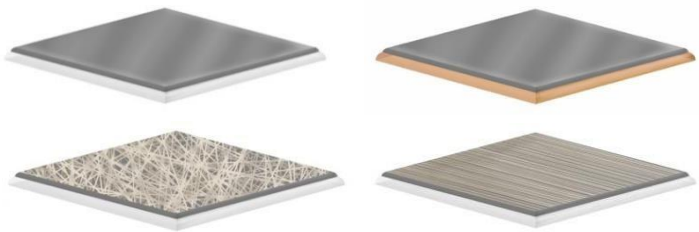

Figure 4.8: Schematic of the Assessed Conductive Constructs. From left to right, Kraton D1152ES (SBS) coated with polymeric platinum (left), Kraton D1152ES (SBS) blended with 10% polyisoprene and coated with polymeric platinum (center), and Kraton D1152ES (SBS) coated with polymeric platinum and layered with P(VDF-TrFE) nanofibers.

However, these properties are completely modifiable based on the thickness of the P(VDF-TrFE) layer. This layer is attached when the polymeric platinum is still wet; therefore, its purpose is two-fold: it acts as an electroconductive substrate, and as an electroconductive adhesive. In thin nanofibrous layers, the P(VDF-TrFE) is completely covered by the platinum, essentially yielding a layer of platinum-coated P(VDF-TrFE) nanofibers affixed to the elastomer. In thicker nanofibrous layers, the P(VDF-TrFE) can act as an insulator, resulting in no conductivity whatsoever. These types of constructs can be used to create elastic, piezoelectric electrodes, which are detailed later on in this chapter. Both are relevant to our purposes and highlight the customizable nature of our construct. Given the complexity and versatility of this construct, we elected to continue our studies of these materials through electrochemical impedance spectroscopy.

Electrochemical impedance spectroscopy (EIS), also known as the AC impedance method, is a non-invasive technique that is used in electrochemical systems analysis. This technique works by applying a stimulus (i.e., a sinusoidal signal) to a material, construct, or cell. This, in turn, provides data used for the creation of equivalent circuit models, which can enable design or electrode functionality optimization. In our own work, EIS can enable further understandings of our soft electrode and soft electrode construct by allowing us to de-couple the various components of our construct.

Electrochemical impedance spectroscopy (EIS) studies were specifically performed in order to understand the resistance and capacitance changes as we created the full construct. Because this construct was designed to function in biological environments (i.e., as an implanted device or in cell culture), we performed EIS studies using samples that had been kept hydrated in PBS and a second set of test utilizing tests performed in dry environments. Hydrated samples were maintained in PBS throughout the course of testing to imitate physiological environments, while dry samples never came in contact with any liquid during the testing process. We were particularly interested in utilizing EIS as each layer of our construct is unique—one hydrophobic, planar elastomer; a second made of textured, polymeric, electroconductive metal; and a third of porous, nanofibrous, piezoelectric fibers. Consequently, we measured the components of the construct as they were built, assessing the elastomer base, platinum and elastomer, and full construct of elastomer, platinum, and piezoelectric.

Figures 4.11 and 4.12 show the Bode and Nyquist plots for the samples kept in hydrated environments prior to testing and assessed in aqueous environments. Impedance was measured for frequencies ranging from 0.1-10000 Hz for samples in wet environments. In each graph, Kraton D1152 is shown in yellow, Kraton D1152 coated with polymeric platinum is shown in green, and Kraton D1152 coated with polymeric platinum and P(VDF-TrFE) is shown in orange. The electric equivalent circuits (EECs) for each sample are shown in Figure 4.11. We utilized the elastomer, Kraton D1152, to show our resistive control, then connected other elastomeric samples with the conductive platinum or platinum-piezoelectric P(VDF-TrFE). The components used to create each circuit are displayed in Table 4.3, and final resistivity and conductivity shown in Table 4.4.

Bode plots recorded for the aforementioned constructs analysed in PBS (pH 7.4) are presented in Figure 4.10. Figure 4.10A shows the logarithm of impedance versus frequency. The logarithm of impedance is much higher for Kraton D1152 compared to any of the platinum-coated alternatives. In the latter, the log of impedance decreases significantly. Nevertheless, when P(VDF-TrFE) fibers are added, increases at lower frequencies occur due to the gain in resistance and capacitance. This shows that overall, the constructs have a frequency dependent response. Figure 4.10B shows that it is possible to observe changes in phase within the different systems. Again, for the two firsts constructs, only one shoulder appears at frequencies below 10 Hz. This corresponds with the membrane resistance in parallel to the constant phase element while the signal becomes more complex with the addition of P(VDF-TrFE). Here, we can observe two shoulders which represent two time constants (τ) in the Bode plot.

Figure 4.11, which displays the Nyquist spectra, shows that all three of our materials form semicircles. Figure 4.11A shows that these semicircles differ substantially in size, with the largest belonging to the most insulating material, Kraton D1152. Kraton D1152 coated with platinum, which has an exposed electroconductive surface, has the smallest semicircle, while the full construct, which has customizable electroconductive/insulating properties, is shown as the median. Figure 4.11A displays these semicircles in more detail, focusing on the highest frequency zone. This figure shows an initial semicircle that corresponds to R1 (R_s), R2 (R_p), and Y0, the first CPE. Generally, the R_S parameter should be not affected by changes occurring on the electrode surface because this variable represents electrolyte resistance from the PBS solution. R_p and Y_0 are related to material resistance and capacitance, respectively. However, since the phase angle is lower than 90º, the capacitance is modelled as a constant phase element (CPE). As more layers are added to the construct, complexity of the obtained signal increases as does fitting the circuit.

A consequence of adding more components to a construct is that new interfaces with multiple interactions originate. The Nyquist plot of the full construct, Kraton D1152 coated with polymeric platinum and P(VDF-TrFE) fibers, presents a second semicircle. This is represented on the equivalent electrical circuit as R3 (R_p) and as a second CPE, which is in line with its more complex circuit. The contributing nature of each element is shown in Table 4.3.

The circuits shown in Figure 4.11 and proposed EEC shown in Table 4.5 were confirmed through triplicates of each sample. Each circuit's data was validated by selecting experimental data with low error, which can be seen in the appendix. Samples with error higher than 30% were removed and are not shown. This is notable as the percentage error associated with each circuit element should typically not be higher than 10%. The maximum error for the individual elastomer and electroconductive elastomer components were between 5.3% and 10.9%; however, the piezoelectric samples contained single components with high error values between 26-30%. In both cases, this was caused by the second constant phase element (CPE) component which is related to presence of the piezoelectric. The Chi Square values from these fitted circuits are also high — the ideal reported values should be < 0.05. The heterogeneity of the electrode surface (i.e. roughness of the platinum and porosity of the piezoelectric fibers) may also influence these value through non-uniform diffusion across its interface. As expected, the resistivity is reduced substantially by the platinum and increased again by P(VDF-TrFE).

A

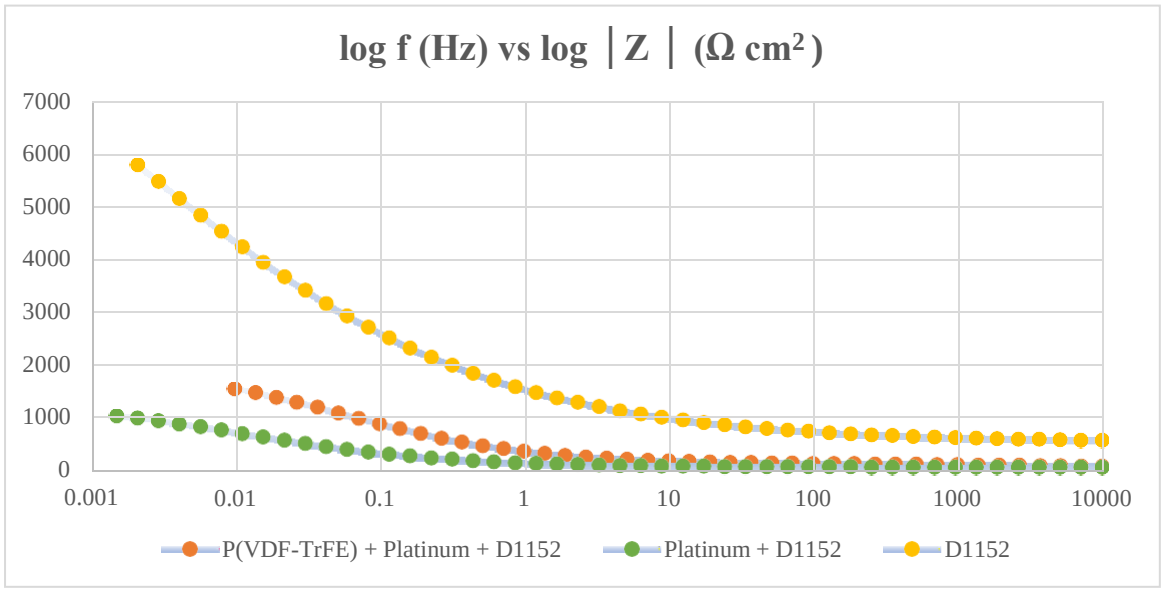

B

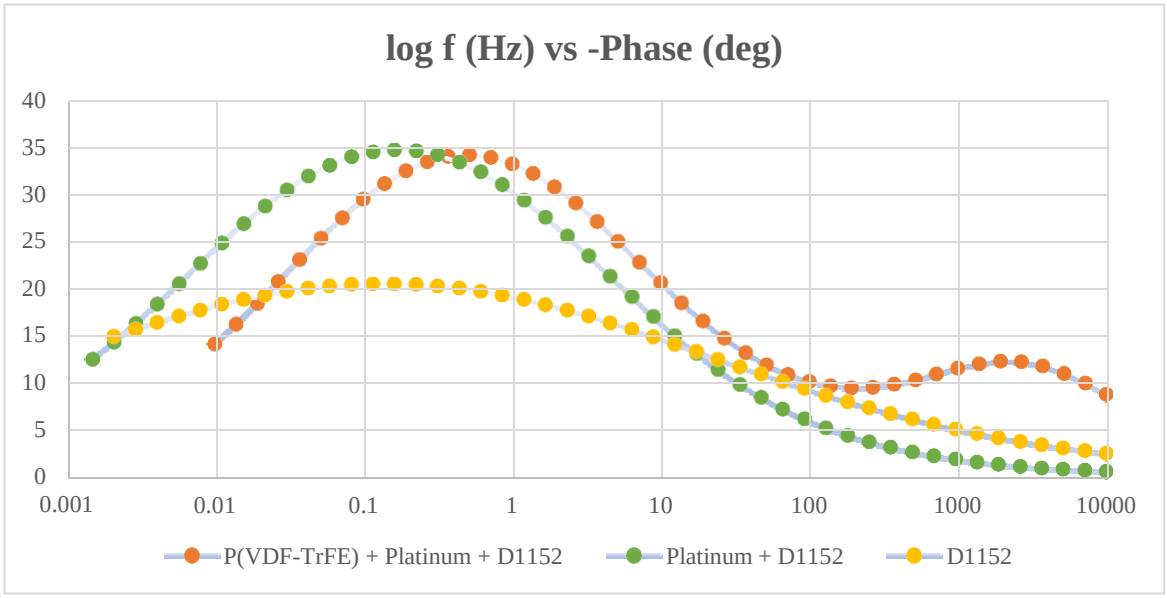

Figure 4.9: Bode Plots of the Full Construct, Electroconductive Elastomer, and Elastomer Base Following Incubation in PBS

A

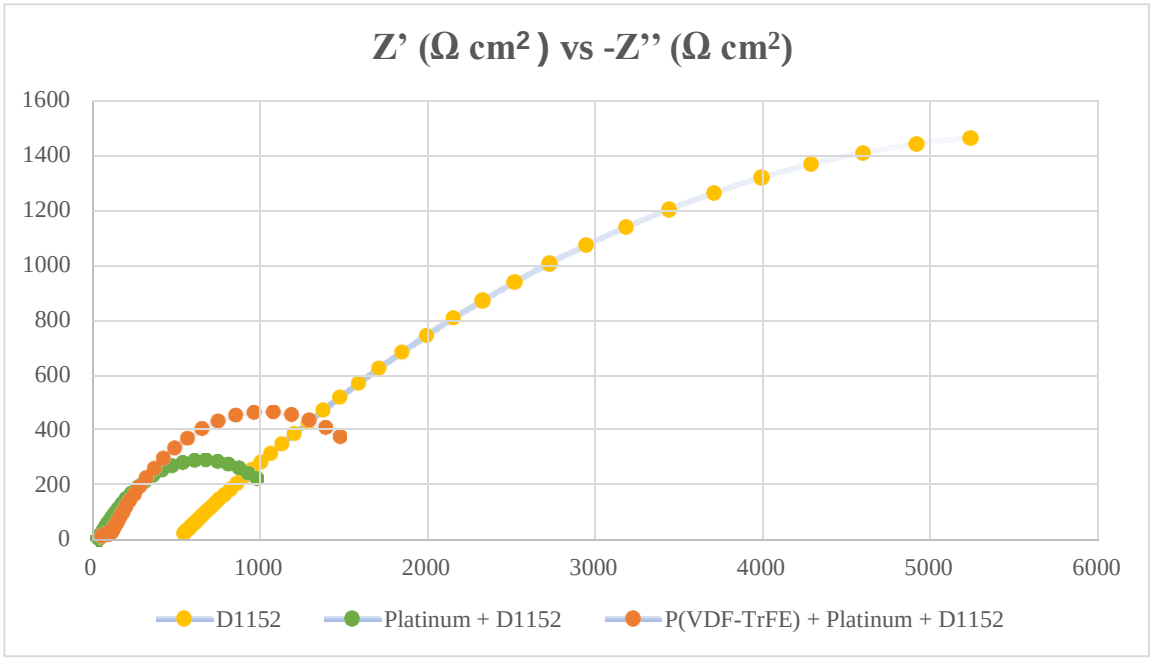

B

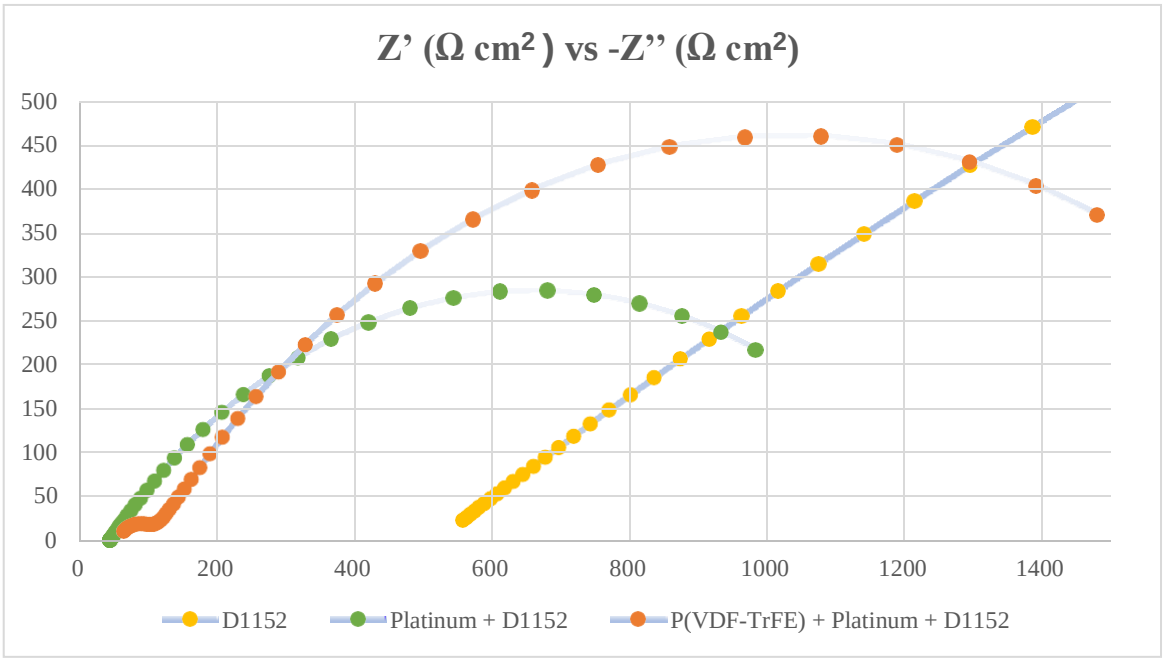

Figure 4.10: Nyquist plots of the Full Construct, Electroconductive Elastomer, and Elastomer Base Following Incubation in PBS

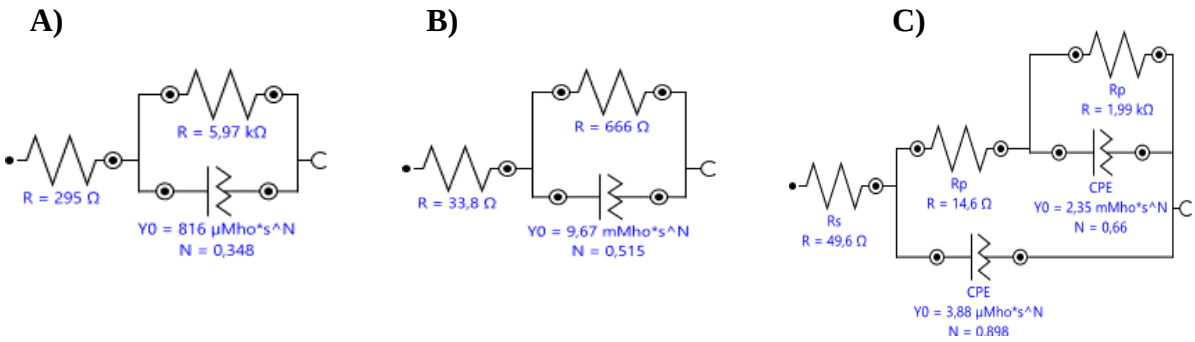

Figure 4.11: Fitted Circuits Following Incubation in PBS. A) Fitted circuits for the elastomer base Kraton D1152ES (SBS), B) Electroconductive elastomer Kraton D1152ES (SBS) coated with polymeric platinum (Gwent), and C) The Full construct.

Table 4.5: Circuit Components Following Incubation in PBS

	R1 (R_s) ($\Omega \cdot cm^2$)	**R2 (R_P) ($\Omega \cdot cm^2$)**	**Y0 (CPE) ($F\ cm^{-2}\ s^{n-1}$)**	***n***	**R_P ($\Omega \cdot cm^2$)**	**CPE ($F\ cm^{-2}\ s^{n-1}$)**	***n***	**X^2**	**Max. % Error**
Kraton D1152	368.21	1884.1	0.0012	0.3708				0.056	5.946
Kraton D1152 Platinum	34	665.72	0.0097	0.5152				0.0999	5.384
Kraton D1152 Platinum P(VDF-TrFE)	24	68	0.001	0.4085	1471.5	0.0011	0.655	0.0366	26.316

The ultimate resistivity and conductivity values are shown in Table 4.6. Membrane conductivity (σ) was calculated using the following equation:

$$\sigma = \frac{L}{R_M A}$$

Equation 4.1: Membrane Conductivity

Here, σ is equivalent of proton conductivity (S/cm), L refers to the thickness of the membrane, A is equivalent to the area, and R_M refers to the resistance of each component.

Table 4.6: Resistances (R) and Conductivity (σ) for the Elastomer, Electroconductive Elastomer, and Full Construct Following Incubation in PBS

Polymer	Thickness (μm)	EEC	R1 (Ω cm^2)	σ1 (S/cm)	R2 (Ω cm^2)	σ2 (S/cm)	R3 (Ω cm^2)	σ3 (S/cm)
D1152	859	[R(RQ)]	523	1.6	10568	0.1		
D1152 Platinum	923	[R(RQ)]	59	16	2337	0.4		
D1152 Platinum P(VDF-TrFE)	939	[R([R(RQ)]Q)]	43	22	121	8	2605	0.4

Ultimately, the elastomer and electroconductive elastomer produced good fitted circuits, but the high error in the results from the full construct called our final results into question. As such, we reattempted the experiments without the influence of the hydrated environment in the hopes it would reduce error. Figures 4.12 and 4.13 show the Bode and Nyquist plots for the samples produced without processing in hydrated environments. These samples did not come into contact with hydrated environments; they were neither incubated nor assessed in PBS or other solutions. In each graph, Kraton D1152 is shown in yellow, Kraton D1152 coated with polymeric platinum is shown in green, and Kraton D1152 coated with polymeric platinum and P(VDF-TrFE) is shown in orange. Impedance was measured for frequencies ranging from 0.1 to 10,000 Hz for samples kept in dry environments. Bode plots recorded for the aforementioned constructs analysed in dry environments are presented in Figure 4.12. Figure 4.12A shows the logarithm of impedance versus frequency. As in Figure 4.10A, the logarithm of impedance is much higher for Kraton D1152 compared to any of the platinum-coated alternatives, and the log of impedance in platinum-coated samples decreases. However, the addition of P(VDF-

TrFE) fibers does not produce the same results, and the same frequency-dependent response cannot be seen. Figure 4.13B echoes this disparity in results.

In Figure 4.13A, the influence of the dry environment becomes clear. Despite the change in frequencies and longer duration of the experiments, there is no semicircle formation, unlike in Figure 4.10. However, if curves were to form eventually, the trend would be similar to that of Figure 4.10: Kraton D1152 is the most insulating material, followed by the full construct, and then the electroconductive elastomer. Similarly, in Figure 4.13B, we can see the formation of a second curve, as we saw in Figure 4.10B. We created an electric equivalent circuit for the full construct analysed in a dry environment, as we had previously. This is shown in Figure 4.15. While the circuit itself is similar, we found that the error for this circuit (in general, but particularly the piezoelectric component) was higher than that of the hydrated samples and therefore less useful to us. Consequently, the full range of data from these samples is not detailed as lack of hydration exacerbates our issues.

A

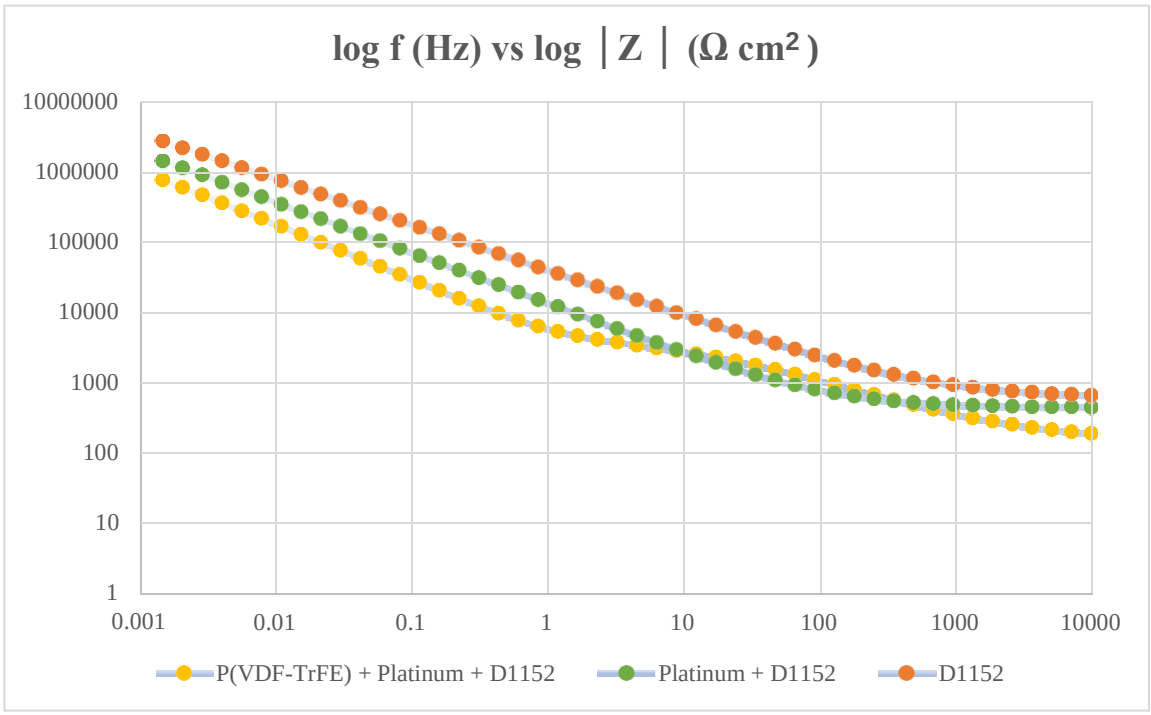

B

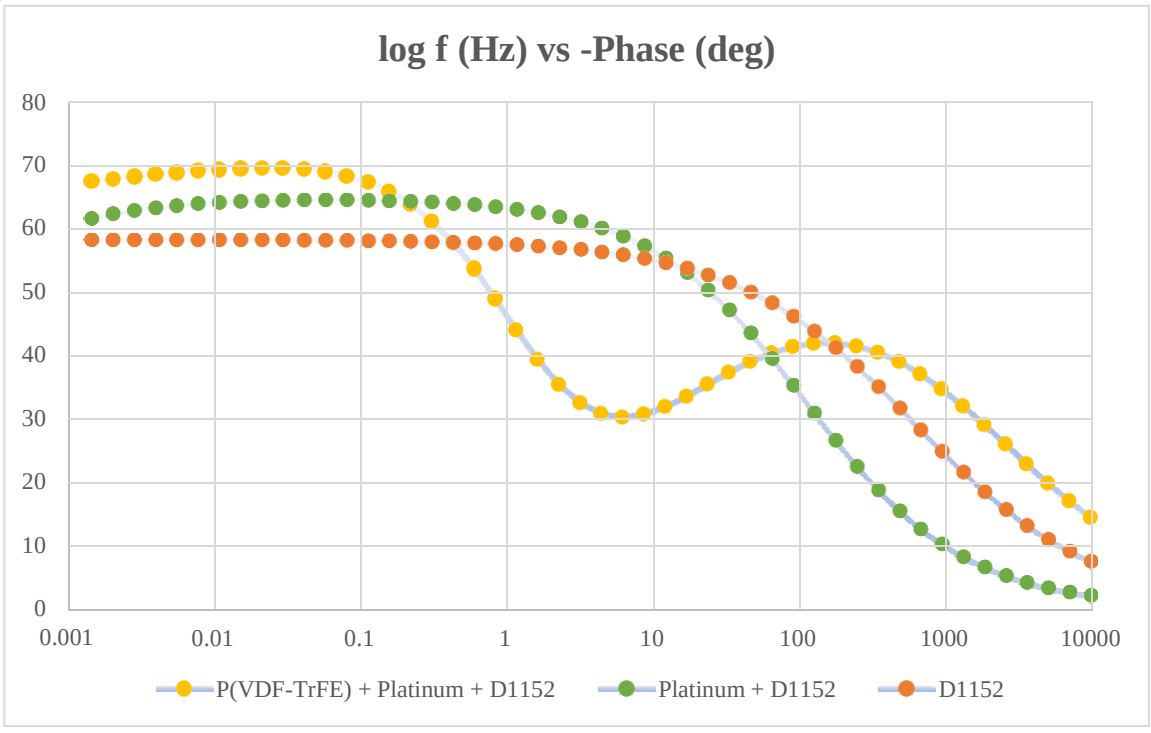

Figure 4.12: Bode plots of the Full Construct, Electroconductive Elastomer, and Elastomer Base without Incubation in PBS

A

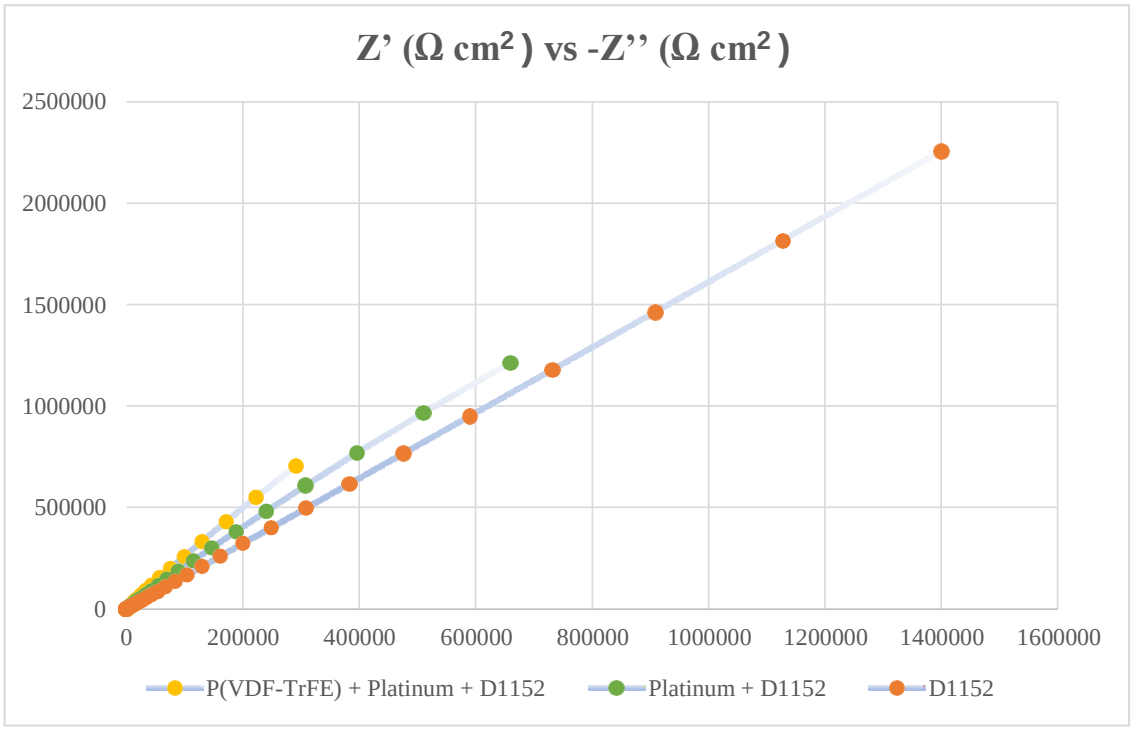

B

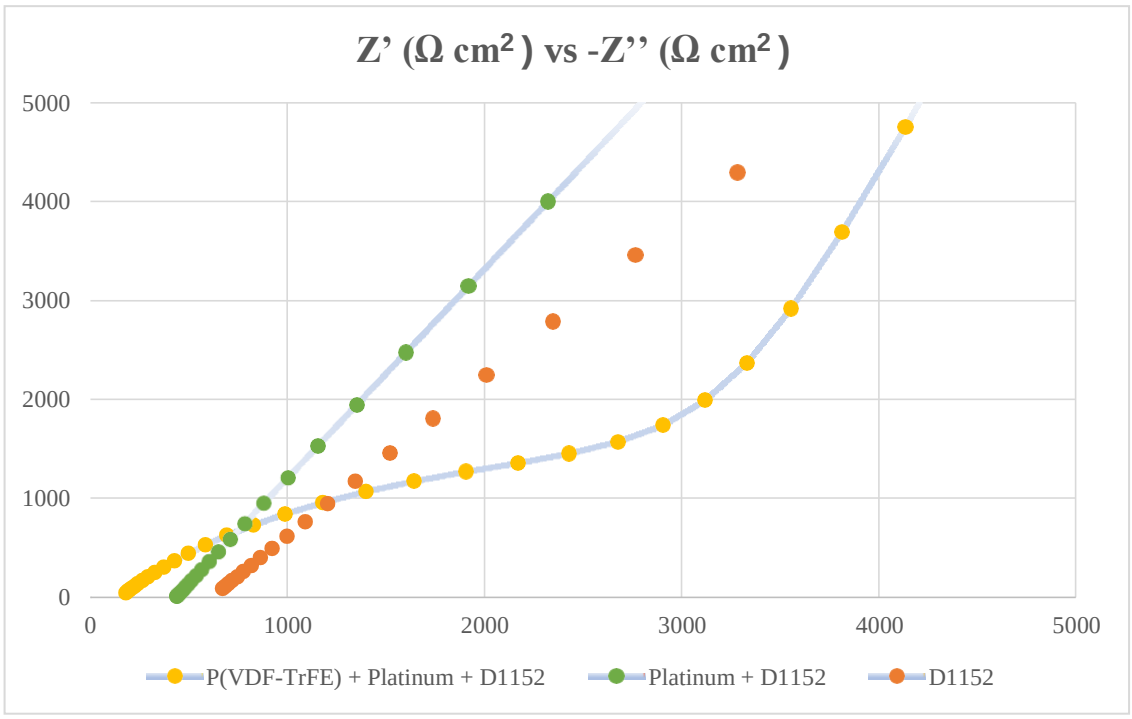

Figure 4.13: Nyquist plots of the Full Construct, Electroconductive Elastomer, and Elastomer Base without Incubation in PBS

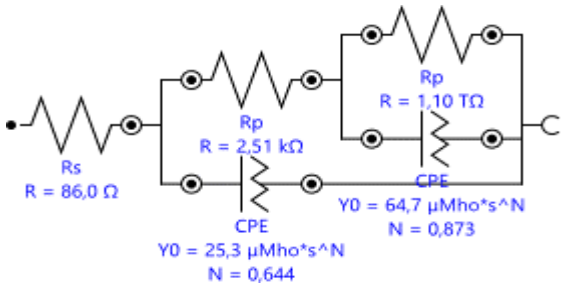

Figure 4.14 Fitted Circuit for the Full Construct without Incubation in PBS

4.6: Electromechanical Assays of the Construct

Having confirmed the conductivity of our electroconductive elastomer, our next priority was confirming that the mechanical properties of the construct had not been excessively negatively affected. Stress-strain and fatigue experiments were performed to assess both Kraton D1152ES (SBS) with polymeric platinum and Kraton D1152ES (SBS) with 10%wt polyisoprene and polymeric platinum. As the majority of the results shown in Figure 4.15 were shown in Chapter 3, they will not be elaborated on excessively.

In the previous chapter, we established heat treatment altered the mechanical properties of the polymers. Notably, when these experiments were repeated with platinum-coated samples, all samples involving platinum had been heat treated. In heat-treated samples without platinum, the failure rate occurs much more rapidly. This is particularly true for samples exposed to high temperatures compared to samples heated to low temperatures (80^{o}C or less), though not room-temperature cured Kraton D1152ES (SBS).

In Figure 4.15, we can see that heating between 37-80^{o}C produces the most ideal stress-strain curves for our work. Kraton D1152 (shown in red) heated to 37^{o}C fails roughly at the machine's maximum: 250%. However, no failure point could be seen for Kraton D1152 heated to 80^{o}C. Kraton D1152 heated to 150 ^{o}C fails at approximately 100% strain. In stark contrast, Kraton D1152 and polymeric platinum (shown in blue), heated to at least 130 ^{o}C but no more than 150 ^{o}C, fails at over 200% strain when undergoing nearly double the stress. The only questionable aspect was slippage of these samples, as can be seen by the deformation markings on the stress-strain curve. These samples were not experiencing fatigue or breaking; instead they were elongating to an extent that the machine's clamps were unable to hold them.

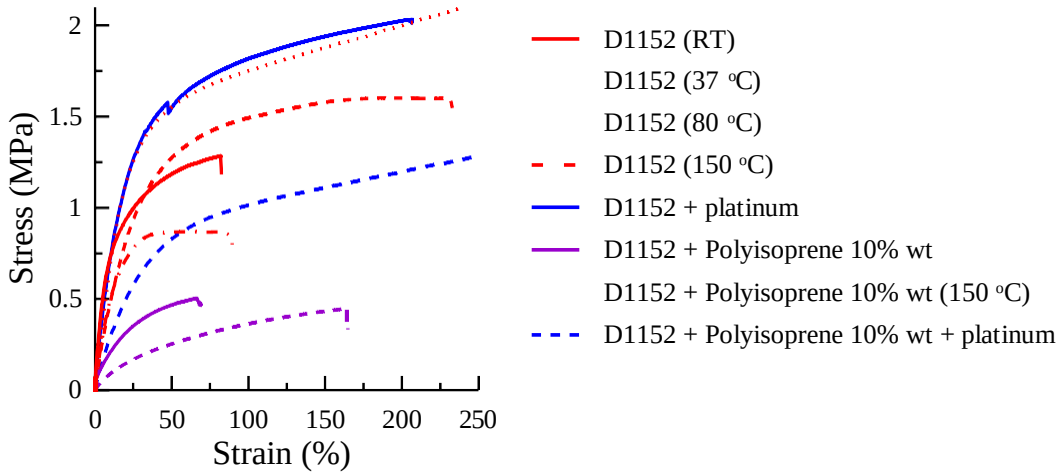

Figure 4.15: Stress-Strain Curves for Kraton D1152 and Kraton D1152-Polyisoprene With and Without Heat Treatments, and With and Without Polymeric Platinum.

Under normal physiological conditions, nerves and other viscoelastic materials undergo repeated mechanical stresses of tensile, compressive, or shear nature. Nerves, skin, and musculature may experience tensile stress from either parallel or perpendicular forces, resulting in longitudinal or transverse stress.[53, 54] In nerves, such stress typically occurs following joint motion, which elongates the nerve in either longitudinal or transverse directions relative to the nerve tract. The nerve, in turn, must accommodate for such stress by elongating and gliding, known as excursion.[53] Our electroconductive elastomers behave in a similar manner. This is noteworthy as this type of behaviour is characteristic of biological tissues—meaning that despite having different stress-strain curves, our selected elastomer has similar mechanical behaviour to materials such as skin and nerves.

Kraton D1152ES (SBS) with 10%wt polyisoprene and polymeric platinum (shown in purple in Figure 4.15), displayed a similar trend. Heated samples of Kraton D1152ES (SBS) with 10%wt polyisoprene failed at strains of approximately 175% under very low stress, while the comparably treated Kraton D1152ES (SBS) with 10%wt polyisoprene and platinum (shown in blue) was capable of withstanding nearly 10 times the stress and had no fail rate.

In Chapter 3, we discussed the suitability of Kraton D1152ES (SBS) when heated to low temperatures, but not high temperatures. In platinum coated samples, heat treatment of approximately 140-150°C not only caused no issues, but produced samples with markedly

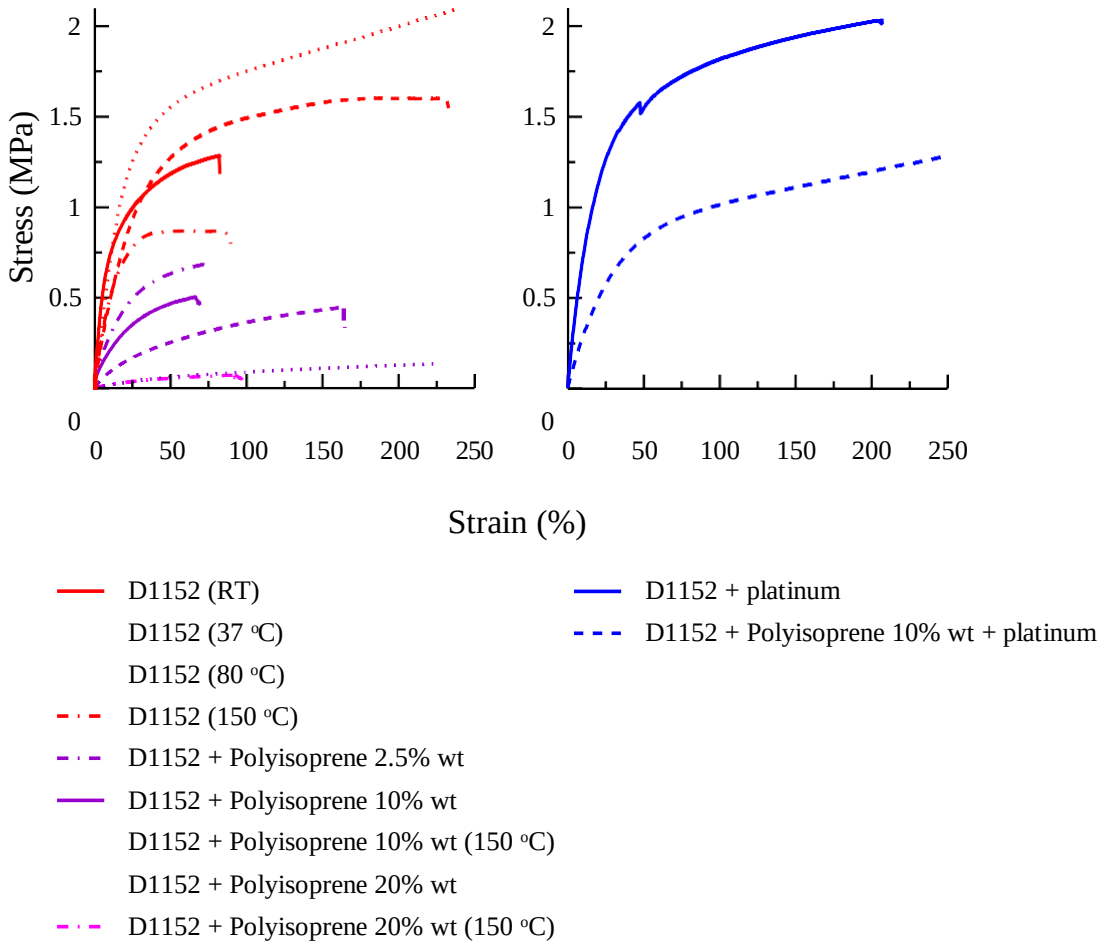

Figure 4.16: Stress-Strain Curves for Kraton D1152 and Kraton D1152-Polyisoprene With and Without Heat Treatments, and With and Without Polymeric Platinum.

improved mechanical properties compared to the non-platinum coated alternatives. The ideal electroconductive elastomer would have stress-strain curves similar to Kraton D1152ES (SBS) when heated to temperatures between 37°C and 80°C. Coincidentally, the average stress-strain curve for Kraton D1152ES (SBS) coated with polymeric platinum, shown in blue in Figure 4.15, is equivalent to these values. The best stress-strain curves we identified for these materials are shown in Figure 4.16. Despite the improvements in mechanical properties due to the platinum coating and heat treatment, the Kraton D1152ES (SBS)-polyisoprene blend is still about half as strong as Kraton D1152ES (SBS).

Continuing our research, we decided to examine the elongation at break properties of our materials to see if they too had been altered by heat treatment and incorporation with the cross-linked polymeric platinum. Elongation at break percentages for heated, unheated, and platinum

coated Kraton D1152 and its 10% and 20%wt polyisoprene blends are shown in Figure 4.17. Furthermore, we chose to perform a one-way ANOVA to assess if the treatments produced

statistically significant differences in elongation at break values, as shown in Table 4.7. We also completed Tukey's significance tests to ascertain whether any between-groups significance was present, as shown in Table 4.8.

A minimum statistical significance of 0.05 was used to assess this data. The p-values are listed in Table 4.7. In Kraton D1152 samples, the p-value corresponding to the F-statistic of the one-way ANOVA was higher than 0.05. This suggests that the heat treatment and heat treatment involving platinum were not significantly different influencing factors on the ultimate point of strain of our Kraton D1152. However, the differences for both polyisoprene blends were found to be statistically significant. Kraton D1152 and 10% polyisoprene samples showed particularly high statistical significance, with a p-value of 0.01.

In order to understand which within-group samples were significantly different, Tukey's significance tests were performed and detailed in Table 4.8. As expected, Kraton D1152 samples presented no significantly different treatment pairs. Although Kraton D1152 with 20% polyisoprene samples presented a statistically significant p value in the ANOVA, no significantly different treatment pairs could be identified in this group. However, Kraton D1152 with 10% Polyisoprene was significantly different to both heat treated Kraton D1152 with 10% Polyisoprene and platinum coated Kraton D1152 with 10% Polyisoprene. No significant difference was found between the heat treated and platinum coated sample.

Based on our analysis, we can conclude that, despite the differences in stress strain curves, heat treatment and platinum coating typically do not result in substantial differences in elongation at break values. This implies that sample integrity is maintained despite heat treatment and neither substantially positively nor negatively influenced by polymeric platinum. All of our samples were capable of withstanding elongation past 100%, the recognized minimum elongation of an elastomeric material. This being said, it is important to note that elongation at break percentages are calculated under fixed strain determined by the machine. The strength of the overall material is more accurately determined by the Young's modulus or stress strain curves, as shown in Figures 4.15 and 4.16.

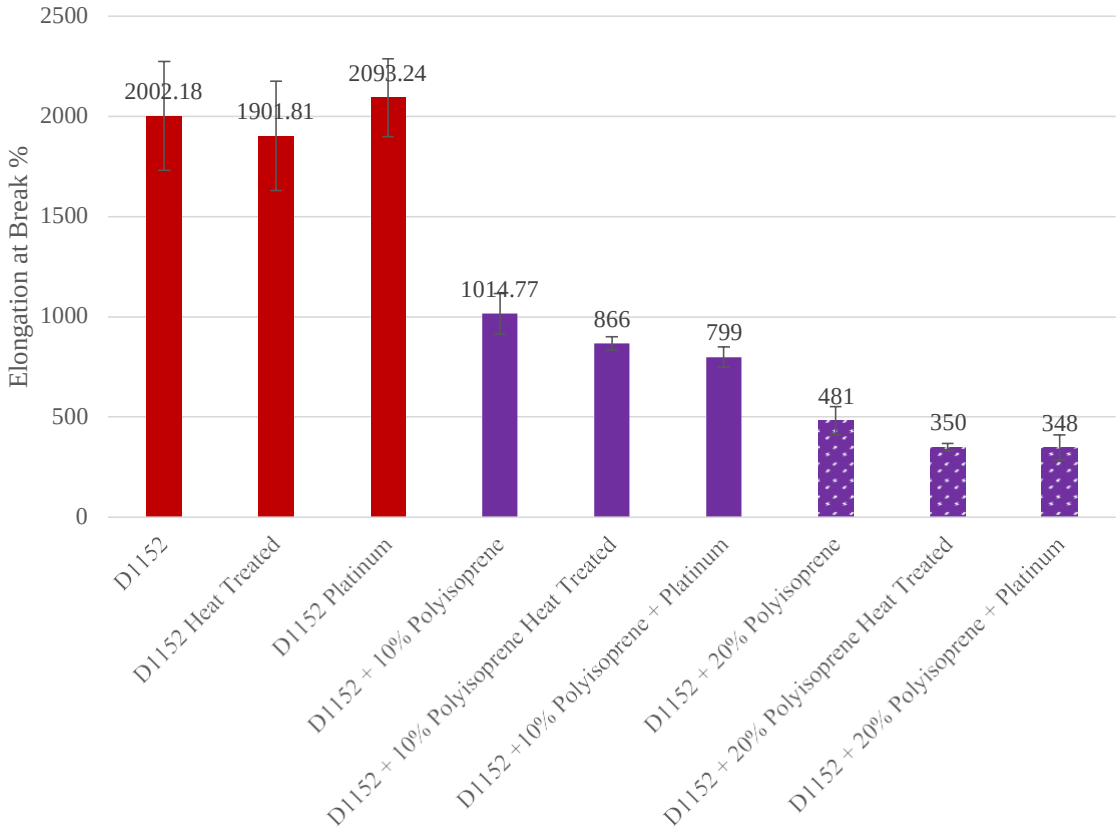

Figure 4.17: Elongation at Break Data of Electroconductive Elastomers

Few of the electroconductive elastomers in Table 4.1 listed elongation at break values. The vast majority of materials had elongation at break values that were similar to our Kraton D1152ES (SBS)-polyisoprene blends (in the range of 200 to 750%). Only the PEG2k-AT6-TMP construct, with an elongation at break value of 1643% and Young's modulus between 3.8 and 7.7 MPa, and Kraton G1645 (styrene-β-ethylbutylene-β-styrene) doped with carbon black, which has an elongation at break percentage between 1,800 and 2,475% and Young's modulus between 8 and 14 MPa, have properties comparable to ours.[7, 10] Given that the maximum achieved conductivity of Latko et al's styrene-b-ethylbutylene-b-styrene doped with carbon black was 9.5 x 10^{-6} S/cm (far less than the conductivity for even the full construct), only the PEG2k-AT6-TMP construct has comparable properties to our own soft electrode. However, it should be noted that Chen et al proposed three different PEG2k-AT6-TMP blends. The strain limitations of PEG2k-AT6-TMP and 2% PANI is 1,644% (YM of 3.8 MPa), with a conductivity of 2.1 x 10^{-4}. In contrast, the 1 S/cm conductivity was achieved by blending PEG2k-AT6-TMP with 20% carbon black, which produces a strain capacity of 1,334% (YM of 10.5 MPa).[10] Additionally, this material was not assessed from an electromechanical perspective; hysteresis, permanent set and similar experiments were not performed.

Table 4.7: One Way Anova for Elongation at Break Samples

Kraton D1152	sum of squares SS	degrees of freedom νν	mean square MS	F statistic	p-value
Treatment	75,993.6527	2	37,996.8263	0.7736	0.5025
Error	294,710.4817	6	49,118.4136		
Total	370,704.1344	8			
Kraton D1152 and 10%wt Polyisoprene					
Treatment	74,046.8322	2	37,023.4161	9.1272	0.0112
Error	28,394.7049	7	4,056.3864		
Total	102,441.5370	9			
Kraton D1152 and 20%wt Polyisoprene					
Treatment	34,850.6667	2	17,425.3333	5.7887	0.0398
Error	18,061.3333	6	3,010.2222		
Total	52,912.0000	8			

We continued on by assessing the mechanical fatigue of the electroconductive elastomers, as shown in Figure 4.18. A similar analysis was performed in Chapter 3. As skin showed failure prior to 10 thousand cycles when subjected to an amplitude around 2.5%, and sustained up to 10^5-10^6 cycles at very low amplitudes of around 0.5%, it was already established that our elastomers had much stronger mechanical properties than *ex vivo* skin.

Table 4.8: Tukey Significance Test for Elongation at Break Samples

Treatment Pairs	**Tukey Q statistic**	**Tukey p-value**	**Tukey Significance Value**
Kraton D1152 vs Platinum Coated Kraton D1152	0.0533	0.8999947	insignificant
Kraton D1152 vs Heat Treated Kraton D1152	1.5493	0.5509874	insignificant
Platinum Coated Kraton D1152 vs Heat Treated Kraton D1152	1.4961	0.5708397	insignificant
Kraton D1152- 10% Polyisoprene vs Heat Treated Kraton D1152- 10% Polyisoprene	4.3117	0.0432319	* p<0.05
Kraton D1152- 10% Polyisoprene vs Platinum Coated Kraton D1152- 10% Polyisoprene	5.8822	0.0102623	* p<0.05
Heat Treated Kraton D1152- 10% Polyisoprene vs Platinum Coated Kraton D1152- 10% Polyisoprene	1.9767	0.3929967	insignificant
Kraton D1152- 20% Polyisoprene vs Heat Treated Kraton D1152- 20% Polyisoprene	4.1461	0.0589550	insignificant
Kraton D1152- 20% Polyisoprene vs Platinum Coated Kraton D1152- 20% Polyisoprene	4.1882	0.0568125	insignificant
Heat Treated Kraton D1152- 20% Polyisoprene vs Platinum Coated Kraton D1152- 20% Polyisoprene	0.0421	0.8999947	insignificant

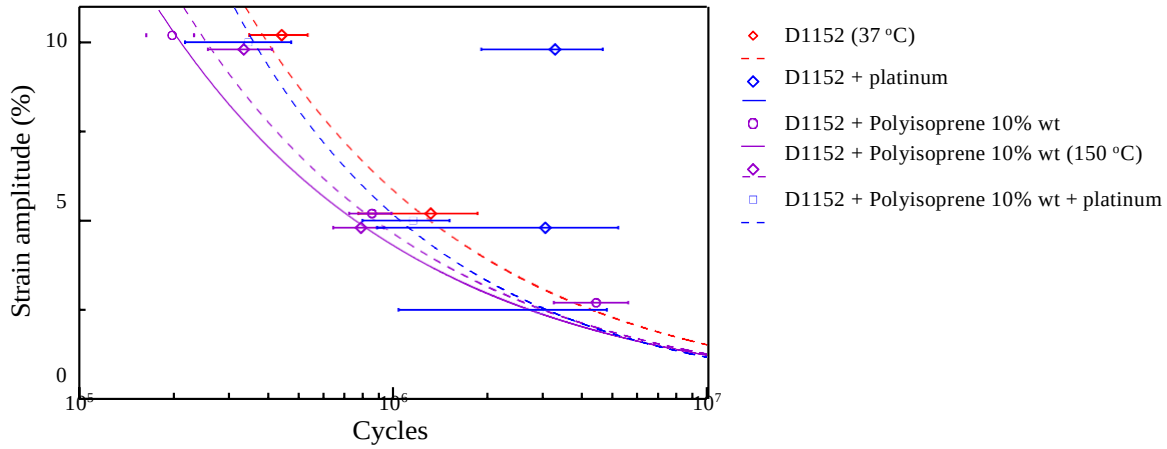

Figure 4.18: Fatigue Analysis of Kraton D1152 and Kraton D1152-Polyisoprene With and Without Heat Treatment and With and Without Platinum

Table 4.9: Fatigue Analysis of Elastomers and Electroconductive Elastomers

Material	Strain Amplitude	Cycles to Failure
D1152 37 °C	2.5%	$>5\times10^6$
	5.0%	1.3×10^6
	10%	4.4×10^5
D1152 + Platinum	2.5%	$>5\times10^6$
	5.0%	3.1×10^6
	10%	3.3×10^6
D1152 + Polyisoprene 10% wt	5.0%	4.0×10^6
	10%	8.5×10^5
	10%	2.0×10^5
D1152 + Polyisoprene 10% wt (150 °C)	2.5%	$>5\times10^6$
	5.0%	7.9×10^5
	10%	3.3×10^5
D1152 + Polyisoprene 10% wt + Platinum	2.5%	2.9×10^6
	5.0%	1.2×10^6
	10%	3.5×10^5

The number of cycles to failure are shown as a function of strain amplitude in these tensile fatigue tests. The error bars correspond to the average of absolute deviations from the mean value. The lines shown are best fits between the three different strain oscillation amplitudes, ε, and the number of cycles to failure, N, assuming: $\varepsilon = aN^{-b}$ behaviour (based on the Coffin-Manson relation). The amplitudes of strain were fixed at 2.5%, 5%, and 10%. The small vertical displacements in polymeric materials are fictive displacements to better visualize the data.

At 2.5%, only polyisoprene-blended materials reached a point of failure. Platinum-coated samples of Kraton D1152ES (SBS) and polyisoprene blends both performed better than non-platinum coated controls in fatigue tests. Kraton D1152ES (SBS) and platinum display the best fatigue resistance; no other sample was able of withstanding 10^6 fatigue cycles at 2.5, 5, and 10%. These tests confirm the improved properties of Kraton D1152ES (SBS) when coated with polymeric platinum. Specific values for each sample are shown in Table 4.9.

Having furthered our understanding of the mechanical fatigue properties of our electroconductive elastomers, we next needed to establish electroconductive fatigue. We had already established that our constructs were more than capable of reaching the maximum *in situ* strain percentage of a human digit's nerves (40%) and skin (75 - 207%).[53, 54, 75] Given that electroconductive elastomers have already been shown to mechanically behave in a manner similar to nerves and skin, the next step was understanding if conduction-related failure would occur in a similar manner.

4.7: Validation of Construct through Electromechanical Assessment

In Chapter 3, the typical *in vivo* strain capacity of nerves in a human toe was shown to be 15%.[53] The maximum strain was 40% before plastic deformation began.[53] We consequently assessed changes in resistivity at points of 15%, 30%, and 45% strain. In Figure 4.19, changes in resistivity are shown for Kraton D1152 coated with polymeric platinum and Kraton D1152 blended with 10%wt polyisoprene and coated with polymeric platinum while these samples are subjected to repeated 15% strain.

We previously stated that the average conductivity of platinum-coated Kraton D1152 was 6.11 S/cm and the average conductivity of platinum-coated Kraton D1152 blended with 10% polyisoprene was 0.585 S/cm. Our methodology for electrocmechanical experiments was not as precise as the four point probe method. As such, the lowest listed resistivity value was 1, implying high conductivity and minimal resistance. In both samples shown in Figure 4.19, resistance in stasis is fully recoverable. However, when subjected to repeated strain, the conductivity of the electroconductive elastomer was reduced to as much as $4 \cdot 10^{-2}$ and $3.57 \cdot 10^{-2}$ S/cm for Kraton D1152 coated with polymeric platinum and Kraton D1152 blended with 10%wt polyisoprene and coated with polymeric platinum, respectively. While our Kraton

D1152-based sample showed a reasonably steady incline in electrical fatigue, as expected, the Kraton D1152-polyisoprene blend showed electrical fatigue that seemed to be somewhat haphazard. This made us suspect hysteresis, which we will discuss later on in this chapter.

In Figure 4.20, we assessed the resistivity of Kraton D1152ES (SBS) coated with polymeric platinum and Kraton D1152ES (SBS) blended with 10%wt polyisoprene and coated with polymeric platinum while being subjected to repeated 30% strain. Again, conductivity in stasis is typically fully recoverable, even after twice as much strain repeated over the same amount of time. However, resistance and electrical fatigue was substantially increased. In this case, maximum conductivity listed was $2.44 \cdot 10^{-2}$ and $8 \cdot 10^{-3}$ S/cm for Kraton D1152 blended with 10%wt polyisoprene and coated with polymeric platinum and Kraton D1152 coated with polymeric platinum, respectively.

In Figure 4.21, we decided to test progressive repeated strain, assessing 15%, 30%, and 45% strain on the same samples. In this case, Kraton D1152 coated with polymeric platinum had relatively a maximum conductivity of approximately $1.5385 \cdot 10^{-2}$ S/cm, which is notably different to the value seen in Figure 4.20. No change in conductivity-in-stasis was seen, even after 10 cycles of repeated 45% strain. In contrast, Kraton D1152 blended with 10%wt polyisoprene and coated with polymeric platinum was not able to give reliable values of resistivity for values of 45% strain. While conductivity-in-stasis was not an issue, at 45% strain our two probe test was not able to confirm detectable or reliable resistivity values. For this reason, sequential conductivity is only assessed up to 30%. The maximum conductivity of this sample is about $1.5385 \cdot 10^{-2}$ S/cm.

The results from these figures are averaged triplicates of samples. Resistivity was assessed using the two probe test connected to the same machinery we used in our elongation-at-break assessments. In such machines, control of stress is defined by the machine and only strain is customizable. We must assume that despite these values, the stress utilized in these experiments is of similar megapascal range to that shown in the stress-strain curves previously. This is relevant due to the unusual changes in these values. Previously, we discussed the influence of stress and strain rate on the maximum elongation of a material. In this case, it is clear that the electroconductivity of the materials is also influenced by stress and strain rate — not directly, but because of factors causing material hysteresis thereby influencing resistivity.

In terms of electroconductivity, we found that no permanent electrical fatigue occurred in most samples. Having identified the potential for electrical fatigue under repeated strain, we attempted a second method of creating the electroconductive elastomer. After initial creation of the construct, we stretched the material to the maximum functional strain percentage we wished it to be electrically conductive at. We then applied a secondary coating of polymeric platinum and allowed the coating to dry. We found that at 100% strain and 1000% strain, this caused no negative impact on Kraton D1152-based samples. We did not repeat the electromechanical fatigue tests to the same extent; however, we did briefly assess resistance in stasis and at the maximum strain percentage. No change in resistance occurred when applying a dual layer of polymeric platinum utilizing this method.

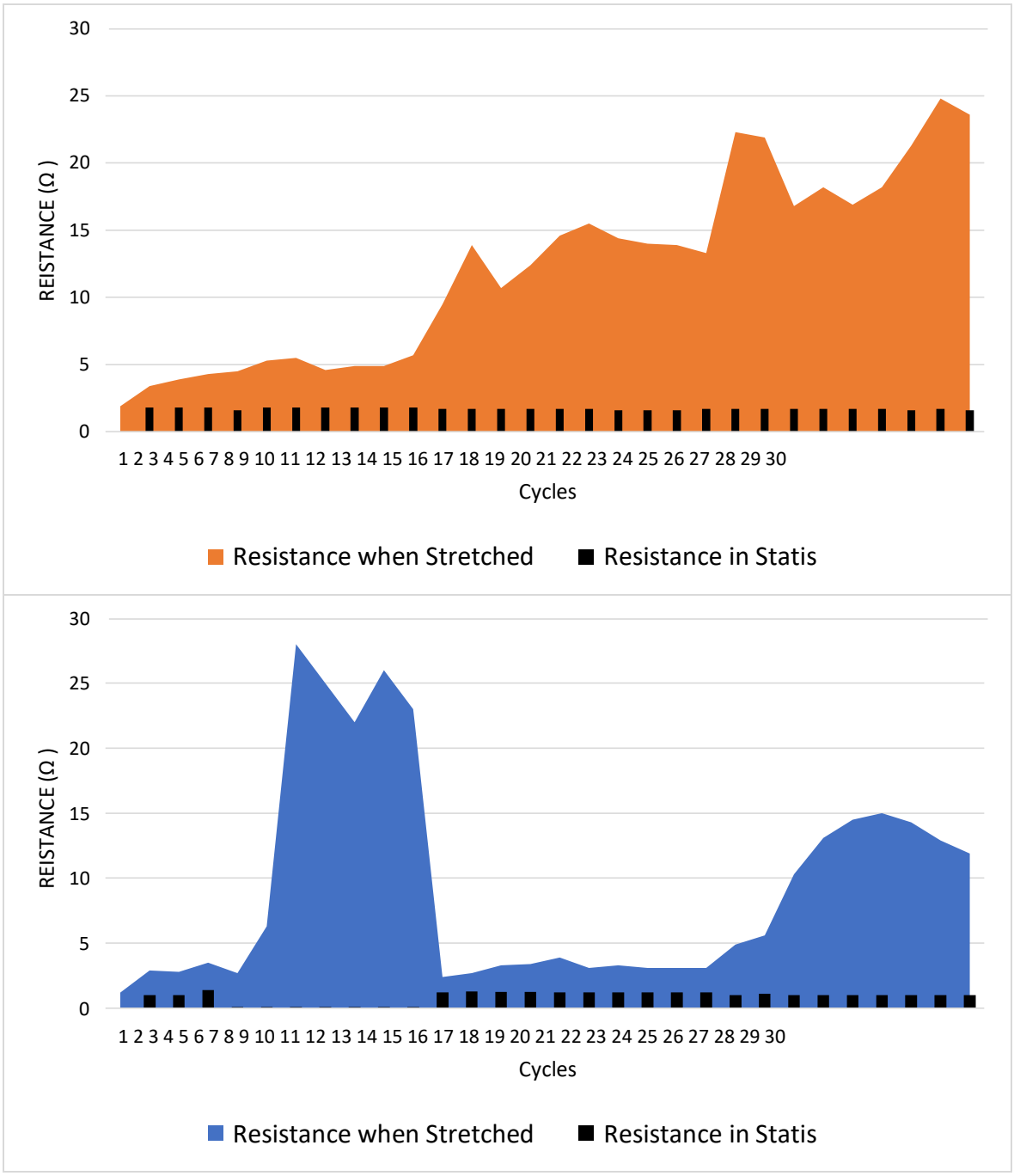

Figure 4.19: Electromechanical Fatigue of Kraton D1152 with Polymeric Platinum and Kraton D1152, 10% Polyisoprene, and Polymeric Platinum under Repeated 15% Strain. Top panel: D1152 and Polymeric Platinum at 15% Strain; Bottom panel: D1152, 10% Polyisoprene, and Polymeric Platinum at 15% Strain

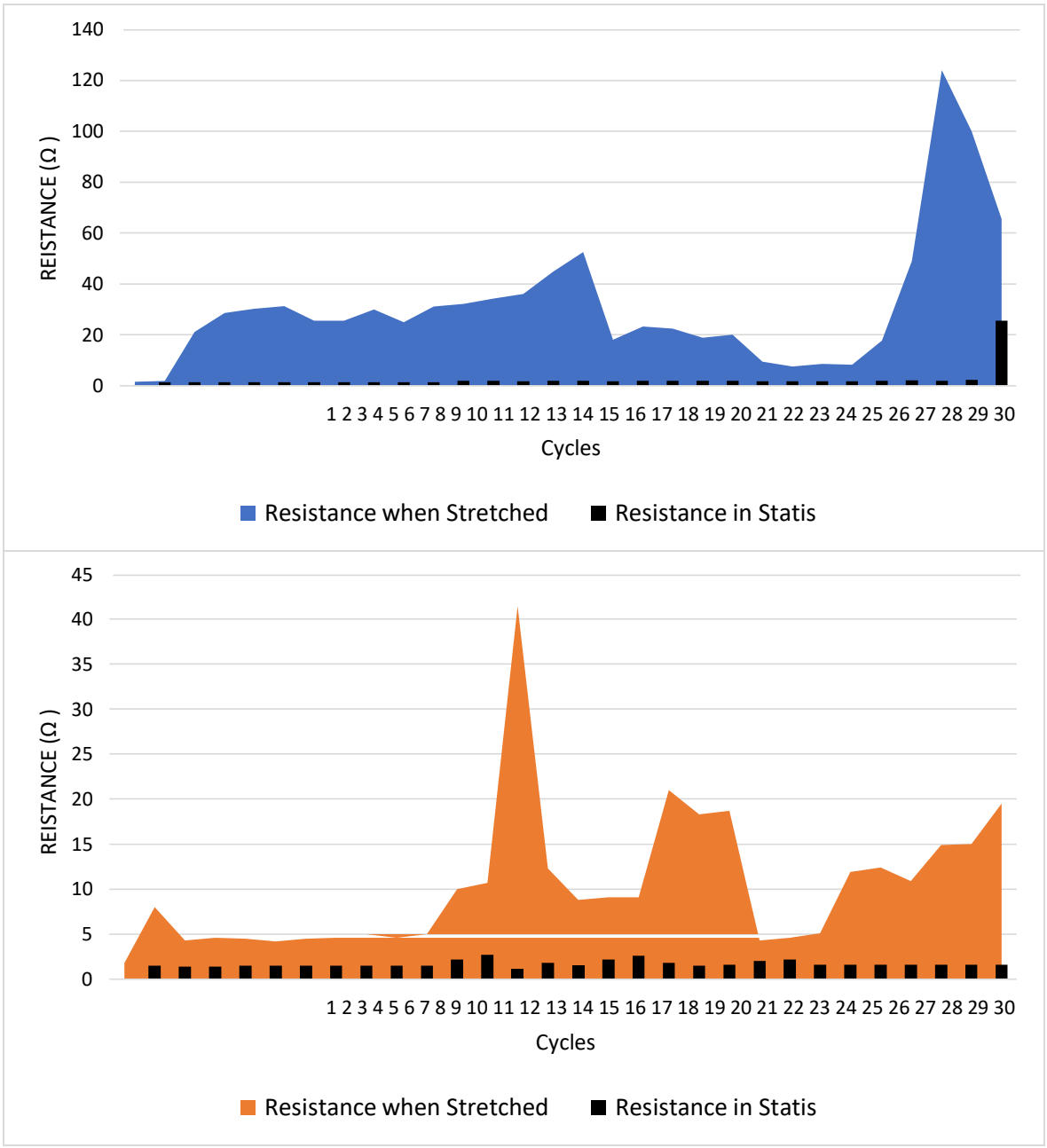

Figure: 4.20: Electromechanical Fatigue of Kraton D1152 with Polymeric Platinum and Kraton D1152, 10% Polyisoprene, and Polymeric Platinum Under Repeated 30% Strain. Top panel: D1152 and Polymeric Platinum at 30% Strain; Bottom panel: D1152, 10% Polyisoprene, and Polymeric Platinum at 30% Strain

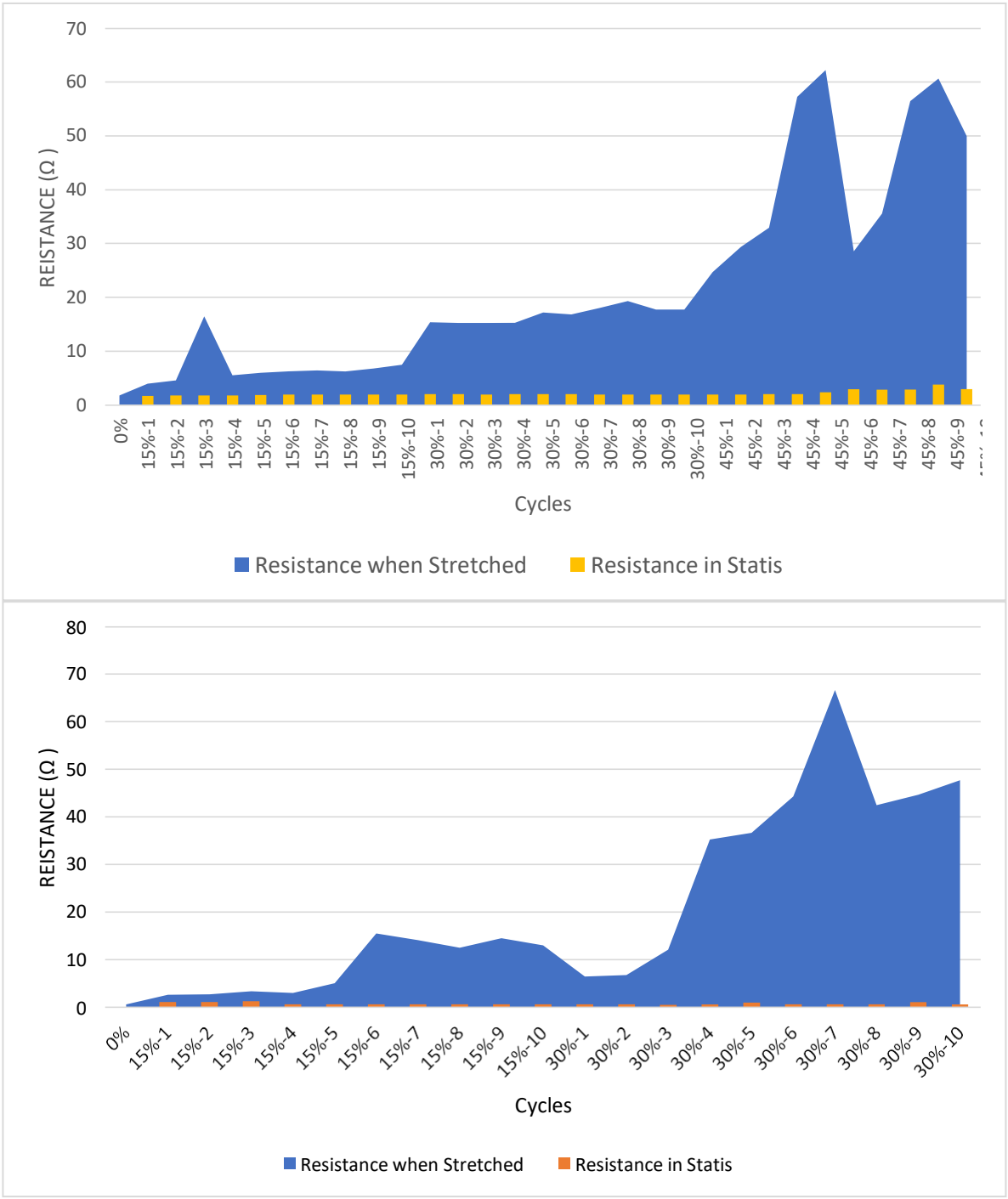

Figure 4.21: Electromechanical Fatigue of Kraton D1152 with Polymeric Platinum and Kraton D1152, 10% Polyisoprene, and Polymeric Platinum Under Progressive, Repeated Strain. Top panel: D1152 and Polymeric Platinum Under Increasing Strain; Bottom panel: D1152, 10% Polyisoprene, and Polymeric Platinum Under Increasing Strain

The hysteresis loops shown in Figure 4.22 are performed at a strain velocity of 10% per minute. The loop goes from 0 to 100% strain and back. The hysteresis loops are the consequence of the difference between the strain rate applied by the machine and the relaxation rate of the material. The material curves are within the elastic region, meaning the material always returns to the

initial state of strain (equivalent to 0) and no plastic or permanent deformation is occurring. However, the visible hysteresis occurs slower than the applied velocity of the machine. These loops allow us to conclude that hysteresis may not be related to the change in electrical properties. Instead, we can hypothesize that the polymeric platinum has a different relaxation

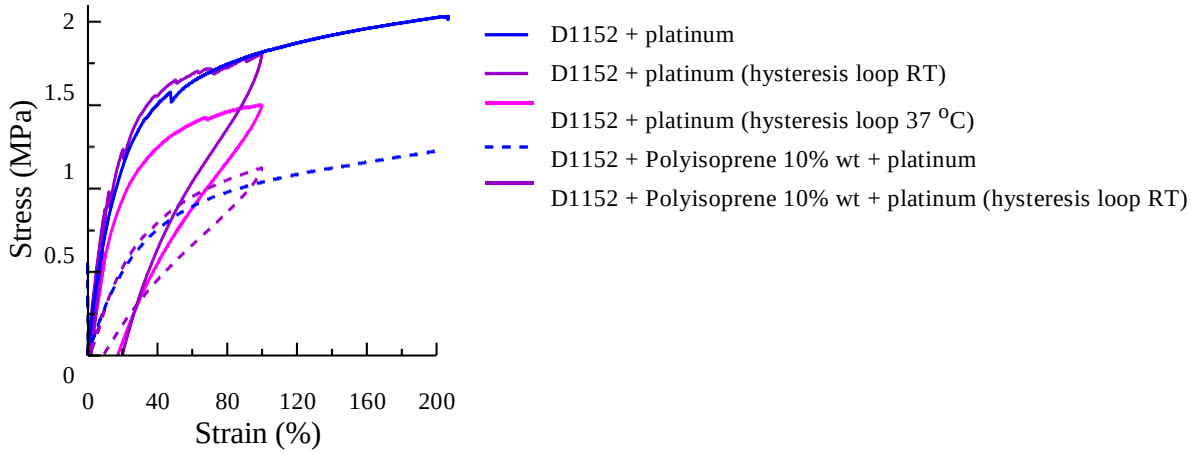

Figure 4.22 Hysteresis Analysis of Kraton D1152 and Kraton D1152-Polyisoprene With and Without Heat Treatment and With and Without Platinum

time compared to the elastomer. The difference in velocity when returning to the original state results in 'misfit' between the electroconductive layer and elastomer. This, compounded with the rapid elongation rate utilized, likely affected the construct's electromechanical properties.

The area inside the loop below the loading curve is larger for the Kraton D1552 compared to that of 10% Polyisoprene. The area shows the energy needed to strain the material, the difference in areas below the loading and unloading curve shows the energy dissipated during the cycle. As such, the hysteresis curves in Figure 4.22 show that Kraton D1552 has a longer relaxation time compared to the 10% Polyisoprene-Kraton D1152 blend at room temperature. Additionally, it implies that this polymer would dissipate more energy during loading and unloading cycles. While this is not immediately relevant, it can affect the piezoelectric properties of the complete construct.

As shown in Figure 4.22, we chose to analyse hysteresis at both room temperature and 37ºC degrees for our Kraton D1152-polymeric platinum sample. The presence of hysteresis is normal in many polymeric materials and depends on various factors, including magnitude of velocity, intrinsic relaxation time of the material, and temperature. Temperature is a particularly relevant factor as the Young's modulus of a material can change substantially with

temperature, depending on the material.

We wished to determine any potential differences in fatigue that might occur if the polymer construct were used in an implanted biomedical device or in cell culture. This data shows that Kraton D1152-platinum's Young's modulus and hysteresis loop are significantly impacted by heat. However, given the improvement in mechanical properties from platinum coating, this alteration in properties do not rule out use of the construct as they are still in line with that of skin. The improvement in mechanical performance due to polymeric platinum coating and heat-treatment processing occurs for unknown reasons, but clearly exists on even a microscopic level that can be investigated in future experiments.

4.8 Piezoelectricity of P(VDF-TrFE) and the Complete Construct

Throughout the course of this chapter, we have discussed the electroconductive elastomer. However, the piezoelectric component, P(VDF-TrFE) has not been remarked upon. We elected not to compare the data from electrospun P(VDF-TrFE) because of the difference in thickness and morphology. While it is possible to create thick, nanofibrous mats of P(VDF-TrFE), we would not need to use mats of such thicknesses in our actual construct. Therefore, their mechanical properties, while comparable, would be irrelevant to us. As we already detailed the mechanical properties of P(VDF-TrFE) in the previous chapter, we opted not to discuss them further in this chapter. Instead, we chose to validate the piezoelectric state and functionality of this polymer.

P(VDF-TrFE) is a flexible polymer with excellent mechanical, biocompatibility, and piezoelectric properties.[55-65] This polymer is often used for pressure sensor or shock gauge applications. Piezoelectric materials give rise to dielectric displacement when undergoing external mechanical stress. As charge is proportional to stretching or pressure and disappears when these cease, piezoelectric materials mimic somatosensory system function. The ease of electrospinning, piezoelectricity, and biocompatibility of P(VDF-TrFE) made it seem like the ideal pressure sensor component system for our construct.

As a piezoelectric, P(VDF-TrFE) is capable of crystallising into four different phases: β, α, γ, and δ.[55-57] The β phase is the only ferroelectric phase. It typically can be produced through the thermal and mechanical treatment of the polymer, or deposition method. In particular,

annealing P(VDF-TrFE) polymers between the Curie temperature (ranging from 90-110ºC) and melting temperature of 150ºC is a successful way of increasing the crystallinity of the polymer and achieving the desired β phase state.[55-57, 59] Published data has shown films annealed at 140ºC are optimal and that polymer morphology can be dramatically altered when cured at temperatures past the melting point.[59-61] In theory, this concept should be simple — curing a piezoelectric polymer should increase the β phase. However, heating is based on various factors, including membrane morphology, thickness, and type of heat. In addition, any mechanical treatments utilized in the preparation of the polymeric membrane can affect β phase. Studies involving piezoelectric films may comment on the heightened piezoelectricity of thin films, which often do not require any post-treatment processing whatsoever.[62] Stretching, which can be accomplished through spin coating or electrospinning, are both capable of increasing β phase — meaning that further heat treatment is not always necessary. However, other studies have shown that β-phase is increased by annealing, even if the material has been stretched through the chosen deposition methodology.[77] Notably, this increase in β-phase content is coupled with reduced mechanical function.[77]

Initially, we assessed P(VDF-TrFE)'s ability to withstand heat between 80-150ºC as this was the temperature range suitable for polymeric platinum. We found that at temperatures above 125ºC, P(VDF-TrFE) sheets and fibers shrink, warp, and melt. At 100ºC, minimal warping and melting of fibers was seen, and no warping or melting of planar sheets was seen. In our previous electroconductivity measurements, the piezoelectric layer of our construct was determined to be as little as 15 μm. Obviously, high temperature heat treatments on such thin layers would likely impact fibers instantaneously and irreversibly. Studies often confirm the β phase state of P(VDF-TrFE) post heat treatment through techniques such as attenuated total reflectance Fourier transform infrared microscopy or Raman spectroscopy. Although this method can confirm the presence of typical piezoelectric peaks and the percentage of β phase in prepared samples, only tests focused on measuring piezoelectric response can validate our model. Other studies have established the important correlation between crystalline morphology and piezoelectric functionality.[63, 64] Typically, high β phase content is correlated with high input (N) and output (V) signals, otherwise known as piezoelectric sensitivity. For this reason, we chose to perform both FTIR spectroscopy and piezoelectric measurements.

FTIR is renowned as a complex analytical method because the interpretation can vary substantially. We identified over half a dozen studies that listed defined values for FTIR β-phase peaks. PVDF and P(VDF-TrFE)'s β phase peaks are most often recognized as 840, 1276, and 1431 cm^{-1}.[64, 65] This has some variability—peaks of roughly 840, 1274 and 1402 cm^{-1} are also accepted.[67, 69] However, the literature has listed other peaks, stating that 474, 510, 1276 cm^{-1} are valid β-phase peaks.[63] Another study listed β-phase peaks as 511 and 840; while 408, 531, 612, 765, 796, 855, 965 are α.[66] This was in line with another article, which listed α-phase peaks at 763, 976, 1150, 1211, and 1384 cm^{-1}, and β-phase peaks at 842 and 1274 cm^{-1}, but did not comment on peaks lower than 763.[68] Faria et al. summarizes the peaks for PVDF and P(VDF-TrFE), listing their attributions and symmetries and compiling α and β-phase peaks listed in the literature.[70] The studies we identified show that β-phase peaks can be identified at approximately 474, 510, 840, 1275, and 1400 cm^{-1}.

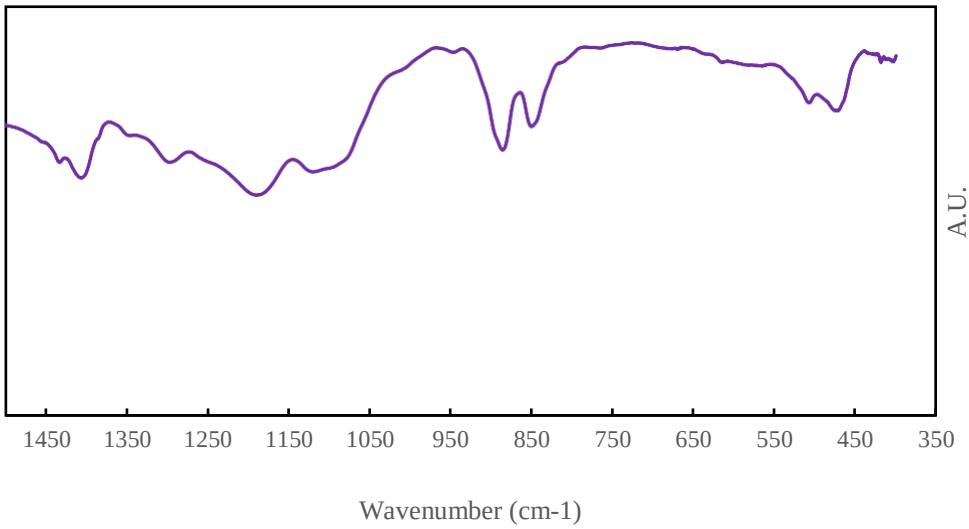

Figure 4.23: FTIR of P(VDF-TrFE) Powder

In our own analysis, P(VDF-TrFE) in powder form was compared to electrospun fibers. Electrospun fibers were analysed as untreated, heat treated for 30 minutes and heat treated for 60 minutes. Heat treatment was performed as ramp heat treatment from room temperature to 140°C. A minimum of 30 minutes was required to reach this temperature when heated at ramp, meaning that the 30 minute heat treatment procedure was primarily performed at low temperatures. We chose to analyse powder as the maker of this polymer (Arkema) lists this P(VDF-TrFE) product as pre-treated for high β-phase content. In Figure 4.23, we can see that powder has peaks at 470 and 507, another two at 848 and 883, and then the last two major

peaks at 1186 and 1403 cm^{-1}. We can conclude that, although small, over half of these peaks can be attributed to β-phase content.

In this figure, the lack of definition of peaks and existence of other peaks can be seen, in accordance with Mahato et al. and Ahn et al.[66, 68] In contrast, peaks for electrospun P(VDF-TrFE) fibers are much more defined. Notable peaks were identified at 470, 846, 883, 1188, and 1400 cm^{-1}, as shown in Figure 4.24. Peaks at 883, 1188, and 1400 cm^{-1} showed the most substantial increases. The dual peak identified as 846 and 883 cm^{-1} seems to be in line with FTIR graphs shown other studies, such as Beringer et al.[64] According to Ito et al., the former peak is specifically referred to as the electroactive phase and can be assumed to be a β-phase peak.[71]

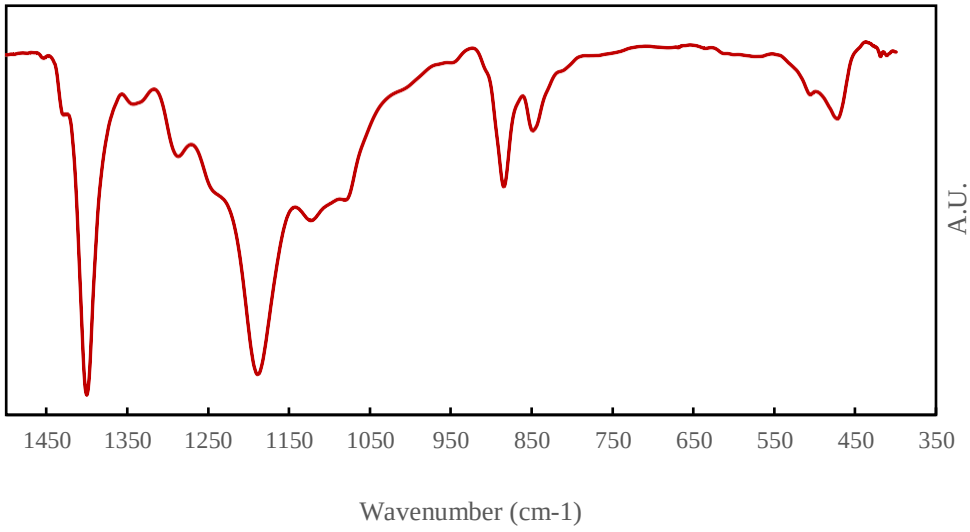

Figure 4.24: FTIR of Unheated Electrospun Fibers

Figures 4.25 and 4.26 are both very similar to the control figure, and virtually identical to one another. Between one another, no major difference can be seen. The difference between these figures and unheated P(VDF-TrFE) also seems minor. However, as shown in Figure 4.27, where these curves are superimposed, heat treatment can be shown to cause a substantial reduction in the β-phase peak at 1188. This reduction can be assumed to be a decrease in crystallinity; often caused by differences in fiber or mat size in other studies, this decrease has been shown to occur through heat treatment alone in our own analysis.

Notably, the P(VDF-TrFE) fibers tested here were random. We did not differentiate between aligned and random fibers for the purposes of this analysis; random fibers are easier to handle

and therefore easier to analyse without destroying fiber integrity or morphology. However, studies have identified the impact of mechanical deposition on β-phase content. We can assume that this β-phase is the minimum achievable through our methodology. This is much higher β-phase content than what could be expected to be seen in a planar sheet; electrospun fibers are typically recognized as having improved β-phase content.[68] P(VDF-TrFE) electrospun fibers collected utilizing a rotating disk or drum, as shown in Yee et al., are also likely to produce improved peaks.[72] We can therefore confirm that we have successfully created functional piezoelectric P(VDF-TrFE) fibers, and only needed to assess if heat treatment and consequent reduction of this peak were impactful on the functionality of P(VDF-TrFE) when assessed in electrode format.

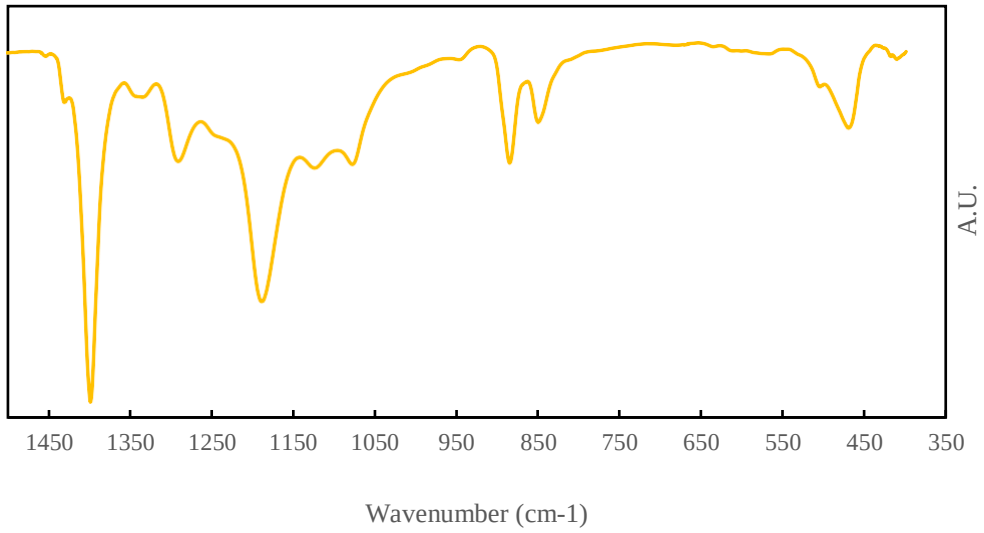

Figure 4.25: FTIR of Electrospun Fibers Heated for 30 minutes

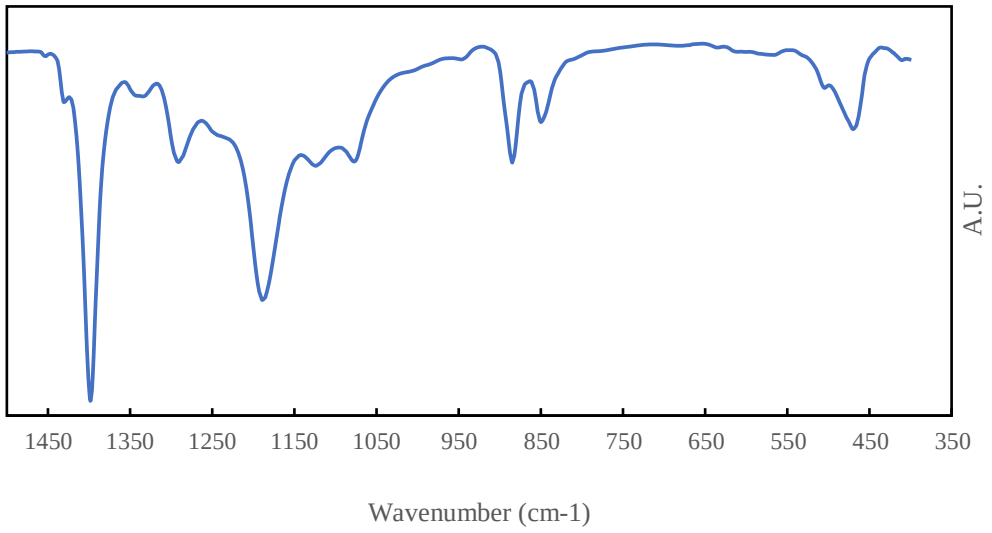

Figure 4.27: FTIR of Electrospun Fibers Heated for 60 minutes

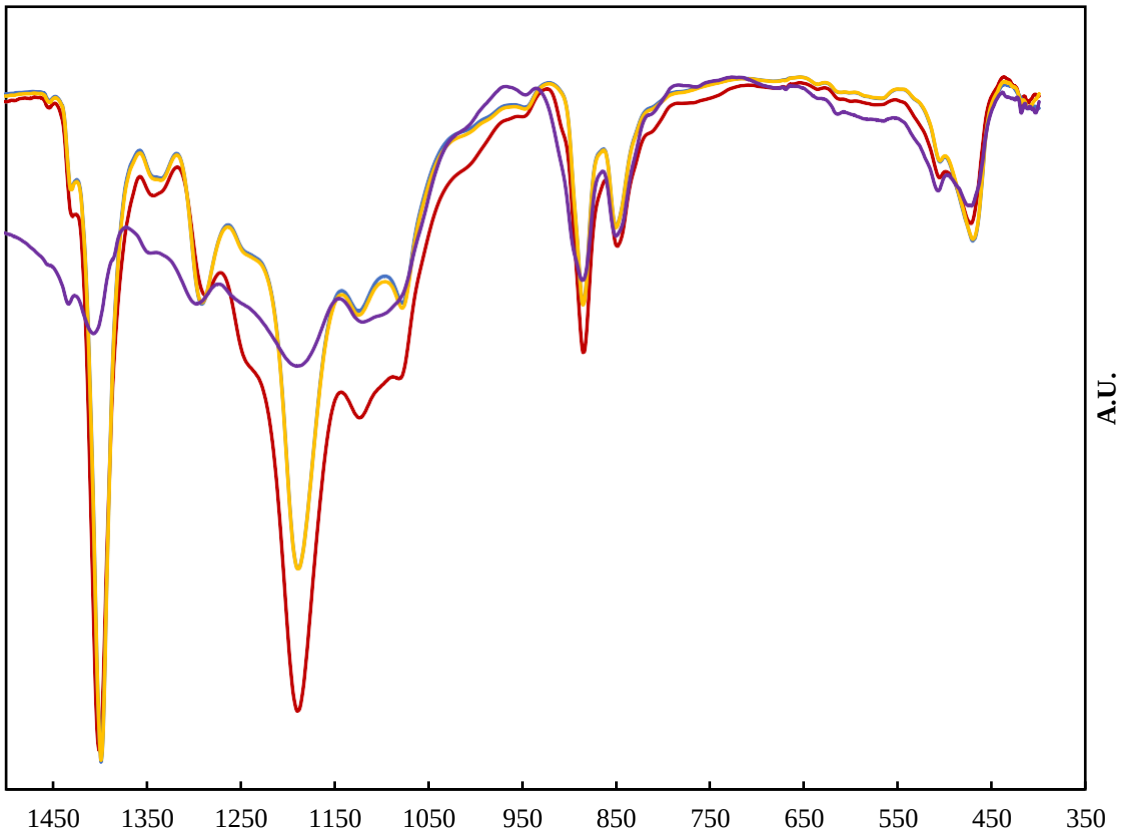

Figure 4.27: P(VDF-TrFE) Compilation of FTIR Analysis

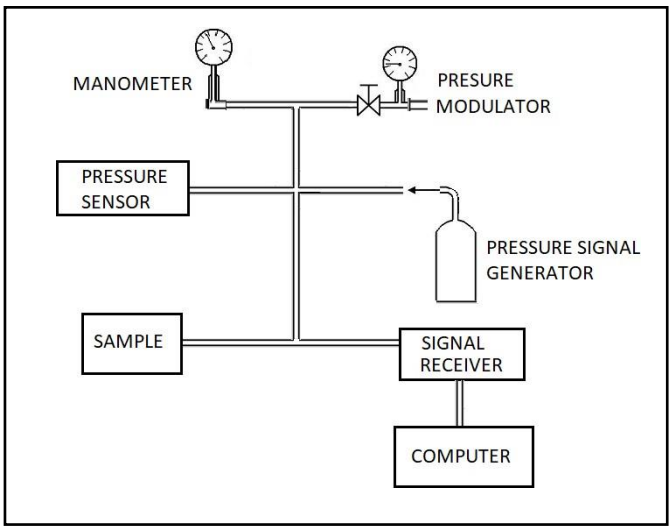

Figure 4.28: Schematic of the Pressurized Pneumatic Circuit

Table 4.10: Piezoelectric Response of P(VDF-TrFE) Electrospun Fibers

Electrode Surface	Peak-to-Peak Piezoelectric Response (mV)
Silver on Glass	45.42
Silver 80 ºC on Glass	40.83
Silver 150 ºC on Glass	61.25
Platinum on Glass	41.67
Platinum 80 ºC on Glass	35.42
Platinum 150 ºC on Glass	51.42
Kraton D1152 (SBS) and Platinum	43.75
Kraton D1152 (SBS) and Platinum 80 ºC	38.75
Kraton D1152 (SBS) and Platinum 150 ºC	45.42
Kraton D1152, 10% Polyisoprene and Platinum	14.58
Kraton D1152, 10% Polyisoprene and Platinum 80 ºC	48.33
Kraton D1152, 10% Polyisoprene and Platinum 150 ºC	51.25

Only P(VDF-TrFE) in fibrous form would be suitable for our purposes based on its mechanical properties, as discussed in Chapter 3, so planar sheets were not assessed. To perform the piezoelectric response tests of P(VDF-TrFE), we first had to design an experimental assembly based on a hermetic and pressurized pneumatic circuit, as shown in Figure 4.28. This circuit utilized about 0.4 - 0.5 bar relative pressure, modulated with a pressure reducer and measured with a precision gauge connected in bypass. Standard electrodes were created using electrospun P(VDF-TrFE) on glass, using silver paint (control) and polymeric platinum. Soft electrodes were created using polymeric platinum and Kraton D1152ES (SBS), or Kraton D1152ES (SBS) with 10%wt polyisoprene. Although the conductivity of polymeric platinum had already been established, we wanted to understand if it was able to act as a comparable electrode substrate compared to a standard metal paint. We chose to assess both Kraton D1152ES (SBS) coated with platinum and Kraton D1152ES (SBS) blended with polyisoprene and coated with platinum in order to determine if differences in soft electrode substrates and resistivity would impact the functionality of the piezoelectric.

Comparing our controls of P(VDF-TrFE) with silver and platinum electrodes on glass, we found that temperature did not play a major role in regards to functionality. Although our values were always improved after heating to 150°C, this can easily be attributed to a small amount of annealing that the piezoelectric has likely undergone. We found that it was the substrate that had a much larger role in piezoelectric response. We experienced lower values in soft electrode substrates compared to glass control electrode substrates. The polymeric platinum used to validate the construct also played a role in reducing the overall functionality, likely due to the polymeric composition within this electroconductive substance (in contrast to the pure non-polymeric silver).

However, ultimately, the majority of these values are still in line with those reported in the literature. P(VDF-TrFE) and aluminium electrodes on plastic have been shown to produce an average of -0.4 to 0.4 V when deformed by 8 mN of cantilever pressure at both 2 and 3 Hz.[64] Other studies using glass/plastic electrodes have shown the highest achievable sensitivity of P(VDF-TrFE) to be 42.00 mV/N.[63] Our highest achievable sensitivity is reported at 61 mV/N under similar parameters. Although this is attributed to our silver, annealed control, it still validates the β phase content in our piezoelectric polymers, as shown through FTIR. In fact, with the exception of the platinum coated, not heat-treated sample of Kraton D1152 blended with 10% Polyisoprene, all of our soft electrodes reported values similar to this range (38.75 – 51.25 mV/N).

Figure 4.29: Schematic of the Soft Piezoelectric Electrodes. Aligned Fibers (Left) and Random (Right).

4.9 : Conclusions

Our attempt to create a customizable, pressure sensitive, electroconductive elastomer, with an easily alterable conductive layer was successful. The methodology used to create this construct is essential for the construct's functionality. Planar sheets created in low-heat solvent chambers are essential for the optimal mechanical functionality of our final constructs. Application of the polymeric platinum does not decrease electroconductivity, as many metal additives do, but strengthens the overall material. Our resulting electroconductive elastomer is sturdy, capable of repeated cyclic loading, and does not experience electromechanical fatigue after such tests when immobile. The ramp temperature heat treatment we developed allows for adherence of the platinum layer that seems to allow the polymeric platinum and elastomer to bond to one another in a way that was not seen following thermal deposition processing. We are able to modify our electroconductive elastomers further by utilizing them as an electrode for electrodeposition, successfully adding substances such as IrOx, or incorporating IrOx nanofibers. Alternatively, stretching, re-painting, and attachment of a piezoelectric layer allows for the creation of an elastomer with electroconductive, pressure-sensitive properties that can be used in wearables and neuroprosthetics.

The customizable conductivity range of our construct makes this construct suitable for *in vitro, in vivo,* and wearable biomedical uses. In stasis, the properties of our construct are extremely stable, even after repeated strain. Elongation at break studies allowed the identification of points of failure and enabled us to make alterations to electromechanical fatigue properties by modifying the process used to create the construct. However, cyclic loading tests show that deformation and hysteresis of our construct is present, which may require future optimization or modification to the protocol involving pre-stress as an essential step.

While this does not destroy conductivity nor functionality of the construct, further studies would aim to correct these issues prior to use in *in vivo* tests as they could result in long-term device fatigue. Finally, piezoelectric analysis has allowed us to confirm the pressure sensitivity of electrospun P(VDF-TrFE), particularly the important impact of heat treatment as this polymer in planar form typically requires complex annealing processes. The β-phase content of the polymer was in line with that of the literature, though further optimization of the polymer could be performed by changing the collector utilized in the electrospinning process and

analysing the effects of heat-treatment (i.e., annealing) on the mechanical properties of this piezoelectric polymer. Analysis of the complete construct in wearables or robotics would enable an extension of electromechanical and piezoelectric fatigue analysis, thereby increasing the construct's potential uses.

4.10 : References

1. Eu.cyberonics.com. (2018). Products « VNS Therapy « Healthcare Professionals, on VNS Therapy for Epilepsy | Cyberonics Europe. [online] Available at: http://eu.cyberonics.com/en/vns-therapy-for-epilepsy/healthcare-professionals/vns-therapy/about-products [Accessed 29 Sep. 2018].
2. Cogan, Stuart F. "Neural stimulation and recording electrodes." *Annu. Rev. Biomed. Eng.* 10 (2008): 275-309.
3. Ortiz-Catalan, Max, Bo Håkansson, and Rickard Brånemark. "An osseointegrated human-machine gateway for long-term sensory feedback and motor control of artificial limbs." *Science translational medicine* 6.257 (2014): 257re6-257re6.
4. Georgiev, Nikola. "Study of two types of sensors of static forces-a piezoelectric sensor and a piezoelectric elastomer sensor." *Techsys 2017* (2017).
5. Greco, Francesco, et al. "Liquid single crystal elastomer/conducting polymer bilayer composite actuator: modelling and experiments." *Soft Matter* 9.47 (2013): 11405-11416.
6. Barkauskas, Jurgis, and Aušra Vinslovait. "Investigation of electroconductive films composed of polyvinyl alcohol and graphitized carbon black." *Materials research bulletin* 38.8 (2003): 1437-1447.
7. Latko, Paulina, Aleksandra Bogucka, and Anna Boczkowska. "Characterization of thermoplastic elastomers based composites doped with carbon black." *Int J Mech Eng Autom*2 (2015): 171-176.
8. Georgousis, G., et al. "Study of the reinforcing mechanism and strain sensing in a carbon black filled elastomer." *Composites Part B: Engineering* 80 (2015): 20-26.
9. Krajči, Juraj, Zdenko Špitálský, and Ivan Chodák. "Relationship between conductivity and stress–strain curve of electroconductive composite with SBR or polycaprolactone matrices." *European Polymer Journal* 55 (2014): 135-143.
10. Chen, Jing, et al. "Super stretchable electroactive elastomer formation driven by aniline trimer self-assembly." *Chemistry of Materials* 27.16 (2015): 5668-5677.
11. Al-Ghamdi, Ahmed A., et al. "Dielectric and microwave properties of elastomer composites loaded with carbon–silica hybrid fillers." *Journal of Applied Polymer Science* 133.7 (2016).
12. Bayer, Ilker S., Adam Steele, and Eric Loth. "Superhydrophobic and electroconductive carbon nanotube-fluorinated acrylic copolymer nanocomposites from emulsions." *Chemical engineering journal* 221 (2013): 522-530.
13. Agrawal, Aditya, et al. "Electromechanically Responsive Liquid Crystal Elastomer Nanocomposites for Active Cell Culture." *ACS Macro Letters* 5.12 (2016): 1386-1390.
14. Xiong, Yuanqin, et al. "Reduced graphene oxide/hydroxylated styrene–butadiene–styrene tri-block copolymer electroconductive nanocomposites: Preparation and properties." *Materials Science and Engineering: B* 177.14 (2012): 1163-1169.
15. Hu, Juan, et al. "Simultaneous improvement in both electrical conductivity and toughness of polyamide 6 nanocomposites filled with elastomer and carbon black particles." *Industrial & Engineering Chemistry Research* 53.6 (2014): 2270-2276.
16. Novikov, G. F., et al. "Effect of small additions of carbon nanotubes on the electrical conductivity of polyurethane elastomer." *Russian Journal of Physical Chemistry A* 88.10 (2014): 1790-1794.

17. Han, Youn Gyu, et al. "Fabrication and evaluation of the novel elastomer based nanocomposite with pressure sensing function." *Materials science forum*. Vol. 544. Trans Tech Publications, 2007.
18. Nadeem, QuratulAin, et al. "Electroconductive Composites from Polystyrene Block Copolymers and Cu–Alumina Filler." *Materials* 9.12 (2016): 989.
19. Kuester, Scheyla, et al. "Hybrid nanocomposites of thermoplastic elastomer and carbon nanoadditives for electromagnetic shielding." *European Polymer Journal* 88 (2017): 328-339.
20. Zhong, Weibing, et al. "Continuously Producible Ultrasensitive Wearable Strain Sensor Assembled with Three-Dimensional Interpenetrating Ag Nanowires/Polyolefin Elastomer Nanofibrous Composite Yarn." *ACS applied materials & interfaces* 9.48 (2017): 42058-42066.
21. Park, Yong-Lae, Bor-Rong Chen, and Robert J. Wood. "Design and fabrication of soft artificial skin using embedded microchannels and liquid conductors." *IEEE Sensors Journal*12.8 (2012): 2711-2718.
22. Zavickis, Juris, et al. "Polyisoprene-nanostructured carbon composite–A soft alternative for pressure sensor application." *Sensors and Actuators A: Physical* 171.1 (2011): 38-42.
23. Pedroni, Lucas G., et al. "Conductivity and mechanical properties of composites based on MWCNTs and styrene-butadiene-styrene block™ copolymers." *Journal of applied polymer science* 112.6 (2009): 3241-3248.
24. Matsuoka, Makoto, et al. "Carbon nanotube-coated silicone as a flexible and electrically conductive biomedical material." *Materials Science and Engineering: C* 32.3 (2012): 574-580.
25. Castillo-Ortega, M. M., et al. "Electrically conducting polyaniline-PBMA composite films obtained by extrusion." *Journal of applied polymer science* 89.1 (2003): 179-183.
26. Koncar, V., et al. "Electro-conductive sensors and heating elements based on conductive polymer composites." *International Journal of Clothing Science and Technology*21.2/3 (2009): 82-92.
27. Zevri, L., et al. "Electrical properties of flexible pressure sensitive chezacarb/silicone rubber nanocomposites." *Nanoscience and nanotechnology,* 13 (2013)
28. Imran, Syed Muhammad, et al. "Carbon nanotube-based thermoplastic polyurethane-poly (methyl methacrylate) nanocomposites for pressure sensing applications." *Polymer Engineering & Science* 56.9 (2016): 1031-1036.
29. Kim, Tae Ann, et al. "Single-walled carbon nanotube/silicone rubber composites for compliant electrodes." *Carbon* 50.2 (2012): 444-449.
30. Urbanchek, Melanie G., et al. "Development of a regenerative peripheral nerve interface for control of a neuroprosthetic limb." *BioMed Research International* 2016 (2016).
31. Del Castillo-Castro, T., M. M. Castillo-Ortega, and P. J. Herrera-Franco. "Electrical, mechanical and piezo-resistive behavior of a polyaniline/poly (n-butyl methacrylate) composite." *Composites Part A: Applied Science and Manufacturing* 40.10 (2009): 1573-1579.
32. Ichkitidze, L. P., et al. "A Conductive Composite Nanomaterial with Biocompatible Matrix and Multilayer Carbon Nanotubes." *Biomedical Engineering* 47.2 (2013): 68-72.
33. Chen, Ling, G. H. Chen, and Liang Lu. "Piezoresistive behavior study on finger-sensing silicone rubber/graphite nanosheet nanocomposites." *Advanced Functional Materials*17.6 (2007): 898-904.

34. Jamal, Daniyal, and Roche C. de Guzman. "Silicone substrate with collagen and carbon nanotubes exposed to pulsed current for MSC osteodifferentiation." *International journal of biomaterials* 2017 (2017).
35. Pan, Lijia, et al. "An ultra-sensitive resistive pressure sensor based on hollow-sphere microstructure induced elasticity in conducting polymer film." *Nature communications* 5 (2014): 3002.
36. Jiyong, Hu, et al. "Electrical properties of PPy-coated conductive fabrics for human joint motion monitoring." *Autex Research Journal* 16.1 (2016): 7-12.
37. Lei, Zhouyue, and Peiyi Wu. "A supramolecular biomimetic skin combining a wide spectrum of mechanical properties and multiple sensory capabilities." *Nature communications* 9.1 (2018): 1134.
38. Georgousis, G., et al. "Strain and damage monitoring in SBR nanocomposites under cyclic loading." *Composites Part B: Engineering* 131 (2017): 50-61.
39. Kim, Jeong Hun, et al. "Simple and cost-effective method of highly conductive and elastic carbon nanotube/polydimethylsiloxane composite for wearable electronics." *Scientific reports* 8.1 (2018): 1375.
40. Li, Hui, et al. "Enhanced electrical conductivity and mechanical property of SBS/graphene nanocomposite." *Journal of Polymer Research* 21.5 (2014): 456.
41. Xu, Cancan, et al. "Synthesis and characterization of conductive, biodegradable, elastomeric polyurethanes for biomedical applications." *Journal of Biomedical Materials Research Part A* 104.9 (2016): 2305-2314.
42. Lipomi, Darren J., et al. "Electronic properties of transparent conductive films of PEDOT: PSS on stretchable substrates." *Chemistry of Materials* 24.2 (2012): 373-382.
43. Chae, Changju, et al. "3D-Stacked Carbon Composites Employing Networked Electrical Intra-Pathways for Direct-Printable, Extremely Stretchable Conductors." *ACS applied materials &interfaces* 7.7 (2015): 4109-4117.
44. Wu, Xiaodong, et al. "Highly sensitive, stretchable, and wash-durable strain sensor based on ultrathin conductive layer@ polyurethane yarn for tiny motion monitoring." *ACS applied materials & interfaces* 8.15 (2016): 9936-9945.
45. Yu, Gui-Feng, et al. "Patterned, highly stretchable and conductive nanofibrous PANI/PVDF strain sensors based on electrospinning and in situ polymerization." *Nanoscale* 8.5 (2016): 2944-2950.
46. Ray, Dipa, ed. *Biocomposites for High-Performance Applications: Current Barriers and Future Needs Towards Industrial Development*. Woodhead Publishing, 2017.
47. Pires, Ana Filipa Soares. "Assessing the use of conjugated polymers and electric fields for cell culture." (2013).
48. Ribeiro, Alexandre Duarte. "Fabrication of Transparent and Electroconductive Scaffolds for Neural Stem Cell Culture Combining 3D Printing and Conjugated Polymers." (2015).
49. Guilak, Farshid, et al. "Control of stem cell fate by physical interactions with the extracellular matrix." *Cell stem cell* 5.1 (2009): 17-26.
50. Discher, Dennis E., David J. Mooney, and Peter W. Zandstra. "Growth factors, matrices, and forces combine and control stem cells." *Science* 324.5935 (2009): 1673-1677.
51. Saha, Krishanu, et al. "Substrate modulus directs neural stem cell behavior." *Biophysical journal* 95.9 (2008): 4426-4438.

52. Carretero González, Nina Magali, and Jaume Casabó i Gispert. "Iridium oxide-carbon hybrid materials as electrodes for neural systems. Electrochemical synthesis and characterization." (2014).
53. Topp, Kimberly S., and Benjamin S. Boyd. "Structure and biomechanics of peripheral nerves: nerve responses to physical stresses and implications for physical therapist practice." *Physical therapy* 86.1 (2006): 92-109.
54. Pawlaczyk, Mariola, Monika Lelonkiewicz, and Michał Wieczorowski. "Age-dependent biomechanical properties of the skin." *Advances in Dermatology and Allergology/Postępy Dermatologii i Alergologii* 30.5 (2013): 302.
55. Müller, Klaus, et al. "Ferroelectric properties of spin-coated ultrathin (down to 10 nm) copolymer films." *Applied Physics Letters* 93.11 (2008): 112901.
56. Kawai, Heiji. "The piezoelectricity of poly (vinylidene fluoride)." *Japanese Journal of Applied Physics* 8.7 (1969): 975.
57. Kepler, R. G. "Piezoelectricity, pyroelectricity, and ferroelectricity in organic materials." *Annual Review of Physical Chemistry* 29.1 (1978): 497-518.
58. Furukawa, Takeo. "Ferroelectric properties of vinylidene fluoride copolymers." *Phase Transitions: A Multinational Journal* 18.3-4 (1989): 143-211.
59. Lau, K., et al. "Effect of annealing temperature on the morphology and piezoresponse characterisation of Poly (vinylidene fluoride-trifluoroethylene) films via scanning probe microscopy." *Advances in Condensed Matter Physics* 2013 (2013).
60. Zeng, Zhi-gang, et al. "Effect of crystallinity on polarization fatigue of ferroelectric P (VDF-TrFE) copolymer films." *Chinese Journal of Polymer Science* 27.04 (2009): 479-485.
61. Li, Weiping, et al. "Annealing effect on poly (vinylidene fluoride/trifluoroethylene)(70/30) copolymer thin films above the melting point." *Journal of applied polymer science* 116.2 (2010): 663-667.
62. Sharma, Tushar, et al. "Patterning piezoelectric thin film PVDF–TrFE based pressure sensor for catheter application." *Sensors and Actuators A: physical* 177 (2012): 87-92.
63. Wang, Y. R., et al. "A flexible piezoelectric force sensor based on PVDF fabrics." *Smart Materials and Structures* 20.4 (2011): 045009.
64. Beringer, Laura T., et al. "An electrospun PVDF-TrFe fiber sensor platform for biological applications." *Sensors and Actuators A: Physical* 222 (2015): 293-300.
65. Dhakras, Dipti, et al. "Enhanced piezoresponse of electrospun PVDF mats with a touch of nickel chloride hexahydrate salt." *Nanoscale* 4.3 (2012): 752-756.
66. Mahato, P. K., et al. "Effect of fabrication technique on the crystalline phase and electrical properties of PVDF films." *Materials Science-Poland* 33.1 (2015): 157-162.
67. Greeshma, T., R. Balaji, and S. Jayakumar. "PVDF phase formation and its influence on electrical and structural properties of PZT-PVDF composites." *Ferroelectrics letters section* 40.1-3 (2013): 41-55.
68. Ahn, Yongjin, et al. "Enhanced piezoelectric properties of electrospun poly (vinylidene fluoride)/multiwalled carbon nanotube composites due to high β-phase formation in poly (vinylidene fluoride)." *The Journal of Physical Chemistry C*117.22 (2013): 11791-11799.

69. Lee, Ju-Hyuck, et al. "Micropatterned P (VDF-TrFE) Film-Based Piezoelectric Nanogenerators for Highly Sensitive Self-Powered Pressure Sensors." *Advanced Functional Materials*25.21 (2015): 3203-3209.
70. Faria, L. O., and R. L. Moreira. "Infrared spectroscopic investigation of chain conformations and interactions in P (VDF-TrFE)/PMMA blends." *Journal of Polymer Science Part B: Polymer Physics* 38.1 (2000): 34-40.
71. Ico, Gerardo, et al. "Size-dependent piezoelectric and mechanical properties of electrospun P (VDF-TrFE) nanofibers for enhanced energy harvesting." *Journal of Materials Chemistry A* 4.6 (2016): 2293-2304.
72. Yee, Wu Aik, et al. "Stress-induced structural changes in electrospun polyvinylidene difluoride nanofibers collected using a modified rotating disk." *Polymer* 49.19 (2008): 4196-4203.
73. Gutiérrez, Jon, et al. "Synthesis, physical and magnetic properties of BaFe12O19/P (VDF-TrFE) multifunctional composites." *European Polymer Journal* 69 (2015): 224-231.
74. Habibur, Rahaman Md, et al. "The effect of RGO on dielectric and energy harvesting properties of P (VDF-TrFE) matrix by optimizing electroactive β phase without traditional polling process." *Materials Chemistry and Physics* 215 (2018): 46-55.
75. Dias, J. R., P. L. Granja, and P. J. Bártolo. "Advances in electrospun skin substitutes." *Progress in Materials Science* 84 (2016): 314-334.
76. Kim, Su-jin, et al. "Electrospun iridium oxide nanofibers for direct selective electrochemical detection of ascorbic acid." *Sensors and Actuators B: Chemical* 196 (2014): 480-488.
77. Jiang, Yonggang, et al. "Aligned P (VDF-TrFE) nanofibers for enhanced piezoelectric directional strain sensing." *Polymers* 10.4 (2018): 364.

CHAPTER 5.

CELL-MATERIAL CHARACTERIZATION AND INTERACTIONS

5.1 : Outline

Chapter 5 discusses the cellular research undergone in order to validate this thesis. We chose to utilize four main cell types in this chapter: L929 fibroblasts, Heka-APF human keratinocyte cells, immortalized human dorsal root ganglion cells, and immortalized Schwann cells. Section **5.2** begins with an introduction to the concept of skin and somatosensory system models, followed by a description of our proposed approach to somatosensory system modelling. This section elaborates upon somatosensory system models in the literature and the selection of cell types that they utilize.

Section 5.3 describes the preliminary ISO-Standard cytotoxicity tests and adhesion assays utilizing fibroblasts. We attempted to elaborate upon these tests by creating different co-culture models that were representative of the somatosensory system. Section 5.4 describes the co-culture model that was set up utilizing four cell types, namely Heka-APF, Dorsal root ganglion cells, Schwann cells, and L929 fibroblasts. We continue on to other assessments of this co-culture, specifically scratch assays in Section 5.5, followed by a validation of the complete construct in Section 5.6 and the overall conclusion in Section 5.7.

5.2 : Skin and Somatosensory System Modeling

5.2.1 : Introduction to Skin and Somatosensory System Models

The somatosensory system is a complex part of the body that extends from the skin through the entirety of the nervous system. The skin, commonly known as the largest organ of the body, contains a myriad of cell types from fibroblasts to different nerve cells. As the aspect of the body that allows humans to perceive the outside world while protecting it, the cells in this organ form a unique, three-dimensional structure. This structure exposes cells like fibroblasts and keratinocytes to the outside world while protecting nerve endings, glands, and components of the immune system in the layers beneath.[1, 2] Despite its complexity and the fact that it is about 16% of a human's body weight, skin is not a well-studied organ—even more so when considered in the context of the somatosensory system.[1, 3]

Modern skin modeling typically involves two types of cells—dermal fibroblasts and epidermal keratinocytes. These two cell types, which are certainly a major component of skin's exterior layers, play an important role in paracrine signalling and the inflammatory, immunological response to external environments.[2] These cells play a particularly important role as the primary form of defence and regulate anything from abrasion-related wound healing to photo- damage.[2] When combined with a collagen matrix, the resulting construct can be used for *in vitro* modeling of skin.

Several three-dimensional, full-thickness models like EpiDermKFT™, Phenion®, and NeoDerm® are now commonly available for cosmetic and pharmaceutical testing.[2, 3] These models are considered advanced compared to the reconstructed human epidermis models containing only differentiated epidermal keratinocytes. Previously used keratinocyte models were grown on insert membranes, exposing the keratinocytes to air and triggering differentiation to mimic the layers of the epidermis: the stratums corneum, granulosum, spinosum, and basale.[4] In contrast, the keratinocyte-fibroblast co-cultures are seeded within a collagen matrix that serves as a scaffold, mimicking the dermal extracellular matrix.[4] Although fibroblasts are often thought to be a cell only useful for proof-of-concept experiments or scar modelling, these cells allow the formation of a basement membrane and create wall-to-wall tissue formation that improves dermal and epidermal modelling.[2] Despite this, these co-culture models remain fairly novel as commercialized products and keratinocyte-only models are still commonly used in chemical, cosmetic, and pharmaceutical testing.[3]

In research, skin modelling may involve fibroblast-keratinocyte co-cultures in collagen produced with the assistance of various techniques, including freeze-drying, three-dimensional bio-printing, electrospinning, and microfluidic lab-on-chip type systems.[3] Other types of co-cultures involving combinations of fibroblasts, keratinocytes, melanocytes, and blood vessel endothelial cells are also being developed.[3, 5] These models provide a much more realistic model of skin, as the human epidermis contains keratinocytes, melanocytes, Langerhans cells, and Merkel cells, while the dermis contains the collagen matrix and fibroblasts.[3] However, the dermis—specifically, the reticular dermis—also contains many of the immunological and nerve cells that make skin into the dynamic and multi-functional organ it is *in vivo*.[3] Additionally, there are hair follicles and blood vessels that traverse this multi-layer organ. Few models take any of this into account.

The most common alternative approach—applicable to both immunological and neurological (or somatosensory) modeling—is the use of skin-on-chip technology.[6, 7] Often, this technology involves a simple skin biopsy that enables all of the important immunological components and specialised nerve endings to be taken and analysed in vitro. This approach is of course heterogenous, but suitable for a personalized medical approach when studying specific donors.[7] However, the same approach using animal models is not nearly as applicable to humans when studying skin in a more generalized sense. For instance, mice, a commonly used mammalian model, possess skin of a different thickness, different hair density, and no sweat glands (except on their footpads.[7]

Somatosensory system modelling focused on skin has historically involved dorsal root ganglion cells. This is because skin is innervated with a variety of peripheral sensory neurons whose cell bodies reside within these ganglia. From Pacinian and Meissner corpuscles to Merkel's disks and Ruffini endings, it is these various nerve pathways that enable us to pick up objects and feel differences in texture and temperature or pleasure and pain. Interestingly, these cells are not only important for the modelling of skin, but very important from a somatosensory perspective.[8]

Sensory neurons have been shown to induce the proliferation of keratinocytes, increasing epidermal thickness and providing improved modeling for both neurological and inflammatory conditions. In turn, epidermal keratinocytes are also known to secrete neurotransmitters that activate these peripheral sensory neurons.[8] These cell-cell interactions and effects on culture morphology make a keratinocyte-dorsal root ganglion co-culture particularly desirable when attempting to model somatosensory system interactions.

5.2.2 Developing a Skin-Related Co-Culture Model

The main obstacle in the co-culture of these cells is that neurons and keratinocytes require different external calcium concentrations. Calcium is important for the development and functionality of both cell types; axonal growth of neural cells requires a high-calcium concentrations while keratinocytes require a low-calcium to proliferate.[9] While fibroblasts and

keratinocytes are able to be co-cultured with ease, keratinocyte-dorsal root ganglion co-cultures are much more challenging given their highly specific media requirements.

Media is not the only important external factor that can play a role in keratinocyte and dorsal root ganglion proliferation and differentiation. Mechanical properties of materials in particular heavily influence their biocompatible desirability. Cellular proliferation and differentiation can be determined based purely on the mechanical properties of their environment.[34]

While neural cells living in the brain reside in tissue with an elasticity of less than 1 kPa, cells such as myofibroblasts require a stiffer matrix of at least 20 kPa.[35] However, this is hardly a matter of decreasing Young's moduli values for optimal cell culture. Extremely soft substrates can inhibit cell proliferation and differentiation, while proliferation and differentiation are promoted in substrates with moduli of at least 500 Pa.[36] Interestingly, neuronal differentiation occurs at moduli in this range, but glial differentiation is improved in substrates with moduli of 1,000-10,000 Pa.[35, 36]

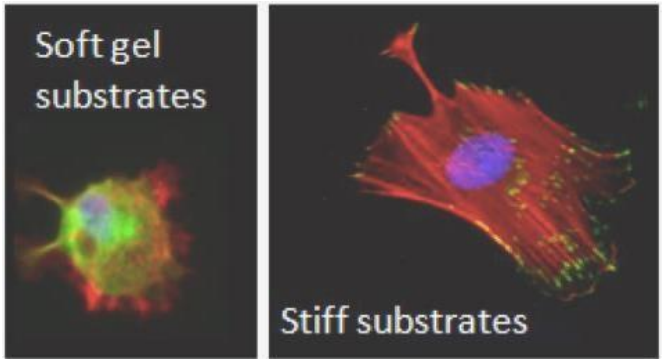

Figure 5.1: Impact of a Cell Culture Substrate's Mechanical Properties on Morphology Reprinted with permission from: Discher, Dennis E., David J. Mooney, and Peter W. Zandstra. "Growth factors, matrices, and forces combine and control stem cells." Science 324.5935 (2009): 1673-1677.50

Our desire to create an electroconductive elastomer suitable for the somatosensory system meant that keratinocytes, fibroblasts, and neuronal cells, particularly dorsal root ganglions and Schwann cells, would have to be receptive to the electromechanical properties and stimulation producible by our construct. Considering both electrical conductivity and mechanical properties in tandem was essential to the progression of our work as any construct produced needed to electromechanically suitable for use with somatosensory system cells.

Our own approach to co-culture expanded upon the established method of culturing primary sensory neurons and keratinocytes.[9] Our objective was to create a co-culture set up that had relevance for both skin and somatosensory system modelling. Since our material substrate has features akin to those of musculature and the peripheral/central nervous system with its electromechanical properties, the cells above it ideally needed to be complete epidermal and dermal layers. This means that a combination of cells would have to used; essentially a co-culture of fibroblasts, keratinocytes, and dorsal root ganglions so that neuronal cells would grow alongside epidermal and dermal ones.

The creation of a skin-based somatosensory model is complex as it requires the optimization of media and validation of cells coexisting harmoniously within the cell model. Furthermore, skin contains differentiated cells. Our model did not take the standard approach of inverting cells to induce keratinocyte differentiation. Instead, this study focused on maintaining keratinocyte and neural proliferation and differentiation, specifically creating a substrate for long-term culture and expansion of these cells. This is particularly distinct from the creation of porous nanofibers made of more natural substrates, like collagen.[37, 38]

Degradable substrates like these are certainly able to encourage cell growth, but are designed for a distinctly different purpose – generally wound healing or temporary integration into the body. However, such porous collagen fibers could potentially be incorporated onto the surface of our construct prior to seeding cells, rather than the standard collagen coating that is recommended for Heka-APF culture. This alternative would influence both cell organization and cell migration, particularly under mechanical stimulation that would directly affect cells two-fold due to the piezoelectric component of our construct. However, the incorporation of such fibers would yield the potential to seamlessly incorporate a more structurally similar extracellular matrix into our co-culture, incorporating not only the relevant cells but layers of collagen and elastic fibers found in skin.

Ultimately, the complexity of a realistic co-culture is extensive. Our final model was purely cellular, and involved a combination of fibroblasts, keratinocytes, dorsal root ganglions and Schwann cells. This produced a model that is most similar to the dermis, rather than the epidermis, as it directly involves innervation. With the exception of the fibroblasts, all cells used were of human origin; none were of primary origin. Schwann cells were included in this

model as their presence allows for the differentiation and proliferation of the dorsal root ganglion cells. Alone, the dorsal root ganglions were overwhelmed by the keratinocytes and fibroblasts in co-culture, but in the presence of Schwann cells, this four-cell co-culture resulted in the formation of 3D tissue. The creation of the final co-culture is detailed more extensively later on in this chapter.

Such an ambitious, untested approach to a co-culture could not be directly attempted on an also untested substrate. A step-wise, experimental approach could be taken increasing the complexity of the experiments, involving:

- Preliminary assessments utilized both primary *Xenopus* and rat neuronal cells, with the simple goal of determining whether or not any cells would adhere to such soft materials.
- More standard assessments were performed shortly after; utilizing mammalian fibroblasts to test the materials to ISO standards.
- Cells were tested individually on standard polystyrene tissue culture plates.
- Two types of somatosensory-skin co-culture [keratinocyte-dorsal root ganglion and fibroblast-keratinocyte-dorsal root ganglion-Schwann cell] were developed and assessed on polystyrene tissue culture plates.
- Cells were tested individually on the polymer substrates.
- Somatosensory-skin co-culture were developed and assessed on the polymer substrates.
- After such validations were completed, co-culture tests were performed as a final validation of the construct.

5.3. ISO-Standard Cytotoxicity Tests and Adhesion Assays with L929 Fibroblasts

As mentioned in previous chapters, the goal of this project was to not only to identify an elastomer that could be used for a somatosensory system interface but to create a biocompatible, electroconductive, elastomeric construct. The first step in the validation of biocompatibility of such a construct was the completion of ISO standard tests. The tests were performed as the preliminary assessments using L929 fibroblasts to determine any cytotoxicity related to direct contact or indirect contact.

We chose to perform cytotoxicity assays for samples of our selected samples, namely:

- Elastomer Kraton D1152ES (SBS) with and without polymeric platinum.
- Kraton D1152ES (SBS) blended with polyisoprene, with and without a polymeric platinum coating.
- Electrospun Kraton D1152ES (SBS) blended with 15 and 25% wt concentrations of iron(III) p-toluenesulfonate hexahydrate and assessed.
- P(VDF-TrFE), the piezoelectric component of our construct which has established biocompatibility and could be used as a control.
- Furthermore, the full construct made of Kraton D1152ES (SBS) coated with polymeric platinum and P(VDF-TrFE) fibers was also tested.

All the tests were performed in accordance with ISO standards, specifically ISO 10993-5:2009(E) for biomaterials. To begin with, the indirect contact assay was performed. This involved incubating the materials with DMEM and 10% (v/v) FBS for 24 hours. The resulting liquid extracts were used as media for the culture of L929 fibroblasts cells. Media incubated with latex (positive control) will not grow, while media incubated with non-toxic materials are unaffected and allow cells to grow normally. Values of cell metabolic activity were obtained using the reagent MTT compared to glass (negative control) and latex (positive control).

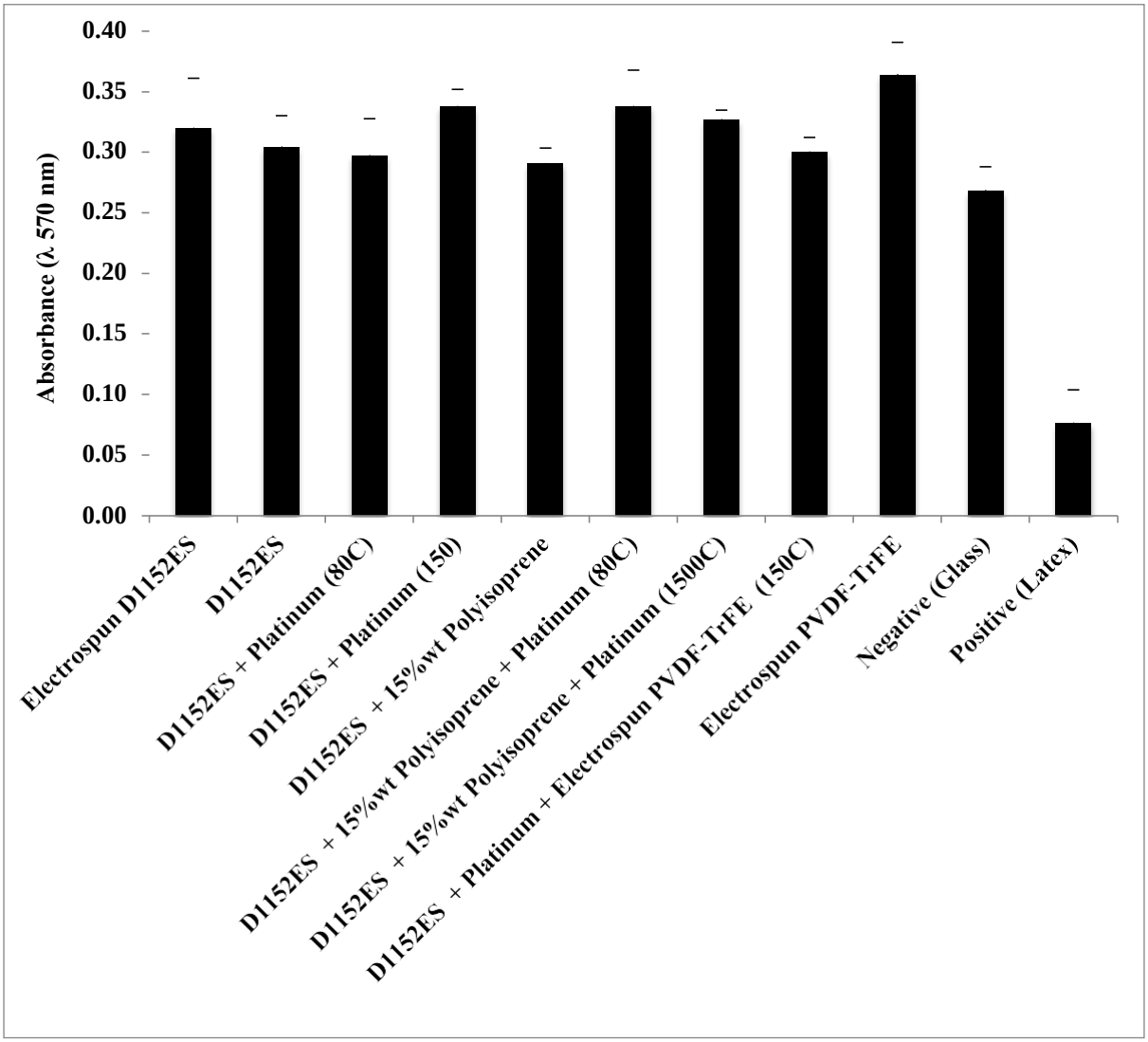

Figure 5.2. MTT Indirect Contact Assay. Showing results of the MTT indirect contact assay for all tested elastomers (Kraton D1152ES (SBS) and polyisoprene blends) and P(VDF-TrFE), where the latter is also utilized as a negative control.

Figure 5.2 depicts the results of an indirect contact assay as a bar chart, where each column depicts the growth of L929 mouse fibroblasts per sample and each error bar represents mean ± SEM of at least three replicates. Indirect contact assays aim to identify the effects of leachates, such as residual solvents, dopants, and cross-linkers from the materials' synthesis or processing. The columns in Figure 5.2 show electrospun P(VDF-TrFE), which is well-known for being a biocompatible material, as the positive control for this test. However, all samples were shown to be non-toxic and presented growth that far surpassed glass (negative conrol). Neither electrospun Kraton D1152ES (SBS), which contained the additive iron(III) p-toluenesulfonate hexahydrate nor polymeric platinum coated samples produced leachates in

the media. Equally, the addition of polyisoprene blended with Kraton D1152ES (SBS) had no detrimental effect on fibroblast growth. As these results were so positive, cytotoxicity assessment continued by examining the morphology and proliferation of cells through a direct contact assay.

The direct contact assay was prepared by culturing L929 fibroblasts on tissue culture polystyrene until confluency, using a glass coverslip as a negative control and a piece of latex glove (toxic) as positive control. As P(VDF-TrFE) is a flexible material with well-established biocompatible properties, this material again served as a secondary negative control of a polymeric nature.

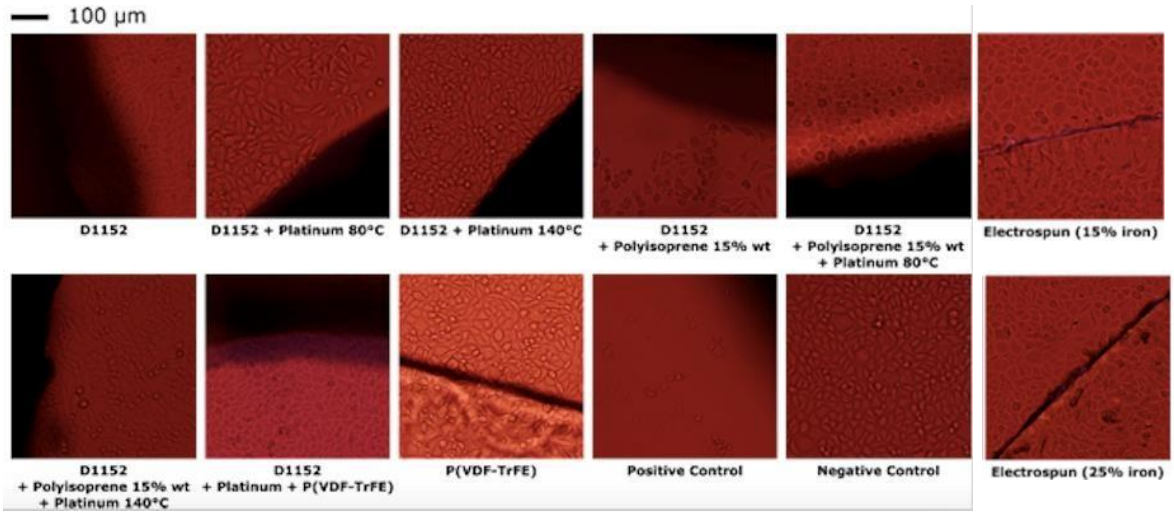

Figure 5.3: Direct Contact Assay. Showing results of the direct contact assay for all tested elastomers (Kraton D1152ES (SBS) and polyisoprene blends) and P(VDF-TrFE), where the latter is also utilized as a negative control.

Figure 5.3 shows direct contact assays for all of the aforementioned samples. Materials toxic to cells produce a halo surrounding the edge of the material, as shown in the positive control. The polymers depicted are not all transparent either due to colour or thickness. As such, pictures of planar materials simply depict the edge of the material and halo extending from this point, or lack thereof. In contrast, electrospun P(VDF-TrFE) and D1152 blended with iron(III) p-toluenesulfonate hexahydrate are fairly transparent. Regardless, cells can be seen proliferating healthily underneath all the materials.

The direct contact assay of these materials on L929 cells shows no halo of inhibition, unlike the latex positive control. According to the ISO standard used, all polymers were non-cytotoxic regardless of the way the materials were processed or the addition of electroconductive materials. All samples except the positive control (latex) show excellent proliferation surrounding the materials. We were interested to know if L929 cells found all materials equally appealing as growth substrates. As such, an extended study of these cells was performed to assess adhesion and proliferation.

Electrospun P(VDF-TrFE) is often a preferred substrate for cells like neural and cardiovascular cells, especially in comparison to smooth, planar substrates such as coverslip glass or polystyrene.[12-14] This is typically thought to be because of its three-dimensional quality and ability to control fibre orientation, both aspects that encourage cell proliferation. However, in the direct contact assay, material samples are placed above rather than underneath cell samples. We wished to perform an assay that assessed adhesion to materials in order to understand whether long-term cultures upon them were feasible. Electrospun materials are well-known as desirable substrates for cell culture. However, given our array of both planar and electrospun materials, we hoped such an assay would provide us with a more direct comparison.

Although they were not part of the ISO standard, we felt including these further studies was important in understanding whether cells could be effectively cultivated long-term on planar and electrospun samples. Figure 5.4 depicts L929 fibroblasts cultured on materials and glass over a period of 14 days in order to assess long term adhesion and proliferation. These tests provided valuable results for our future analyses.

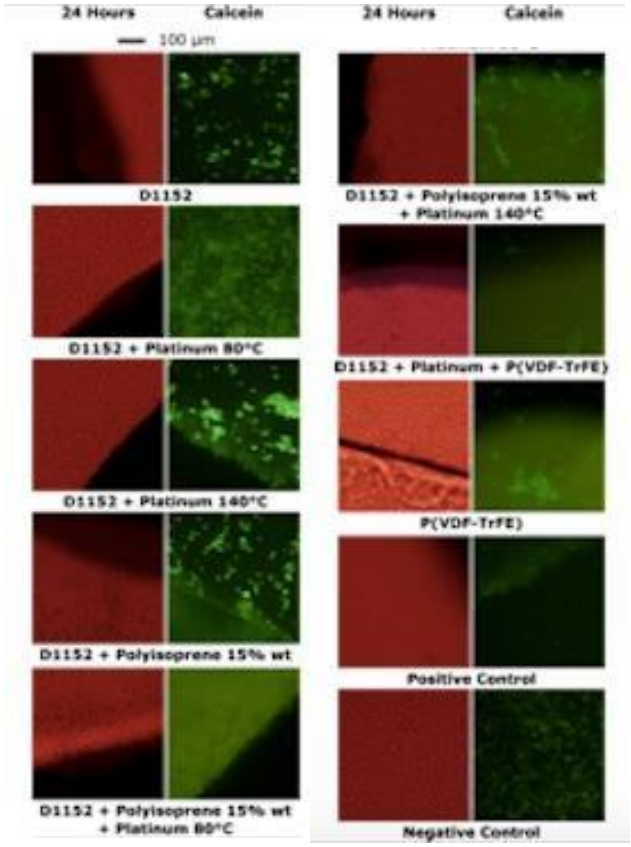

Figure 5.4: Direct Contact Assay and Calcein Staining. A long-term adhesion assay showing the viable long-term culture of L929 fibroblasts on Kraton D1152ES (SBS), Kraton D1152ES (SBS)-polyisoprene blends, and P(VDF-TrFE) at 14 days.

Long term proliferation and adhesion assays typically recommend the fixation and staining of cells and substrates. In most cases, a simple live-dead stain would work perfectly. However, it was discovered that our materials absorb immunofluorescent stains, making them complicated to analyze. Eventually, we realized that it was not the stains but the use of fixatives that were invading the substrates. This meant that live stains like calcein, as shown in Figure 5.4, allowed us to identify cells, but could not be comparatively analysed with the coupled dead stain (typically ethidium homodimer-1). Figures 5.4 and 5.5 show some of the most preliminary results we obtained, proving that live cells existed alongside samples.

We discovered that the fixation process caused the elastomeric samples to absorb dye, resulting in indistinct imaging of cells and making microscopy-based cellular analysis of our construct problematic. While no issue occurred in samples of P(VDF-TrFE) or controls, any culture attempting to utilize an elastomeric base produced fluorescence and cell-like artefacts highlighted throughout the polymer. Given the nature of our results, the next step was to determine if cells could be identified growing on or permeating our substrates. Our initial tests

were analysed by SEM, as shown in Figures 5.5 and 5.6. Cells (which had been fixed) can be seen in most samples, though they often appear obscured, resembling shadows. This was due to the lack of transparency of most materials, as well as the three-dimensional depth of fibrous constructs.

We continued with adhesion and proliferation assays, initially attempting to image the surface of our samples through different forms of microscopy. As is shown, the thickness and multi-dimensional nature of the constructs prevented us from clearly identifying cells present in or on the materials in many samples.

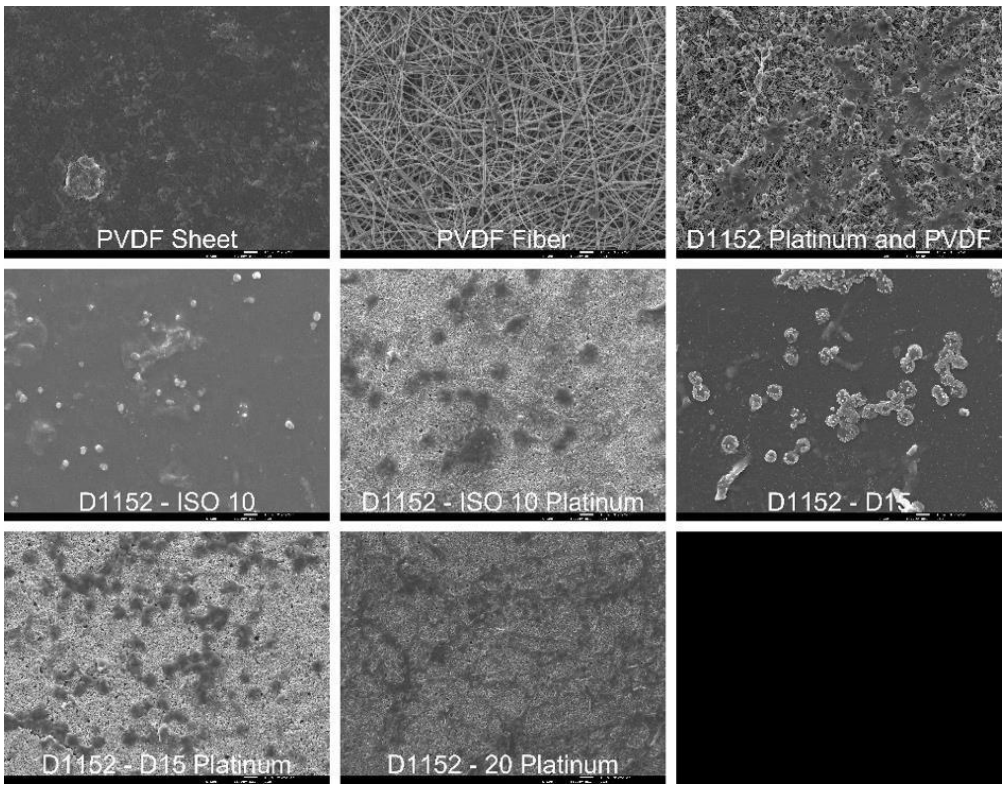

Figure 5.5: SEM of the substrates used for long-term culture of L929 fibroblasts on Kraton D1152ES (SBS), Kraton D1152ES (SBS)-polyisoprene blends, and P(VDF-TrFE) after 14 days.

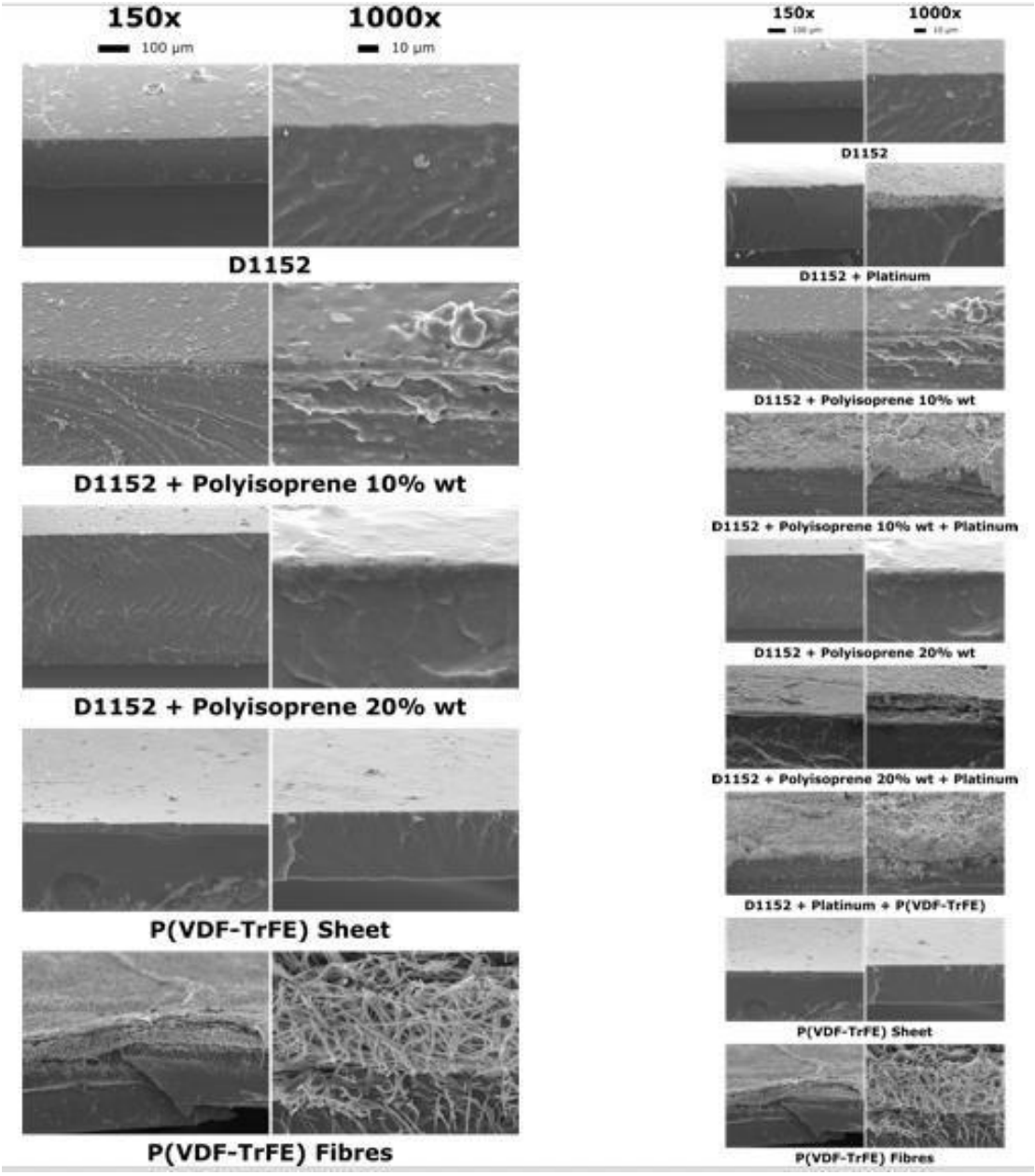

Figure 5.6: SEM Cross Sections of Adhesion and Proliferation Analysis. SEM cross-sectons of scaffolds following long-term culture of L929 fibroblasts on Kraton D1152ES (SBS), Kraton D1152ES (SBS)-polyisoprene blends, and P(VDF-TrFE) at 14 days.

Despite the existence of many cells around scaffolds on the direct contact assays, and cells suspected on scaffolds during preliminary adhesion and proliferation assays, their identification remained a mystery for some time. Calcein staining was attempted successfully, yet cells seemed to almost disappear when fixed and stained or trypsinized. When cells on scaffolds were trypsinized (in order to prepare them for FACS or other similar tests), then re-

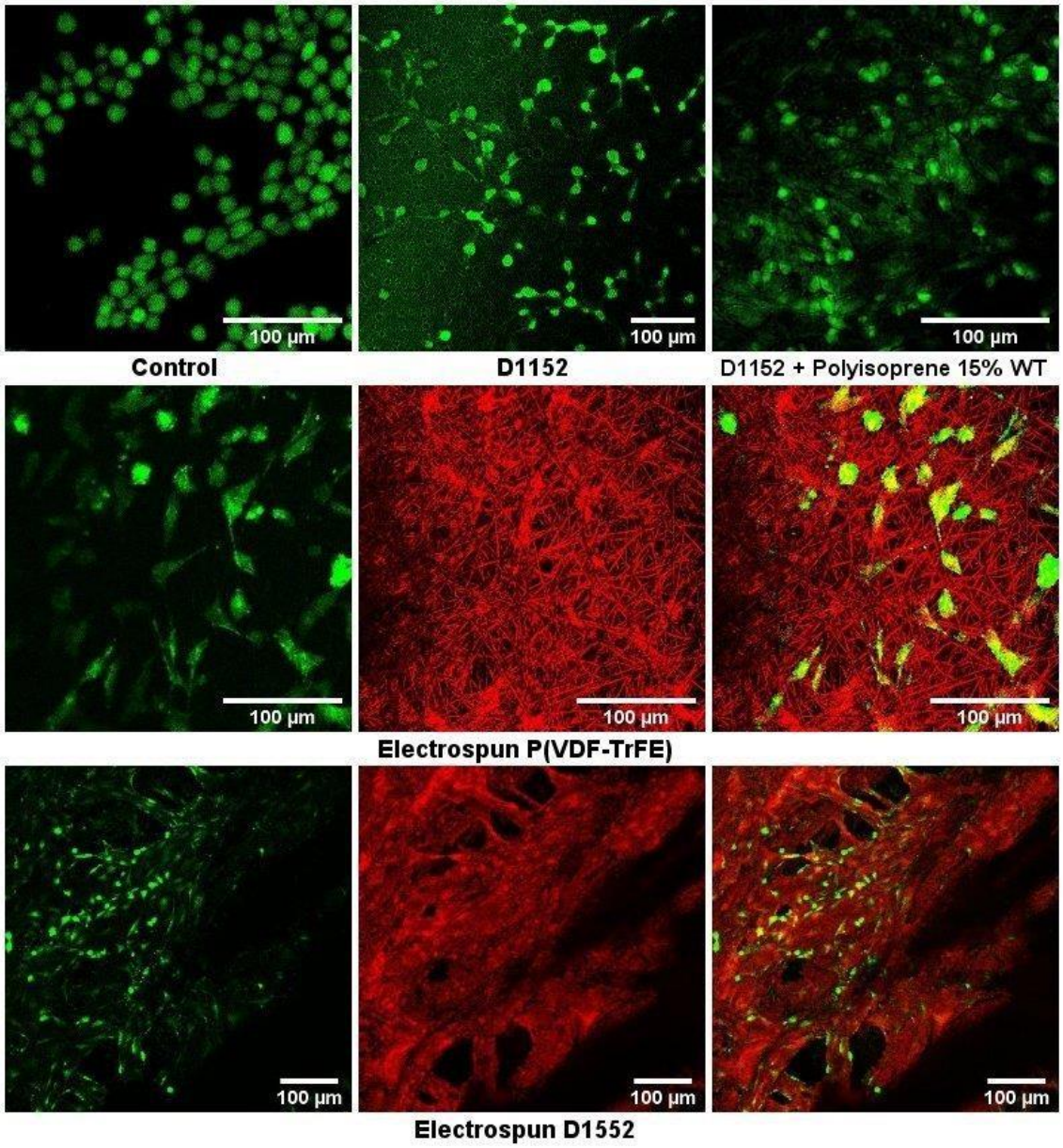

Figure 5.7: Adhesion and Proliferation Assay of Planar and Electrospun Materials through Confocal Microscopy. Confocal microscopy of L929 fibroblasts stained with alkaline phosphatase on Kraton D1152ES (SBS), Kraton D1152ES (SBS)-polyisoprene blends, and P(VDF-TrFE).

stained with calcein, stained cells were still present. We attempted to cross-section scaffolds in order to identify the location of cells, hypothesizing that they could have permeated the membrane or 3D component of the scaffold. However, cells could not be imaged any better using this method. We consequently decided that SEM was also not the appropriate method of analysing our cellular tests. We therefore continued on to confocal experiments that would enable us to visualize the cells across multiple planes. Live cell staining and confocal microscopy were found to be the most consistently reliable way to analyse these cellular experiments.

Alkaline phosphatase was used to identify and image live L929 fibroblast cells through confocal microscopy. Cells can be seen in every sample, even permeating through the 3D electrospun scaffolds and growing along their fibres, as shown in Figure 5.7. In fact, cellular adhesion and long term proliferation were comparable to culture on glass. This provides clear confirmation of the excellent biocompatibility of our base materials, both planar and electrospun.

5.4 Co-Culture Model Development

5.4.1 Justification of the Co Culture Model

Traditionally, somatosensory co-cultures are made of range of differentiated skin cells.[2-5] More advanced cultures also involve neural cells, but these cells are known for being fickle and hard to maintain. Cultivating neuronal cells alongside highly-proliferative cells or in new media is particularly challenging. This is due, in part, to the absence of valuable experimental models allowing precise control of the environment.

The cell-cell interactions between sensory neurons and keratinocytes partially resolve such issues. However, the establishment of such cocultures produces some practical problems. Neurons and keratinocytes require different external calcium concentrations for their development and proper functioning. In particular, axonal growth requires a higher calcium concentration than that occurring in epidermis, whereas keratinocytes require a low-calcium environment in order to proliferate.[9] However, the importance of a well-established co-culture—not only involving a basic two-cell culture but the creation of three-dimensional, innervated skin—cannot be understated.

The concept of an accurate, long-term somatosensory model has historically been somewhat impossible — co-cultures of cells such as keratinocytes and dorsal root ganglion cells have been successful for the last few decades, but typically, dorsal root ganglions are primary cultures and have limited lifespans. It is only in recent years that immortalized cells have come into existence—first rat, then human.[15] This novel development has meant that immortalized human dorsal root ganglions can be co-cultured alongside not only standard cell culture lines,

like fibroblasts and keratinocytes, but also neural cells important in myelination and wound healing, such as Schwann cells.

Our own decision to create a co-culture was based on the well-established understanding that skin is densely innervated with sensory neurons. These cell bodies reside within the ganglion cells dispersed throughout the human body, providing skin with varied tactile and thermal sensations.[16] This makes dorsal root ganglion cells the ideal cell type to incorporate into a somatosensory co-culture. However, these nerve fibers may differ dramatically based on factors such as myelination, conduction velocity, and size.[17, 18] It also highlights the importance of other cell types, such as Schwann cells, which myelinate neuronal cells.[19] In fact, removal of the myelinating aspect of a neural cell culture may inadvertently create a disease model and plays an important role in the malfunction of the somatosensory system.

This understanding led us to the creation of two different potential somatosensory system models with two different philosophies: a keratinocyte model with dorsal root ganglion cells to act as a basic somatosensory system model, and a more complex somatosensory system model, featuring fibroblasts and Schwann cells alongside the other two main cell types. The inadequacy of current skin cell models has been discussed previously, highlighting the importance of certain cell types - such as Schwann cells and fibroblasts - being constantly overlooked. In tissue engineering, these cells are a crucial component of cell-cell communication and the formation of morphological structures. Their importance can be seen histologically in both healthy and disease models.[19, 20] There are even well-established interactions between fibroblasts and Schwann cells, resulting in the release of cell factors that can induce morphological changes.[21] Furthermore, the interaction between Schwann cells and fibroblasts increases the ability of Schwann cells to ensheathe neurites. This is not necessary for dorsal root ganglions to achieve their final mature phenotype, but is for other neuronal cells, such as superior cervical ganglion neurons.[22]

It is recognized that epidermal keratinocytes in a culture secrete neurotransmitters that can activate peripheral sensory neurons. Consequently, the keratinocyte-dorsal root ganglion co-culture model is hardly useless, but we felt that it was inadequate as the sole focus of the development of a somatosensory system model for the aforementioned reasons. However, the keratinocyte-dorsal root ganglion model has been successfully achieved with several types of

primary cultures.[9] Together, keratinocytes and dorsal root ganglions are able to substantially affect differentiation and proliferation in a variety of ways.[25, 28] This co-culture is now a well-known model with established cell-cell interactions, release of neuropathic growth factors, and distinct morphological formations, and has even been used to further understanding of certain diseases, like atopic eczema.[9, 23-30] We felt that at a minimum, the keratinocyte-dorsal root ganglion co-culture could be used as a control model system that could help us establish the appropriate media, identify cellular structures, and validate our model.

Primary culture of keratinocytes and dorsal root ganglion cells is the most common method of producing a skin or somatosensory-based co-culture. We based our fundamental design and seeding ratios on primary rat keratinocyte and dorsal root ganglion cell co-culture (optimized in the Rajnicek lab at the University of Aberdeen and detailed in the appendix) prior to moving on to the culture of immortalized cell lines.

We utilized two types of co-cultures for the validation of the three-dimensional somatosensory construct. Both of these involved keratinocytes and dorsal root ganglion cells. We believed that an optimal somatosensory model would involve fibroblasts, keratinocytes, and dorsal root ganglion cells at a minimum. Ideally, Schwann cells could also be involved—however, an alternative approach is to involve the growth factors they release, which are sufficient to induce differentiation of neural cells. In addition to analyzing our chosen cells, we also needed to assess the role of our materials. Our chosen substrates also have the potential to provide direction for orientation and differentiation within the culture microenvironment.[35]

Modeling of the epidermis and dermis would be more complex and is only truly perfect when using skin-on-chips utilizing biopsies). These particular dorsal root ganglion cells were obtained from Drs. Ahmet Hoke and Weiran Chen from John Hopkins. These researchers were able to immortalize and characterise nociceptive dorsal root ganglion sensory neuronal lines from rats, and now humans.[15] We were able to use these immortalized human dorsal root ganglion cells alongside human keratinocyte cells to create our first co-coculture; to our knowledge, the first co-culture of immortalized human keratinocytes and dorsal root ganglions (hK-DRG). Utilizing this model presented limitations as dorsal root ganglions of this type require the presence of other cells, such as Schwann cell growth factors, in order to differentiate.

The creation of an accurate model is highly challenging particularly since, unlike the majority of other models, our models did not utilize primary cultures. However, we found that the presence of Schwann cells in this co-culture system was sufficient for the growth and differentiation of the dorsal root ganglion cells, improving our model of the somatosensory system. Schwann cells myelinate DRG neurons and are considered to be important when modeling a variety of conditions, including somatosensory pathologies like neuropathies and chronic pain.[29-32]

In summary, we created the fundamentals for the creation of two somatosensory system co-culture models, neither of which require primary cells. We focused on optimizing the culture of these cells both alone and together with one another, which consequently focused on appropriate media, appropriate seeding densities, and an attempt to understand cell-cell interactions.

5.4.2 Cell Culture Media and Co-Culture

Historically, keratinocyte-dorsal root ganglion cocultures are maintained using keratinocyte-based media due to their calcium levels. Such media are essentially supplemented Epilife medium, the standard used to sustain keratinocytes. When neural cells were cultured in these media, no specific issues were initially found—but proliferation of neural cells halted and other markers of growth, such as elongated neurites, ceased. Long-term culture of neural cells in these media were unsustainable. Attempts to confirm the long-term viability of both keratinocytes and dorsal root ganglions in co-culture confirmed the unsuitability of these media, compounded by differences in cellular growth rates. While neural cells seemed to be present and their differentiated or undifferentiated state could affect staining, long-term co-cultures in Epilife did not show the presence or expansion of neural cells (as shown in Figure 5.8).

According to Le Gall-Ianotto et al (2012), low calcium media are optimal for the co-culture of keratinocytes and dorsal root ganglions.[27] This type of medium is ideal as it allows for an analysis of the interaction between these two cell types. However, there are a wide variety of other factors involved in the selection and optimization of media. For example, Gingras et al (2003) discussed the necessary addition of growth factors like NGF for sensory neuron's neurite outgrowth, but noted that this growth factor was not critical for survival.[28] Similarly, B27 and glial cell co-culture was not essential for stable, long-term co-cultures. These studies were the basis for our own co-culture creation – although growth factors are not necessary for co-culture, they can help us create accelerated co-cultures in shorter periods of time, thereby allowing us to understand whether or not our co-culture models would be successful in longer studies. Similarly, the level of calcium in media was also critical and was optimized in our tested media.

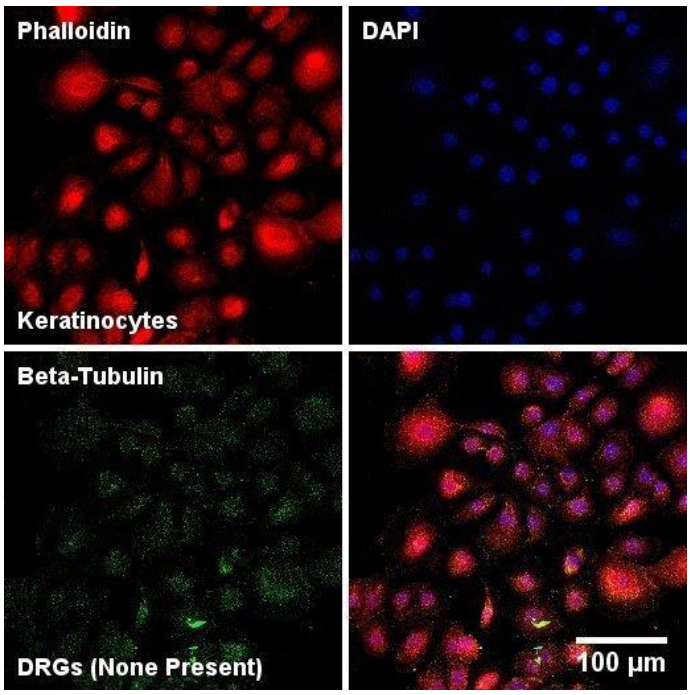

Figure 5.8: Keratinocyte-DRG in Epilife. Confocal microscopy of fixed Heka-APF and DRG cells co-cultured in Epilife media

We chose to analyze multiple media types while establishing these cocultures; some culture media caused cultures to remain planar, while others formed 3-D structures. Said structures were induced by the presence of media suited to dorsal root ganglions and Schwann cells; essentially the presence of the aforementioned growth factors. There were no such structures seen with fibroblasts or keratinocytes or co-cultures utilizing fibroblast or keratinocyte media alone. Excessive formation of these structures eliminated the presence of keratinocytes in the

culture, making the model unrealistic for somatosensory system analysis. However, these morphological differences were most likely not due to media alone. According to Tsutsumi et al., keratinocytes and dorsal root ganglion cells are capable of generating a wide variety of structures depending on the seeding conditions. Whether or not cells are plated together or in sequence (essentially plating the second type of cells on top of the first, already adherent cells) can also play a major role in structure formation.[22, 25]

Analysis of the cell cultures in various media showed that viability was much improved when a 2:1 ratio of Epilife to DRG medium was used to seed the cells. This particular ratio of media allowed for the growth of all cell types while allowing neurons to be retained in culture long term. Most importantly, it established the adherence of cells initially upon seeding and ensured the presence of all necessary growth factors. Structural formation only occurred when culture density was quite high, showing cellular growth in sworl-like clusters, rather than an even, planar spread typical of cell culture. Growth was found to be preferential in regions prone to forming structures in high-density cultures. This medium allowed for adherence of multiple co-culture types (complex: fibroblast-keratinocytes-dorsal root ganglions-Schwann cells vs simple: keratinocyte-dorsal root ganglions). Furthermore, it allowed for these cells—usually difficult to passage repeatedly and retain in the accurate proportions—to be retained and reseeded over multiple passages. Dense co-culture structures are shown in Figure 5.9. Areas that lack structural formation are primarily populated by keratinocytes. Penetration of these populations by neuronal cells is to be expected over time.

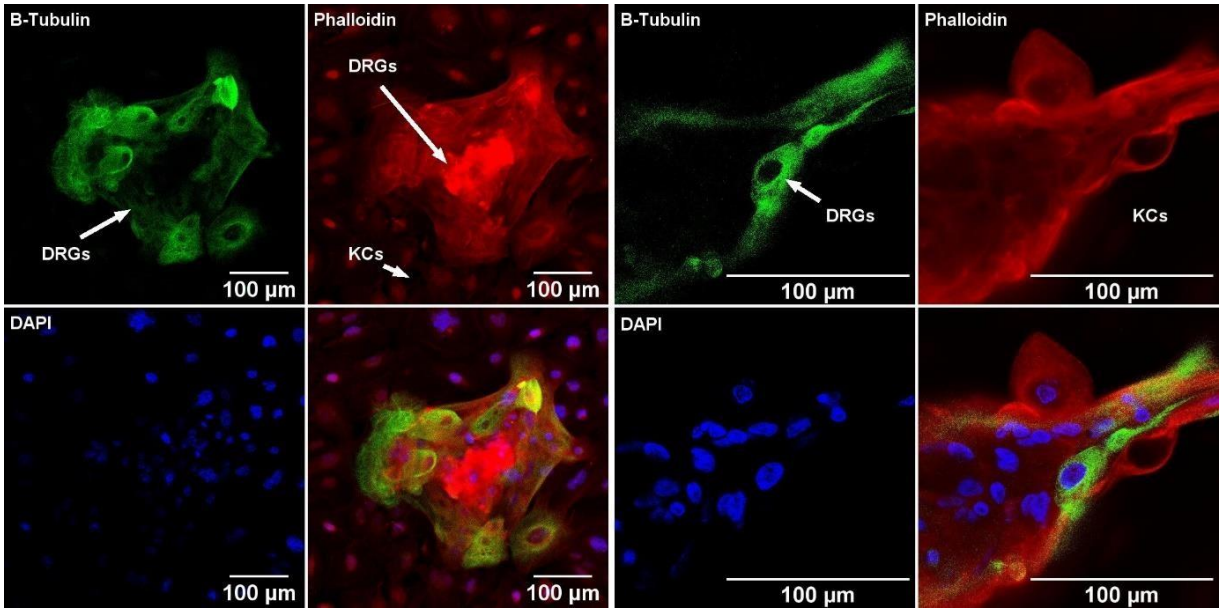

Figure 5.9: Mixed Media Culture of Keratinocytes and Dorsal Root Ganglion Cell. Confocal microscopy of fixed Heka-APF and DRG cells co-cultured in mixed media (Epilife-DRG).

Despite our progress with this cell model system, the struggle with using this co-culture was due to analysis on actual constructs. We were restricted to using live-cell staining in order to avoid the autofluorescence issues caused by our materials. While we were able to assess a variety of stains, including neural cell stains, progenitor-cell stains, and universal stains (such as cell trackers), we found that these stains did not stain differentially when used as live-stains (although they did when used in the traditional fixative method). This meant that we were unable to differentiate between cells like Schwann cells and DRGs due to our lack of markers. Similarly, we were unable to differentiate DRGs from keratinocytes. While we attempted to rectify this issue, we assessed all of our chosen cells alone in an attempt to observe morphological differences.

Our primary concerns were finding a way to differentiate between neuronal cells like Schwann cells and dorsal root ganglion cells, and skin cells like fibroblasts and keratinocytes. Our original hope was that the live cell stains would be able to help us differentiate between these cell types, considering that both of these cells are not considered to be progenitors though they are both of neural origin. Unfortunately, as shown in Figure 5.10, Schwann cells (and other neural cells) did not stain positive when utilized as a live neural-cell stain. Although the Nissl neurotrace stain (depicted in red in Figure 5.10) is present, but does not seem to stain the cell bodies like the alkaline phosphatase (AP) progenitor stain.

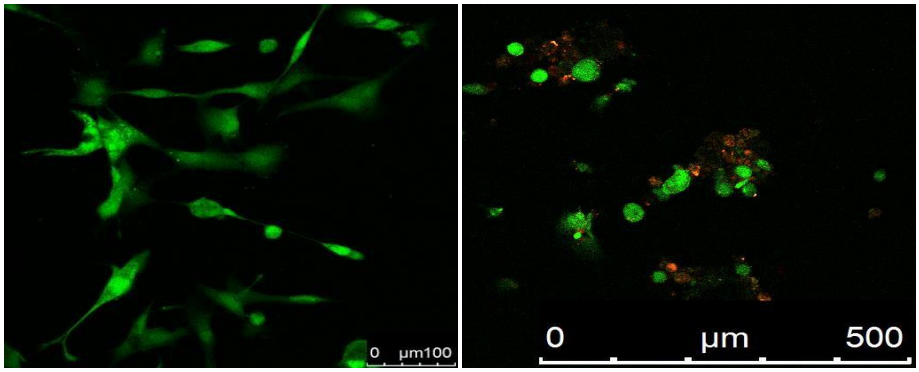

Figure 5.10: Schwann Cells on Glass (AP and Nissl Live Stain). Confocal microscopy of Schwann cells stained with AP and Nissl live stains. AP is shown in both left and right images; Nissl staining is only shown on the image on the right.

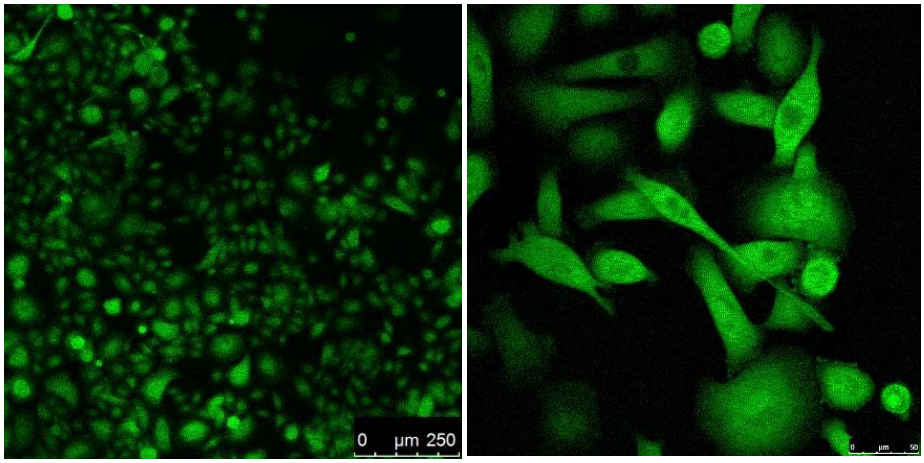

Figure 5.12: Keratinocytes on Glass (CMAC Stain). Confocal microscopy of keratinocyte cells stained with CMAC live stain.

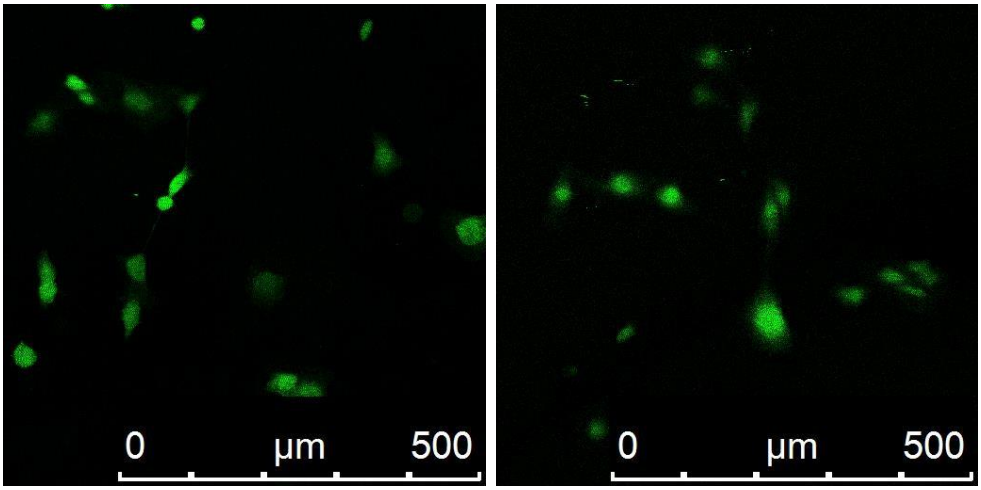

Figure 5.11: Dorsal Root Ganglion Cells on Glass (AP Live Stain). Confocal microscopy of dorsal root ganglion cells stained with AP live stain.

As shown in images of single cell populations, the AP stain also did not function as intended. This stain was found to stain all cell populations, as is shown later throughout this section. Despite this, clear staining of the Schwann cells allowed us to assess the morphology of this cell type. The dorsal root ganglions, stained in the same manner, are shown in Figure 5.11. They are clearly different from one another when kept in separate populations, and were found to grow at substantially different rates. However, comparing more than two populations of cells (e.g., the fibroblasts, as shown in the control of Figure 5.10, Schwann cells in Figure 5.10, dorsal root ganglions shown in Figure 5.11, and keratinocytes shown in Figure 5.12) was impossible using only a morphological analysis. This made the concept of a four-cell construct unusable, despite its physiological accuracy.

To continue our validation of this model while taking these limitations into consideration, we took an alternative approach. The adhesion and proliferation assay that had been performed with the fibroblasts was repeated and expanded upon utilizing our other two main cell types: keratinocytes and dorsal root ganglion cells, which is discussed in section 5.5. The keratinocytes, as shown in Figure 5.12 are typically cultured using a collagen or fibronectin base. In our case, we utilized a collagen-fibronectin pre-coating on all surfaces, regardless of whether they were glass or polymer, to enhance adherence. The coating is critical to the culture of these cells; keratinocytes cultured without this coating did not grow and would not migrate to surfaces that had not been coated.

This result was exaggerated on the polymeric constructs due to their hydrophobicity, making them quite distinct from fibroblasts. Keratinocytes also formed certain morphological agglomerations, expressing clear and unique growth patterns compared to fibroblasts and even the cells of neural origin. Notably, once coated, a material can be re-used—even following trypsination and other methods. The only way to remove the coating is seemingly through abrasion—as shown in the scratch analysis in section 5.4. In can be assumed that the combination of the collagen-fibronectin coating and the natural morphological agglomerations were contributing factors to the structures previously shown.

5.5 Scratch Assay of Co-culture Model

Our final validation of our co-culture model utilized a wound healing model in order to assess how cells would interact in mixed media cultures following injury. Realistically, cell-cell interactions in physiological models are crucial to wound healing. Neuropathic damage of the somatosensory system always involves neural cells such as dorsal root ganglions; often it is the myelination (or lack thereof) involving Schwann cells that causes side effects such as neuropathic pain. Poor signalling, presenting as somatosensory issues (e.g., burning, stinging, aching) occur in the surrounding areas, implying underlying nerve damage.

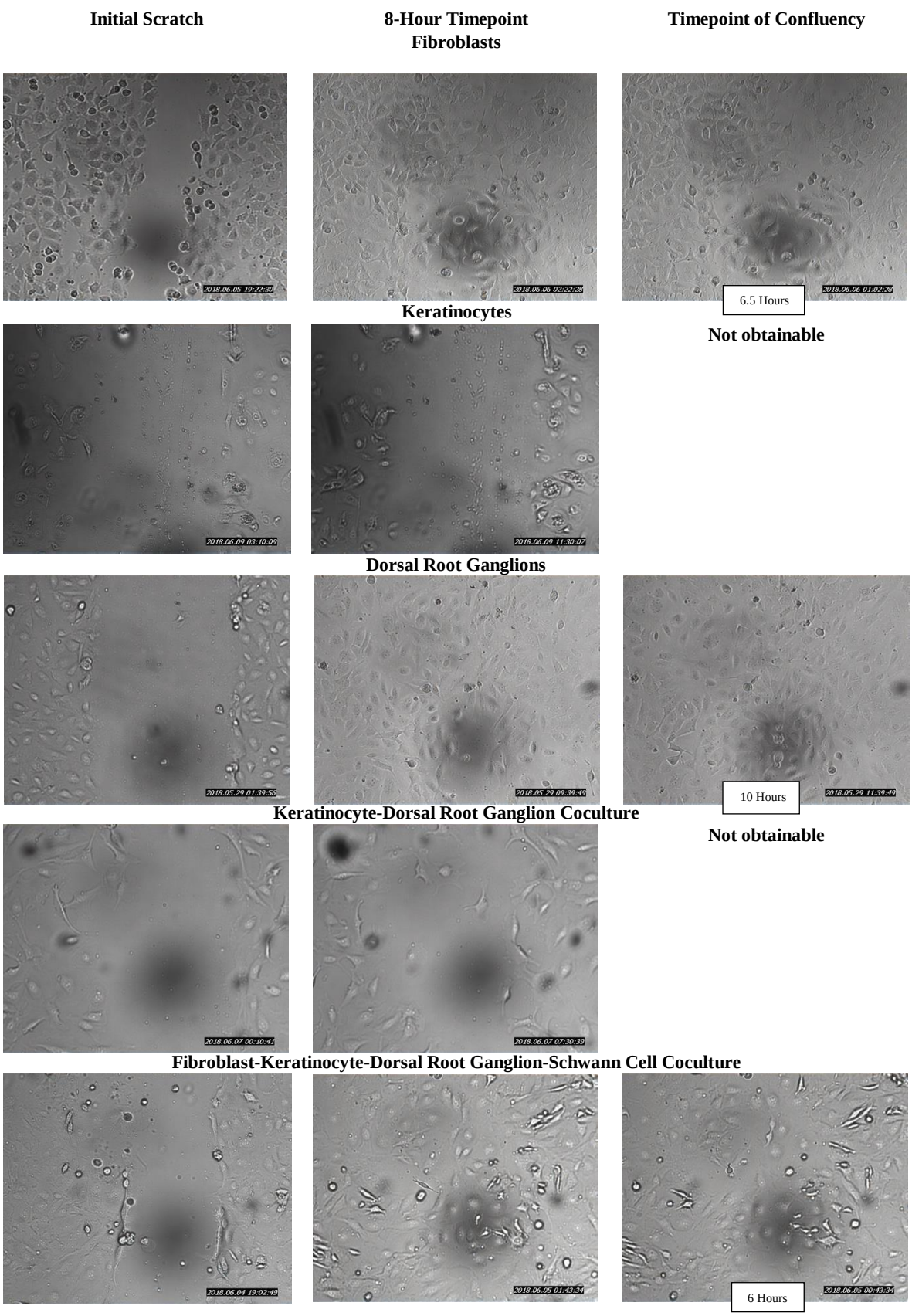

Figure 5.13: Wound Healing Analysis

Through the scratch analysis in this section, we wished to see the responses of individual cells, as well as co-cultures of cells and complex cultures. Given the novelty of these cells, both individually and in the form of co-cultures, we wished to assess their responses to injury. In all cases, we simply wished to validate the occurrence of cell migration across a site of injury and calculate the speed at which this occurred. The results of these experiments highlighted the importance of the substrate coating for keratinocytes, importance of myelinating Schwann cells in wound healing, and speed of fibroblast growth—all important factors in setting up our co-cultures for long-term growth.

Figure 5.13 shows cells individually cultured alongside a simple co-culture (keratinocyte-DRG) and complex co-culture (fibroblast-keratinocyte-DRG-Schwann cells). An extension of this work would involve the complex co-culture, which is a more realistic and representative model of the somatosensory system. However, given our issues with imaging (discussed in the previous section) we primarily pursued the simple co-culture model. A similar wound healing analysis was also attempted utilizing our constructs and live-cell stains, but the microscope was not able to image cells on these constructs due to their dense nature. An alternative approach, utilizing confocal microscopy to assess cells at fixed timepoints (not shown) was also attempted—but cells were found to be minimally affected. This phenomenon is discussed later on in this chapter. Consequently, this section only details a validation of wound healing of our co-culture on tissue culture substrates. All wounds were made using a 20-200 ul pipette tip and monitored for 8 hours or up to one full day, if necessary.

Figure 5.13 highlights the comparatively rapid growth of fibroblasts, cells with long-standing repute for being easy to grow, maintain, and expand. Within 6.5 hours the wound was fully sealed and cells had returned to complete confluency. Minimal changes occurred between 6.5 and 8 hours. In contrast, keratinocytes scratched showed proliferation at the 8 hour timepoint, but no migration into the wounded site, even after a full 24-hour period of monitoring the wound. Given the sensitivity of keratinocytes to substrate coatings, the issue here may more likely be related to the lack of fibronectin and collagen rather than the migratory ability of the cells themselves. Neural cells dorsal root ganglions had no such issues, and good migration was seen at the 8 hour time point. These cells only achieved confluency at 10 hours. Schwann cells grew slowly and struggled to grow independently; the data for these cells is not shown in this figure as a control.

Co-cultures of keratinocytes and dorsal root ganglions experienced a similar issue to keratinocytes alone; migration can be assumed to be based on the neural cells rather than keratinocytes given the control's results. Confluency in this case was not achieved, meaning that cell-cell signalling within the co-culture impeded wound healing or that fewer neural cells were surviving within this culture. The larger Fibroblast-Keratinocyte-Dorsal Root Ganglion-Schwann cell co-culture had no issues with wound healing; this tissue-like co-culture was able to proliferate at a faster rate than fibroblasts alone (6 hours). Staining is not shown to define which cells are which in the image, but appears to be depicting mixed migration based on morphology. Given Schwann cell's importance in wound healing and neural cell myelination, this supports our hypothesis; these results highlight the importance of using full co-cultures in tissue modeling and future studies.

5.6 Validation of the Construct Using Human Somatosensory System Cells

Given the fact that fibroblasts were able to be cultured on various planar constructs and electrospun substrates (Figure 5.10), validation of the complete construct was necessary. Figure 5.14 shows L929 fibroblasts seeded on the construct, with images depicting where on the construct cells can be found, as well as the corresponding overlay of cells on electrospun fibers of P(VDF-TrFE) (shown in red) and on the platinum-based region of the polymer, coated in platinum (shown in green). Figure 5.14 shows that the majority of cells in both aligned and random constructs can be found on the planar surface, indicating that fibroblasts have preference for planar substrates over electrospun substrates. However, despite this, there were distinctly more cells on aligned fibers than random ones.

Keratinocytes assessed in the same way expressed the opposing preference. Figure 5.15 shows keratinocytes primarily adherent to the platinum-coated polymer on aligned constructs, but evenly distributed between the platinum-coated polymer and electrospun fibers in the random construct. Keratinocytes had been previously shown to preferentially form certain types of morphological agglomerations. As they reached confluency on constructs, they seemed to prefer structures that did not impede their desired growth patterns. Aligned fiber constructs were consequently found to be undesirable in comparison to random fiber constructs and/or

platinum-coated planar substrates. Both substrates were coated with collagen-fibronectin solution; this was not a determining factor.

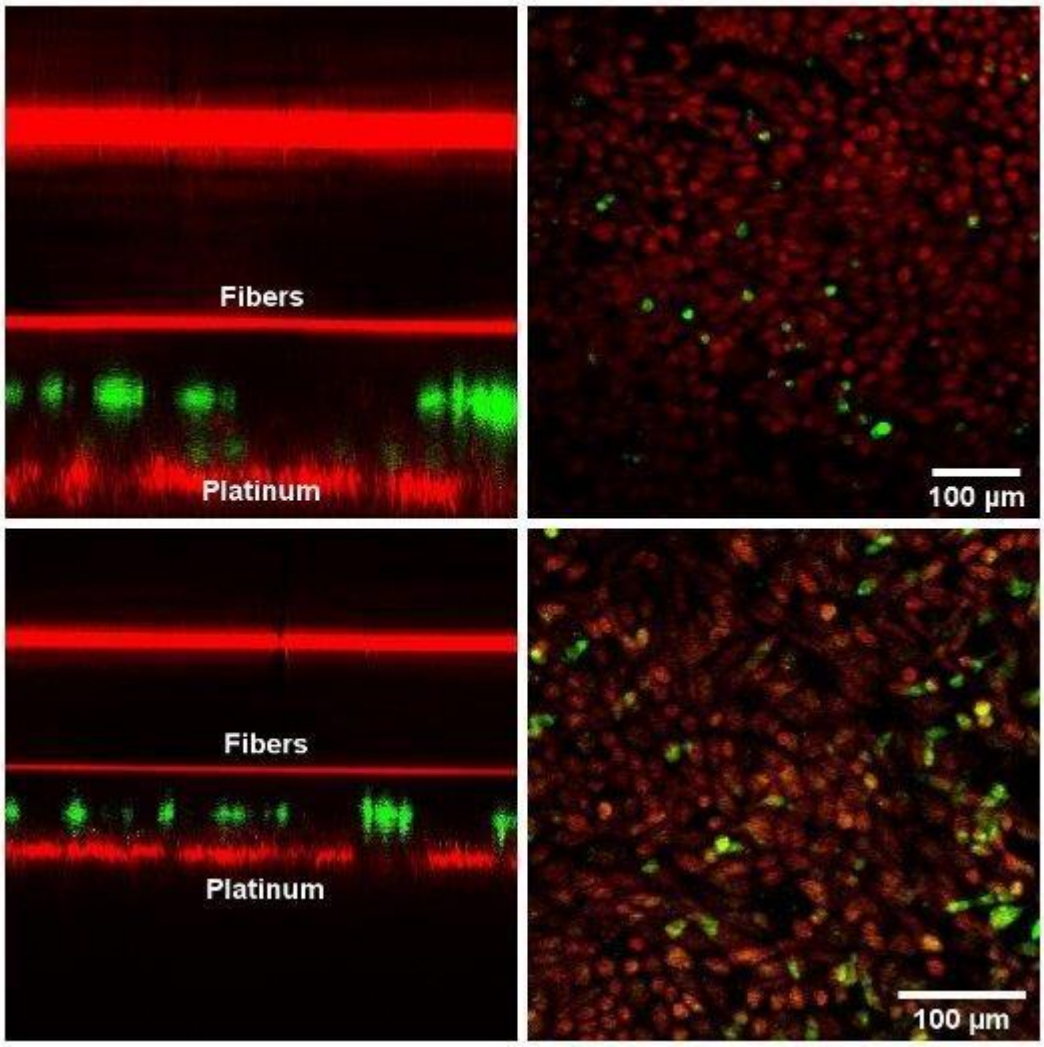

Figure 5.14: Fibroblasts on Aligned (Top) and Random (Bottom) Full Construct. Confocal microscopy L929 fibroblasts. Cells can be seen penetrating the fibrous layer of the scaffold, adhering primarily between the fibrous and platinum layers.

Dorsal root ganglion cells (depicted in Figure 5.16) alone also presented no issues on the full construct. They were shown to grow on both fibers and platinum-coated polymer, but present in different manners based on the substrate they had adhered to. Typically, neurons are meant to preferentially adhere to fibers. This was observed; however, other adherent neurons could be seen as ball-like structures on the planar substrate. Proliferation on these constructs was found to occur at a much slower rate compared to tissue culture substrates. However, clear morphological differences were found even between tissue culture substrates and planar polymer.

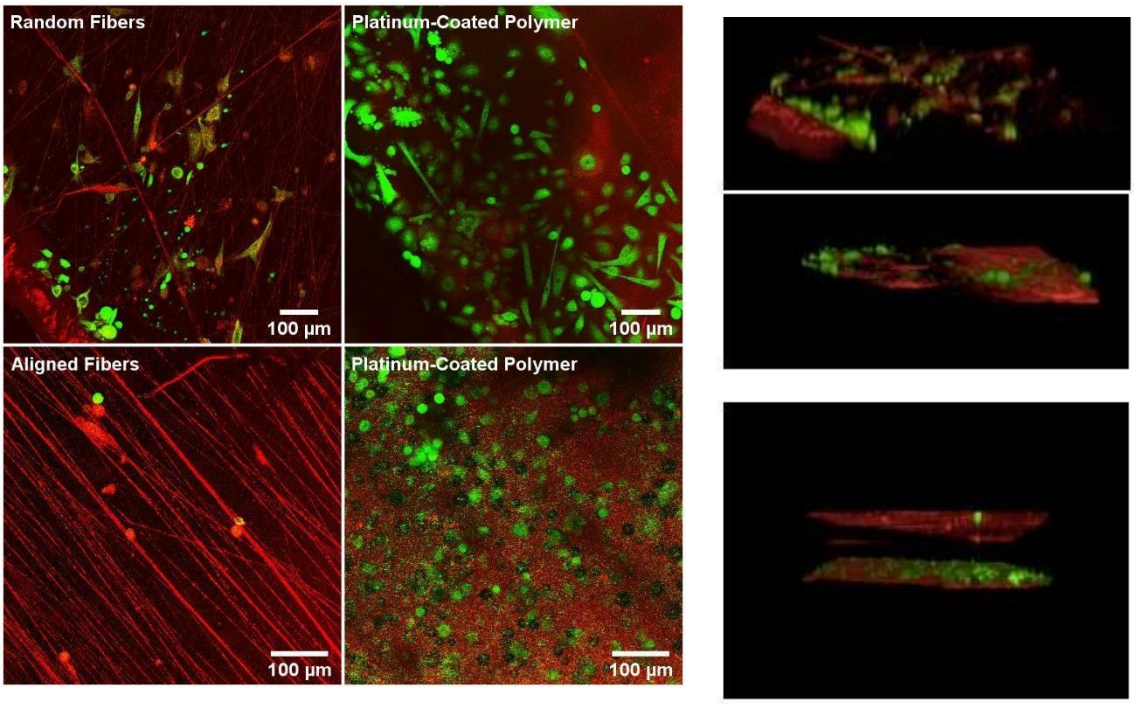

Figure 5.15: Keratinocytes on Random (Top) and Aligned (Bottom) Full Construct. Confocal microscopy of Heka-APF cells on the full construct. Heka-APF cells preferentially adhere to the planar platinum-coated construct or random P(VDF-TrFE) fibers.

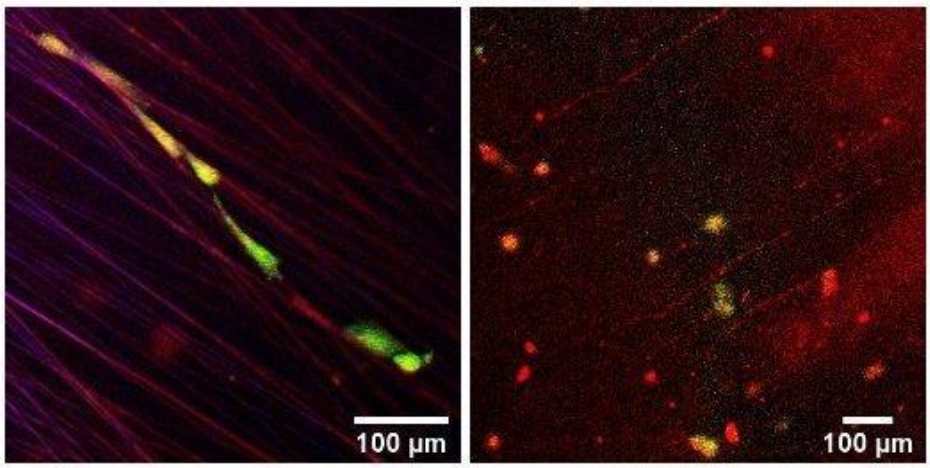

Figure 5.16: Dorsal Root Ganglions on Complete Construct. Confocal microscopy of DRG cells on aligned fibers, highlighting the preference for neuronal cells to adhere to aligned fibers though cells are also seen on the platinum layer.

Our assessment of the co-culture on our constructs was much more complete, looking at the individual polymer, platinum-coated polymer, and full constructs. Figure 5.17 shows both controls in the style of the adhesion and proliferation assay, depicting live cell staining of the keratinocyte-dorsal root ganglion co-culture on planar substrates (left) and platinum-coated

planar substrates (right). Adherence was not an issue on either of these controls; however morphology was clearly different between the two. Cells were adherent to both substrates, but cells on the planar substrate proliferated and formed stronger bonds with one another than the substrate, while platinum-coated substrate provided an adherent surface for cells to attach to.

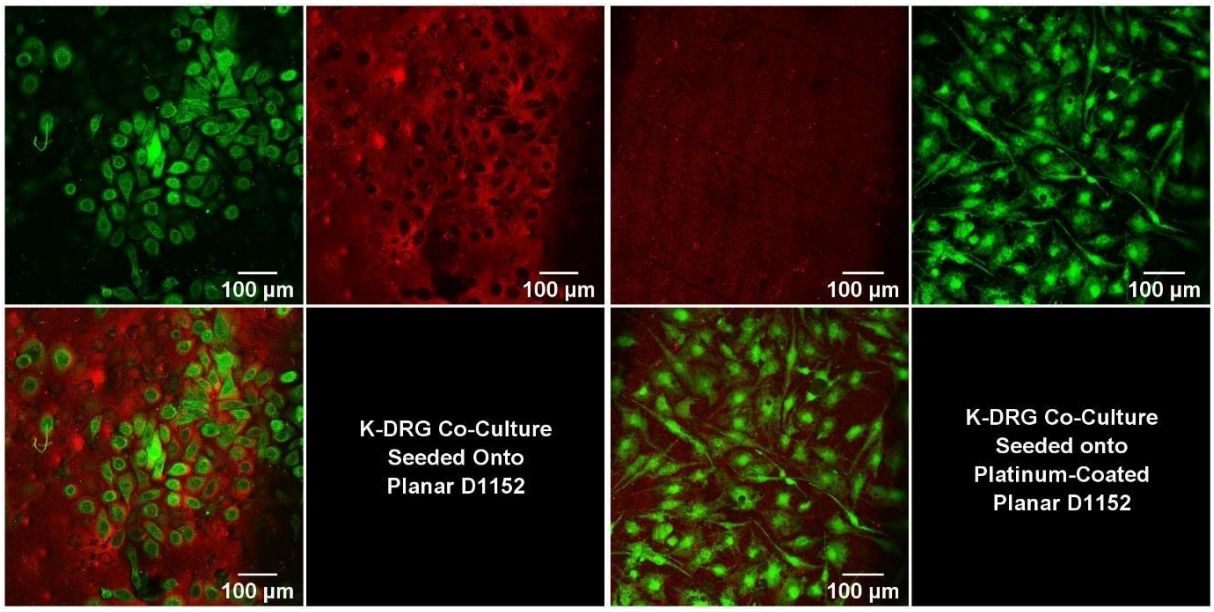

Figure 5.17: Keratinocyte-Dorsal Root Ganglion Co-Culture on D1152 & Platinum-Coated D1152. Confocal microscopy of keratinocyte and DRG co-culture showing adherence of cells to both Kraton D1152ES (SBS) (left) and polymeric platinum coated Kraton D1152ES (SBS) (right).

We found that on certain planar substrates a secondary biological scaffold formation was occurring, despite being identical to platinum-coated substrates in every respect besides the platinum coating. This far surpassed the cell structures seen in previous figures; scaffold formation was so substantial that these structures were forming sheets of skin-like structures and peeling of the elastomer in their entirety. These cells, which were clearly conglomerating rather than spreading and adhering as they would normally, had naturally unattached from the majority of the substrate as they proliferated and spread. The tissue structure and cells within can be seen in Figure 5.18. Collagen-fibronectin stained equally along with cells, making this structure difficult to image and too fragile to fix and re-stain, but a noteworthy phenomenon promoting additional potential uses for the D1152 polymer. The natural encapsulation and release of complete tissue structures could potentially present an alternative way of creating skin for burn victims or 3-D cultivation systems more representative of skin. Clearly, this type of analysis requires further investigation.

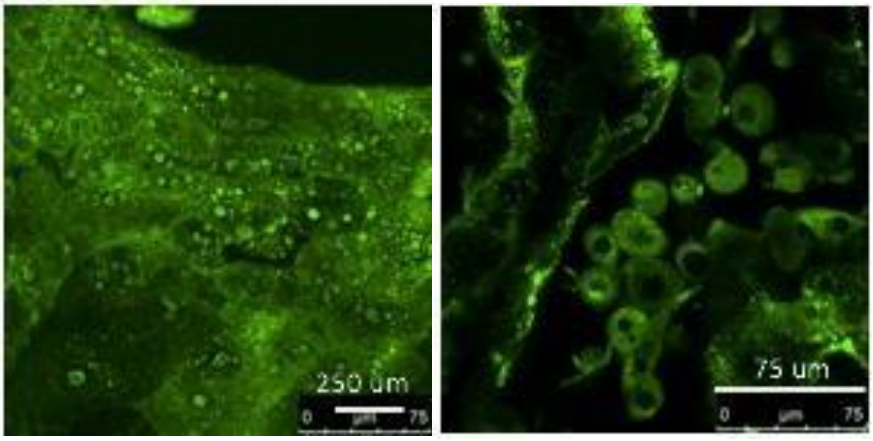

Figure 5.18: Keratinocyte-Dorsal Root Ganglion Biological Scaffold Formation. Confocal microscopy of the biological scaffold formation resulting from long-term keratinocyte-dorsal root ganglion co-culture on Kraton D1152ES (SBS).

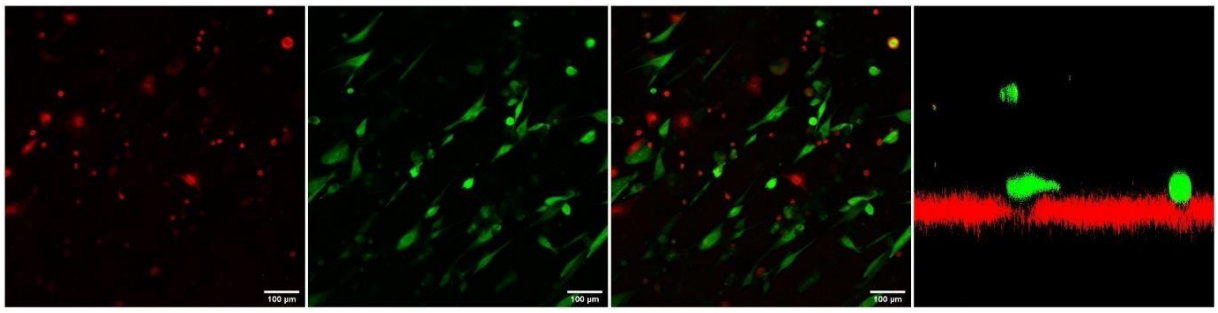

Figure 5.19: Keratinocyte-Dorsal Root Ganglion Co-Culture on Aligned Complete Construct. Confocal microscopy of keratinocyte-dorsal root ganglion co-culture cells on aligned construct. Cells are seen adherent to both platinum-coated polymer (left) and fibers (second from left); overlay is the second from right. Microscopy allows the visualization of cells sinking into soft substrate, potentially highlighting cellular encapsulation.

Ultimately, the complete construct was able to support both keratinocytes and dorsal root ganglions in co-culture regardless of whether fibers were aligned or random. Cells were also shown to grow on both the platinum layer and the electrospun substrate. No structural formation occurred in this case; the presence of the nanostructured electrospun fibers seemed to prevent any such phenomena. We were not able to differentiate between the keratinocytes and dorsal root ganglion cells at this time due to the aforementioned problems with differential staining and fixation.

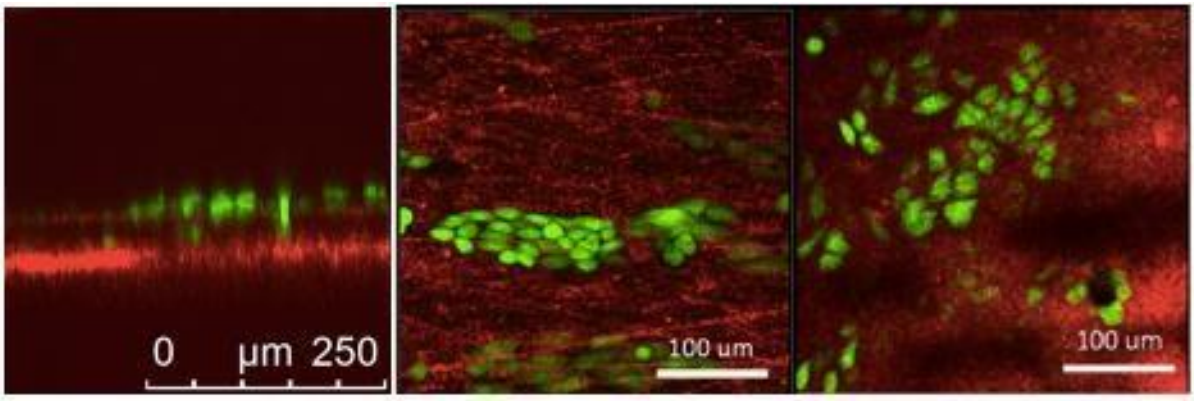

Figure 5.20: Fibroblast-K-DRG-Schwann Co-Culture on Aligned Complete Construct, Confocal microscopy of keratinocytes, DRGs and Schwann cells on the aligned complete construct. Bundles of cells are seen to form in structures throughout the construct, following the alignment of the fibers.

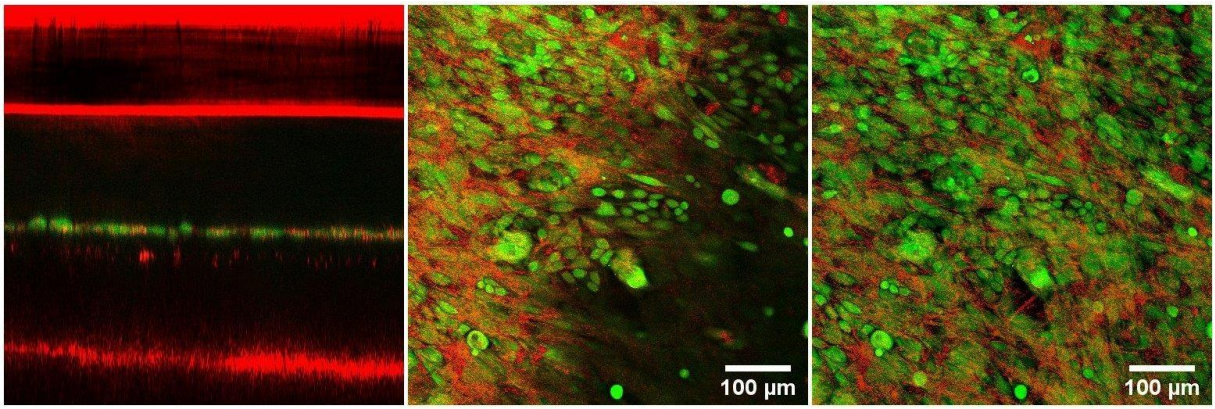

Figure 5.21: Fibroblast-Keratinocyte-DRG-Schwann Co-Culture on Random Complete Construct. Confocal microscopy showing the dispersion of keratinocytes, DRGs, fibroblasts, and Schwann cells on the random complete construct.

The same assessment was performed with the complete co-culture of cells in the interest of discovering any potential morphological differences. Structural formation was much more evident, and while aligned constructs allowed an even distribution of cells both on the polymeric platinum substrate and electrospun fibers, random constructs resulted in the formation of dense cellular structures that preferentially adhered only to the electrospun layer.

As cells were cultured for longer durations, increasingly defined structures formed, though these were somewhat more complex than those that had been reported in the literature previously.[18, 25] Although the staining is not differential, the presence of such reticular structures are meant to encourage neuronal growth and we can assume that an even distribution

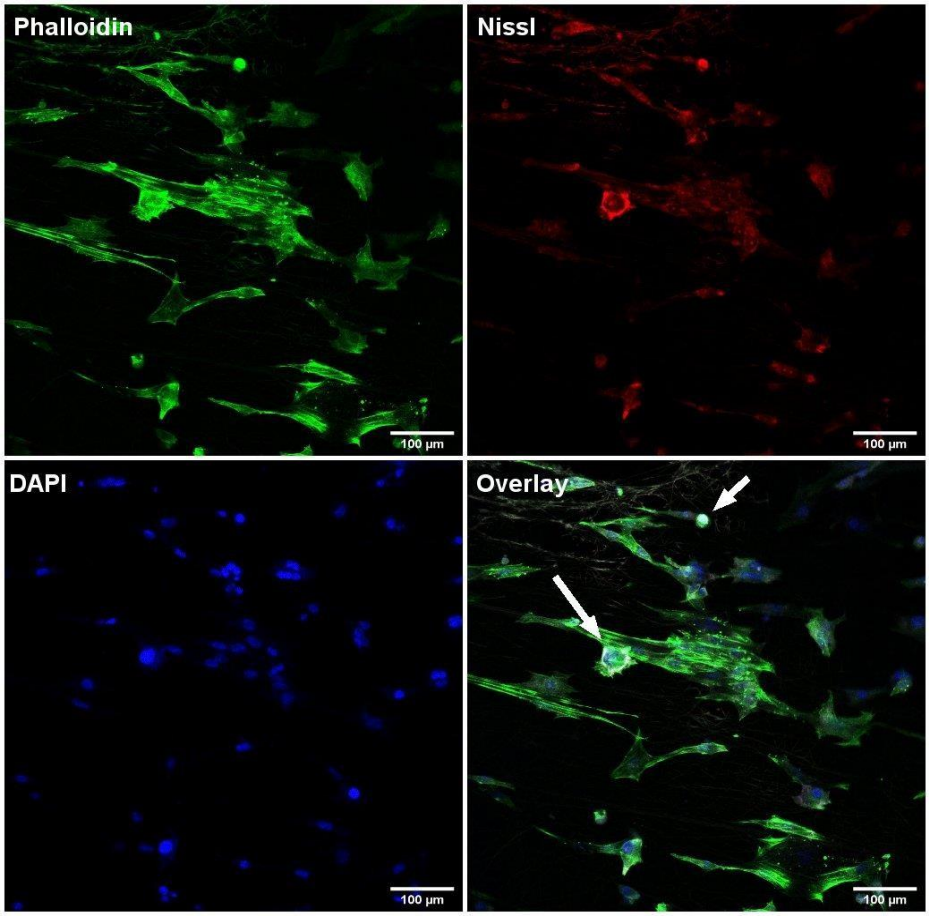

Figure 5.22: Fixed Fibroblast-K-DRG-Schwann Co-Culture on Complete Construct. Confocal microscopy of fibroblast, keratinocyte, DRG, and Schwann cells co-cultured and fixed on construct. Fixed staining supports the identification of neuronal vs. non neuronal cells through Nissl and Phalloidin staining.

of cells has survived in the population long-term for the maintenance of these structures. One sample of this four-cell co-culture was also able to be fixed and stained — insufficient for this complex construct, but proving that there were neural cells present amongst keratinocytes and fibroblasts. Figure 5.22 shows that there is potential to fix these constructs in BSA over short periods and stain differentially in order to image neuronal and non-neuronal cells. This will prove essential for the validation of future research utilizing these scaffolds, particularly any electrical field experiments or expansion and differentiation assays.

Furthermore, suitable dyes must be identified; stains such as the Nissl neuronal stain are not meant to be used in fixatives such as BSA, explaining the dampened signal present in Figure 5.22. Ultimately, cultivation of this co-culture on the electrospun construct would also be performed long term to see if tissue formation and unattachment is also a possibility, as with the planar uncoated construct shown in Figure 5.21.

Electrical Field Experiments

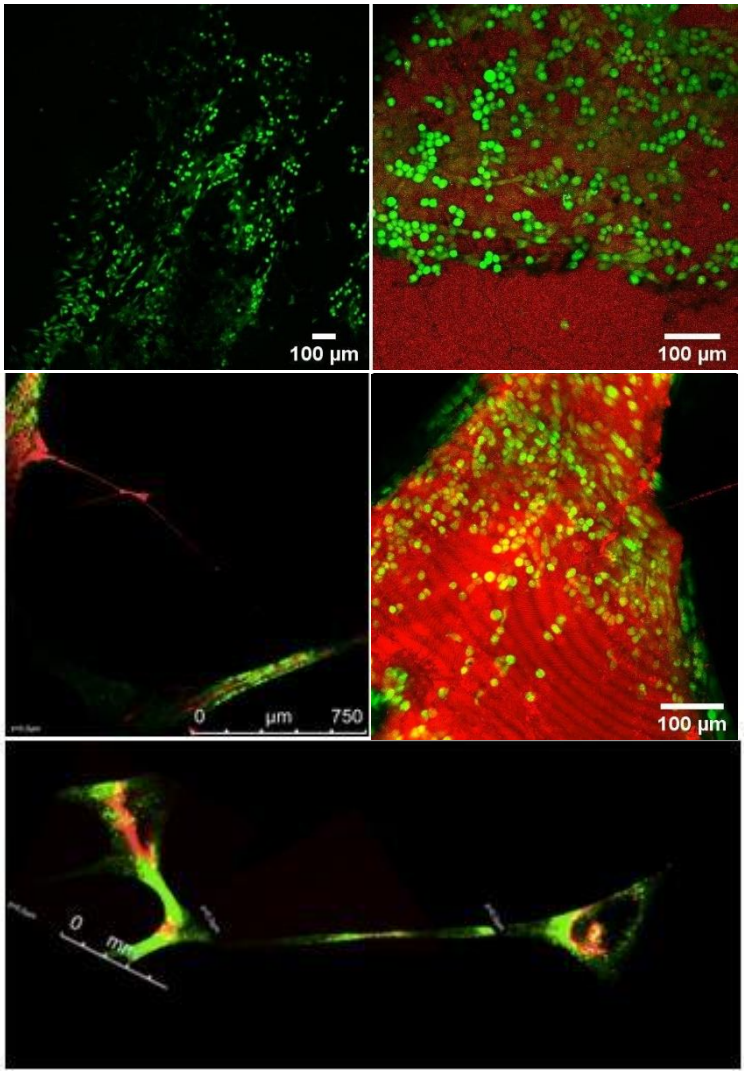

Figure 5.23: Electrically-Stimulated Fibroblast-K-DRG-Schwann Co-Culture on Aligned (Top) and Random (Bottom) Constructs.Electrically stimulated fibroblast-keratinocyte-dorsal root ganglion-Schwann cell co-culture, highlighting the formation of macroscopic structures after stimulation.

Neural cell differentiation is often performed alongside electrical-stimulation expansion experiments.[33] Our inability to analyse cells on our scaffolds extensively made such experiments in the context of somatosensory system co-cultures fairly limited. The only judgement expected was qualitative expansion and validation that electrical stimulation would not destroy the cell culture. However, the ease with which these co-cultures created tissue structures may also be a component. Figure 5.23 shows this co-culture seeded on aligned constructs (top) random constructs (middle and bottom) and the consequent tissue formation (bottom) that was found to occur along the path that fibers traversed. No such fiber formation occurred on random fiber constructs; only aligned.

5.7 Conclusions

This chapter provides a substantial amount of positive preliminary data to support the electroconductive elastomers created in this thesis. It highlights the wide range of applications, from engineering of 3-D tissues to cellular expansion, that polymer D1152 and its derivatives can provide bioengineers with. Ultimately, to further this data, one main problem must be addressed: a lack of suitable staining techniques. Whether this issue is addressed by utilizing more specific live-cell stains or by fixation utilizing BSA-friendly cell markers, it is essential to find suitable methods of staining in order to understand the structural formation, cellular differentiation, and cellular migration occurring in samples. Ideal markers would highlight the varied range of keratinocytes and neurons in culture, rather than act as broad-spectrum markers.

An alternative approach to this issue would be to find a secondary method of analysis. However, the inability to remove cells from the substrates through typical techniques requires the creation of a special methodology to be developed in order to attempt other traditional analytical techniques, such as FACS. Despite this, other alternatives may be used now that the formation of tissue is able to self-release; while the population of cells is incomplete, fixation and analysis of such tissue structures is now possible. Such tissues can be digested and analysed through FACS and other similar methodologies. Histological assessments, both of the complete construct with adherent cells and the tissues, are also potential options for further assessment.

Ultimately, the nanofibrous, electroconductive elastomer has provided a unique substrate with the potential for a multidisciplinary range of applications. However, crucial hurdles related to the analysis of both co-cultures and seeded scaffolds must be overcome before this material can be utilized as an implantable. Miniaturization of other similar devices, such as vagus nerve stimulators are made of similar materials and allow for long-term implantation. Analysis of these materials as they are removed from patients may allow us to gain an understanding of how our own materials would interact in the body.

5.7 References

1. Edwards, Christopher, and Ronald Marks. "Evaluation of biomechanical properties of human skin." *Clinics in dermatology* 13.4 (1995): 375-380.
2. Hayden, P. J., et al. "Epiderm (TM) full thickness (Epiderm-FT), a dermal-epidermal skin model with a fully developed basement membrane." Toxicological Sciences. Vol. 72. OXFORD UNIV PRESS, 2003.
3. Yun, Ye Eun, et al. "Artificial skin models for animal-free testing." *Journal of Pharmaceutical Investigation* (2018): 1-9.
4. Rademacher, Franziska, et al. "Skin microbiota and human 3D skin models." *Experimental dermatology* 27.5 (2018): 489-494.
5. Bergers, Lambert IJC, et al. "Immune-competent human skin disease models." *Drug discovery today* 21.9 (2016): 1479-1488.
6. Wufuer, Maierdanjiang, et al. "Skin-on-a-chip model simulating inflammation, edema and drug-based treatment." *Scientific reports* 6 (2016): 37471.
7. Wagner, Ilka, et al. "A dynamic multi-organ-chip for long-term cultivation and substance testing proven by 3D human liver and skin tissue co-culture." *Lab on a Chip* 13.18 (2013): 3538-3547.
8. Roggenkamp, Dennis, et al. "Epidermal nerve fibers modulate keratinocyte growth via neuropeptide signaling in an innervated skin model." *Journal of Investigative Dermatology*133.6 (2013): 1620-1628.
9. Ulmann, Lauriane, et al. "Trophic effects of keratinocytes on the axonal development of sensory neurons in a coculture model." *European Journal of Neuroscience* 26.1 (2007): 113-125.
10. Müller, Franciélli, et al. "New sulfonated polystyrene and styrene–ethylene/butylene–styrene block copolymers for applications in electrodialysis." *The Journal of Physical Chemistry B* 116.38 (2012): 11767-11779.
11. Elkovitch, Mark D., L. James Lee, and David L. Tomasko. "Effect of supercritical carbon dioxide on PMMA/rubber and polystyrene/rubber blending: Visosity ratio and phase inversion." *Polymer Engineering & Science* 41.12 (2001): 2108-2125.
12. Hitscherich, Pamela, et al. "The effect of PVDF-TrFE scaffolds on stem cell derived cardiovascular cells." *Biotechnology and bioengineering* 113.7 (2016): 1577-1585.
13. Arinzeh, Treena L., Norbert Weber, and Michael Jaffe. "Electrospun electroactive polymers for regenerative medicine applications." U.S. Patent Application No. 10/052,412.
14. Hoop, Marcus, et al. "Ultrasound-mediated piezoelectric differentiation of neuron-like PC12 cells on PVDF membranes." *Scientific reports* 7.1 (2017): 4028.
15. Chen, Weiran, et al. "Immortalization and characterization of a nociceptive dorsal root ganglion sensory neuronal line." *Journal of the peripheral nervous system* 12.2 (2007): 121-130.
16. Basbaum, A. I., D. M. Bautista, et al. (2009). "Cellular and molecular mechanisms of pain." Cell 139(2): 267-284.
17. McGlone, Francis, and David Reilly. "The cutaneous sensory system." *Neuroscience & Biobehavioral Reviews* 34.2 (2010): 148-159.
18. Lumpkin, E. A. and M. J. Caterina (2007). "Mechanisms of sensory transduction in the skin." Nature 445(7130): 858-865.

19. Bunge, Richard P. "Expanding roles for the Schwann cell: ensheathment, myelination, trophism and regeneration." *Current opinion in neurobiology* 3.5 (1993): 805-809.

20. Obremski, Valerie J., Patrick M. Wood, and Mary Bartlett Bunge. "Fibroblasts promote Schwann cell basal lamina deposition and elongation in the absence of neurons in culture." *Developmental biology* 160.1 (1993): 119-134.

21. Obremski, V. J., M. I. Johnson, and Mary B. Bunge. "Fibroblasts are required for Schwann cell basal lamina deposition and ensheathment of unmyelinated sympathetic neurites in culture." *Journal of neurocytology* 22.2 (1993): 102-117.

22. Tsutsumi, Moe, et al. "In vitro formation of organized structure between keratinocytes and dorsal-root-ganglion cells." *Experimental dermatology* 21.11 (2012): 886-888.

23. Klusch, Andreas, et al. "Coculture model of sensory neurites and keratinocytes to investigate functional interaction: chemical stimulation and atomic force microscope-transmitted mechanical stimulation combined with live-cell imaging." *The Journal of investigative dermatology* 133.5 (2013): 1387.

24. Kumamoto, Jun-ichi, et al. "Coculture system of keratinocytes and dorsal-root-ganglion-derived cells for screening neurotrophic factors involved in guidance of neuronal axon growth in the skin." *Experimental dermatology* 23.1 (2014): 58-60.

25. Tsutsumi, Moe, et al. "Morphological and functional differences in coculture system of keratinocytes and dorsal-root-ganglion-derived cells depending on time of seeding." *Experimental dermatology* 20.6 (2011): 464-467.

26. Roggenkamp, Dennis, et al. "Atopic keratinocytes induce increased neurite outgrowth in a coculture model of porcine dorsal root ganglia neurons and human skin cells." *Journal of Investigative Dermatology* 132.7 (2012): 1892-1900.

27. Le Gall-Ianotto, C., et al. "Characterization of the first coculture between human primary keratinocytes and the dorsal root ganglion-derived neuronal cell line F-11." *Neuroscience* 210 (2012): 47-57.

28. Gingras, Marie, et al. "In vitro development of a tissue-engineered model of peripheral nerve regeneration to study neurite growth." *The FASEB journal* 17.14 (2003): 2124-2126.

29. Kumar, CD Mounesh, et al. "Osteosarcoma of maxilla mimicking neurofibroma." *Clinical Cancer Investigation Journal* 1.4 (2012): 233.

30. Vincent, Andrea M., et al. "Sensory neurons and schwann cells respond to oxidative stress by increasing antioxidant defense mechanisms." *Antioxidants & redox signaling* 11.3 (2009): 425-438.

31. Scholz, Joachim, and Clifford J. Woolf. "The neuropathic pain triad: neurons, immune cells and glia." Nature neuroscience 10.11 (2007): 1361.

32. Taveggia, Carla, and Alessandra Bolino. "DRG Neuron/Schwann Cells Myelinating Cocultures." *Myelin*. Humana Press, New York, NY, 2018. 115-129.

33. Pires, Filipa, et al. "Neural stem cell differentiation by electrical stimulation using a cross-linked PEDOT substrate: expanding the use of biocompatible conjugated conductive polymers for neural tissue engineering." *Biochimica et Biophysica Acta (BBA)-General Subjects* 1850.6 (2015): 1158-1168.

34. Guilak, Farshid, et al. "Control of stem cell fate by physical interactions with the extracellular matrix." Cell stem cell 5.1 (2009): 17-26.

35. Discher, Dennis E., David J. Mooney, and Peter W. Zandstra. "Growth factors, matrices, and forces combine and control stem cells." Science 324.5935 (2009): 1673-1677.
36. Saha, Krishanu, et al. "Substrate modulus directs neural stem cell behavior." Biophysical journal 95.9 (2008): 4426-4438.
37. Yannas, I. V., et al. "Progress in design of an artificial skin." *Federation Proceedings*. Vol. 38. No. 3. 9650 Rockville Pike, Bethesda, Md 20814-3998: Federation Amer Soc Exp Biol, 1979.
38. Chin, Curtis D., Krishn Khanna, and Samuel K. Sia. "A microfabricated porous collagen-based scaffold as prototype for skin substitutes." *Biomedical microdevices* 10.3 (2008): 459-467.

CHAPTER 6.
OVERVIEW OF THE COMPLETE CONSTRUCT, CONCLUSIONS, AND FUTURE DIRECTIONS

6.1 : Overview of the Complete Construct and Future Directions

This work demonstrates four main accomplishments in regards to the creation of an electroconductive elastomer with piezoelectric properties. Work related to mechanical properties, electroconductivity, piezoelectricity, and biocompatibility were all elaborated and validated during the course of this work.

6.1.1 : Mechanical Elaboration and Validation of the Construct

Various flexible and elastic polymers were studied in order to identify their mechanical properties, as detailed in Chapter 3. Perdurable thermoplastic elastomers with the best potential for use in relation to biomedical purposes were identified. The Young's moduli values and fatigue properties of these polymers were assessed and the properties of these polymers were compared to those of porcine skin.

Many of the flexible materials assessed in the course of this work were not suitable as substitutes for artificial skin. However, they have interesting mechanical properties that may make them potentially useful as components of neural or cardiac implants or other biomedical devices. Similarly, certain elastic polymers such as styrene-isoprene-styrene and styrene-butylene-styrene polymers were insufficiently similar to skin. Although these polymers were not found to be capable of the same strain as skin, they may be ideally suited for use as soft cell-culture substrates, medical wearables or a component of bioelectronic implants.

Out of the assessed elastomers, styrene-butadiene-styrene (SBS) polymers were found to have the closest properties to skin, given the capacity of their stress-strain curves. In fact, this polymer is capable of a higher strain capacity compared to skin, as shown in Figure 3.13. The fatigue properties of excised skin, which is incapable of regeneration, were incomparable to those of Kraton D1152 (SBS). However, these values can only be taken as theoretical, given skin's regenerative properties *in vivo.* Despite this, the combination of elastic styrene-butadiene-styrene polymers' strain capacity and fatigue properties imply that these elastic styrene-butadiene-styrene polymers are potentially optimal for long-term implantation. In certain cases of lower strain (i.e., 2.5% strain amplitude) there was not even an identifiable fatigue point after 5,000,000 cycles.

Although Kraton D1152ES (SBS) is perdurable, it lacks skin's regenerative properties. This study provides the basis of information required for creating products that can be implanted or used as wearables for long-term periods. Since this polymer only experiences deformation after undergoing substantial elongation, its use as a substrate for a neural cuff implant in bioelectronic medicine is already a possibility. This polymer may also be well-suited for implantation into certain regions of the body given its strength; the joints, hips, and skin on feet regularly contract and elongate to 55% when performing basic movements, like walking.[1] However, use as a perdurable human-machine interface system may require further modifications, given skin's elongation at break value at 207%.[2] Optimal use of this polymer may require it to be modified, even considering products produced with the mindset of built-in obsolescence, or substituted for another soft material with regenerative properties.[3]

Our own research could be furthered by performing fatigue tests in a humidified environment in order to prevent dehydration-based fatigue failure, which occurred to skin in this study at an accelerated rate. Dehydration-based issues also influenced the rate of material fatigue, though this is present in certain polymers (i.e., electrospun Kaneka D1152ES (SBS)) more than others. A humidified, controlled environment during testing would almost certainly influence results.

As skin is capable of regeneration, an extensive, in-depth analysis of fatigue would be required in order to produce a ready-for-market product. This would involve deformation tests focused on mimicking the anisotropic properties of skin affixed to a body in order to understand if these materials could be used as wearables or biomedical devices. These results could be compared to *in vivo* skin in order to provide a more comprehensive understanding of material perdurability.

6.1.2 : Electroconductive and Piezoelectric Elaboration and Validation of the Construct

Given the mechanical properties of our selected materials, no singular material was likely to contain the electroconductive components that would make it well-suited as an implantable material usable in bioelectronic medicine. However, in the course of this work, we identified an electroconductive cross-linked polymeric platinum that was able to seamlessly integrate with our elastomeric material. Unlike other conductive polymers, which are often water-

soluble, or conductive materials, which are likely to interfere with the mechanical properties of the elastomer, this polymeric platinum was miscible with Kraton D1152ES (SBS) and could bond to its surface, resulting in an effect similar to thermal evaporation but necessitating lower levels of heat treatment. The result was a soft, electroconductive substrate with modifiable properties that can be used as an adhesive or electrode.

Although a variety of constructs were created in the elaboration of this work, not all were fully analysed. The development of iridium oxide coated constructs should be explored in more detail; the elaboration of this research would require an assessment of conductivity and electromechanical fatigue, re-validation of the piezoelectric response on this soft electrode, and confirmation of the biocompatibility of this construct. Similarly, these parameters should be explored in the context of a fully nanofibrous construct, utilizing PVP-IrOX fibers as the electrode substrate. This construct would be much more limited from a mechanical perspective, but may prove to be of more interest given additional properties, like porosity.

The SBS-platinum-P(VDF-TrFE) construct we created performs adequately based on the findings of conductivity, electrical impedance spectroscopy, and electromechanical assessments, as discussed in Chapter 4. However, further tests on both long-term electromechanical fatigue and hysteresis are required to utilize this construct in a clinical setting or as a wearable device.

Preliminary assessments of pre-stressed materials showed that no conductivity-related failure occurs when applying polymeric platinum to a pre-stressed material. Similarly, no conductivity-related failures occur when applying polymeric platinum to a material, stressing it, then allowing it to return to its original state. However, conductivity was altered after repeated strain (cite percentage) and during the incorporation of other materials into the final construct (i.e., P(VDF-TrFE)).

Given the functional elongation at break value of 207% for skin [3] and our preliminary data on elastomer deformation and hysteresis, an alteration is likely required in the methodology for the creation of this construct. Specifically, materials would ideally need have polymeric platinum applied, be pre-stressed to a set value (e.g., 200%), have polymeric platinum re-applied, and then undergo the heat-treatment process. Alternatively, polymeric platinum could

be applied a single time if the elastomer could maintain the desired elongation under heat. Our assessments found that not all elastomers (e.g., styrene-butylene-styrene) are capable of elongation during heat treatment. This procedure has been attempted with styrene-butadiene-styrene and but has not been fully optimized.

This optimization is particularly essential for the functionality of a construct with piezoelectric properties. The piezoelectric construct will only function as it should if its surface electrode continues to maintain conductivity. A loss in conductivity will interfere with the detection of the piezoelectric response. Future modifications should additionally focus on a more precise understanding of the polymeric platinum layer and piezoelectric layers interactions, as the piezoelectric acts as an insulator in stasis.

On a similar note, piezoelectric fatigue is a distinct issue given our choice of piezoelectric polymer. Piezoelectric fatigue is a much more serious issue given the potential for mechanical fatigue in P(VDF-TrFE), given the inability for piezoelectrics to regenerate. In fact, P(VDF-TrFE) is known for experiencing rapid mechanical fatigue. Films have shown cracks after as little as 2,000 cycles at a strain amplitude of 0.8%, and a 20% reduction in function after 30,000 cycles at the same strain.[4] This implies that it must be applied in a very specific manner to the complete construct in order to optimize its qualities. It should, in theory, be able to function in accordance with skin's elongation at break properties, or at least function after being subjected to strain at this level. Current studies imply that the latter would be unfeasible. However, nanofibrous conformation and the construction of the construct are both likely to play a major role in piezoelectric functionality.

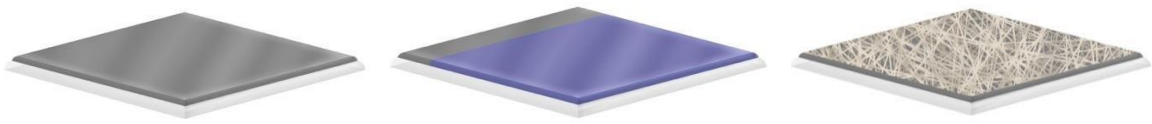

Figure 6.1: Novel Electroconductive and Piezoelectric Constructs Developed. Showing schematic of customizable electroconductive elastomers, e.g., alkene-styrene elastomers such as planar Kraton D1152ES (SBS) coated with cross-linked polymeric platinum (left), polymeric platinum covered by electrodeposited IrOx (center), and polymeric platinum with nanofibrous P(VDF-TrFE).

6.1.3 : Construct Biocompatibility

The lack of cytotoxicity and long-term biocompatibility of our selected polymers and constructs has validated all of the materials through ISO standard biocompatibility tests using L929 fibroblasts. Cellular adhesion and long term proliferation experiments using these cells and Heka-APF, DRG, and Schwann cells also have shown great promise. However, the analysis of 3D constructs was challenging. We should elaborate upon the cellular validation of this construct by exploring alternative techniques, such as histology in order to fully understand the structural formations occurring on our constructs.

There is also electroconductive work that must be performed in order to further the study of this construct in relation to cells. Specifically, the electrical stimulation of this construct should be analysed under cell culture. These experiments were attempted, but most did not produce results due to experimental failure of the setup. The few results that were obtained produced intriguing results, as seen in Figure 5.26. Experiments studying cultures undergoing repeated strain were not assessed at all, and the piezoelectric response on cells was not able to be determined. Ultimately, this means that experiments performed in stasis require different set-ups compared to those performed under mechanical strain.

Our group has already published work on cells that have been electrically stimulated.[5] However, these studies have focused on flexible polymers for use in neural tissue engineering, and are made of flexible polymers which have substantially different properties to those discussed in this work.

In addition to this, any *in vivo* setting will involve calculating the combined mechanics and consequent piezoelectricity for each potential region of implantation. Hence, mathematical modelling will be required to further research in this segment of the construct's development. Novel set ups in relation to mechanical stimulation of cells (and as such, piezoelectric constructs), are also equally relevant approaches to incorporate into cell culture.

In conclusion, given the results obtained thus far, the created construct can be explored for use in products such as wearables. Prolonged assessments of the material in the form of a wearable would also allow for long-term fatigue and deformation to be explored. Animal studies,

focused on the long-term biocompatibility of these materials when utilized as nerve cuffs or similar implants, would act as next steps in the development of this material from a clinical perspective.

6.2 Conclusions

In summary, this work shows that Kraton D1152ES (SBS) is a very promising biocompatible elastomer with easily modifiable mechanical properties when combined with additives such as polyisoprene or iron(III) p-toluenesulfonate hexahydrate. Unlike most elastomers, this material has a low Young's modulus but nonetheless has a high strain capacity.

Kraton D1152ES (SBS) can be used as a component of both electroconductive and piezoelectric constructs without its insulating capacity interfering with overall construct functionality, making it useful in a variety of fields. In combination with our selected polymeric platinum and piezoelectric P(VDF-TrFE), we have produced a biocompatible piezoelectric, electroconductive elastomer. Our only identified mechanical limitation to this polymer is hysteresis and deformations due to permanent set, which are typical of thermoplastic elastomers.[7-9]

According to Yamada et al, conventional strain sensors are typically limited to low strain that is approximately 5%.[1] At 5% strain amplitude, our selected elastomers were capable of between 280,000 cycles (for Kraton D1152ES (SBS)-polyisoprene blends) and 1,300,000 cycles (Kraton D1152ES (SBS)). Even P(VDF-TrFE) is not a limiting factor in this sense, as it should only experience deformation starting at 45% strain. Similarly, conductivity-related limitations that were identified also occurred around 45% strain – though these were primarily due to hysteresis of the base elastomer rather than faults with the polymeric platinum.

The selected materials were not only well-suited given our desired mechanical, electroconductive and piezoelectric properties. They also have excellent biocompatibility, bringing a next step as the assessment of the construct *in vivo,* perhaps as a component of nerve cuffs or electrodes used in both external and implantable stimulation (e.g., vagus nerve implants). However, given the range of different conductivities required in each circumstance,

individual modeling is required before producing each distinct product; the most complex modeling being required prior to any integration with a neurally-controlled prosthetic.

Finally, the approximate cost of our selected materials when used to produce different products forecasts scale up as highly affordable. Given the structure of the construct, only our two polymers and third electroconductive material (polymeric platinum) are needed – no binders or other additional materials. The most expensive of these materials is the Gwent Polymeric Platinum, forecasted at approximately 1,309 EUR per 0.025 kilograms as of the date of publication. However, out of these three materials, both the piezoelectric fibers and polymeric platinum are produced to nanometer-sized thicknesses – which means that the bulk of the construct is the Kraton D1152ES polymer. Given the fact that Kraton polymers are sold for as little as 0.10 USD cents per pound, scale up and mass manufacture of these polymers is both cost-effective and easy.

In an era where built-in obsolescence is rapidly becoming the norm, our chosen materials allow for the creation of a construct that can be easily and affordably produced, scaled-up, and integrated into a variety of different devices. Given the easily modifiable properties of both the electroconductive and piezoelectric components, we have created a construct that has potential uses in both wearables and as a component of implanted biomedical devices. This construct would also have a range of applications related to virtual reality, robotics, and monitoring systems.

6.3 References

1. Yamada, Takeo, et al. "A stretchable carbon nanotube strain sensor for human-motion detection." *Nature nanotechnology* 6.5 (2011): 296.
2. Dias, J. R., P. L. Granja, and P. J. Bártolo. "Advances in electrospun skin substitutes." Progress in Materials Science 84 (2016): 314-334.
3. Tee, Benjamin CK, et al. "An electrically and mechanically self-healing composite with pressure-and flexion-sensitive properties for electronic skin applications." Nature nanotechnology 7.12 (2012): 825.
4. Singh, Deepa, and Ashish Garg. "The combined effect of mechanical strain and electric field cycling on the ferroelectric performance of P (VDF-TrFE) thin films on flexible substrates and underlying mechanisms." *Physical Chemistry Chemical Physics* 18.42 (2016): 29478-29485.
5. Pires, Filipa, et al. "Neural stem cell differentiation by electrical stimulation using a cross-linked PEDOT substrate: expanding the use of biocompatible conjugated conductive polymers for neural tissue engineering." Biochimica et Biophysica Acta (BBA)-General Subjects 1850.6 (2015): 1158-1168.
6. Lam, Tu-Ngoc, et al. "Tuning mechanical properties of electrospun piezoelectric nanofibers by heat treatment." Materialia (2019): 100461.
7. Qi, Hang Jerry, and Mary C. Boyce. "Stress–strain behavior of thermoplastic polyurethanes." *Mechanics of Materials* 37.8 (2005): 817-839.
8. Cho, Hansohl, et al. "Deformation mechanisms of thermoplastic elastomers: Stress-strain behavior and constitutive modeling." *Polymer* 128 (2017): 87-99.
9. Bergström, J. S., and M. C. Boyce. "Large strain time-dependent behavior of filled elastomers." *Mechanics of materials* 32.11 (2000): 627-644.

APPENDIX

Section 2.A: Materials and Methodology

Other polymers were assessed as potential materials and material blends in the creation of the construct. The polymers in Table 2.A were not successfully electrospun nor cast as homogenous sheets, with the exception of PDMS.

Table 2.A: Other Polymers Assessed for Electrospun Mesh Creation

Polymer	Solvent	Young's Modulus	Notable Properties
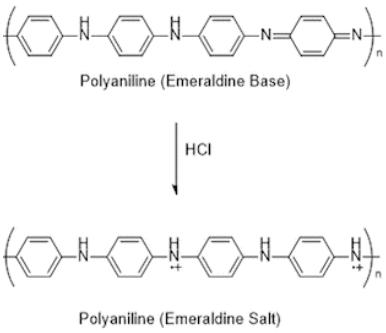 Polyaniline (PANi)	m-Cresol Chloroform	1.5-2.2 GPa[4,5]	Undoped 6.28×10^{-9} S/m; Doped (4% HBr) 4.60×10^{-5} S/m[4,5,6]
Poly(phenylene oxide) 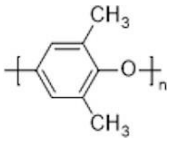	Chlorobenzene DMF	2.7 GPa[14]	Insulator
Poly (dimethylsiloxane) (PDMS) 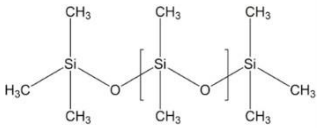	DMF THF	3.6-8.7 x 10^5 Pa (varies based on mixing ratio)[16]	Insulator

PDMS was prepared for multiple other purposes (listed in Chapter 2) but was not usable as a base material in this work. This polymer was prepared using Sylgard® 184 Silicone Elastomer

Kit (Dow Corning). Elastomer and curing agent were combined in a 1:10 weight proportion. The two were mixed together for one minute using a stirrer, then placed in a desiccator under vacuum for 30 minutes before use.

Combinations of PEDOT, P3HT, PPy with Elastic and Flexible Polymers

PEDOT, P3HT, and PPy are not available in sufficiently viscous states to electrospun independently. However, these solutions were able to be combined with other polymers so long as a miscible solvent had been used. Combinations of P3HT and SIBS (Kaneka SIBSTAR™), which are both miscible in chloroform, were attempted in ratios of 1:10, 1:8, 1:6, and 1:4. The same proportions of PEDOT-PSS and PVP, which are both miscible in ethanol, were attempted. Blends of PEDOT-PSS and PVP with KANEKA SIBSTAR™ (SIBS) were not successful. While blends of KANEKA SIBSTAR™ (SIBS) and P3HT polymers were successfully made, such solutions could only be spin coated, rather than electrospun. The electroconductivity and viscosity of electroconductive polymers combined with elastomers, such as in the case of was incompatible with the electrospinning process; the resulting material was too resistive to detect when measured with a two-point probe.

Section 3.A: Materials and Mechanics

Kraton D1152ES (SBS) electrospun fibers were produced as detailed in Chapters 2 and 3. This material could produce sputtering, and in turn, elastomeric sheets (Fig. 3.A.1). However, this material was also able to produce electrospun fibers with minimal beading (Fig. 3.A.2).

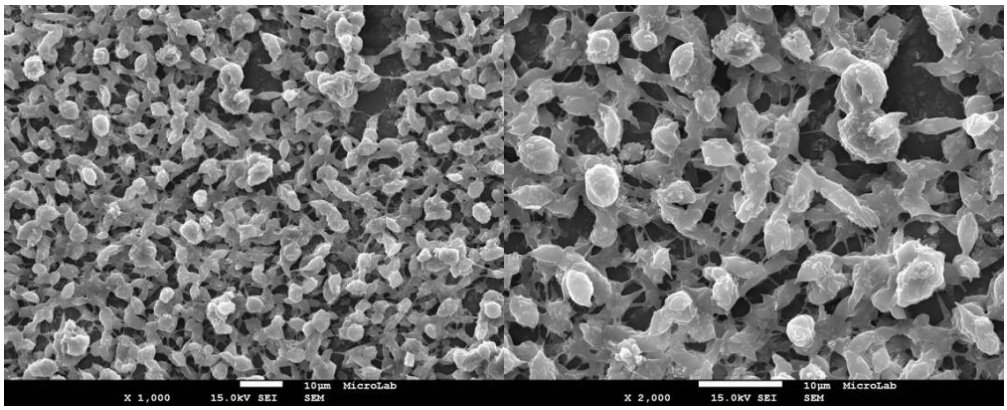

Figure 3.A.1: Sputtering of Kraton D1152ES (SBS)

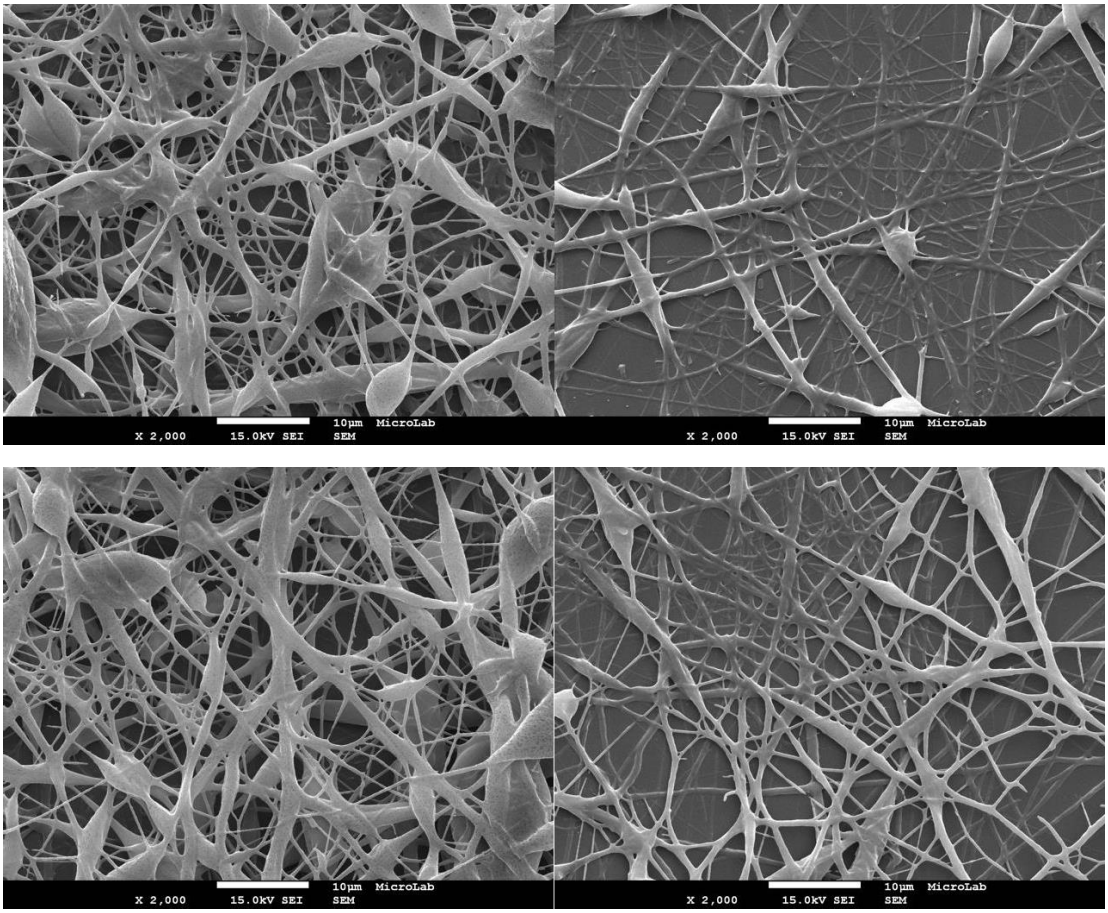

Figure 3.A.2: Additional Images of Electrospun of Kraton D1152ES (SBS)

As elongation at break data is not listed for all polymers is one graph in Chapter 3, this complication of information has been provided here. This data should not be considered comparative beyond the purposes of this thesis, given the differences in thickness of the samples and the machine parameters that were applied accordingly.

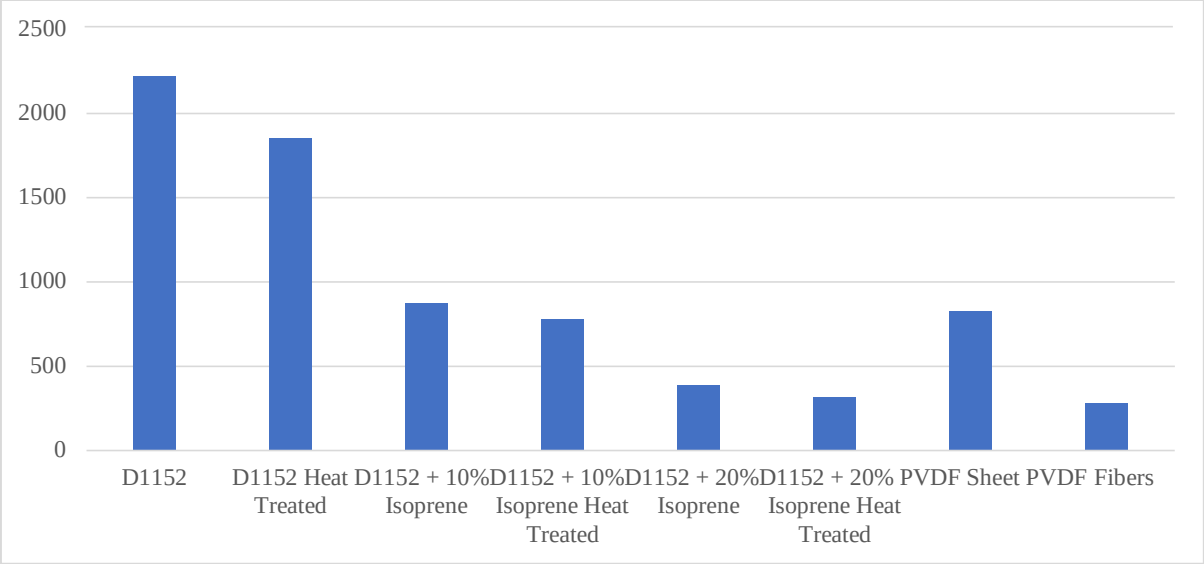

Figure 3.A.3: Elongation at Break Graph for Flexible and Elastic Polymers

Figure 3.A.4: Maximum Elastomer Deformation

Elastomer deformation was identified after repeated strain, as in the fatigue experiments shown in Figure 3.16 and Table 3.6. At this stage, permanent deformations were observed; as such, the polymer was unable to return to its original length. This loss of elastic recovery was due to permanent set (i.e., unrecoverable strain that occurs due to plastic deformation). Deformation of this type is to be expected of thermoplastic elastomers and has been identified in many alkene-styrene polymers and their blends.[1-3] As was expected, we found that permanent set primarily occurred in the first cycle of strain, with minimal changes occurring in following cycles.

Hysteresis was not explored until Chapter 4, following the electromechanical assessments. This data is shown in Figure 4.23. Hysteresis and elastomer deformation are concepts which can occur in variable amounts following repeated strains. Further hysteresis and permanent set are also likely to occur following cycles at higher strain amplitudes.

The concepts of permanent set and hysteresis must be more thoroughly explored in order to optimize construct functionality or the final product risks. Both piezoelectric functionality and conductivity of the construct (as shown in Figures 4.19, 4.20, and 4.21) can be affected should the elastomer experience issues due to permanent set. An affected elastomer would produce non-reversible deformations, which would lead to variable and non-reproducible results. Although this is not truly seen in stasis at low strain amplitudes (i.e., Figure 4.19) for Kraton D1152ES (SBS), it is immediately notable in Kraton D1152ES (SBS)-polyisoprene blends. Changes in resistance after repeated strain are seen after just 10 cycles when stretched at strain amplitudes of 15%, 30%, and 45%, highlighting the lack of reproducible conductivity and the functional limitations of the complete construct.

Thermogravimetric analysis was not performed as part of the assessment for our polymers. However, a sample analysis was performed on Kaneka SIBSTAR™ 062M. Further analysis of our selected elastomers would expand upon this analysis.

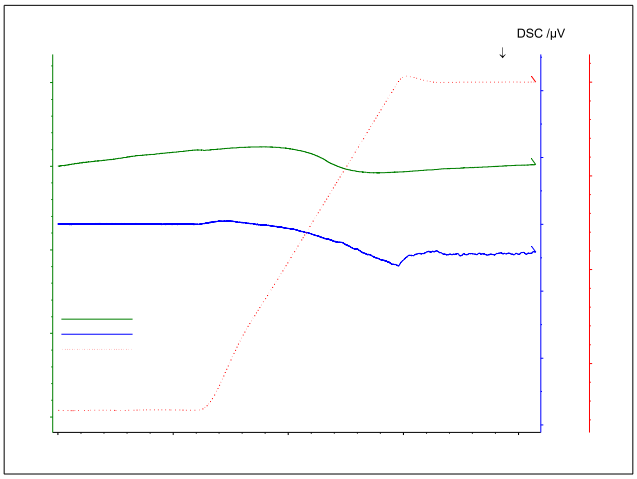

Figure 3.A.5: Thermogravimetric Analysis of Drop Cast Kaneka SIBSTAR™ 062M. Analysis performed courtesy of the Universitat Autònoma de Barcelona.

Contact angle assessments were performed prior to this thermogravimetric analysis; the results of the latter showed how this polymer retains liquid (both solvent and electrolyte solutions, like PBS). We assessed the contact angle of Kraton D1152ES in both wet and dry states.

Table 3.A: Contact Angle of Hydrated and Dehydrated SBS

Material	Contact Angle (º)	SD
Hydrated Kraton D1152ES (SBS)	87.69	0.57
Dehydrated Kraton D1152ES (SBS)	81.29	0.19

Section 4.A: Electrochemical Analysis

Electrochemical Properties of Gwent Polymeric Platinum Products

Differences between C2050804P9 and C2020322P6 are minimal. However, there are key aspects that make one polymer more suitable than the other. We were able to electrodeposit iridium oxide onto platinum-coated Kaneka SIBSTAR™ (SIBS), which had been applied via thermal evaporation. However, the cyclic voltammetry graphs shown in Figures 4.A.1 and 4.A.2 imply that this might not translate in the same way when using C2050804P9 and C2020322P6 given the quantity of polymer in the platinum. Example cyclic voltammetry and electrodeposition graphs utilizing thermally evaporated platinum and IrOX on glass are shown in Figure 4.A.3.

These cyclic voltammetry graphs of Gwent products C2050804P9 and C2020322P6 (Figures 4.A.1 and 4.A.2) were obtained in triplicate utilizing silver or silver chloride as the reference electrode. Graphs were provided by Silver Merkoci, courtesy of Gwent and Sun Chemical Ltd.

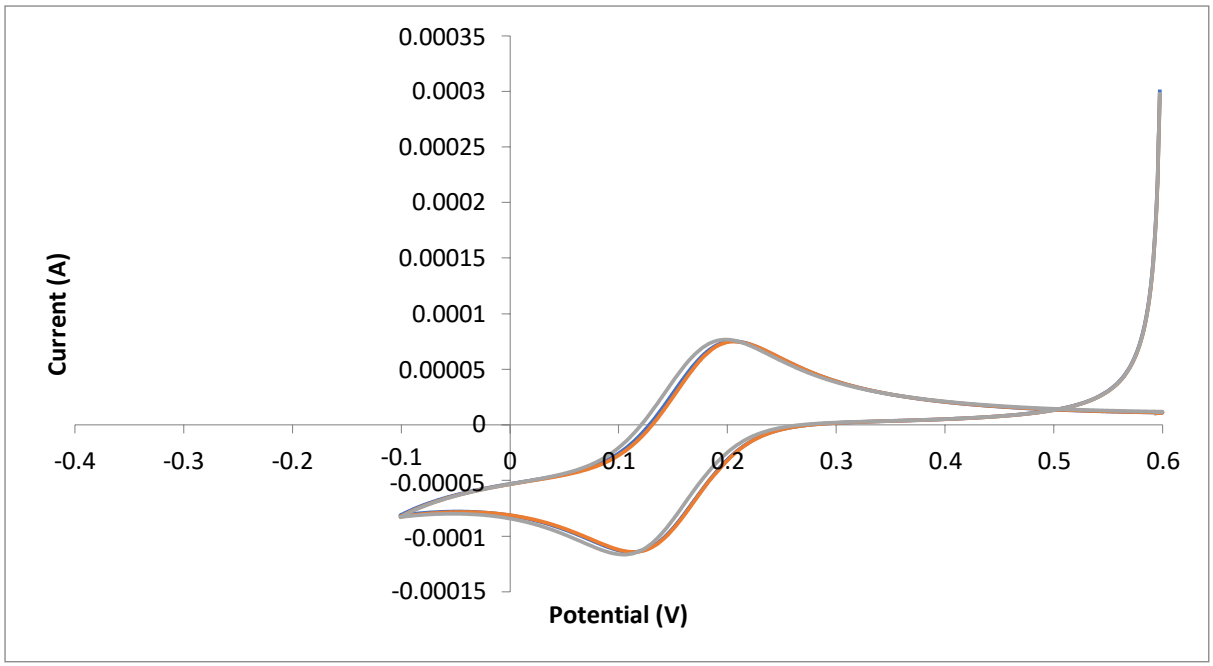

Figure 4.A.1: Cyclic Voltammetry of Gwent Polymeric Platinum C2050804P9

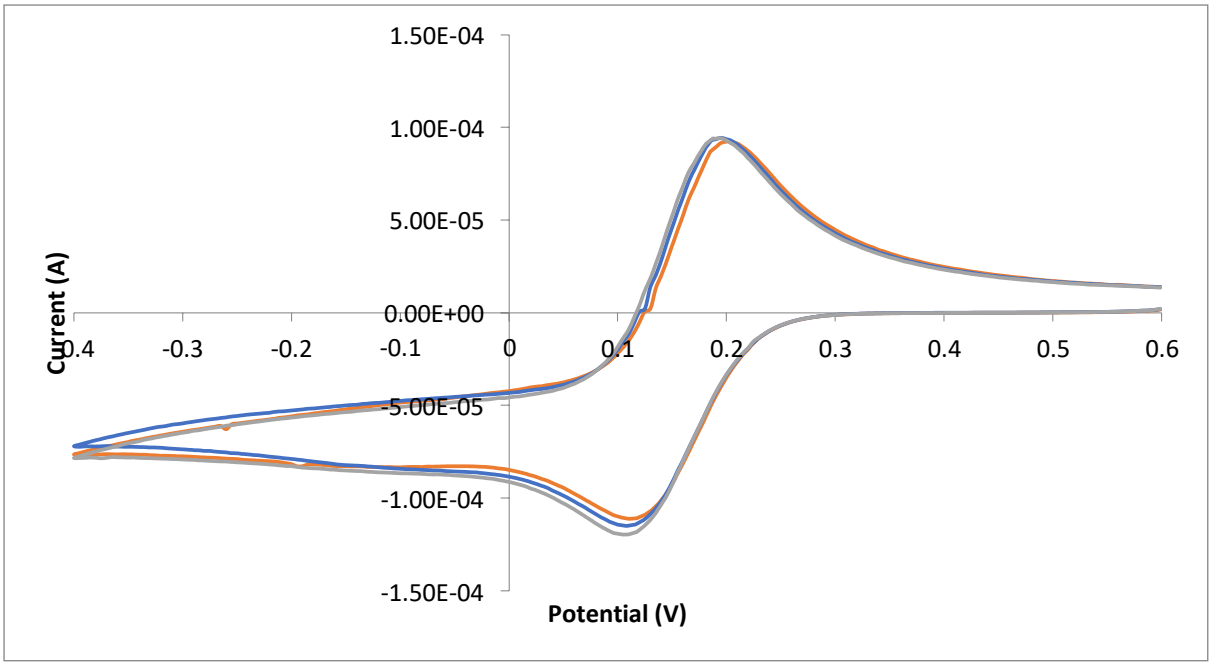

Figure 4.A.2: Cyclic Voltammetry of Gwent Polymeric Platinum C2020322P6

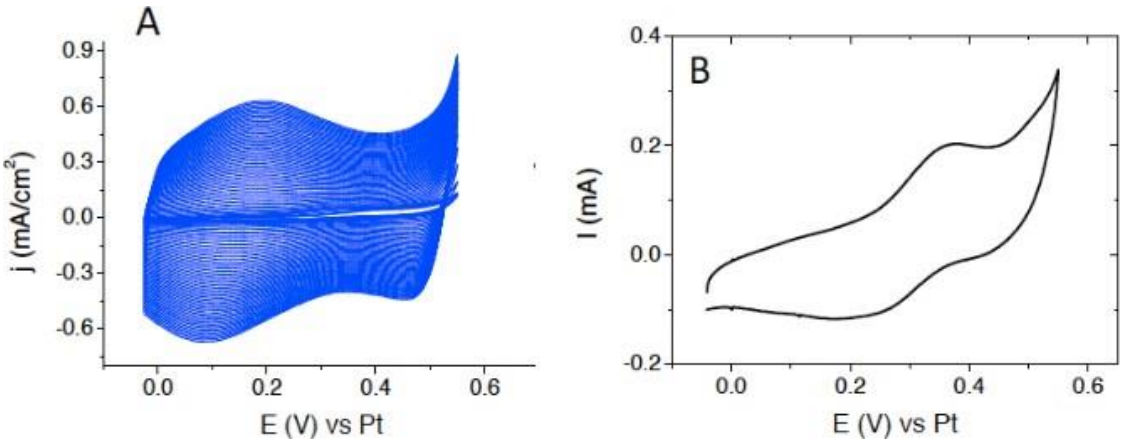

Figure 4.A.3: Example of IrOx Electrodeposition on Thermally Evaporated Platinum
Reprinted with permission from: Cruz, A. M., et al. "Iridium oxohydroxide, a significant member in the family of iridium oxides. Stoichiometry, characterization, and implications in bioelectrodes." The Journal of Physical Chemistry C 116.8 (2012): 5155-5168. (Copyright 2012 American Chemical Society) and detailed in: Carretero González, Nina Magali, and Jaume Casabó i Gispert. "Iridium oxide-carbon hybrid materials as electrodes for neural systems. Electrochemical synthesis and characterization." (2014).[4]

The total combinations of electroconductive materials blended with or deposited onto elastomers is detailed in Figure 4.A.4. There are 78 combinations in total; these numbers are expressed in percentages, with iridium oxide, gold nanoparticles, and carbon nanoparticles ranked as the three most tested materials.

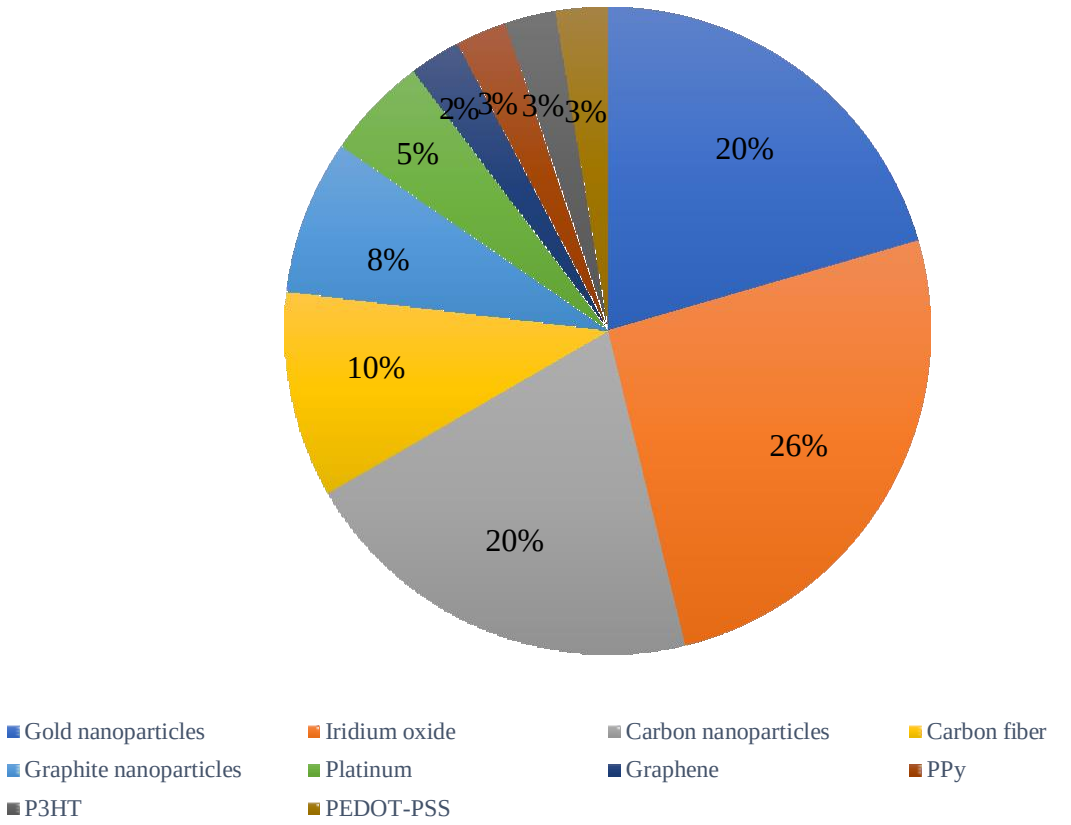

Figure 4.A.4: 78 Electroconductive-Elastomer Combinations Assessed

Further details on the way that these materials were combined with polymers can be found in Tables 4.A.1 and 4.A.2 and 4.A.3. Table 4.A.1 details the selected materials and the way they were incorporated into the polymer blend (i.e., through blending, coating or multiple types of processes). All materials were believed to be biocompatible, though some had reported issues based on their method of preparation.

Tables 4.A.2 and 4.A.3 detail more precise information on how materials were combined and their approximate conductivity based on a 2-point probe assessment. Table 4.A.2 depicts the controls, while 4.A.3 shows the combinations assessed. These tables were the primary methods used for the elimination of the 78 combinations shown in Figure 4.A.4.

Table 4.A.1 Electroconductive Materials Analysed for Use in Interface Construct

MATERIAL	BLENDED VS. COATED	ASSESSED
P3HT	Either	Yes
PEDOT	Coated	Yes
PPy	Coated	Yes
Gold nanoparticles	Either	Thermally Evaporated
IrOx (solid)	Either	Yes
IrOx (liquid for electrodeposition)	Either	Yes
Graphene oxide	Either	Yes
Graphene oxide (electrodeposited)	Either	No
Graphite	Either	Yes
Carbon Fiber	Either	Yes
Carbon nanotubes (CNTs)	Inside	Yes
Platinum	Coated	Thermally Evaporated
Platinum Paint	Either	Yes
Silver Paint	Coated	Yes

Table 4.A.2 Controls for Preliminary Assessment of Polymer-Electroconductive Material Blends

10% wt Polymer	Solvent	Electroconductive material(s)	Material Ratio	Range of Electroconductivity	Elasticity or flexibility
SIBS 062M	THF	None- control	-	200 M Ω	Elastic
SIBS 062M	Chloroform	None- control	-	200 M Ω	Elastic
SIBS 102T	THF	None- control	-	200 M Ω	Elastic
SIBS 102T	Chloroform	None- control	-	200 M Ω	Elastic
Polyimide	DMF	None- control	-	200 M Ω	Flexible
Polyimide	DMAc	None- control	-	200 M Ω	Flexible
	None	Platinum- control	-	200 Ω	None
	Chloroform	Iridium solid- control	-	200 Ω	None
	None	Iridium, electrodeposition control	-	200 Ω	None
	None	Carbon fiber	-	2 K Ω	Flexible

Table 4.A.3 Preliminary Assessment of Polymer-Electroconductive Material Blends

10% wt Polymer	Solvent	Electroconductive material(s)	Material Ratio	Range of Electroconductivity	Elasticity or flexibility
SIBS 062M	THF	Graphene oxide	1:1	200 M Ω	Elastic
SIBS 062M	Chloroform	Graphene oxide	1:1	200 M Ω	Elastic
SIBS 102T	THF	Graphene oxide	1:1	200 M Ω	Elastic
SIBS 102T	Chloroform	Graphene oxide	1:1	200 M Ω	Elastic
SIBS 062M	THF	Graphite (0.15nm)	1:1	200 M Ω	Elastic
SIBS 062M	Chloroform	Graphite (0.3nm)	1:1	None	Elastic
SIBS 102T	THF	Graphite (0.15nm)	1:1	None	Elastic
SIBS 102T	Chloroform	Graphite (0.3nm)	1:1	None	Elastic
SIBS 062M	THF	Carbon nanotubes	5:3	200 M Ω	Flexible
SIBS 062M	Chloroform	Carbon nanotubes	5:3	200 M Ω	Flexible
SIBS 102T	THF	Carbon nanotubes	5:3	200 M Ω	Elastic
SIBS 102T	Chloroform	Carbon nanotubes	5:3	200 M Ω	Elastic
SIBS 062M	THF	Iridium oxide (solid)	3mls SIBS: 1mg Iridium	200 K Ω	Elastic
SIBS 062M	Chloroform	Iridium oxide (solid)	3mls SIBS: 1mg Iridium	200 K Ω	Elastic
SIBS 102T	THF	Iridium oxide (solid)	3mls SIBS: 1mg Iridium	200 K Ω	Elastic
SIBS 102T	Chloroform	Iridium oxide (solid)	3mls SIBS: 1mg Iridium	200 K Ω	Elastic
SIBS 062M	THF	Iridium oxide (blended)	1 ml IM Iridium: .67 ml SIBS	2 K Ω	Flexible
SIBS 062M	Chloroform	Iridium oxide (blended)	1 ml IM Iridium: .33 ml SIBS	200 Ω	None
SIBS 102T	THF	Iridium oxide (blended)	1 ml IM Iridium: .67 ml SIBS	2 K Ω	Flexible
SIBS 102T	Chloroform	Iridium oxide (blended)	1 ml IM Iridium: .33 ml SIBS	200 Ω	None
SIBS 062M	THF	Iridium oxide (atop SIBS)	1:1	200 K Ω	Uneven
SIBS 062M	Chloroform	Iridium oxide (atop SIBS)	1:1	200 K Ω	Uneven
SIBS 102T	THF	Iridium oxide (atop SIBS)	1:1	200 K Ω	Uneven
SIBS 102T	Chloroform	Iridium oxide (atop SIBS)	1:1	200 K Ω	Uneven
SIBS 062M	THF	Carbon fiber (layered atop)	N/A	None	Flexible
SIBS 062M	Chloroform	Carbon fiber (layered atop)	N/A	None	Flexible
SIBS 102T	THF	Carbon fiber (layered atop)	N/A	None	Flexible
SIBS 102T	Chloroform	Carbon fiber (layered atop)	N/A	None	Flexible
SIBS 062M	THF	Carbon fiber (immersed)	N/A	None	Flexible
SIBS 062M	Chloroform	Carbon fiber (immersed)	N/A	None	Flexible
SIBS 102T	THF	Carbon fiber (immersed)	N/A	None	Flexible
SIBS 102T	Chloroform	Carbon fiber (immersed)	N/A	None	Flexible
SIBS 062M	Chloroform	Platinum (under, on glass)	N/A	200 M Ω	None
SIBS 062M	THF	Platinum (under, on glass)	N/A	200 M Ω	None

Section 5.A: Cell Culture and Preliminary Biocompatibility Tests

Section 5.A.1: Primary Cell Culture

This section details the work done at the University of Aberdeen on rat keratinocytes and dorsal root ganglion cells and xenopus neurons. Their extraction and cultivation is detailed below.

Rat Dorsal Root Ganglion (rDRG) Cells

Rat dorsal root ganglion cells are sourced as primary cultures. These processes of dissection, cell extraction, and cell culture are detailed below.

rDRG Cell Media

Dorsal root ganglion cells can be kept in Epilife media (Thermo Scientific; M-EPI-500-CA) supplemented with S7 (Thermo Scientific; S-017-5) and 1% Pen-Strep, or alternatively in Bottenstein and Sato's Fluid ++ Media, detailed in Table 5.A.1.

Table 5.A.1: Bottenstein and Sato's Fluid and Bottenstein and Sato's Supplemented Fluid

Bottenstein and Sato's Fluid (BSF)		**Bottenstein and Sato's Fluid (BSF) ++**	
Transferrin	1 ml (10mg/ml stock)	BSF	20 ml
30% BSA	1 ml	Insulin (Sigma, I9278)	20 µl (20mg/ml stock)
Pen/Strep	1 ml (10000U/ml stock)	NGF (Sigma, N6009)	20 µl (100µg/ml stock)
Progesterone	100 µl (60µg/ml stock)		
Putrescine	1 ml 1.6mg/ml stock)		
Sodium Selenite	10 µl 1.6mg/ml stock)		
Hams F-12 (Zenbio, F12020)	94 ml		

rDRG Cell Harvesting

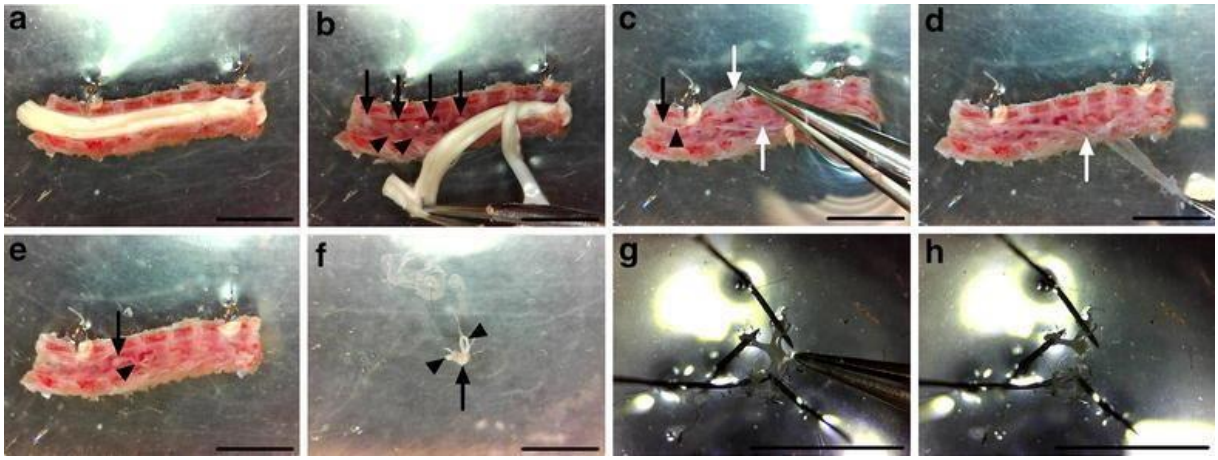

Figure 5.A.1: Dissection of the rat spinal column after a sagittal cut along the midline. Black arrows point to dorsal root ganglia; white arrows mark residual tissue and meninges (a, b, c). The spinal cord is removed to expose the vertebrae (d, e). As meninges and residual tissue are removed, dorsal root ganglia can be removed with forceps (f). The final product is a dorsal root ganglion with roots floating in a dish (f). The roots are fixated with forceps or needles and cut close to the dorsal root ganglion body (g, h.)

Dorsal root ganglion cells were obtained from postnatal Sprague-Dawley rat pups two to four days after birth. Rat pups were killed through cervical decapitation in accordance to the UK Animals (Scientific Procedures) Act 1986 and approval from the University of Aberdeen ethics committee. Dissection of the rat spinal column was done to extract removal rDRGs. Axonal roots were cut proximal to the ganglion prior to dissection, as shown in Figure 5.A.

rDRG Substrate Pre-coating and Cell Culture

Plates for rDRG cells can be precoated to optimize cell adherence. PLS (1 mg/ml stock diluted to 10-50 ug/ml) coating is done first, and cell culture plates can be kept in the fridge long-term. Subsequent laminin coatings can be done the day before cell culture work and are diluted to 2 ug/ml for overnight incubations.

Dissociated cells were incubated in an enzymatic solution of 50U Papain and retinal buffer solution (pH=7.4) for 30 minutes at 37°C, 5% CO_2. Resuspension of the cells was carried out in retinal buffer and trypsin inhibitor DNAse (TID) solution. Retinal buffer is made of bovine serum albumin, C-L-cysteine, HEPES buffer, D-Glucose, CaCl2, MgSO4, MgCl2, NaHCO3,

Phenol Red, 1M KCl, and HBSS, as detailed in Table 5.A.2. TID solution is made of DNAse, Bovine Serum Albumin, Trypsin Inhibitor, and HBSS, as detailed in table 2.1.8. The composition of these solutions is detailed below. Cells were then pipetted up and down repeatedly with a 1000µl pipette.

Table 5.A.2: Retinal Buffer (Rb) and Papain-Rb Dissociating Solutions

Retinal Buffer Solution Component	**Quantity**	**Supplier**	**Catalogue Number**
Bovine Serum Albumin (BSA)	40 mg		A7030
D-L cysteine	40 mg	Sigma	C7352
HEPES	239 mg	Sigma	H3375
D-glucose	578 mg	Sigma	G7021
Calcium Chloride	38 mg	Sigma	C3881
Magnesium Chloride	20 mg	Sigma	M2670
Magnesium Sulphate	14 mg	Sigma	M1880
Sodium Bicarbonate	16 mg	Sigma	S5761
Phenol Red Solution	0.4 ml	Sigma	P0290
Potassium Chloride Solution (2M)	2 mL	-	-
Hanks Balanced Salt Solution (HBSS)	Final volume made up to 200 mL with HBSS -		
RB-Papain Dissociating Solution			
RB Solution	1 ml	-	-
Papain	10 U/ml	Sigma	P3125

Table 5.A.3: Trypsin Inhibitor Dnase (Tid) Solution

Solution Component	Quantity	Supplier	Catalogue Number
BSA	1 g	Sigma	A7030
DNase	2 mg	Sigma	DN25
Trypsin Inhibitor	25 mg	Roche	10 109 886 001 101
Hanks Balanced Salt Solution (HBSS)	Final volume made up to 100ml with HBSS	Zenbio	HBSS011

The cell suspension was subsequently diluted in 0.9ml of cell culture medium in order to create the final solution used for plating. Each rat spinal cord typically yielded three cell culture dishes of rDRGs. Monoculture experiments were conducted after an outgrowth of a minimum of two neurites within 60% of neurons that had been plated. Media on cells was changed every 48 hours.

Rat Keratinocyte Cells

Various components are used in rat keratinocyte cell culture as these are primary cultures. These coating solutions and reagents necessary for dissection, pre-coating, and culture are detailed in Tables 5.A.4 and 5.A.5.

Table 5.A.4: Fibrogen-Collagen Coating Solution

Coating Solution Component	Quantity	Supplier	Catalogue Number
Bovine Serum Albumin (BSA)	0.5 ml	Sigma	A7030
L-15 Leibovitz	100 ml	Sigma	L5520
Collagen Type I	1 ml	Sigma	C3867
Fibronectin	1 mg	Roche	11051407001
HEPES	2 ml	Sigma	H3375

Table 5.A.5: Calcium-Based Media Solutions

Component	Quantity	Supplier	Catalogue Number
Lo-Ca medium (0.05mM)			
Calcium-free EMEM	450 ml	Lonza	BE06
Calcium-stripped FBS	40 ml	Labtech International	FB-100-C/100
Penicillin/streptomycin	5 ml	Life Technologies	15140-122
Hi-Ca medium (1.35 mM)			
LoCa medium	495 ml	-	-
0.25 M$CaCl_2$	2.6 ml	-	-
Antibiotic/Antimycotic	2 ml	Thermo Scientific	SV30079.01
CaCl2 (1M) Stock Solution			
$CaCl_2 \cdot 2H_2O$	1.47 g	Sigma	C3881
MilliQ water	10 ml	-	-

rKeratinocyte Cell Media

Rat keratinocytes are kept Epilife media. Each 500 mLs are supplemented with Supplement S7 and 1% Pen-Strep, as mentioned previously.

rKeratinocyte Harvesting

Keratinocytes were obtained from postnatal Sprague-Dawley rat pups two to four days after birth. Rat pups were killed through cervical decapitation in accordance to the UK Animals (Scientific Procedures) Act 1986 and approval from the University of Aberdeen ethics committee. Harvesting was done in sterile conditions according to a modified protocol from Lichti, et al. (2012). Pups were inserted into a 50ml falcon tube containing 10ml of 70% ethanol and gently shaken. Distilled, sterile water was then used repeatedly to wash off debris and alcohol. The limbs and tail of the rat were removed, and the skin of the pup was sliced dorsally in order to facilitate removal of the skin from the body. Extracted skin was flattened on a 100mm Petri dish containing 10ml Trypsin (Sigma; T4424) and incubated overnight at 4°C. After incubation, the intact skin was transferred to a second 100mm dish. With the epidermis faced down, the dermis was lifted off and discarded. The epidermis was then transferred to another dish containing keratinocyte culture media, and cut into small pieces using surgical

scissors. The solution and epidermis were moved to tube, pipetted up and down gently to further break down the epidermis, then centrifuged for four minutes at 1000rpm at 4°C. Following centrifugation, the supernatant was removed, and 5ml of media was added to resuspend the pellet. Using a 100um mesh cell strainer, the suspension was subsequently filtered into a 50ml falcon tube and again centrifuged for four minutes at 1000rpm at 4°C. The supernatant was removed and the final pellet was resuspended in 10ml of cell culture media, then plated.

rKeratinocyte Cell Culture

All rat keratinocyte cell cultures were seeded on 35mm CellStar tissue culture dishes which were previously coated with 0.5 ml 3mg/ml Collagen (Sigma) and 1mg Fibronectin human plasma (Calbiochem) for 1 hour at 36°C, 5%CO_2. Cells were typically plated at approximately 1,000,000 cells/dish.

Rat Keratinocyte-Dorsal Root Ganglion Co-Culture

Co-culture of cells was first optimized for rat keratinocyte-dorsal root ganglion cells. Rat keratinocytes and DRGs were obtained from P2-P4 rats. 30mm dishes were pre-coated with 0.5ml of collagen and fibronectin and kept in an incubator for 30 minutes to 2 hours. Dishes were washed with distilled H20 and Epilife medium before any cells were plated.

Keratinocytes were cultured at 1,000,000 cells per dish. Epilife medium supplemented with S7 and antibiotics, as previously detailed, was used for the culture of these keratinocytes. After one hour to confirm adhesion of keratinocytes, DRG neurons were added to the cell culture at 20,000-50,000 cells per plate. Higher proportions of DRG cells may inhibit growth of keratinocytes. Media should be removed within 24 hours and replaced with fresh media, then every 48 hours thereafter. Neuronal outgrowth should be apparent within one day. Confluency and neuronal outgrowth can be observed within seven days. DRG neurons appear as larger and rounder cell bodies compared to mosaic-appearing keratinocytes. It is possible to adjust calcium levels in order to control the proliferation of keratinocytes and outgrowth of DRG neurons, as described by Roggenkamp et al., 2012.[5]

Xenopus Cell Culture

Xenopus neuronal cells are sourced as primary cultures. These processes of dissection, cell extraction, and cell culture are detailed below.

Xenopus Cell Media

A variety of solutions are used in the xenopus microsurgical technique to isolate neuronal cells, namely Steinberg's solution, Calcium and Magnesium-Free Steinberg's Solution, MMR, and Culture Medium. Steinberg's solution and MMR being the most complex. MMR is similar to pond water and is used for xenopus embryo incubation, while Steinberg's solution acts like extracellular fluid. Calcium and Magnesium-Free Steinberg's is used to maintain a calcium ion free environment that helps cell clusters break down into individual cells, facilitating plating. Both types of Steinberg's solution and MMR were created at the concentrations listed below, and are made up to 1L with MilliQ water. Steinberg's is kept at a pH of 7.8-7.9, while MMR solution is kept at a pH of 7.4. The MMR solution listed below is diluted to create 0.1X solution in MilliQ water before use. All solutions were filtered before use and kept at 4C otherwise.

Xenopus Harvesting and Culture

Xenopus embryos extracted from frogs are kept in 0.1X MMR solutions and placed into incubators at different temperatures ranging from 12C to 22C. Embryos kept at lower temperatures mature less rapidly; only embryos that have reached stage 20-22 can be used for neuronal cell dissections.

Each embryo should be passed through separate solutions of ethanol, MMR, Steinberg's solution, and 8-10 mg/ml of collagen dissolved in Steinberg's solution. The outer layer is removed, followed by the transparent inner layer. Once the layers have been removed, the remainder of the procedure must be done inside solution; embryos that reach the top will explode. The embryos should then be cut in half, with the stomach on one end and the head/spine on the other. Embryos should be moved into collagenase solutions and incubated there for 20 minutes. Following this period, neural tubes were extracted and placed in CMF-Steinberg's solution. Once disintegrated, each neural tube is moved to 200ul culture media, which is composed of 20% modified L-15, 1% calf serum, and 2% pen/strep in Steinberg's solution. The pH of this media should be between 7.8 and 8.0.

Table 5.A.6: Xenopus Dissection and Culture Solutions

	Concentration	g/L	Working Dilution (ml per L)	Final Concentration (mM)
Steinberg's Solution				
Nacl	1 M	58	58	58
KCl	0.1 M	7.46	6.7	0.67
$Ca(NO_3)_2 \cdot 4H_2O$	0.1 M	23.62	4.4	0.44
$MgSO_4 \cdot 7H_2O$	0.1 M	24.65	13	1.3
Trizma Base	0.1 M	12.11	46	4.6
Calcium & Magnesium Free Steinberg's Solution				
Nacl	1 M	58	58	58
KCl	0.1 M	7.46	6.7	0.67
Trizma	0.1 M	12.11	46	4.6
EDTA		0.1117		0.4
10X MMR				
NaCl	1 M	58		
KCl	20 mM	1.49		
CaCl2. 2H2O	20 mM	2.94		
MgCl2 .6H2O	10 mM	2.03		
HEPES	50 mM	11.91		

Xenopus Cell Fixation and Permeabilization

Formaldehyde at concentrations of 37-40% was used to stain Xenopus cells. Once fixed, PBS-Triton was applied to allow cell dye to be properly absorbed. Cells can be left in PBS (as mammalian cells) or staining can be subsequently performed.

Xenopus Electrical Field Experiments

As with mammalian electrical field experiments, the electrical field experiments used for xenopus cells are composed of two power supplies. The first is the main power supply

(electrophoresis power supply). This is connected to a second power supply that has been linked to a variable resistor in series that can be dialed up or down as necessary.

Electrodes are connected to silver-silver-chloride electrodes, which sit in beakers of Steinberg's solution. The size of beakers used are relevant to the size of the agar bridges used to connect the plates. Agar bridges are made up at 25mls of Steinberg's solution in proportion to each 0.5g of agar. They are placed half in beaker and half in plate. Electrophoresis of media through bridges can occur, which is relevant to size of beakers and consequent size of bridges. Steinberg's solution is used within these beakers because the majority of media used is of the same type.

All plates to be tested were set at the same range, which can be confirmed by the electroconductivity set-up. The voltage can be measured across each chamber using the voltimeter. Chambers typically yield equivalent length in cm to voltage (V) (e.g., 5 cm long chamber □ 1000 mV per mm = field needs to yield 5 V). Electrical fields were applied for 3-5 hours in humidified environments, and stained afterwards.

Section 5.A.2: Preliminary Biocompatibility Assessments

Preliminary tests of our materials were performed using primary *Xenopus* neurons and rat cortical neurons. These tests were performed to determine the biocompatibility of the different Kraton materials, Kraton D1152 and Kraton D1161. Kraton D1152 and D1161 were initially not particularly different from a structural or mechanical perspective (as shown in the initial results of Chapter 3). The primary difference between these materials is the different elastomeric component within the copolymer and its ratio compared to polystyrene: Kraton D1152 uses butadiene, with 30% polystyrene and 15% diblock. while Kraton D1161 uses isoprene, with 15% polystyrene and 19% diblock. Given the hydrophobicity of the materials and the sensitive nature of neurons, which typically require their substrates to be specially coated, it was important to determine if either (or both) of these materials could be used as a somatosensory construct.

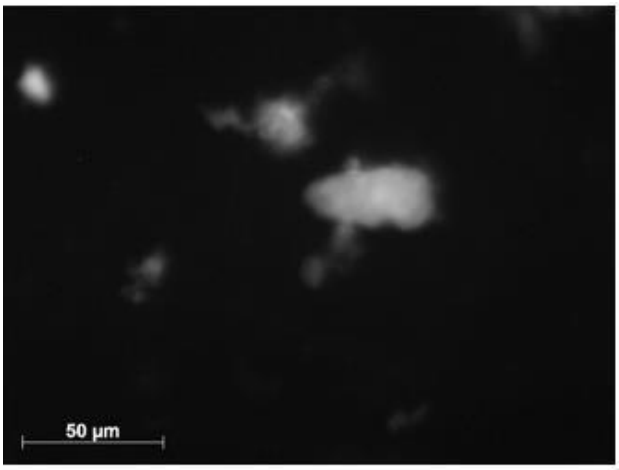

Figure 5.A.2: Xenopus Neurons on (10%) Kraton D1161PT (SIS). Minimal neuronal adherence of xenopus cells on Kraton D1161PT (SIS)

Preliminary biocompatibility tests were performed in conjunction with mechanical experiments in order to select between Kraton D1152ES (SBS) and Kraton D1161PT (SIS). These first figures show the results of the initial biocompatibility testing performed, using *Xenopus* neurons and rat cortical neurons. These experiments were performed on planar sheets of both materials that had been prepared using 10%wt concentrations of both polymers. The purpose of these tests was primarily to validate a lack of toxicity and solvent retention. However, it also served as a fundamental test to assess the hydrophobicity of the materials, assess if adhesion proteins could effectively adhere, and determine if neuronal cells may have any preference for either material given the difference in mechanical properties.

As shown in Figures 5.A.1 there was no neuronal outgrowth on the SIS polymer. However, there was substantial outgrowth was seen on various neurons on the SBS polymer, as shown in Figure 5.2. Neurite outgrowth is clearly defined by rhodamine phalloidin, as well the arrows designating elongated filopodia. Interestingly, neuronal outgrowth on Kraton D1152 seemed to be related to substrate topography. On a macroscopic level, these polymers were smooth and transparent materials without structure. However, on a microscale and nanoscale level, cells may be interacting with the materials. These results inspired us to perform confocal analyses in the following systems that were tested.

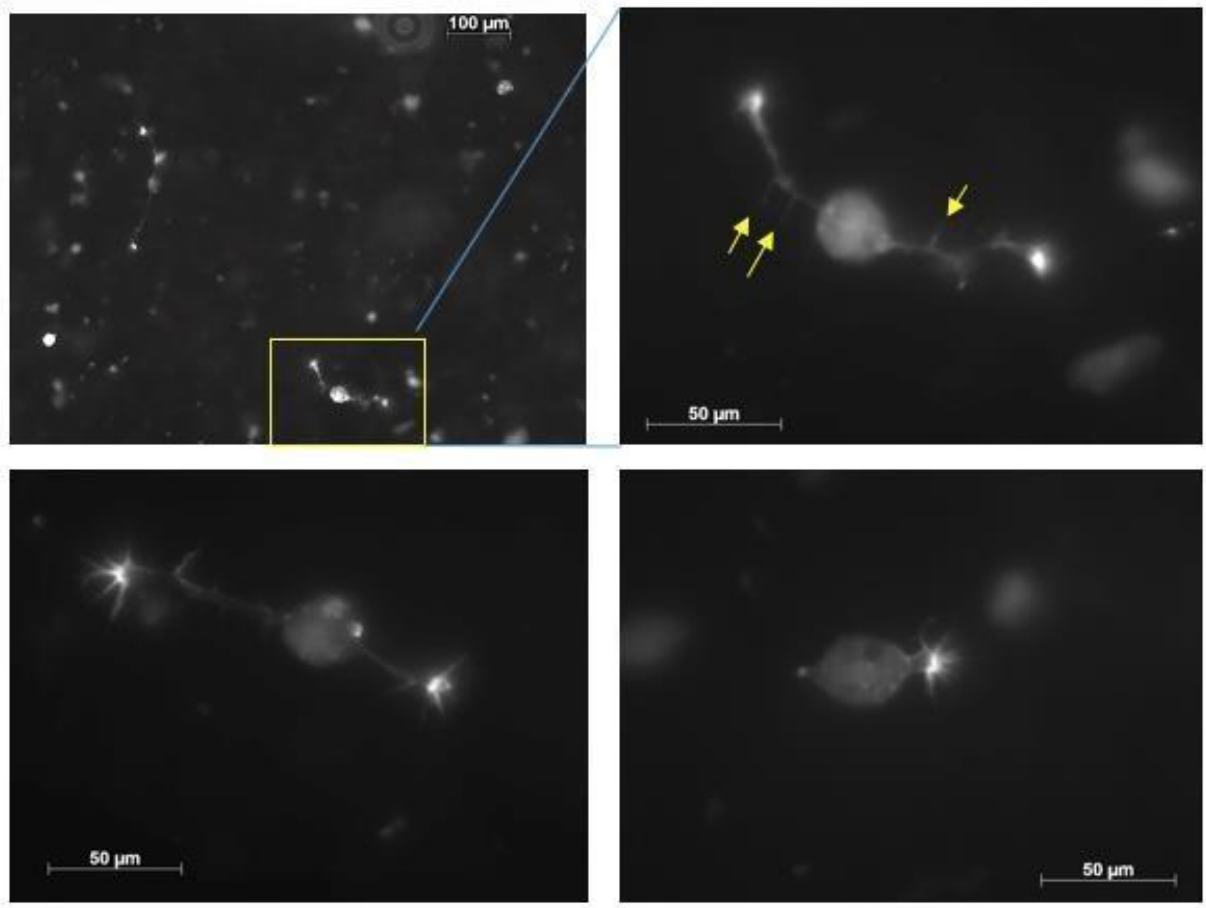

Figure 5.A.3: Xenopus Neurons on (10%) Kraton D1152ES (SBS). Various xenopus neurons, showing neurite outgrowth, adherent to Kraton D1152ES (SBS)

Preliminary experiments of this nature were also performed using mammalian cells; specifically, rat cortical neurons. As shown in Figure 5.A.3 and Figure 5.A.4, the results between our amphibious and mammalian models were essentially the same. While cells adhered to the Kraton D1161 material, no convincing outgrowth was seen in most cells. The rat cortical neurons showed a single cell with neurites on Kraton D1161PT (SIS) (Figure 5.A.4), whereas multiple can be identified easily on Kraton D1152ES (SBS) (Figure 5.A.3). Given our results, the primary polymer we chose to utilize for the rest of our experiments was Kraton D1152ES (SBS). We assumed that, given the fairly similar mechanical properties of these materials, the structural content and consequent differences in hydrophobicity may have influenced the differences in adherence and elongation on neurites. These differences were not explored further, but were considered sufficiently adequate as a rationale for the elimination of Kraton D1162PT (SIS).

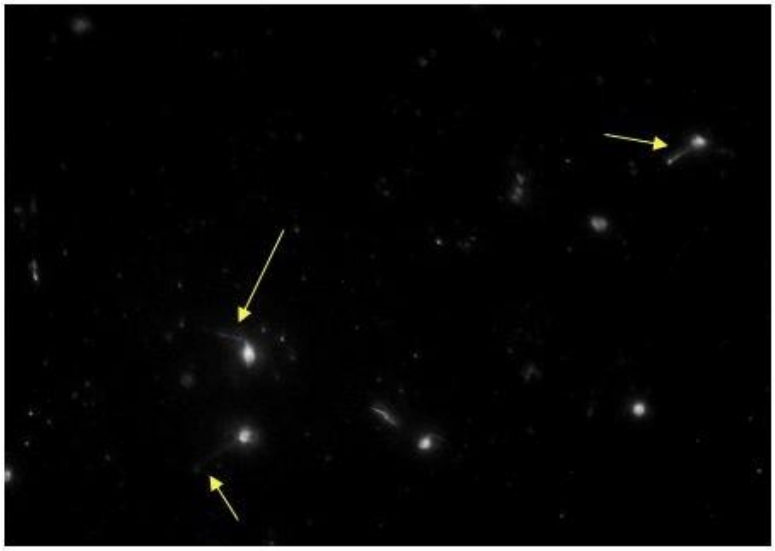

Figure 5.A.4: Rat Cortical Neurons on (10%) Kraton D1152

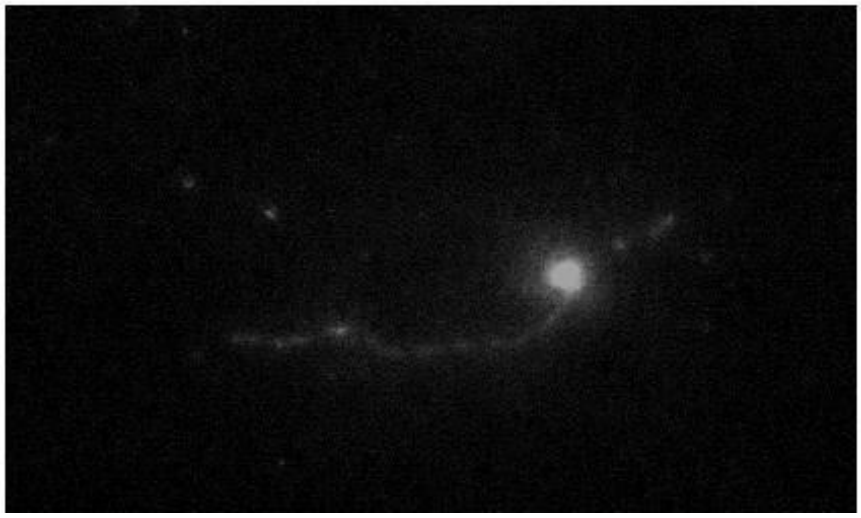

Figure 5.A.5: Rat Neuron on (10%) Kraton D116

6.A: References:

1. Qi, Hang Jerry, and Mary C. Boyce. "Stress–strain behavior of thermoplastic polyurethanes." *Mechanics of Materials* 37.8 (2005): 817-839.
2. Cho, Hansohl, et al. "Deformation mechanisms of thermoplastic elastomers: Stress-strain behavior and constitutive modeling." *Polymer* 128 (2017): 87-99.
3. Bergström, J. S., and M. C. Boyce. "Large strain time-dependent behavior of filled elastomers." *Mechanics of materials* 32.11 (2000): 627-644.
4. Cruz, A. M., et al. "Iridium oxohydroxide, a significant member in the family of iridium oxides. Stoichiometry, characterization, and implications in bioelectrodes." The Journal of Physical Chemistry C 116.8 (2012): 5155-5168.
5. Carretero González, Nina Magali, and Jaume Casabó i Gispert. "Iridium oxide-carbon hybrid materials as electrodes for neural systems. Electrochemical synthesis and characterization." (2014).
6. Roggenkamp, Dennis, et al. "Atopic keratinocytes induce increased neurite outgrowth in a coculture model of porcine dorsal root ganglia neurons and human skin cells." Journal of Investigative Dermatology 132.7 (2012): 1892-1900.
7. Sleigh, James N., Greg A. Weir, and Giampietro Schiavo. "A simple, step-by-step dissection protocol for the rapid isolation of mouse dorsal root ganglia." BMC research notes 9.1 (2016): 82.